IDENTIFYING NOVEL REGULATORS OF IMMUNE EVASION IN HUMAN PAPILLOMAVIRUS-POSITIVE HEAD AND NECK SQUAMOUS CELL CARCINOMA

By

Nicholas Scott Giacobbi

A DISSERTATION

Submitted to
Michigan State University
in partial fulfillment of the requirements
for the degree of

Physiology – Doctor of Philosophy

2024

ABSTRACT

The incidence of Human Papillomavirus positive (HPV+) head and neck squamous cell carcinoma (HNSCC) threatens the health of thousands of people each year, with cases projected to rise in the coming decade. HPV is now the etiologic agent accountable for nearly all oropharyngeal cancers. Despite the effectiveness and relatively favorable prognosis of current treatments for HPV+ HNSCC, many patients do not respond and are left facing uncertainty about their health and future. What is sure is that there is an urgent need to develop novel strategies for the treatment of HPV+ HNSCC.

Viruses have evolved a myriad of mechanisms to evade the immune system. Some high-risk HPV strains can elude detection by disrupting host DNA methylation patterns, altering genome-wide cellular transcription, and depleting key signaling molecules necessary for the infected cell to mount an effective immune response. Including those that are initiated by viruses, the epigenetic dysregulation of DNA methylation or chromatin structure has been observed in tumor cells across many cancers. This suggests that there are common mechanisms that both viruses and tumor cells can exploit to evade immune detection, predisposing the cell toward cancer progression.

Through the application of genome-wide gene knockout screening in HPV+ HNSCC cells, we have revealed several factors which disrupt the normal cellular epigenetic landscape. Among them were the lysine acetyltransferase 2A (KAT2A) and members of the polycomb repressor complex 2 (PRC2). Interestingly, PRC2 is part of an evolutionarily conserved mechanism known to contribute to cancer immune evasion and resistance to immunotherapies by downregulation of the major histocompatibility complex

I (MHC-I). We validated our screening results with additional genetic knockouts and identified multiple small molecule inhibitors that may help remediate the pathologic epigenetic changes. We have also identified novel targets within the pathway of MHC-I downregulation that we hope will aid in the development of future treatments for HPV+ HNSCC.

Prior to this study, we identified a homeostatic signaling molecule, CXCL14, as a crucial antitumor factor that is epigenetically silenced in HPV+ cancer progression. Rescued CXCL14 expression in HPV+ tumor cell lines suppressed tumor growth and suggested that its restoration may help to treat some HPV+ cancers. Here we provide new developments in understanding CXCL14 antitumor properties, and we outline the development of a novel transgene therapeutic platform to further study CXCL14 antitumor immunity.

ACKNOWLEDGEMENTS

There are many people to whom I owe respect and praise for their help in completing my dissertation. First, I wish to express my sincere thanks to Dr. Dohun Pyeon for his encouragement and for providing me with the opportunity to pursue this work in his laboratory. My deep gratitude extends to all past and present members of the Pyeon lab for their help and support, without whom this work would truly not have been possible.

I also wish to thank: My guidance committee, Drs. Hua Xiao, Yasser Aldhamen, Karen Liby, Kathleen Gallo, and Eran Andrechek for their patience, understanding, and direction. Dr. Gina Leinninger for her wisdom, empathy, and student advocacy. Our department is truly a better place with your leadership. The DO/PhD program, Drs. Brian Schutte, Justin McCormick, Andrea Amalfitano, and John Goudreau, in addition to Michelle Volker, Bethany Heinlen, and Rusti Sidel. I am forever grateful. My fellow students and friends in BMS, who are a constant source of support and inspiration. Especially my friends on the fourth floor of BPS who were there for me throughout the years.

I am honored to acknowledge the following individuals who directly contributed to the technical completion of this work, and I express my thanks to them: To Dr. Andrew Olive, whose expertise was instrumental in the genesis and completion of our CRISPR/Cas9 screens. I am very grateful for your support in this work along the way. A special thanks goes to John Vusich for providing the CUT&RUN assay. He was crucial for experimental design, technical handling, optimization, and data analysis/interpretation. To Sarah Roosa, Dr. Aldhamen, and Dr. Amalfitano for their supervision, guidance, and provision of reagents during the preparation of adenoviral

vectors. To Canchai Yang, for his help in the preparation of our screens, troubleshooting of western blots, discussion of experimental procedures, and stalwart diligence to our lab. To Lexi Vu, for your dedication at the bench, contribution to cloning and analysis of the screens, troubleshooting qPCRs, and the data for Figure 7B. To Dr. Mohamed Khalil, for your help in screen preparation, supervision at the flow cytometry core, and help processing of my flow samples. To Shreya Mullapudi for qPCR repeats, sample processing, and contributions to the CXCL14 manuscript. To Will Eckerman for sample processing and western blot repeats. To Harrison Nabors for his perseverance in the CXCL14 project and philosophical debates. To Smriti Chadha for help with luciferase assays and stoic perspective. To Evelyn Gomez for qPCR repeats, and to Anthony Schulte and Alex Wahl for TIDE troubleshooting.

TABLE OF CONTENTS

CHAPTER 1

Introduction

Part of this chapter was adapted from the original article entitled, "The Chemokine CXCL14 as a Potential Immunotherapeutic Agent for Cancer Therapy" published in Viruses. 2024 Feb 16;16(2):302. doi: 10.3390/v16020302.

Authors: **Nicholas S. Giacobbi**, Shreya Mullapudi, Harrison Nabors, and Dohun Pyeon

1.1 Epidemiology of Human Papillomavirus Cancers

Human Papillomavirus (HPV) is the etiologic agent linked to ~4-5% of all human cancers worldwide[1,2]. Of the known cancer-causing infectious agents, HPV is second, accounting for nearly one third of the infections which lead to cancer[3]. High-risk HPV subtypes are responsible for multiple cancer types including ≥95% of cervical cancers, ≥80% of anal cancers[4], and >50% of penile, vulvar, and vaginal cancers[5]. Coinciding with a gradual decrease in HPV-negative HNSCC since the last decade of the twentieth century, HPV+ HNSCC has steadily increased[6,7]. HPV+ HNSCC now is estimated to account for ~90% of all oropharyngeal cancers and may reach an annual incidence of >30,000 cases by 2030, eclipsing cervical cancer as the leading HPV associated cancer[8].

As of 2012, HPV+ HNSCC incidence increased the most in higher-income western countries and was lowest in Africa, the Middle East, or east Asia, with similar trends in the anogenital cancers[9]. Conversely, incidence rates of cervical cancer were highest in Sub-Saharan Africa and lowest in the United States or Western Europe[9]. Although lacking a definitive explanation, these observations may be attributable to differential rates of HPV-vaccination, screening, or possibly differences in regional variants within high-risk subtypes[9-15].

Demographically, HPV+ HNSCC has predominately affected males of advanced age. Although similar rates afflicting both sexes are documented, males are still projected to have an ~5-fold greater incidence of HPV+ HNSCC by 2030, when controlling for ethnicity and region in the United States[16]. It is also projected that HPV+ HNSCC incidence will wane among those born after 1990, but will increase in those over age 55 by the 2030 projection[16].

Other significant risk factors for all HNSCC includes the use of tobacco, alcohol, and reduced immunity[2,17]. DNA Damage, with the formation of DNA adducts, can result from tobacco consumption and alcohol (ethanol)[18,19]. For HPV+ HNSCC, the obvious risk factor for disease is HPV infection, that can further be increased with an increased number of sexual partners (increasing HPV infection risk)[20]. Infection with high-risk HPV subtypes are key to HPV cancer development, and they drive cancer progression through the expression of the oncoproteins E6 and E7[21], although at least one report includes E2, E4, and E5 expression as sufficient for carcinogeneis[22]. At least 13 of 200 known[9] subtypes are high-risk (carcinogenic), with HPV-16 overwhelmingly the most dangerous, accounting for about half of cervical cancer and up to 90% of HPV+ HNSCC[12,23]. Deeper analysis of variants within high-risk strains indicates varying levels of risk toward cancer progression[12], and a better understanding of what pathologic effects are propagated by a respective virus to make a given strain truly “high-risk” compels further scrutiny.

1.2 HPV Biology and Tumorigenesis

Human Papillomaviruses are one of the small (~8000 base pairs in length), circular, double stranded DNA (dsDNA) tumor viruses[24,25], and can sometimes cause persistent infections that contribute to cancer progression[26]. HPV infection occurs in basal keratinocyte stem cells found in cutaneous or mucosal squamous epithelium. Normally, undifferentiated keratinocytes in the stratum basale stop proliferating and progress apically as they commit to a path of differentiation, forming the layers of the epithelium along the way[27]. Following HPV infection, normal differentiation is delayed, and epithelial homeostasis is dysregulated to accommodate the viral life cycle[26,28]. Instead, viral DNA replication and production of viral progeny is orchestrated by the temporal expression of virus proteins, early (E1,2,4,5,6,7) to late (L1,2), with early genes mediating replication

and cell proliferation, and late genes required for virion assembly and release[28]. Impaired cellular differentiation is regulated in large part by the expression of the HPV oncoproteins E6 and E7[29-32], which also set the stage for viral genome production and cell proliferation[28]. Sometimes through this process, E6 and E7 from high-risk HPV subtypes can induce cellular transformation and cancer progression[21,28]. E7 promotes cell proliferation by inhibition of the retinoblastoma tumor suppressor family members pRB, p107, and p130, permitting the release of E2F transcription factors that promote the G1 to S-phase cell cycle transition[33,34].

An important aside is that the family of E2Fs (1-8) have differential effects on the cell cycle, with some promoting it and others negating it[35]. Although, despite their differences, the various E2Fs are highly homologous and may exhibit overlapping activity in the right context[36,37]. E7 can also interact with cellular DNA methyltransferase enzymes (DNMTs), which results in widespread DNA methylation changes, subsequent effects on gene expression, and even the silencing of tumor suppressor genes[38,39].

High-risk E6 variants contribute to tumorigenesis as a result of E6 mediated degradation of the p53 tumor suppressor protein via E6AP ubiquitin-protein ligase binding[40]. E6 also immortalizes cells in conjunction with the c-MYC (cellular MYC, or sometimes interchangeably “MYC”[41]) proto-oncogene by increasing telomerase expression[42-44], and E6 can also limit antitumor immunity in HPV+ HNSCC by driving degradation of death receptors[45]. In an aggressive HPV+ neuroendocrine cervical cancer, c-MYC has even been proposed as the primary driver of cellular transformation rather than E6 and E7[46]. High-risk HPV genomes also tend to integrate into certain “hotspots,” specifically c-*MYC* and *SOX2,* with both c-MYC and (neuronal MYC) N-MYC overexpressed as a result[47]. The expression of N-MYC is typically restrained to tissues

during embryonic development, but in an adult, its expression is low and is observed in only a few tissue types (e.g., brain, heart, or developing B-cells)[48]. The amplification of N-MYC gene expression, like the other MYC family members, has been observed in high-risk HPV+ cancers previously[49,50], but its specific impact on HPV+ cancer progression (if any) is unknown. Aberrant expression of N-MYC can influence cancer progression by promoting cellular transformation[51], and N-MYC can transform cells through collaboration with ras[52]. Rapid cancer progression of neuroblastomas and decreased progression-free survival have been linked to N-MYC overexpression[53,54], and likewise, even to a lack of therapeutic response and poor patient prognosis[55]. Importantly, N-MYC can drive oncogenic transcriptional programs in conjunction with the lysine acetyltransferase (KAT2A) as part of greater transcriptional co-activator Spt-Ada-Gcn5-acetyltransferase (SAGA) complex, and loss of SAGA decreased N-MYC chromatin binding and transcription[56]. Interestingly, an important early discovery was the amplification N-MYC expression and its relationship with evasion of the immune system by downregulation of MHC-I[57].

1.3 Innate Immunity and HPV Infection

The control and clearance of both viral infections and cancer cells is mediated by the shared activity of both innate and adaptive (acquired) immunity. Innate immunity is readily available, broad spectrum, and typically the first defense against pathogens. It is comprised of such elements as physical barriers (e.g., membranes), secreted antimicrobial proteins (e.g., lysozyme found in tears), antimicrobial peptides (e.g., defensins), the complement system (i.e., pathways that detect and destroy microörganisms)[58], and cellular components that mediate the process in response to “non-self” threats (e.g., neutrophils and macrophages)[59].

Physical barriers protect the body from the outside environment, and the epithelium (e.g., skin and mucosal surfaces) is arguably the very first line of defense. Epithelium comprises the skin, and lines the body's vessels, digestive tract, and other organs[60]. There are many types of epithelium[61], and squamous epithelium, for example, exists in the mouth, pharynx, esophagus, and in the cervix[62]. HPV has evolved to infect and exploit some of the most vulnerable cells (i.e., keratinocytes) in the epithelial barrier for its own growth, and regrettably, infection sometimes contributes to cancer progression[63-65]. Yet after immune system clearance of the virus (i.e., under the clinical range of detection), the virus can persist in long-lived "stem-like cells"[66], and with immune regression, can reactivate[67,68]. Interestingly, the "stem-cells" exhibit a state of limited immunity, with reduced expression of HLA genes and attenuated anti-apoptotic mechanisms[68,69]. Hence, those cells could provide the perfect haven needed for HPV to help stoke cancer progression.

Beyond standing barriers, innate defense mechanisms can be triggered non-specifically by pathogen associated molecular patterns (PAMPs) that are detected through the cell's pattern recognition receptors (PRRs).[70] An important group of PRRs are the toll-like receptors (TLRs), which are distributed in compartments throughout the cell and on the cell surface, to detect a range of ligands[71]. Some of these ligands include components of bacterial cell walls (e.g., lipoteichoic acid detected by TLR-2), double-stranded RNA (via TLR-3), or unmethylated dsDNA (via TLR-9)[71]. In many cell types (including keratinocytes), TLR-9 can detect unmethylated CpG DNA typically found in bacteria or viruses (e.g., HPV), as it is less common in mammalian DNA where it's expected that ~70% of CpG dinucleotides are methylated[72,73]. HPV as a result, has evolved strategies to downregulate TLR9 as a mechanism of immune evasion[74,75]. Hasan

et al. showed that TLR9 transcription is down regulated by expression of HPV16 E6 and E7[74], and similarly, Pacini et al. showed that HPV38 can downregulate TLR9 expression by recruitment of Enhancer of Zeste Homolog 2 (EZH2)[75].

TLR9 is found in the endoplasmic reticulum (ER) and translocates to endosomes containing its ligand (i.e., CpG DNA) for binding and subsequent signaling[76]. The membrane protein UNC93B1 is necessary for the trafficking and activation of some TLRs, including TLR9, to the endolysosomes[77]. Ligand binding to TLR9 initiates a signaling cascade by association with the myeloid differentiation primary response 88 (MyD88), IL-1 receptor-associated kinase family members 1 and 4 (IRAK1/4), and TNF receptor-associated factor 6 (TRAF6), associations that lead to the liberation of nuclear factor kappa-light-chain-enhancer of activated B cells (NFkB) allowing its translocation to the nucleus to foster expression of a number of important transcriptional networks[78,79]. NFkB transcription factor is one of the major conductors regulating immune responses against infections, and depending on context (e.g., cell type), NFkB translocation to the nucleus fires the transcription of many inflammatory genes, including interleukin-12 (IL-12), tumor necrosis factor alpha (TNF-a), type I interferon alpha and beta (IFN-α, IFN-β), and type II IFN-gamma (IFN-γ) pathways[80]. Interferon stimulated pathways can then activate such elements as the signal transducer and activator of transcription 1 (STAT1) to drive the production of hundreds of interferon stimulated genes (ISGs) to mitigate viral infection, among many other known functions[81]. STAT1 signaling is crucial in propagation of an antiviral state[82], and in HPV+ *in vivo* tumor models, the loss of STAT1 resulted in accelerated tumorigenesis[83].

IFN-γ signaling can upregulate the expression of MHC-I. Initiation of IFN-γ signaling triggers the phosphorylation, dimerization, and mobilization of (STAT1) to the

nucleus[84], and in conjunction with NFkB and interferon response factor 1 (IRF1) activity, promotes the expression of MHC-I genes[85]. Stimulation by IFN-γ also drives expression of genes needed for antigen presentation via MHC-I, including the Transporter-associated antigen processing (TAP) genes and proteasomal genes[86,87].

Cellular innate immune responses involve a multitude of specialized cell types[88]. For example, neutrophils are some of the earliest responders to infections, and will swarm infection sites, and cast neutrophil extracellular traps (nets) to help reduce viral infections[89]. Eosinophils and Basophils are granulocytic cells typically associated with their role in mediating TH2 responses (i.e., responses to extracellular insults like allergens or parasites)[90], and cancer[91,92]. Natural Killer (NK) cells are innate immune effector cells that can kill tumor cells that have low surface levels of MHC-I receptors (and diminished cytotoxic T cell responses)[93]. NK cells mediate tumor cell killing by a unique mechanism that involves the expression of the natural killer group 2D (NKG2D) receptor on the NK cell surface and the binding of NKG2D ligands (e.g., MHC I Chain-related molecules A and B, MIC A/B) on the surface of cancer cells, not typically expressed on healthy cells[94]. NK cells and some T cells express the other NKG2 receptor classes, A, B, and C, and have been shown to be the receptor for the non-classical MHC-I heavy chain, HLA-E. Interestingly, in keratinocytes expressing HPV16 E7, HLA-E expression is highly downregulated, suggesting that the control of HPV+ cells may be regulated in part by HLA-E expression[38]. Lastly, monocytes, macrophages, and dendritic cells (DCs) are necessary to maintain homeostasis and modulate innate immune activation[95]. These cells are highly phagocytic and are well equipped with PRRs to detect and promote subsequent immune responses. Phagocytized pathogens can be destroyed in macrophages following recognition of PAMP signals[96]. Following their activation, both macrophages and DCs can

release the cytokines and chemokines necessary for the movement (i.e., chemotaxis) of additional immune cells to sites of infection or tumors[97,98]. Macrophages and DCs are also crucial in processing and presenting antigens via MHC-II molecules to other immune cells, effectively bridging innate and adaptive immunity[99,100].

1.4 Chemokines and Cancer

Chemokine signaling is part of the unique language by which the immune system communicates with itself and other cell types. Chemokines were initially identified as chemical attractants for immune cells but were later discovered to modulate a broad range of homeostatic functions and responses to pathogens and diseases[101-103]. Given these broad roles and functions, it is not surprising that certain chemokines can also play important roles in cancer progression and the modeling of the tumor microenvironment (TME)[104].

A recent comprehensive profiling of the chemokine signaling governing the TME of patient-derived melanoma was shown in the study by Hoch et al. [105]. Hoch et al. have shown that so-called immunologically “cold” tumors lack chemokine expression and T-cell infiltration. In contrast, immune “hot” tumors show high T-cell infiltration within areas exhibiting relatively high levels of the chemokines CXCL9, CXCL10, CXCL13, and CCL4[105]. The role of CXCL9 and CXCL10 in T-cell infiltration has been well established, representing their importance for tumor clearance by T-cell responses[106,107].

Galeano Niño et al. have also shown that CD8+ T cells within the TME induce the recruitment of distant CD8+ T cells via the expression of CCL3/4, establish a positive feedback loop, and eventually “swarm” the tumor with CD8+ T cells[108]. Additionally, the B-cell homing chemokine, CXCL13[109], was newly implicated in mediating the formation of tertiary lymphoid structures and infiltrating T and B cells into tumors, specifically,

ovarian cancer[110].While these studies suggest the importance of chemokines in activating and perpetuating a variety of cellular antitumor immune responses, chemokines can also promote the opposite effect, establishing a protumor and immunosuppressed TME. For example, Li et al. have shown that activating the CCL2-CCR2 axis results in the recruitment of myeloid-derived suppressor cells and tumor-associated macrophages (TAMs) into the TME, leading to immunosuppression and tumor promotion[111]. Similarly, Xu et al. have shown that TAMs upregulate CCL5 expression in renal cell carcinoma, creating an immunosuppressive TME associated with poor patient prognosis[112]. Together, these studies indicate that chemokines have the capacity to both enhance and negate antitumor immune responses. Identifying the most applicable conditions and relevant chemokines in the right context (e.g., cancer type) may offer the potential to utilize chemokine signaling as a novel cancer immunotherapeutic.

For example, CXCL14, a homeostatic chemokine in squamous epithelia, is known for its association with cancer as being abundantly expressed in normal tissue but significantly downregulated in some tumors[113,114]. High levels of CXCL14 expression are correlated with overall patient survival in colorectal, breast, endometrial, intraepithelial, and head and neck cancers[98] and suppress tumor progression[115-119]. In contrast, other studies have shown protumor effects of CXCL14 in nasopharyngeal carcinoma, prostate cancer, glioblastoma, non-small-cell lung cancer, and microsatellite-stable colorectal tumors[120-124]. We have previously shown that CXCL14 expression is epigenetically downregulated in human papillomavirus-positive (HPV+) head and neck squamous cell carcinoma (HNSCC) and cervical cancer (CxCa)[38,125]. Our findings suggest that CXCL14 is critical for the antitumor control of HPV+ cancers. For example, by rescuing the expression of CXCL14 in HPV+ HNSCC cells, we observed increased MHC-I expression

and CD8+ T cell infiltration into the TME[125,126], resulting in tumor suppression *in vivo*. Similarly, Kumar et al. have shown that elevated CXCL14 resulted in increased CD8+ T-cell infiltration into tumors with improved survival using an *in vivo* malignant glioma model[116]. Dolinska et al. have shown that CXCL14 expression is absent in bone marrow niche cells of chronic myeloid leukemia patients. However, with CXCL14 restoration, leukemia-initiating stem cells were suppressed, and their sensitivity to imatinib treatment was enhanced[126,127]. Parikh et al. have revealed that CXCL14 expression inhibits tumor growth and increases tumor-infiltrating lymphocytes in HPV-negative squamous-cell carcinoma of the oral cavity[128]. Interestingly, single cell-RNA sequencing has revealed that CXCL14 downregulation is most prominent in malignant cells within tumor-draining lymph nodes as well as the primary tumor cells, suggesting that CXCL14 may play an important role in limiting nodal metastasis[128]. The effect of CXCL14 on metastasis has previously been observed in other cancer types[98,126,129,130]. Conversely, metastasis enhanced by CXCL14 has been shown in pancreatic and breast cancers[98,131,132]. Overall, these findings suggest CXCL14 has diverse and likely context-specific functions in both antitumor immunity and metastasis[98,119,133,134].

1.5 Adaptive Anti-tumor Immunity, Immunosurveillance, and Immunosuppression

Infiltration of tumors by cytotoxic CD8+ T cells and other lymphocytes is critical to tumor clearance, and has been well documented[135-139], [140,141]. The canonical paradigm of mounting a productive adaptive CD8+ T cell response begins with activation, followed by expansion, and then migration of CD8+ T cells to tumor sites[142]. Activation of antigen specific CD8+ T cells need three activating “signals.” First, antigen presenting cells (APCs) (e.g., DCs) will phagocytize, process, and display specific cancer cell derived antigens s via their MHC-I receptor molecules to naïve mature CD8+ T cells in lymph

nodes, which responsive T cells will bind through their respective T cell receptor[143]. APCs also express costimulatory molecules (i.e., B7.1/CD80 and B7.2/CD86) that bind to CD28 on the T cell to ensure activation[140,144]. A third set of secreted signals (e.g., IL-12 or IFN-γ) are released from APCs to further promote T cell proliferation and differentiation into effector cells[145]. Once primed and activated as effector cells, the CD8+ T cells will undergo clonal expansion, enter circulation, and can migrate to sites of infection or tumors[146]. Upon arrival at the target cell, an activated CD8+ T cell will recognize an MHC-I molecule loaded with its cognate antigen on the infected/tumor cell surface (through its T cell receptor)[147]. This encounter triggers the killing of the target cell by the effector CD8+ T cell by the release of perforin and granzymes at the immunological synapse between the cells, or by activation of Fas (death) receptors on the cancer cell, triggering apoptosis[148]. After acute stimulation and expansion and clearance of target cells, CD8+ cells will eventually decrease in numbers, leaving a persistent subset called memory T cells which will quickly respond to the same tumor cell or foreign pathogen if again encountered at a later time[149,150].

Nuancing the canonical paradigm for antitumor CD8+ T cell activity are new observations that involve the presence of stem-like T cells to maintain durable anti-tumor responses[151]. Jansen et al. showed that the presence of stem-like CD8+ T cells at antigen-presenting-cell niches in tumors were critical for effective infiltration by CD8+ T cells and help to explain why only some tumors become infiltrated by CD8+ T cells[152]. Later, Prokhnevska et al. put forth that contrary to canonical models, tumor-specific CD8+ T cells will proliferate in tumor draining lymph nodes as stem-like CD8+ T cells, migrate to tumor sites, and only then are they co-activated to acquire canonical effector functions -and not prior[142]. This concept is specifically relevant for HPV+ HNSCC, with the findings

that HPV-specific CD8+ T stem-like cell populations exist, are important to sustain T cell responses with prolonged antigen stimulation, and may dictate responses to immune checkpoint blockade[153].

Given these mechanisms, it is no wonder that the process of antigen presentation and MHC-I expression in both APCs and cancer cells are paramount for effective immunosurveillance and mounting successful cytotoxic CD8+ T cell responses. Antigen peptide processing (APP) is facilitated by an assemblage of cellular machinery, aptly named the antigen processing machinery (APM). The process beings in the cytoplasm where proteins that are endogenously produced (including those made in tumor cells) or of intracellular pathogen proteins (e.g., virus), are ubiquitinated and targeted for degradation by the cellular immunoproteasome to produce antigenic peptides[154]. Dendritic cells (and potentially many other phagocytic cell types) may also capture exogenous antigens through phagocytosis for cross-presentation via MHC-I[155]. In either case, processed peptides are moved into the ER via TAP, receive additional processing, and along with the help of chaperone proteins (e.g., calnexin and calreticulin), are associated with HLA heavy chain and β2M light chain to finalize peptide loading of the MHC-I complex[156]. After peptide is loaded, MHC-I is dissociated from the ER, enter the Golgi apparatus, and the new MHC-I molecules are shuttled to the cell surface for T cell interaction[157]. Any disruption to this process (e.g., in tumor cells) can limit MHC-I expression and subsequent CD8+ T cell tumor infiltration or lysis, allowing cancer cells to persist[141]. A pertinent example of this comes from Dersh et al., who conducted a genome wide screen of human diffuse large B cell lymphomas to identify genes negatively regulating antigen presentation and MHC-I expression important for CD8+ T cell immunosurveillance[158]. They found that EZH2 and EED of the histone methyltransferase

PRC2 were top hits from the screen, and that treatment with two EZH2 inhibitors (GSK126 and tazemetostat) restored MHC-I expression, alleviated H3K27me3 (the repressive histone mark distributed by PRC2) at HLA-B and NLRC5 promoters, and increased T cell responses *in vitro*[158].

Another captivating zoologic example of these mechanisms highlighting the importance of the relationship between APP, CD8+ T Cells, and recognition of MHC-I on cancer cells is Devil Facial Tumor Disease (DFTD)[159]. DFTD is observed in the Tasmanian devil and is one of the few transmissible cancers. The cancer has a mortality rate of 100% and is so deadly due to the fact that the tumor cells totally lack MHC-I expression and are “invisible” to the immune system[160,161]. Interestingly, the mechanism leading to downregulation of MHC-I was determined to be reversible and mediated through the epigenetic modification of histones and the downregulation of β2M, TAP1, and TAP2 expression[161].

Immunosuppressive tumor microenvironments can also undermine CD8+ T cell responses against tumor cells. Immune cells in the TME including T-regulatory cells (Treg), M2 macrophages (M2), and myeloid-derived suppressor cells (MDSCs) can all inhibit anti-tumor activity[162]. For example, the release of immunosuppressive cytokines like IL-10 and transforming growth factor-beta (TGF-β), from Treg cells can inhibit the activation of both CD8+ and CD4+ T cells[163]. Like Tregs, MDSC cells can also secrete IL-10 and TGF-β[164]. MDSC can also disrupt the homing of CD8+ cells by downregulating their expression of L-selectin adhesion molecules[165,166]. MDSCs can even promote tumor progression by directly stimulating tumor angiogenesis and supporting metastasis[167]. Both MDSCs and M2 macrophages can “starve” effector T cells through the expression of Arg-1 and iNOS enzymes, consuming L-arginine in the TME and limiting availability to

effector T cells[168]. Some tumors can secrete IL-10 and TGF-β1, tilting macrophage differentiation toward M2, and results in increased Treg infiltration of the TME[169].

A recent profiling of HPV+ and HPV-negative head and neck cancer tumors showed that HPV+ samples had fewer associated MDSCs prior to treatment and increased CD8+ T cells after therapy, relative to HPV-negative samples[170]. However, other evidence indicates that patient prognosis does not appear to correlate with increased presence of M2 macrophages in HPV+ tumors compared to HPV-negative[171]. Regardless, the tumor immune cell profiles in HPV+ HNSCC patients who do not respond to therapy or experience recurrence are still not well delineated, nor is it completely understood if immunosuppressive cell types (i.e., M2, MDSC, Treg) are actually contributing to immune evasion. Instead, these results may speak to the overall "good" prognosis of HPV+ HNSCC, but still fail to adequately represent patients who have advanced disease.

Irrespective of the relative incidence of effector CD8+ T cell infiltration into the TME, over time the anti-tumor responses of T cells can become inhibited through 'exhaustion'. In a general sense, exhaustion describes how T cell responses against tumor cells or virally infected cells can diminish following chronic antigen stimulation[172]. Under normal circumstances, activated T cells upregulate inhibitory receptors (e.g., PD-1, LAG3, TIM-3, TIGIT) to balance T cell responses, but after prolonged exposure to antigens (like when responding to tumors), proliferation potential is decreased, expression of inhibitory receptors increases, and effector function diminishes allowing cancer progression[173]. The use of immune check point blockade therapy (e.g., Pembrolizumab) has sometimes been effective in overcoming exhaustion and maintaining antitumor T cell responses[174], and their use has also demonstrated some

efficacy in treatment of head and neck cancer[175]. However, use of immune checkpoint blockade fails in many patients, or provide only a limited increase in survival, therefore more research is required to understand how to increase their usefulness[176].

1.6 Therapeutic Strategies and Potential Novel Treatments in HPV+ HNSCC

Despite an existing vaccine that is effective for prevention of some high-risk HPV subtypes, it cannot prevent infection by viral strains not covered by the current vaccine formulation, nor can the vaccine be used to treat patients with existing HPV infections. The notion of vaccine effectiveness is also mostly based on its use in cervical or anogenital cancers, and is less well understood for HPV+ HNSCC[177]. Exacerbating the problem further is that all patients risk developing lasting functional and/or cosmetic complications as a result of receiving standard care, and that up to 20% of patients will fail to respond to treatment and develop a more severe disease (i.e., treatment resistance or metastasis)[178-181]. These issues highlight that HPV+ HNSCC encompasses a diverse spectrum of pathologies[182,183], although current treatments for head and neck cancer are still not greatly diversified.

The standard of care for all locally advanced head and neck cancer is based on estimating stage and then risk for disease severity and recurrence, and is subsequently addressed by single or combined use of minimally invasive surgical resection, adjuvant radiotherapy, and chemotherapies (e.g., cisplatin)[184]. Nuances to staging and treatments are guided mostly by the anatomical location, associated comorbidities, development of resistance and recurrence, and as of the publishing of the 8th edition of the American Joint Committee on Cancer staging guidelines, HPV(+/-) status[185]. The changes in treatment guidelines toward HPV positivity were related, in part, to the more favorable prognosis of most HPV+ HNSCC[1]. For example, early ipsilateral node involvement is more common

with HPV+HNSCC (than HPV-negative), and it is often detected prior to the primary lesion[186]. This is mechanistically related to the absence of connective tissue beneath the oral tonsils and “leakage” of tumor cells, but it does not necessarily equate with tumor invasiveness or with increased prognostic value[187].

HPV+ HNSCC, when juxtaposed to HPV-negative disease, has >80% vs >50% overall survival, respectively[188,189]. Although, irrespective of type, all head and neck cancers still receive essentially the same modalities of treatment[190]. Differing outcomes may relate to the average age of diagnosis, relative lifestyle, physical fitness of individuals, and underlying molecular mechanisms. HPV-negative patients typically exhibit advanced age, a history of alcohol and tobacco use, and correlate with the accrual of mutations in tumor cells, making it more difficult for the immune system to overcome[177,188,191]. HPV+ HNSCC tends to have a more inflamed tumor microenvironment, higher rates of lymphocyte infiltration. Data from Solomon et al. indicate that increased CD8+ T cell infiltration correlates with a positive prognosis[139,192]. Irrespective of these trends, it still leaves ~15% of HPV+ HNSCC patients with limited treatment options and increased risk of advanced disease[189,193-195].

Newer strategies to combat treatment resistant or recurrent HNSCC utilize immunotherapies, including immune checkpoint inhibitors (ICI) (e.g., anti-PD-1/ anti-PDL-1). Over the past two decades, several clinical trials have reported on the use of checkpoint blockade in recurrent or metastatic HNSCC patients. The CheckMate 141 phase III study with Nivolumab (PD-1 antibody) treatment showed a better response than control in recurrent HNSCC patients, with an increased median overall survival of 2.4 months[196]. Another phase III study, KEYNOTE-040, showed that Pembrolizumab (PD-1 antibody) performed better (8.4 vs 6.9 months median overall survival) than other single

agent drugs (control) and was able to prolong overall survival[197]. More recently, KEYNOTE-048 phase-III compared the use of pembrolizumab, pembrolizumab plus platinum-5-fluorouracil, or cetuximab (EGFR inhibitor) plus platinum-5-fluorouracil in recurrent or metastatic HNSCC patients[198]. It was concluded that pembrolizumab alone is an effective first-line option for PD-L1+ patients, and that the addition of platinum-5-fluorouracil would be effective as a general first-line treatment for recurrent or metastatic HNSCC.[198]. Unfortunately, data still suggests fewer than 10-20% of patients who receive ICI therapy will respond to the treatment, and for those that do, the response may be limited[199].

At present, it is still not completely understood why ICI therapies work in some patients, but fail in others. However, it is reasonable to postulate that in some patients, the success of ICI therapy depends on the antitumor activity of CD8+ T cells, stimulated by their activation through MHC-I expression on tumors. Therefore, any impediment to MHC-I expression on cancer cells would ultimately nullify the efficacy of certain ICI therapies. Decreased MHC-I expression certainly will not explain all ICI failure, but in tumors with decreased MHC-I, those patients may benefit from strategies geared to increase MHC-I and subsequent CD8+ T cell response.

A substantial effort has been made to understand the mechanisms of downregulation of MHC-I in HNSCC[200]. Notably, the use of an Enhancer of Zeste Homolog 2 (EZH2) inhibitor, GSK126, can effectively increase MHC-I expression and the efficacy of ICI treatment in models of HPV-negative HNSCC[201]. This study parallels the work of Burr et al., who revealed an evolutionarily conserved cancer mechanism of MHC-I inhibition mediated by the histone methyltransferase activity of PRC2[160]. This evidence suggests the potential for combination therapies that include EZH2 inhibitors to augment

standard therapy for some HNSCC patients. Albeit conclusive evidence for this same mechanism in HPV+ HNSCC has yet to be elucidated.

Other novel strategies may also be effective in combination with the administration of standard radiotherapy. With the application of ionizing radiation, dsDNA breaks are introduced, and cancer cells can resist the therapy by increasing DNA repair through non-homologous end joining (NHEJ)[202-204]. The naturally occurring histone acetyltransferase inhibitor, Garcinol, can increase the radiosensitization of tumor cells by blocking NHEJ, limiting DNA repair, and impeding the ability of cancer cells to respond to DNA damage[202,205,206]. Garcinol can also promote antitumor immunity by suppressing STAT3 inflammation in HNSCC, in addition to other antitumor effects[207]. Hence, the incorporation of drugs like garcinol, or those which act similarly (i.e., histone acetyltransferase inhibitors), may have potential for use in combination therapies for HPV+ HNSCC treatment.

Additional innovative directions for the treatment HPV+ tumors involve the use of therapeutic vaccines and transgene therapy[208-210]. In the MASTERKEY-232 clinical trial, Talimogene laherparepvec (T-VEC), an oncolytic immunotherapy approved for advanced melanoma, was used in combination with Pembrolizumab to treat HNSCC patients[211]. Although the combination was safe for patients, there was no significant improvement over pembrolizumab alone[211]. However, other viral transgene studies have offered some interesting preclinical results. For instance, Peng et al., incorporated the expression of a high-risk HPV E6 and E7 epitope vaccine, in combination with anti-PD-1 antibodies, and were able to effectively decrease tumor growth and increase the survival *in vivo*[212]. Oncolytic vectors loaded with interleukin -7 and -12 also showed effective tumor regression and increased systemic effectiveness of immune checkpoint blockade[213].

Despite the neutral response by T-VEC in HNSCC patients, these newer strategies with HPV epitope vaccines and cytokines offer new hope for future development.

1.7 Epigenetic Gene Regulation and Implications in Cancer

Epigenetics can be defined simply as changes in gene expression without an accompanying change in the underlying DNA sequence[214]. This concept can be extrapolated to a cell's entire genome, encompassing its 'epigenetic landscape,' a concept first introduced by Conrad Waddington in 1957[214]. Epigenetic signatures are heritable, guide cell differentiation, maintain cell identity, and their disruption can lead to cell transformation and cancer progression[215-217].

The normal consequences of epigenetic regulation are evident by the differences in gene expression across the different cell types of a given organism. That is, because all cells in a given organism have fundamentally identical genotype, but are not all phenotypically the same, epigenetic regulation can account for these differences[218]. Epigenetic changes include DNA methylation, post-translational modifications to chromatin, and effects by some non-coding RNAs.

Mammalian DNA methylation refers to the covalent (but reversible) linkage of methyl (-CH3) groups to cytosine (5-methylcytosine), positioned 5-prime to guanosine, and exhibiting a phosphodiester bond between them (CpG)[218]. Hypermethylation of regions in gene promoters with GC-rich stretches, called CpG "islands" (CGI), can significantly repress gene transcription by limiting access of the transcriptional machinery[219]. DNA methyltransferase enzymes are responsible for establishing the pattern of DNA methylation, and their dysregulation can have profound effects on global transcription[220].

As mentioned above, DNA methylation is highly dysregulated by the E7 oncogene in HPV+ HNSCC[38], with high risk HPV16 E7 binding to DNA methyltransferase 1 (DNMT1) and upregulating its activity[39,221]. HPV16 E6 also upregulates DNMT1 indirectly by inhibition of p53[222], and HPV+ tumor cells exhibit higher levels of DNMT3a expression and higher rates of DNA methylation at PRC2 (histone methylator) regulated genes when compared to HPV-negative tumors[223] Notably, Holland et al., indicated that the catalytic core of PRC2, EZH2, was transcriptionally activated by E7 mediated release of E2Fs[224].

The abolishment of DNA methylation with DNMT inhibitor (DNMTi) (i.e., decitabine) treatment has been successful in the restoration genes important for antitumor immunity in HPV+ cancer cells[126]. DNMTi treatment has also been effective at treating some blood cancers[225,226], and bodes well for use in solid tumors[227,228]. However, despite what is known in HPV+ cancer cells regarding the dysregulation of global DNA methylation[183,229,230], a thorough enough rationale to warrant the application of DNMTi treatment in HPV+HNSCC is currently unavailable, and many mechanistic questions are unanswered. For instance, DNMT1 is known to be responsible for maintaining DNA methylation patterns during replication, however, DNMT3a and 3b are recognized as necessary for any *de novo* DNA methylation[218]. Although, how HPV interacts in concert with DNMTs to facilitate the methylation of DNA, how targets are determined, the breadth of effect on cancer related gene expression, and potential other regulators and intermediates are unknown.

As part of the regulation of DNA, within the nucleus, the DNA strand is wound about histone protein octamers, forming nucleosomes, and packed nucleosomes comprise chromatin. Histones (specifically histone tail domains) are modified by many post-translation modifications[231]. The overall breadth of modifications, which can be

interpreted by cellular proteins resulting in changes (e.g., altered gene expression), encompasses the “histone code”[232].

Although they are not mutually exclusive, the methylation of histone protein tails contributes to the formation of compacted chromatin (i.e., heterochromatin) limiting gene transcription, and acetylation forms open chromatin (i.e., euchromatin) permitting transcription[217,233]. There is also new evidence suggesting that euchromatin is not “open” per se, but instead possess condensed, “liquid-like,” domains that affect accessibility and the potential for transcription[234]. Regardless, it does still hold that euchromatic states have a greater abundance of histone acetylation marks than do heterochromatin[234].

Two histone methylation sites well-known to control gene expression include H3K27 and H3K4. Genes with “bivalent” promoters have both H3K27me3 and H3K4me3, and are toggled “on and off” through these marks[235]. PRC2 mediates H3K27 methylation and is considered a transcriptionally repressive mark, whereas H3K4me3 (mediated by trithorax genes) is an activating mark which resists PRC2 and readies genes for transcription[236,237]. Conclusively, the balance in activity between polycomb repressor genes, trithorax genes, and their respective marks, is thought to dictate the level of gene expression at these sites[238,239]. Promoter bivalency is connected to maintaining pluripotency during embryonic development and controls tissue specific gene expression[236]. PRC2 is normally active during embryonic stem cell development and regulates the homeobox (HOX) family of genes[240]. Interestingly, PRC2 target genes tend to overlap with OCT4, SOX2, and NANOG transcription factors, known for their influence on stem cell formation[241-243]. PRC2 is also active in some adult stem cells (e.g., muscle cells) managing their differentiation[244]. Dysregulation of PRC2 is associated with the progression of many cancer types[245] and has been linked to cancer immune

evasion[160,246]. In patients with oral leukoplakia which may progress to head and neck cancer, EZH2 expression was associated with malignant phenotypes and could predict oral cancer development[247]. Mechanistically, PRC2 members can interact directly with oncogenes like MYC[248,249], and MYC is able to upregulate all core PRC2 genes[250,251].

PRC2 is responsible for all H3K27 methylation[252]. The core PRC2 genes are *EZH2* (or *EZH1*), Embryonic Ectoderm Development (*EED*), and Suppressor of Zeste 12 (*SUZ12*). EZH2 is a methyltransferase and primary catalytic subunit of the complex, however, it requires EED and SUZ12 to efficiently methylate targets and to avoid autoinhibition (i.e., all three genes are required for methylation to propagate)[253,254]. EED recognizes an initial H3K27me3 mark and facilitates an increase in PRC2 activity by allosteric activation[255,256]. SUZ12 is required for site targeting and chromatin binding[252,257,258].

Coordinated action between PRC2 and DNMTs may lead to gene specific silencing[259]. In mammals, PRC2 is recruited to specific genes, often those with hypomethylated CGI promoter regions, and mediates H3K27me3[260,261]. This may act as a recruitment signal for DNMTs, who then facilitate de novo methylation of target CGIs to silence a target gene[259,262-264]. This process may be required during development to ensure the long-term silencing of genes that are not required for a given cell's differentiation pattern. However, this mechanism may be incomplete, context dependent, and is in some sense controversial[258,265]. Deviating from the sequential mechanism, another PRC2 accessory subunit, AEBP2, can bind to methylated DNA[266], and H3K27me3 can coexist with DNA methylation[258]. Other models indicate that H3K27me3 and H3K4me3 at bivalent promoters resist DNMTs and DNA methylation[267].

Many contemporary studies have focused on specifically understanding PRC2 specific targeting and its facilitation of H3K27me3[254,268,269]. Importantly, Højfeldt et al. revealed that with complete abrogation of H3K27me3 and PRC2 knockout, rescued expression of PRC2 shows that SUZ12 directs the complex to reestablish H3K27 methylation patterns, de novo, consistent with the original H3K27 methylation patterns[252].

The exact chain of events behind polycomb group regulation of chromatin and gene expression is highly complex, involving canonical and non-canonical modes of activation, a multitude of modular protein subunits, and a range of contextual factors which has made articulating full processes challenging[270,271]. Concisely, PRC1 complexes catalyze H2AK119ub1 and PRC2 catalyzes H3K27me3; the activity of PRC1/2 is often localized, cooperative, and results in maintenance of gene silencing[245]. However, Fursova et al. showed that canonical PRC1 complexes are not required for gene repression, but variant PCGF1-PRC1 mediated ubiquitination (H2AK119ub1) was essential for H3K27me3 establishment and gene repression[272]. Sparbier et al. found that PCGF1 and the PRC2 accessory subunit MTF2 had specific roles in maintaining bivalency and ultimately repression of MHC-I molecules[246]. The core members of PRC2 with the MTF2 subunit in complex (PRC2.1), facilitates recruitment to unmethylated CGIs[273-275]. Perino et al. also suggested that PRC2.1-MTF2 binds to DNA more readily than PRC2.2 with the alternative JARID2 subunit, and is less dependent upon prior PRC1 activity[276]. Petracovici et al. used an inducible protein degradation system with PRC2.1 depleting MTF2 or PRC2.2 depleting JARID2, and showed that the PRC2.1/2 subtypes have separate target genes[277]. MTF2 target genes had CpG sites in their promoters and were marked with high amounts H3K27me3, and JARID2 target genes were pre-marked with H2AK119 ubiquitination and were downregulated as cells became more

differentiated[277]. **Figure 1** below illustrates the relationship of DNA methylation to relative to transcription and a simplified polycomb group interaction at a bivalent promoter.

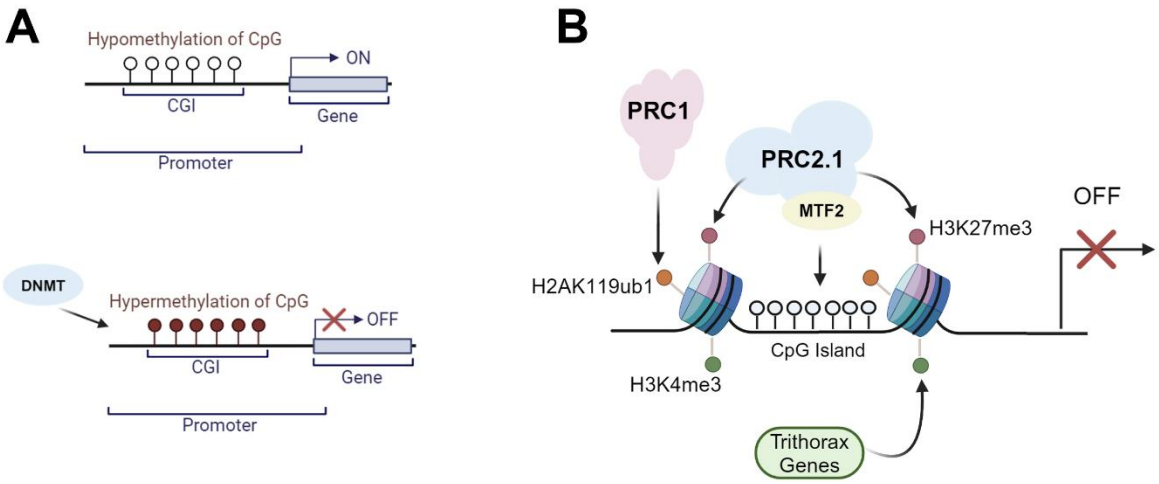

Figure 1. **Epigenetic Regulation of Transcription by DNA methylation or Posttranslational Modification of Histones**. **A**) CGI methylation state relative to transcriptional activation of promoters. **B**) Simplified diagram of the interactions of PRC1, PRC2.1, and trithorax genes and at a bivalent promoter region. Diagram adapted from the following sources: MTF2-PRC2.1 binds hypomethylated CGI and PRC2 facilitates methylation at H3K27[275]. PRC1 mediates ubiquitination at H2AK119. Trithorax genes contribute to H3K4me3 deposition[246,272]. PRC1/2 maintain gene repression[272]. Illustrations created with BioRender.com.

The third important element of epigenetic control beyond DNA methylation and Histone modifications is by non-coding RNA interactions. There is still much to understand in regard to these interactions, but they are known to have far-reaching implications on epigenetic regulation, gene expression, and cancer[215,218]. In non-small cell lung cancer (NSCLC), some micro-RNAs (miRNAs) can bind to DNMTs, preventing aberrant DNA methylation, and upregulate tumor suppressor genes[278]. Conversely, DNMT downregulation of miRNAs induced by SOX2 and Oct4, upregulates glioblastoma cell stem-like properties and tumor formation[279]. In triple-negative breast cancer, MYC facilitates DNMT3A silencing of miR-200b transcription, permitting cancer progression by

de-repressing SOX2[280]. MYC inhibition of miR-26a tumor suppressor, mediated through the recruitment of EZH2, was associated with lymphoma aggressiveness[281]. Interestingly, application of EZH2 inhibitor (DZNEP) and BET bromodomain inhibitor (JQ1) inhibited MYC and restored miR-26a expression[281].

Another class of RNAs involved in epigenetic regulation and cancer are the PIWI-interacting RNAs (piRNAs)[282]. They associate with Argonaute family members and can regulate transposons and gene expression[283]. In HPV+ HNSCC, specific piRNA expression signatures were distinctly associated with HPV16 and 18 driven cancer, and piRNA expression was used to predict overall patient survival[284].

The binding of RNA signals can also directly regulate the activity of PRC2[285,286]. For example, Kaneko et al. found that PRC2-interacting nascent RNA inhibits H3K27me3 activity[287], and Friedman et al. showed that miR-101 directly represses EZH2 in bladder transitional cell carcinoma[288]. Notably, the long non-coding RNA (lncRNA) Homeobox transcript antisense intergenic RNA (HOTAIR) can function as a scaffold to facilitate the aggregation of PRC2 and subsequent H3K27me3 at target genes[289,290]. Beyond PRC2, HOTAIR has been implicated in cancer progression and chemotherapy resistance mechanisms[289]. In NSCLC, the silencing of HOTAIR inhibited activation of cellular autophagy by blocking ULK1 phosphorylation, and decreased drug resistance in the cancer cells[291]. In HPV-16 cervical cancer cells, HOTAIR is upregulated, and its knockdown decreased cell proliferation and increased apoptosis, likely limiting its ability to sequester miR-214-3p[292]. Given their connections toward the promotion of other cancers, HOTAIR guided PRC2 may also drive cancer progression in head and neck cancer and may be a valuable axis to investigate as novel targets for patient treatment[293].

1.8 KAT2A and the SAGA Complex

The lysine transferase 2A (KAT2A), also known as general control non-repressible 5 (GCN5), plays a prominent role in the acetylation of histone tails and activation of gene transcription. KAT2A, or its paralog, KAT2B aka p300/CBP-associated factor(PCAF), can serve as the main acetyltransferase enzyme in two transcriptional co-activator complexes, SAGA and Ada-2-A containing (ATAC)[294]. Generally, transcriptional coactivators bind to transcription factors, and can potentiate transcription through the modification of chromatin and histones[295]. For example, SAGA binds to the transcription factor MYC through its TRRAP (Transformation/Transcription domain Associated Protein) subunit[296]. SAGA's histone acetyltransferase (HAT) domain then facilitates the acetylation of lysine residues on histone tails via KAT2A's "writer" function, permitting accessibility by RNA-polymerase II and the recruitment of accompanying transcriptional machinery on the chromatin at target genes[297-299].

Both SAGA and ATAC are multidomain protein complexes with a vast array of differential functions[294,300]. The SAGA complex is found both inside the nucleus and in the cytoplasm, whereas ATAC is thought to be exclusively nuclear[300]. Both complexes have a HAT module comprised of KAT2A/B, SGF29, TADA3, and TADA2A (found in ATAC) or TADA2B (found in SAGA)[301], with histone acetylation taking place primarily at H3K9 or H3K14 sites, among others[302-305]. Within the HAT domain, the Sgf29 subunit is required for chromatin targeting and histone "reading" at H3K4me3 sites through its tandem tudor domain[306-308]. KAT2A can also "read" acetylated histone residues through its bromodomain and allows anchoring to nucleosomes[309,310]. ATAC has two main structural regions, the HAT domain, and a core region comprised of six additional subunits (YEATS2, NC2β, ZZZ3, WDR5, MBIP, and CSRP2BP)[311]. The structure of SAGA has

been solved[299], and is comprised of 18-20 subunits with five functional modules: HAT, deubiquitinase (DUB), activator binding, splicing, and core[311]. DUB activity is mediated in large part by USP22[312,313]. The transcription factor/activator-interacting module connects TRRAP, and the core module includes the TATA binding protein (TBP)-associated factor (TAFs)[300,314-316]. **Figure 2** below illustrates the SAGA complex, the respective members, and summarizes some of the major functions of its different modules.

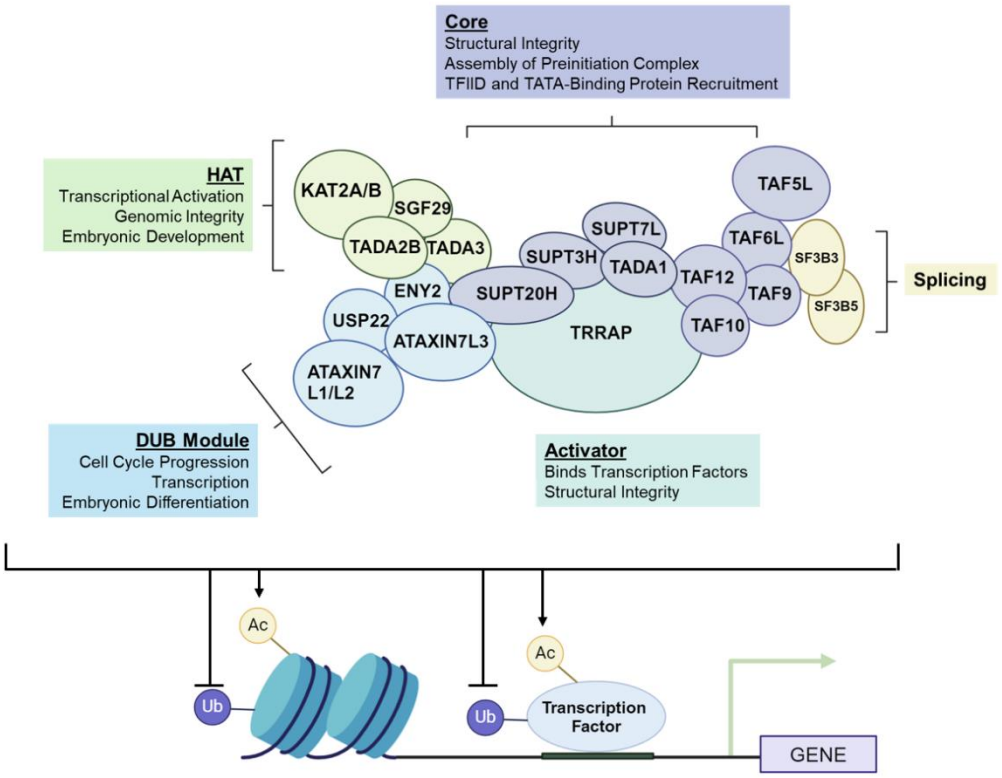

Figure 2. SAGA Structure and Function. The various subunits of SAGA make up its multi-modular (HAT, DUB, Core, Activator, and Splicing) structure and influence variety functions important to transcription and cellular phenotype. SAGA can acetylate and deubiquitinate histone tails and non-histone substrates, which both affect gene transcription. Respective colors make up the different domains as labeled. This figure was adapted from several sources[297,299,300,317]. Illustrations created with BioRender.com.

KAT2A and the SAGA complex are frequently dysregulated in cancer, and they may promote cancer progression through multiple mechanisms[318,319]. First, SAGA and

KAT2A are central players in the activation of the proto-oncogene MYC driven transcription[296,320-324]. It was originally demonstrated by McMahon et al. that TRRAP binds to MYC or E2F1 and is crucial for their transcription[314], and they later showed that KAT2A was recruited via TRRAP to c-MYC for its acetyltransferase activity[296,320]. The relationship of KAT2A in MYC and E2F1 dysregulation in cancer is evident in many studies. For example, Malone et al. demonstrated that specifically the KAT module of SAGA is responsible for oncogenic progression in N-MYC driven neuroblastoma[56], Han et al. found that KAT2A/E2F1 promotes colon cancer and metastasis[325], and Mustachio et al. showed that blocking KAT2A represses c-MYC expression in NSCLC[326]. More recently, Chen et al. showed that SAGA is required for MYC promoted oncogenic transcription in multiple myeloma[327].

The indictment of KAT2A/B in cancer is furthered by KAT2A's ability to directly acetylate non-histone substrates in the cytoplasm[328]. KAT2A acetylates MYC *in vivo*[322], and in cervical cancer cells, KAT2A also stabilizes MYC by direct acetylation[329]. KAT2B promotes lung adenocarcinoma by stabilizing EZH2 through direct acetylation[330], and similarly, E2F1[331]. KAT2A can also act both as a transcriptional activator and a repressor of NFkB[332]. In addition to acetylation, KAT2A can succinylate protein substrates, and in gastric cancer, succinylation of pyruvate kinase M2 (PKM2) decreases its activity resulting in increased aerobic glycolysis and the "Warburg Effect"[333]. Similarly, USP22 can have direct effects on MYC to promote its stability through its DUB activity[318], and is required for its transcription[334]. USP22 by itself can mediate immune evasion and drug resistance mechanisms in cancer[335].

KAT2A and SAGA activity is important for stem cell development, maintenance, and self-renewal[336]. Yamauchi et al. found that KAT2A is necessary for normal embryonic

development[337]. Deletion of KAT2A resulted in embryonic lethality in mice, and with KAT2A deletion in embryonic stem cells, cells exhibited an abnormal phenotype that coincided with the loss of OCT4 and Nodal, indicating a loss of pluripotency[338]. KAT2A has also been implicated in pluripotent reprogramming in association with MYC[297,339,340]. In keratinocytes, KAT2A supports an undifferentiated state and maintains self-renewal by mediating global H3K9Ac[341]. Additionally, SAGA members TAF5L and TAF6L can maintain embryonic self-renewal through MYC[342].

KAT2A may help drive cancer progression by inducing the formation of cancer stem cells. A pRb-RBL2-E2F1/4-KAT2A axis regulates cancer stem cell formation in prostate and breast cancer, and it is driven by KAT2A mediated WNT signaling[343]. Additionally, in genome-wide screens to detect regulators of pluripotent stem cell reprogramming, KAT2A, along with several other SAGA complex and PRC1.3 members, were “top hits” from the screen[344]. In acute myeloid leukemia, KAT2A propagates leukemia stem cells by buffering transcriptional “noise” to maintain self-renewal[345]. In other words, transcriptional noise is reduced by KAT2A, and pluripotency is retained by limiting variability in transcriptional programs[346].

1.9 Dissertation Overview

Immune evasion is an important hallmark of cancer and encompasses the strategies utilized by cancer cells to avoid recognition and elimination by the body’s immune system. Human Papilloma Virus is linked to the progression of most head and neck cancer, with a significant number of patients experiencing relapse, metastasis, and treatment failure (i.e., cancer immune evasion)[1,8]. Thus, it is imperative to identify and interdict the mechanisms of immune evasion propagated by HPV to increase therapeutic efficacy and to ultimately improve patient outcomes. The overarching goal of this

dissertation was to elucidate the pathways governing immune evasion in human papillomavirus-positive head and neck squamous cell carcinoma (HPV+ HNSCC).

A common strategy of viral immune evasion mechanisms is to inhibit the expression of the MHC-I molecules and antigen presentation pathways[141,347]. These pathways are critical to the activation of cytotoxic CD8+ T cells, whose response is needed to eliminate virally infected and/or cancer cells. Like other viruses, HPV can downregulate MHC-I by several different mechanisms[348]. For example, most of the class I heavy-chain genes required for MHC-I expression are transcriptionally downregulated in HPV+ keratinocytes by high-risk HPV oncoprotein E7[38]. That observation was partially explained by HPV mediated dysregulation of host epigenetic machinery and aberrant DNA promoter methylation of *HLA-E*, the non-classical MHC-I gene[38]. However, the complete mechanism(s) to explain the downregulation of other MHC-I genes are still not completely understood. Thus, we hypothesized that HPV downregulates MHC-I gene transcription by an uncharacterized epigenetic mechanism outside of promoter DNA hypermethylation.

In **Chapter two,** we explored this hypothesis by conducting a genome-wide genetic knock-out analysis to identify candidate genes that negatively regulate MHC-I expression in HPV+ HNSCC. Interestingly, the analysis identified several epigenetic regulator genes among the top hits. Those genes were subsequently validated as negative MHC-I regulators by additional genetic knockout, pharmacologic, and *in silico* studies, and we conclude that MHC-I transcription is downregulated through epigenetic dysregulation.

An interesting observation made during our investigation (described in chapter two), was that the neuronal MYC (N-MYC) proto-oncogene was upregulated in our HPV+

HNSCC cell lines, and it was identified as a negative regulator of MHC-I by the genome-wide screens. We hypothesized that N-MYC is a driver of MHC-I downregulation in HPV+HNSCC. In **Chapter three,** we validated our hypothesis by pharmacologic induced degradation of N-MYC to show subsequently increased MHC-I expression. Interestingly, the impact of N-MYC abrogation also extended to decreased expression of the E3 ubiquitin ligase Membrane-associated RING-CH protein 8 (MARCHF8), which we have previously verified can degrade several surface immune receptors[45]. We conclude that N-MYC is a critical node for MHC-I inhibition and control of antitumor immunity by HPV.

In addition to MHC-I, HPV also epigenetically downregulates the cellular chemokine, CXCL14, during cancer progression[126]. Restoration of CXC14 expression increases tumor infiltration of CD8+ T cells, MHC-I expression, and suppresses tumor cell growth[125]. We hypothesized that CXCL14 suppresses HPV+ HNSCC by upregulating antigen presentation on tumor cells and CD8+ T cell responses against tumors. However, the mechanism(s) by which CXCL14 elicits those responses is unknown. In **Chapter four**, we investigated the structure CXCL14 and its potential signaling pathways, with the hope of identifying the specific features of CXCL14 and cellular intermediates necessary for its antitumor activity. We also reviewed the viability of developing CXCL14 as an immunotherapy, and we described the construction of an adenoviral-based transgene platform to deliver CXCL14 into HPV+ HNSCC tumors. Overall, our results show that CXCL14 has robust antiviral activity, and our results provide new footholds and tools from which to investigate CXCL14 mediated antitumor mechanisms.

Chapter five provides a discussion of our results and suggestions for future research directions respective for each chapter. Finally, **Chapter six** details our experimental methodology. In summation, the work described in these chapters harvests

new insights from multiple experimental directions regarding the mechanisms underlying immune evasion in HPV+ HNSCC. In doing so, we hope that this work provides novel targets and directions for future investigations, along with the improved hope to one day end the scourge of HPV+ HNSCC.

CHAPTER 2

Genome-wide CRISPR/Cas9 screens reveal epigenetic immune evasion mechanisms in human papillomavirus-positive head and neck squamous cell carcinoma

Contributions to Science

The work in this chapter was conceptualized by Nicholas Giacobbi. The final figures for this chapter were generated by Nicholas Giacobbi. The experiments in this chapter were performed by Nicholas Giacobbi with contributions from others listed below, respectively. The preparation, analysis, and validation of the CRISPR/Cas9 screens in this work were a collaborative effort involving Dr. Andrew Olive, Dr. Dohun Pyeon, Dr. Mohamed Khalil, Nicholas Giacobbi, Lexi Vu, and Conchai Yang. *In silico* analyses were performed by Nicholas Giacobbi with contributions from Lexi Vu. Quantitative PCR reactions were performed by Nicholas Giacobbi with contributions by Shreya Mullapudi, Lexi Vu, and Evelyn Gomez. Western blots were performed by Nicholas Giacobbi with contributions by Conchai Yang, and Will Eckerman. Flow cytometry experiments were performed by Nicholas Giacobbi with contributions from Dr. Mohamed Khalil. The CUT&RUN experiment was a collaboration between Nicholas Giacobbi and John Vusich. John Vusich was crucial for experimental design, technical handling, optimization, and data analysis/interpretation.

2.1 Abstract

Human papillomavirus-positive head and neck squamous cell carcinoma (HPV+ HNSCC) cells frequently exhibit low expression of MHC-I molecules for antigen presentation which can contribute to cancer immune evasion. To identify negative regulators of MHC-I expression, we performed genome-wide CRISPR/Cas9 screens in HPV+ HNSCC cell lines. The top negative regulators of MHC-I expression include core members of the polycomb repressive complex 2 (PRC2). PRC2 is known to repress MHC-I-related gene expression via histone methylation (H3K27me3) as part of an evolutionarily conserved developmental mechanism. We found increased expression of PRC2 and H3K27me3 levels in HPV+ HNSCC cells. Interestingly, our pathway analysis identified the Spt-Ada-Gcn5 acetyltransferase (SAGA) complex as the top gene network responsible for the downregulation of MHC-I expression. The SAGA complex, via the histone lysine acetyltransferase (KAT2A), is a transcriptional coactivator for E2F and MYC targeted transcription, whose activity is highly upregulated in HPV+ HNSCC cells. We show that KAT2A and SAGA complex expression is upregulated in HPV+ HNSCC, and that inhibition of PRC2, KAT2A, or other SAGA complex members resulted in increased MHC-I expression. These results suggest that elevated KAT2A/SAGA potentiates E2F- and MYC-mediated transcription of PRC2 genes, contributing to the downregulation of MHC-I. Thus, manipulation of the KAT2A/SAGA:E2F/MYC:PRC2 axis may be a novel pathway to increase antitumor immunity by restoring MHC-I expression in HPV+ HNSCC.

2.1 Introduction

Human papillomaviruses-positive head and neck squamous cell carcinoma (HPV+ HNSCC) accounts for nearly all oropharyngeal cancers[8]. Despite a relatively good prognosis for HPV+ HNSCC patients following standard chemoradiation therapy, about ~15% of patients will lack a treatment response or experience cancer relapse[189,193,194]. New immunotherapies using immune checkpoint inhibitors (ICIs) also show very limited success, further necessitating the development of novel therapeutic strategies to treat patients. Diminished or lack of treatment response is frequently associated with the nullification of antitumor immunity, and thus, better understanding of cancer immune evasion will provide new targets to overcome treatment failure.

A key factor for the stimulation of antitumor immunity is MHC-I antigen presentation, which when limited, can contribute to cancer immune evasion[200]. We have previously described that the relative expression of nearly all MHC-I alpha subunits is significantly downregulated by high-risk HPV[1]. HPV is known to have several mechanisms that inhibit the presentation of viral epitopes on MHC-I[348]. Notably, human leukocyte antigens (HLA), specifically HLA-B, -C, and -E, were transcriptionally downregulated in normal keratinocytes expressing the HPV oncoprotein E7 from high-risk subtypes[38]. The downregulation in HLA-E expression is mediated by increased CpG promoter (hyper)methylation, although a direct correlation with decreased HLA-B/C expression was not readily apparent. Others have observed that cutaneous HPV E7 recruits EZH2 to the promoter of toll-like receptor 9 (TLR9) and downregulates TLR9 expression through chromatin trimethylation at histone-3 lysine-27 (H3K27me3) in the TLR9 promoter region[75]. EZH2 is the catalytic core of PRC2, and it is responsible for

H3K27me3 of histone tails[268]. Importantly, HPV16 E7 dysregulation of E2F increases transcription of EZH2, as found by Holland et al., 2008[224].

A recent landmark study revealed that dysregulation of PRC2 downregulates the antigen presentation process and MHC-I transcription through increased H3K27me3, and is a conserved mechanism across cancers[160]. Likewise, in HPV-negative HNSCC, inhibition of PRC2 upregulates MHC-I expression and enhances ICI therapy responses[201]. Elevated levels of PRC2 are correlated with disease progression in many cancers[349-351], including HPV+ HNSCC[352,353]. However, the possibility of a PRC2 related mechanism contributing to MHC-I downregulation and immune evasion in HPV+ HNSCC has yet to be firmly established.

Beyond changes in chromatin methylation, aberrant histone acetylation has been increasingly implicated in cancer progression, enhancing the activity of oncogenic transcription factors[354]. Lysine acetyltransferase 2A (KAT2A), is a key component of the SAGA complex. KAT2A functions as a coactivator for MYC and E2F targeted transcription[296,314,320,355-358], both of which are highly activated in HPV+ cancer cells by the viral oncoproteins E6 and E7, respectively[21,42,359]. KAT2A is overexpressed in many cancers, and the transcription of KAT2A itself is also induced by E2F and MYC[329,360]. The KAT module of the SAGA complex was recently demonstrated to maintain the oncogenic gene expression program observed in N-MYC-driven neuroblastoma, further indicating that the dysregulation of SAGA and KAT activity can promote cancer progression[56]. To the best of our knowledge, in HPV+ HNSCC, KAT2A nor the SAGA complex has yet been implicated in cancer progression or mechanisms of immune evasion.

Here, we identify that dysregulation of the SAGA complex and PRC2 causes MHC-I downregulation in HPV+ HNSCC. Our results offer new insights into a common

evolutionary strategy of cancer immune evasion and provide potential targets for new immunotherapies in HPV+ HNSCC.

2.2 **Results**

CRISPR/Cas9 screens identify regulators of MHC-I in HPV+ HNSCC cells

To elucidate mechanisms of MHC-I expression in HPV+ HNSCC cells, we performed genome-wide CRISPR/Cas9 screens using the Brunello sgRNA library that contains over 75,000 sgRNAs targeting 19,114 genes in three HPV+ cell lines, SCC90 and SCC152 derived from patient tumors[361] and N/Tert-1_E6E7, immortalized human keratinocytes that overexpress HPV16 oncoproteins E6 and E7 (**Figure 3A**). Following transduction of the sgRNA library[362], we sorted for the top and bottom 5% of MHC-I expressing cells. From those cells, positive and negative regulator genes of MHC-I expression were enriched by sequencing sgRNAs in the sorted cells. Next, we utilized the Model-based Analysis of Genome-wide CRISPR/Cas9 Knockout (MAGeCK) to statistically rank each gene by negative-binomial distribution[363]. Significant positive (red) or negative (blue) regulators were categorized in each screen by exhibiting ≥ (+/-)2 LFC; p-value = (≤0.05). The volcano plot in **Figure 3B** visualizes the position of each gene from our SCC90 screen as negative regulators (blue), positive regulators (red), or non-significant (gray). In the plot, significant cutoffs are gated by the dashed lines. To begin validation of our screens, we examined known positive regulators of MHC-I, TAP1 and TAPBP[364]. In the HPV+ HNSCC cell lines, we performed individual sgRNA depletion experiments and evaluated surface MHC-I expression relative to scrambled controls by flow cytometry. We confirmed that with the knockout of the TAP1 or TAPBP genes, MHC-I surface expression significantly decreases (**Figure 4A & 4B**, respectively). **Figure 4C** shows the success of sgRNA production and CRISPR editing in the sgRNA treated cells

lines by tracking of indels[365]. Next, to identify common regulator genes across our screens, we normalized all genes in each of the three screens (Z-score), ranked them, and selected a cutoff of Z=(±)1.5 (i.e., negative regulators candidates are Z≤-1.5 and positive are Z≥1.5). We identified (12) common genes from top positive regulators and (15) common genes from the top negative regulators (**Figure 3C and 3D, respectively**). Reassuringly, the (12) positive regulators included TAP2 and TAPBP at the very top of positive regulators, both critically involved in MHC-I antigen presentation[366,367]. Interestingly, we found that (5) out of the (10) genes in the negative candidates were members of polycomb repressor complexes (PRC) (i.e., EZH2, EED, and PCGF1) or of the SAGA complex (i.e., KAT2A and TADA3). Both complexes are known chromatin modifiers, suggesting that epigenetic dysregulation may play a significant role in negative MHC-I regulation in HPV+ cells.

We next sought to identify pathways involving the candidate genes that negatively regulate MHC-I expression. Using the MAGeCK ranked list from our SCC90 cell screen, we analyzed protein-protein interactions using the STRING database[368]. STRING analyzes the ranked list to identify known network clusters and segregates them by the top end (most positive regulators of MHC-I) and bottom end (most negative MHC-I regulators). STRING revealed that the SAGA complex, composed of transcriptional coactivators and histone modifying proteins, was overwhelmingly the most significant network cluster responsible for negative regulation of MHC-I expression (NES = 1.74; FDR =1.14E-05) (**Figure 3E**). However, the only network cluster identified as positively regulating MHC-I was exclusively the “MHC class I peptide loading complex” (NES = 5.54; FDR = 1.14E-05). In **Figure 3F**, we show the SAGA complex genes from the SCC90 screen as its own volcano plot. Most SAGA complex genes were identified as significant

negative regulators of MHC-I expression in our screen. Specifically, KAT2A was the most significant gene and was identified in all three screens (**Figure 3B and 3D**). In addition to the SAGA complex, KAT2A is also known to be associated with the Ada-2-A containing (ATAC) complex which is also responsible for histone modification and histone acetyltransferase (HAT) activity[301]. However, beyond KAT2A, SGF29, and TADA3, which are overlapping members between SAGA and ATAC complexes, any genes that are exclusive to the ATAC complex were not identified as significant negative MHC-I regulators in any of the three cell line screens (**Figure 3G** shows SCC90 results for ATAC members). These results suggest that the role of KAT2A as a negative MHC-I regulator is mediated through SAGA complex-associated activity. Analysis also revealed that the core members of PRC2, EZH2, EED, and SUZ12 alongside the PRC2.1 subunit MTF2, were identified as significant negative MHC-I regulators. (**Figure 3H**)[160]. In contrast, other PRC2.2-associated genes (e.g., JARID2 or AEBP2) fell into the positive regulator category. This suggests a specific role for PRC2.1-MTF2 in the negative regulation of MHC-I expression relative to other subtypes.

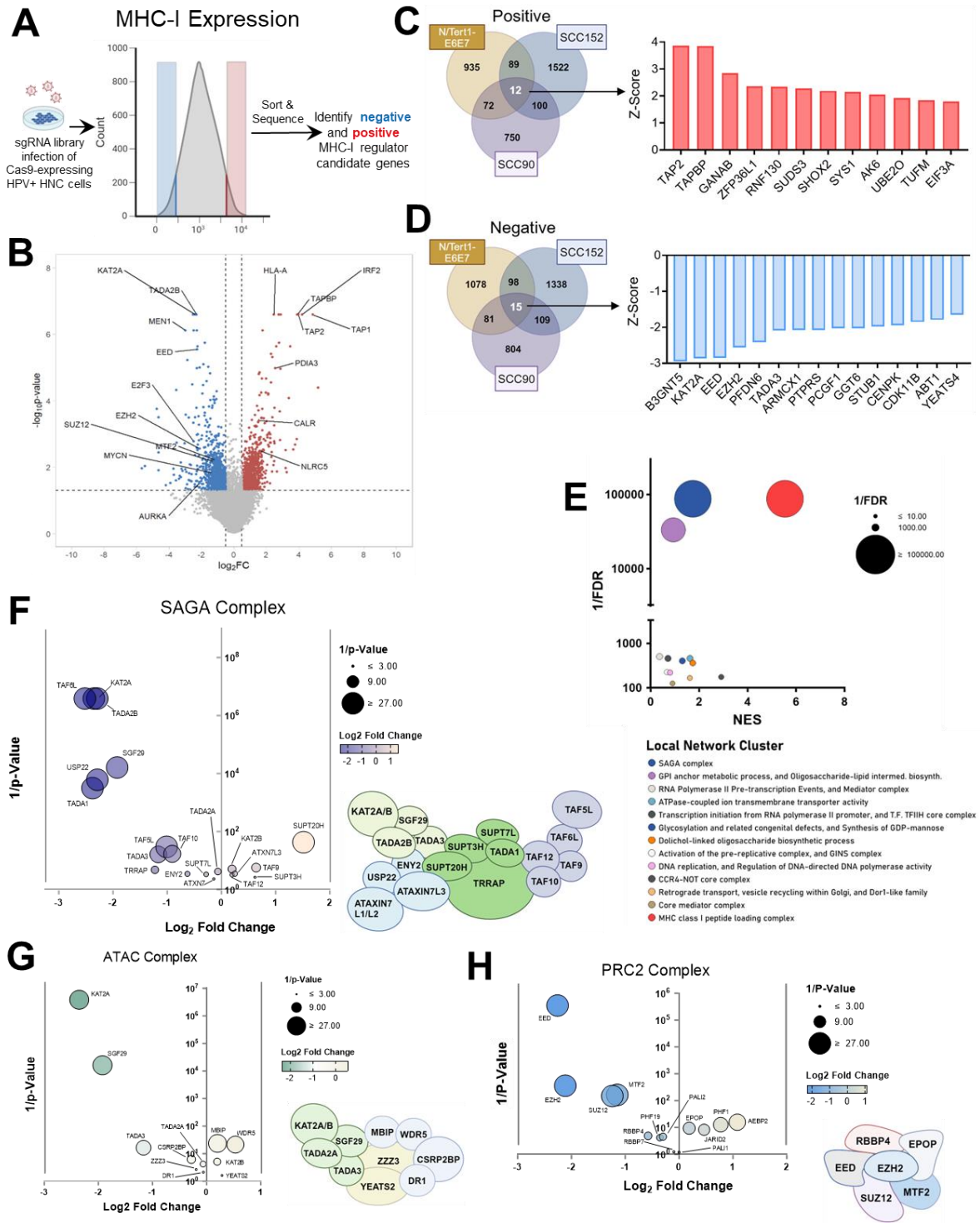

Figure 3. Genome-Wide CRISPR/Cas9 Screens Identify Positive and Negative Regulators of MHC-I Expression. **A)** Screen experimental schematic. Briefly, HPV+ cell lines expressing Cas9 were transduced with the Brunello sgRNA library via lentivirus. Cells were sorted by MHC-I expression via flowcytometry. Top/bottom 5% MHC-I

Figure 3. (Cont'd)
expressing cells were sequenced along with the input library by NGS. **B)** Volcano plot of SCC90 screen candidate genes based on log2 fold change (>1) and significant p-value (p≤0.05) as determined by the MAGeCK algorithm. **C and D)** Venn diagrams of top regulator (Z≤-1.5 ; Z≥1.5) candidate genes ranked by MAGeCK and normalized across screens (z-score=[(log2FC-mean FC) / SD of mean]). The top 15 common candidate positive or 12 negative regulator genes, and their respective z-score, are shown in the histograms. **E)** Local network cluster analysis hierarchy identified by STRING analysis (https://string-db.org/). The top panel depicts network clusters based on normalized enrichment score (NES) and respective false discovery rate (FDR) from MAGeCK ranked list. **F-H)** Volcano plots of SAGA, ATAC, and PRC2 family members, respectively. Significance is based on log2 fold change (>1), and significant p-value (p≤0.05) as determined by the MAGeCK algorithm from SCC90 ranked list. Diagrams of the respective complex genes are illustrated on the right of each plot. Illustrations created with BioRender.com.

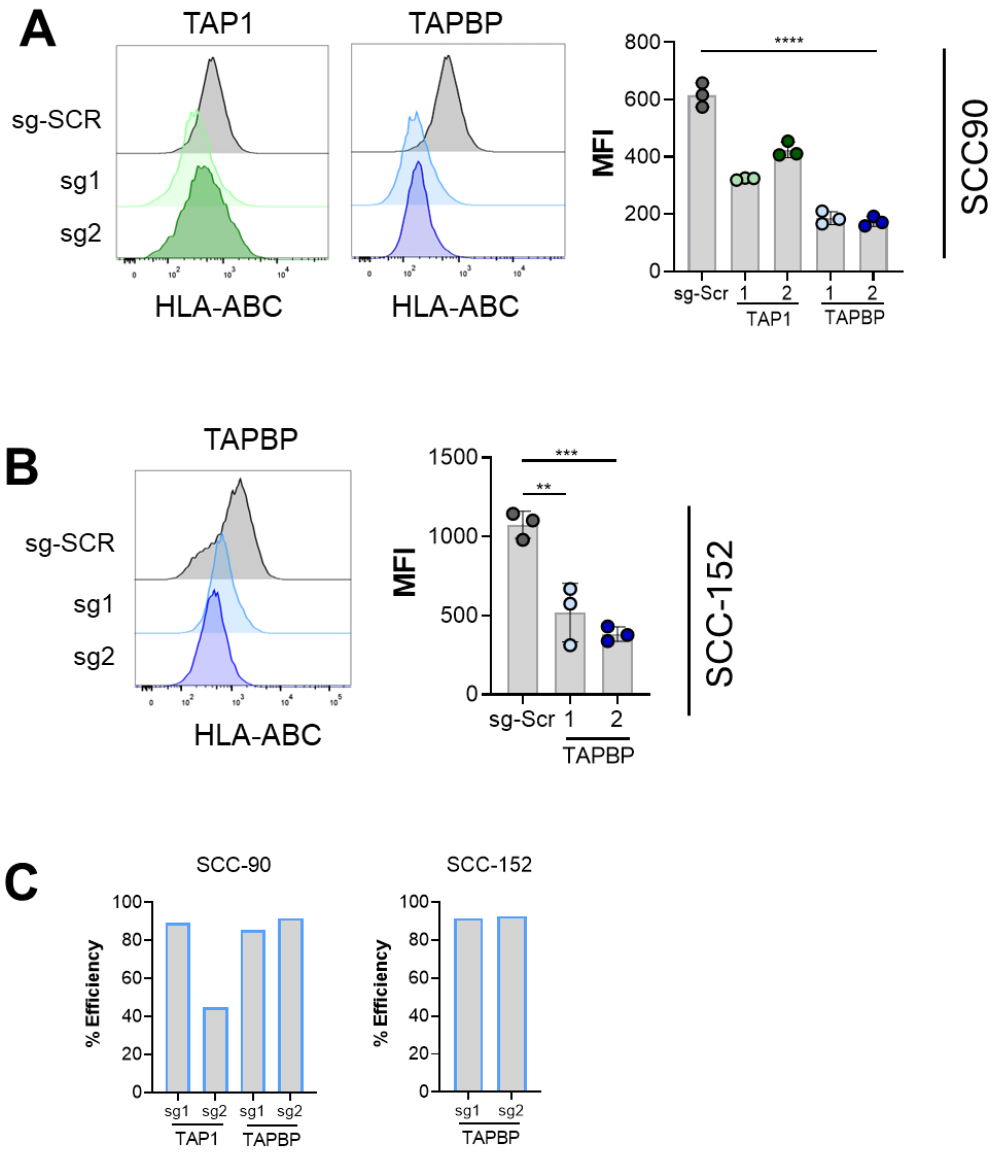

Figure 4. **CRISPR/Cas9 sg-RNA depletions of known positive MHC-I Regulators**. **A)** HLA-ABC surface expression following treatment with scramble sg-RNA control (sg-Scr) with either TAP1 or TAPBP sg-RNAs in the SCC90 cell line. **B**) TAPBP sg-RNA treatment in SCC152. Statistical significance was determined by One-way ANOVA comparing sg-Scr (control) to each sg-RNA treatment. ****p<0.0001, ***p<0.001, **p<0.01, *p<0.01. Error bars represent standard deviation of three independent experiments. (**C**) Tracking of Indels by Decomposition (TIDE) provides percent efficiency of CRISPR/Cas9 editing (https://tide.nki.nl/).

PRC2 and SAGA complex genes are upregulated in HNSCC

PRC2 components are known to be upregulated or have increased activity in many cancers[349,350,369]. There is also increasing evidence that histone acetyltransferases, like KAT2A, are dysregulated in cancer and potentially associated with cancer progression[325,354,370]. To determine if the epigenetic regulators identified in our study are dysregulated in HNSCC patients, we examined The Cancer Genome Atlas Program (TCGA) HNSCC datasets for the levels of PRC2 genes and KAT2A. In **Figures 5A and 5D**, we show that PRC2 members and KAT2A are significantly upregulated in patient TCGA-HNSCC samples (n=546), respectively[371,372]. We also gauged the relative expression of PRC2, KAT2A, and three additional SAGA complex members in exclusively (HPV+) HNSCC patient samples (n=97) versus normal individuals using Timer2.0 software (**Figure 6**)[373-375]. The choice of the SAGA members—KAT2A, USP22, TAF6L, and TADA1—in HPV+ HNSCC patients was based on their representation across the major SAGA domains by meeting significance criteria in the CRISPR screens (**Figure 3F**). Timer2.0 analysis revealed that all PRC2 and SAGA members are upregulated in the HPV+ HNSCC patients compared to normal samples (n=44) and relative to HPV- HNSCC patients (n=421)[373-375]. In three HPV+ cancer cell lines, we confirmed the upregulation of the PRC2 components, EZH2, EED, SUZ12, and MTF2 (**Figure 5B, C, and E**), and KAT2A (**Figure 5F**) by reverse transcription-quantitative PCR (RT-qPCR). In **Figure 7**, we detected that in N/Tert-1_E6E7 cells or in mouse oral epithelial cells over-expressing subtype HPV16 E6 and E7 (mEERL),that KAT2A and/or EZH2 was upregulated. Together, these data support the notion that the epigenetic modifiers found in our screens are upregulated in HPV+HNSCC or in cells expressing the HPV16 oncogenes E6 and E7.

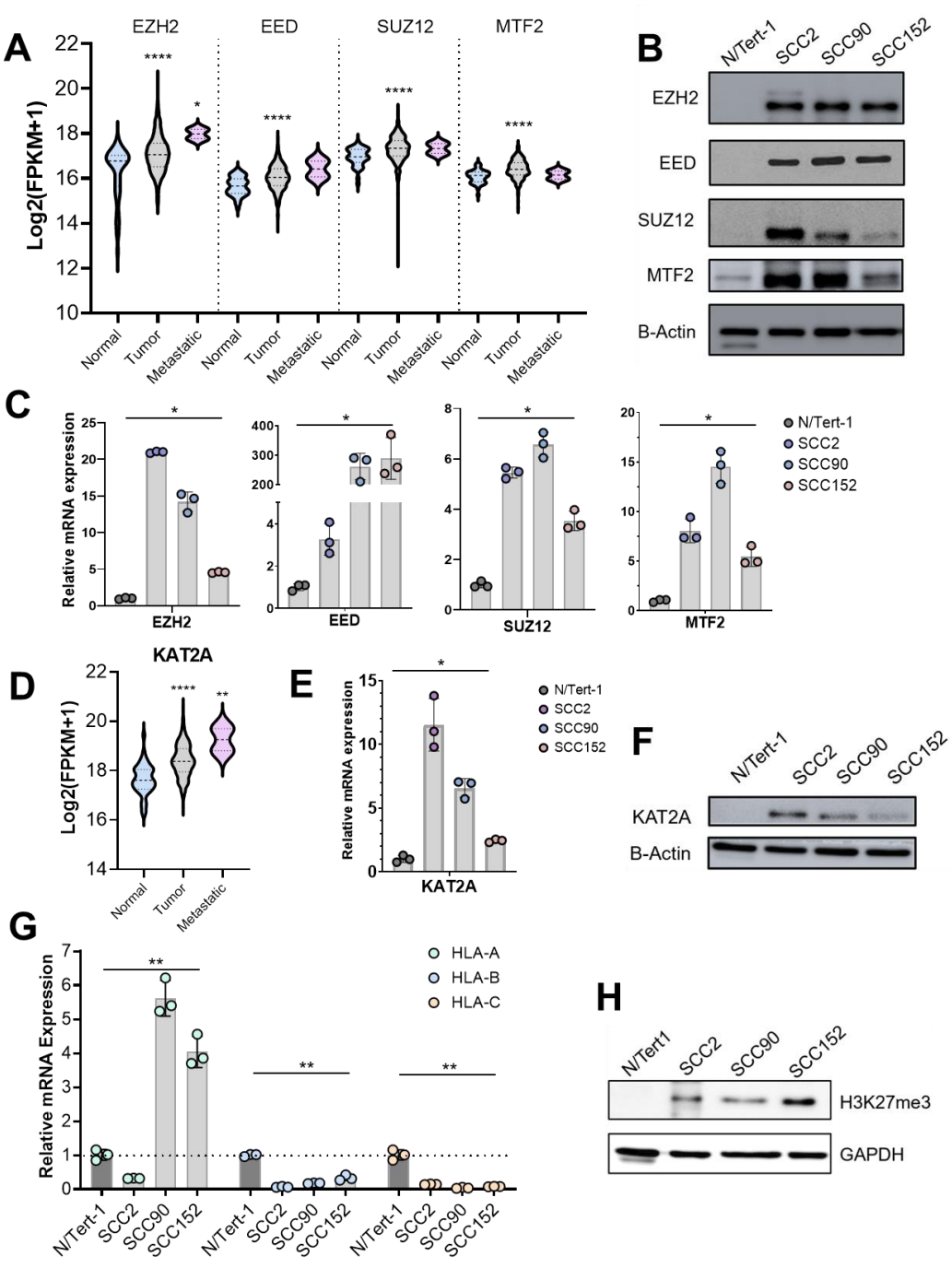

Figure 5. KAT2A and PRC2.1 Family Members are Upregulated in Head and Neck Cancer. **A)** GDC TCGA Head and Neck Cancer data (n=546) (acquired from UCSC [https://xenabrowser.net/]) for PRC2.1 complex genes EZH2, SUZ12, EED, and MTF2. Y-axis shows fragments per kilobase of transcript per million mapped reads, log2(FPKM+1). Statistical significance was determined by One-way ANOVA and Dunnett's multiple comparison test. **B)** Western blot analysis of whole cell lysate from HPV+ HNSCC tumor cell lines relative to N/TERT-1 keratinocyte control cells for total levels of core PRC2.1

Figure 5. (Cont'd)
complex genes. **C)** Quantitative PCR (RT-qPCR) for relative mRNA expression (ΔΔCT) normalized to GAPDH and compared to N/TERT-1 keratinocyte control cells. Significance p-values were calculated using an unpaired student's T-test comparing N/Tert-1 (control) relative to each SCC cell line individually. Each SCC line compared to N/TERT-1 met at least a significance threshold of *p<0.05, and is represented with the single asterisk for simplicity. **D**) GDC TCGA Head and Neck Cancer data (n=546) (acquired from UCSC [https://xenabrowser.net/]). Statistical significance was determined by One-way ANOVA and Dunnett's multiple comparison test. **E**) Quantitative PCR for relative mRNA expression (ΔΔCT) normalized to GAPDH control and compared to N/TERT1 keratinocyte control cells. Significant p-values were calculated using an unpaired student's T-test. **F**) Western blot analysis of whole cell lysates for KAT2A expression. **G**) Quantitative PCR (ΔΔCT) for HLA-A, B, and C normalized to B-actin control. The dotted line indicates the relative threshold value for each gene's expression in N/Tert-1 cells (approximating a value of 1). Significant p-values were calculated using Dunnett's multiple comparison test. Each comparison met at least a significant threshold of **p<0.01. **H**) Western blot analysis of whole cell lysates for global H3K27me levels. In qPCR experiments, error bars depict standard deviation (SD). For significance testing, ***p<0.0001, ***p<0.001, **p<0.01, *p<0.05. For all RT-qPCR data plots in this figure, three independent experiments were completed, each with three technical repeats per condition. The triplicated experiments demonstrated similar results and data from one experiment is represented, respectively.

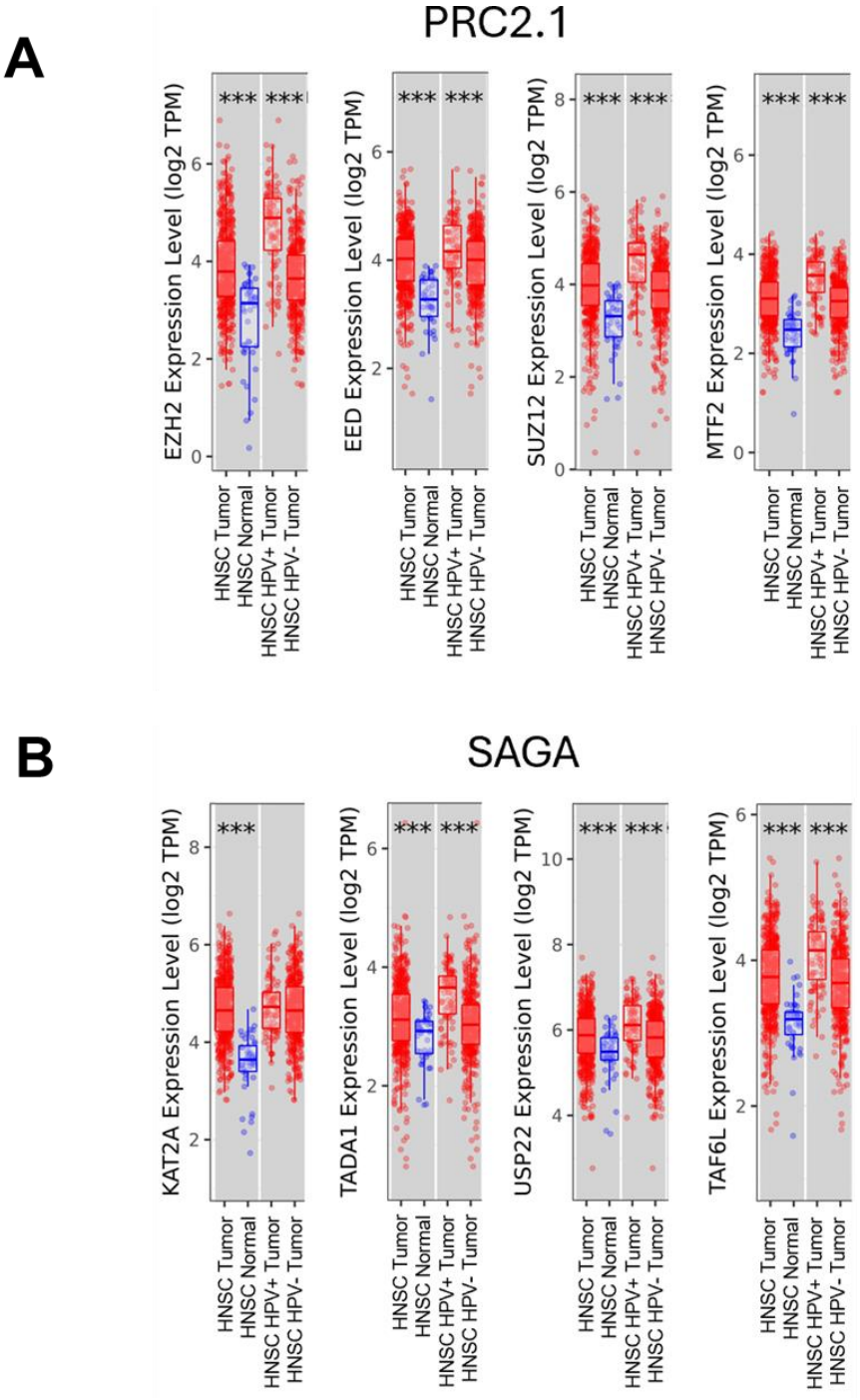

Figure 6. **PRC2.1 and SAGA Complex Members are Upregulated in HPV+HNSCC**. Differential gene expression data obtained from Timer 2.0 comparing expression of PRC2 members (**A**) or SAGA complex members (**B**) between HNSC Tumor (n=520), HNSC Normal (n=44), HNSC HPV+ Tumor (n=97), and HNSC HPV- Tumor (n= 421). The statistical significance computed by the Wilcoxon test with ***p<0.001, **p<0.01, *p<0.05.

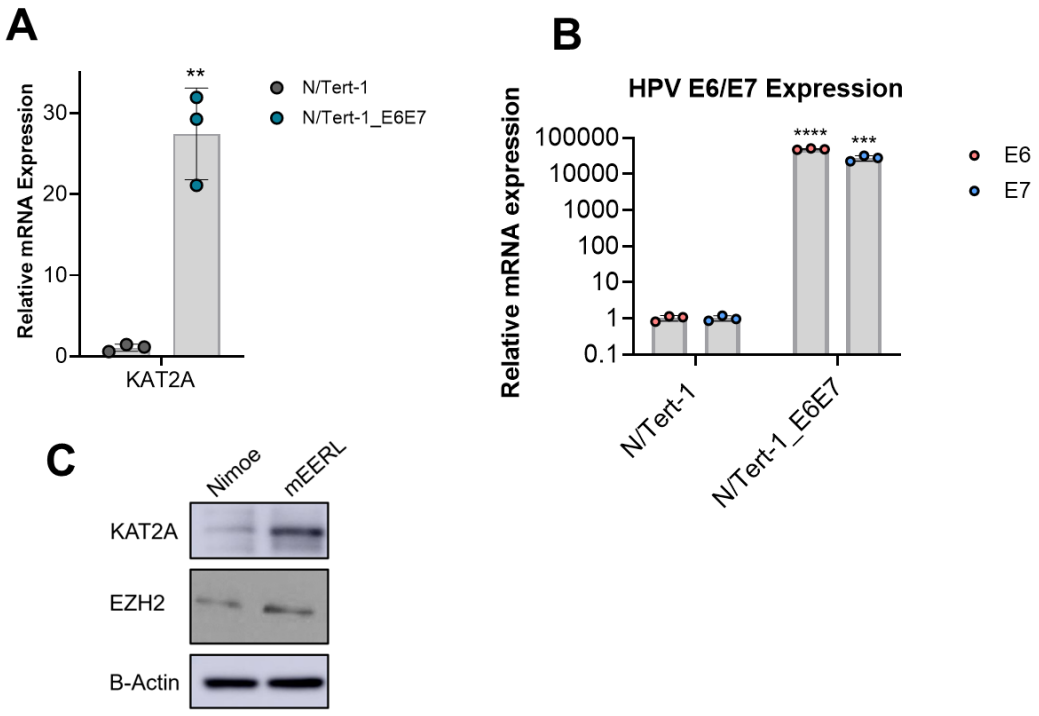

Figure 7. **Expression of Epigenetic Regulators in human and mouse cell lines**. **A**) Relative mRNA expression (ΔΔCT) normalized to GAPDH control for by RT-qPCR. **B**) Relative E6 and E7 mRNA expression normalized to GAPDH control for N/Tert-1_E6E7 cells relative to N/Tert-1 control cells by RT-qPCR. Significant p-values were calculated using an unpaired student's T-test. ****p<0.0001, ***p<0.001, **p<0.01, *p<0.05. These graphs represent single experiments with three technical repeats per condition. Error bars depict SD. **C**) Western blot analysis of whole cell lysates for KAT2A or EZH2 in mEERL relative to NiMOE control cells.

MHC-I Expression Negatively Correlates with H3K27me3 in HPV+ HNSCC

Given the observed increase in PRC2 expression in HPV+HNSCC, we evaluated the potential of increased PRC2 activity via global changes in H3K27me3 levels and the corresponding levels of MHC-I gene expression[268]. **Figure 5G** shows the mRNA levels of HLA-A, B, and C genes relative to healthy keratinocyte controls. As expected from our previous observations[38], HLA-B and HLA-C are transcriptionally downregulated in all HPV+ HNSCC cell lines. HLA-A was significantly downregulated only in SCC2, but it was increased in SCC90 and SCC152 cells. The overall changes in MHC-I heavy chain gene

expression (i.e., HLA-B/C) across cell lines negatively correlated with increases in H3K27me3 (**Figure 5H**), suggesting that PRC2 mediated histone methylation is negatively impacting the levels of MHC-I mRNA expression.

Genetic knockout of PRC2 or SAGA complex members increases MHC-I expression

To validate the observations made from our screens, we knocked out the core PRC2 members, *EZH2*, *EED*, or *SUZ12*, in SCC90 cells (**Figure 8A**). Following knockout, there was significant increases in total protein (**Figure 8B**) and cell surface expression of MHC-I (**Figure 8C**). There was also a corresponding significant increase in relative mRNA expression of HLA-B/C, with less pronounced change in HLA-A (**Figure 8D**). The Increased MHC-I levels paired with a concomitant loss in global H3K27me3 levels in all the PRC2-depleted cell lines (**Figure 8E**), supporting our hypothesis that PRC2-mediated H3K27me3 limits MHC-I gene expression. These findings were corroborated by additional knockouts of *EZH2*, *EED*, or *SUZ12* in the SCC152 HPV+ HNSCC cell lines (**Figure 9A** and **9B**).

Knockout of *KAT2A* in SCC90 cells followed the trend of PRC2 showing increase in total (**Figure 8F**) and cell surface (**Figure 8H**) MHC-I protein levels significantly increased. Loss of KAT2A correlated with decreased histone 3 lysine-9 acetylation (H3K9Ac) levels, which are governed in large part by KAT2A functions[56,302].

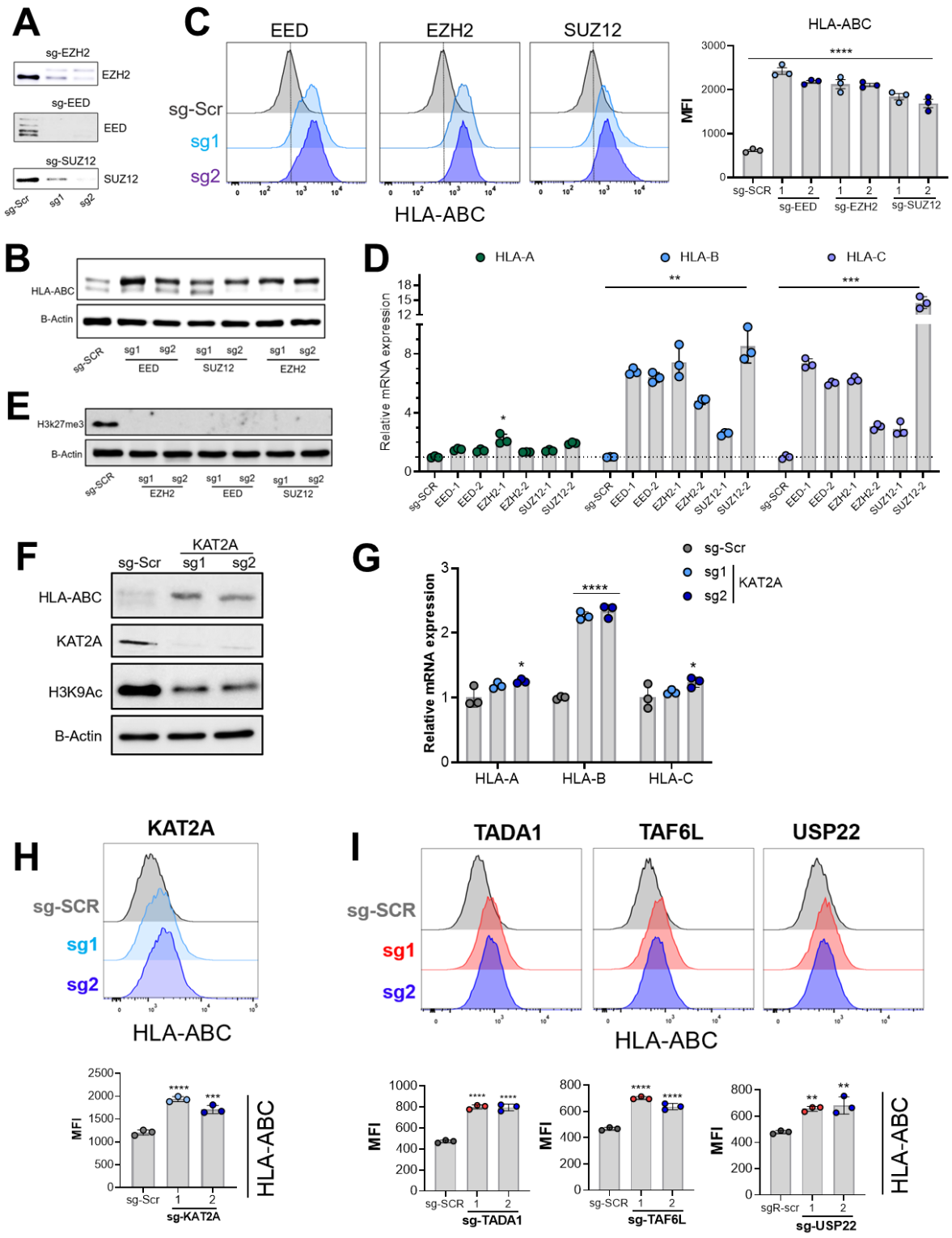

Figure 8. Genetic depletion of PRC2 or SAGA increases MHC-I expression. A) Western blot of WCL from sg-RNA treated cells for total EZH2, EED, or SUZ12 levels. **B**) Western blot of WCL from sg-RNA treated cells for total HLA-ABC. **C**) Surface expression

Figure 8. (Cont'd)
of total HLA-ABC detection by flow cytometry. **D**) Relative mRNA expression (ΔΔCT) by RT-qPCR normalized to GAPDH control. Significant p-values were calculated using an unpaired student's T-test. **E**) Western blot of WCL from sg-RNA treated cells for global H3K27me3. **F**) Western blot of WCL from sg-RNA treated cell lines for total HLA-ABC, KAT2A, global, or H3K9Ac. **G**) Relative mRNA expression (ΔΔCT) by RT-qPCR normalized to GAPDH control. Significant p-values were calculated using an unpaired student's T-test. **H & I**) Surface expression of total HLA-ABC detection by flow cytometry with respective sg-RNA depletions. Significant p-values were calculated using One-way ANOVA Test. ****p<0.0001,***p<0.001, **p<0.01, *p<0.05. Quantitative PCR experiments were performed in duplicate with similar results and graphs represent one experiment with three technical repeats. Error bars depict SD.

However, KAT2A knockout cells significantly upregulated the mRNA levels of HLA-B, with some accompanying increase in HLA-A and -C (**Figure 8G**). To confirm our findings, we again knocked out *KAT2A* in SCC152 cells (**Figure 9C** and **9E**) and found that both mRNA (**Figure 9D**) and cell surface protein (**Figure 9C**) levels of MHC-I are increased in KAT2A-depleted cells. The effect on MHC-I surface expression with *KAT2A* knockout followed suit with sg-RNA gene knockouts of SAGA complex members *TADA1*, *USP22*, and *TAF6L* (**Figure 8I**). **Figure 9F** shows the knockout efficiency of *TADA1*, *USP22*, and *TAF6L* via TIDE. With each gene responsible for differential functions of the SAGA, our data suggest that activity mediated by the whole SAGA complex is responsible for downregulation of MHC-I in HPV+ HNSCC cells. Together, these results demonstrate that the depletion of the PRC2 or SAGA complexes alters the chromatin modifications (i.e., decreased histone methylation or acetylation) that coincide with increased transcription of HLA genes and MHC-I expression.

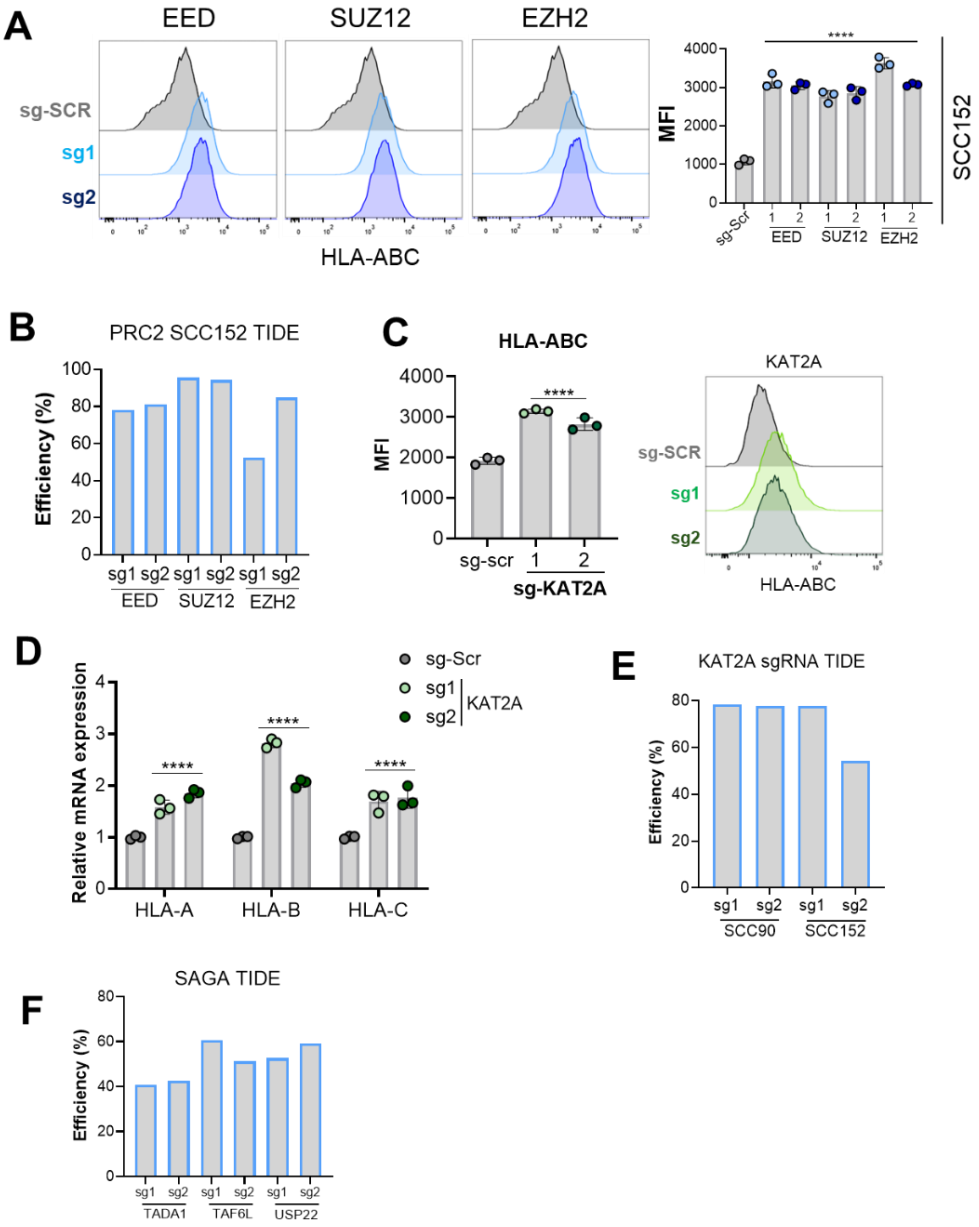

Figure 9. Genetic depletion of PRC2 or SAGA increases MHC-I expression. A) Surface expression of total HLA-ABC detection by flow cytometry with respective sg-RNA depletions for SCC152 PRC2. **B)** TIDE analysis for PRC2 genes in SCC152. **C)** Surface expression of total HLA-ABC detection by flow cytometry with respective sg-RNA depletions for SCC152 KAT2A. **D**) Relative mRNA expression (ΔΔCT) by RT-qPCR normalized to GAPDH control. Significance p-values were calculated using Dunnet's Multiple Comparisons Test. ****p<0.0001, ***p<0.001, **p<0.01, *p<0.05. **E)** TIDE analysis % efficiency for sg-RNA depletion of KAT2A genes in SCC90 and SCC152. **F)** TIDE analysis for sg-RNA depletion of SAGA genes in SCC90. Quantitative PCR experiments were performed in duplicate with similar results and graphs represent one experiment with three technical repeats. Error bars depict SD.

Pharmacologic inhibition of epigenetic modulators increases MHC-I expression

To complement our genetic validation of PRC2 or SAGA complexes as negative MHC-I regulators in HPV+HNSCC, we sought to evaluate the abolishment of PRC2 or SAGA activity using pharmacologic inhibitors. Utilizing our original ranked gene list data, we performed Ingenuity Pathway Analysis (IPA)-upstream regulator analysis[376] to identify relevant compounds based on the directionality, significance of observed gene expression changes, and incidence of known target genes within our screen (**Figure 10A**). The most significant compound predicted to inhibit MHC-I negative regulators (and thereby increase MHC-I) was, garcinol, a histone acetyltransferase inhibitor naturally derived from Garcinia species[377] (**Figure 10A**). Garcinol can target several HATs, including KAT2A[376,378]. Among the other most significant compounds identified were the FDA-approved EZH2 inhibitor, tazemetostat[379], and the global DNA methyltransferase (DNMT) inhibitor, decitabine[380], which blocks DNMT-mediated CpG island methylation[381] (**Figure 10A**). Given the prominence of KAT2A and PRC2 members as negative MHC-I regulators from our screens, we choose to evaluate garcinol, two EZH2 inhibitors (tazemetostat and GSK126)[349], and decitabine for their ability to affect MHC-I expression in HPV+ HNSCC cells. As predicted, treatment with all compounds significantly increased total protein, cell surface expression of MHC-I, and the relative mRNA levels of HLA-B and C (**Figure 10B-E and Figure 11**). Both tazemetostat or GSK126 reduced global H3K27me3 levels which correlated with MHC-I upregulation[160] (**Figure 10C; Figure 11A** and **11C**, respectively). Significantly increased MHC-I expression following garcinol treatment correlated with decreased levels of both H3K9Ac and KAT2A protein (**Figure 11B)**. Interestingly, garcinol also reduced

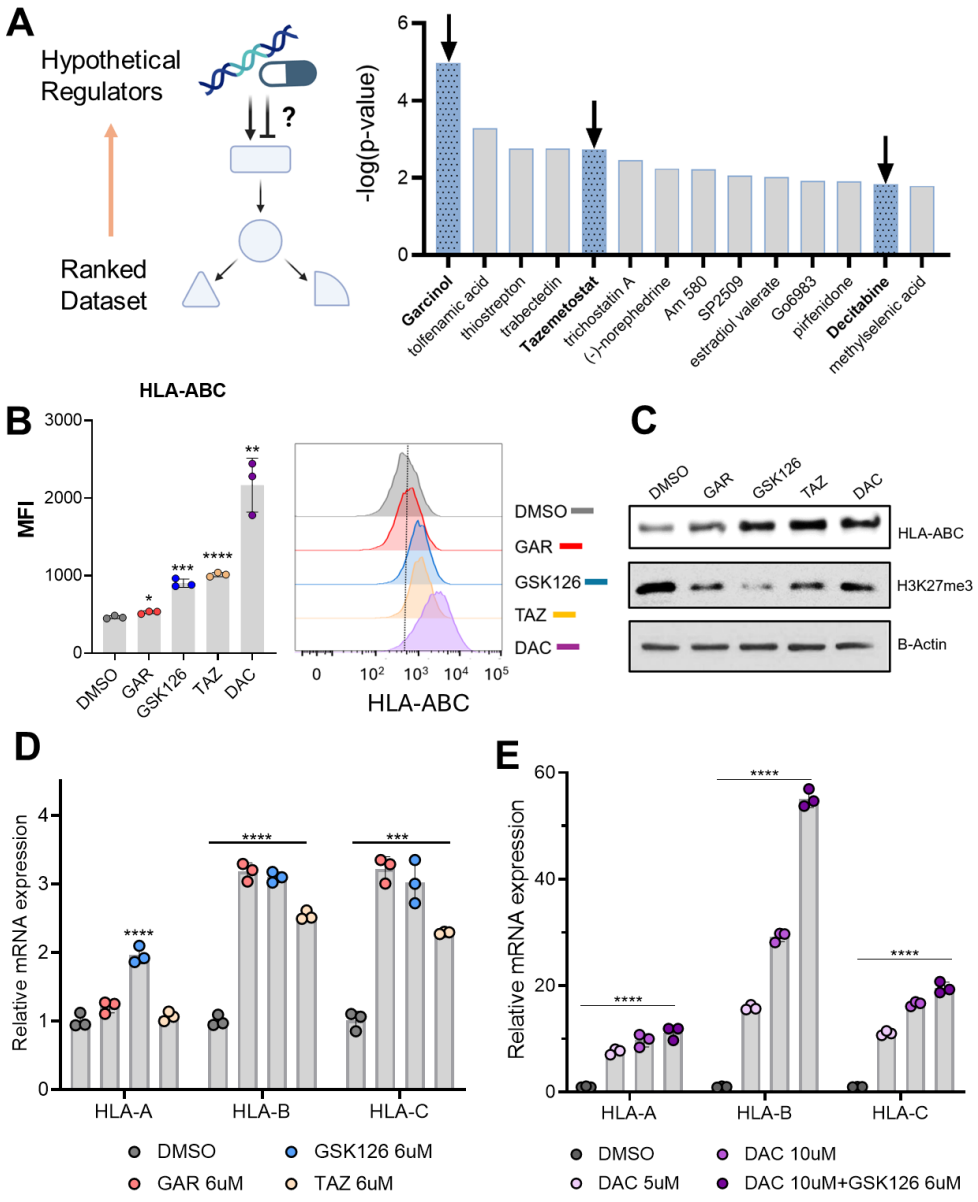

Figure 10. Prediction and Evaluation of Pharmacologic Inhibitors on MHC-I. A) Upstream Regulator Analysis of SCC90 ranked genes to predict hypothetical regulators (histogram). **B**) Surface expression of total HLA-ABC by flow cytometry following inhibitor treatment. SCC90 cells were treated for 7 days with DMSO (0.1%), Garcinol [6uM], GSK126 [6uM], Tazemetostat [6uM], or Decitabine [10uM]. Significant p-values were calculated using an unpaired student's T-test. **C**) Western blot of WCL from treated cells for total HLA-ABC, global H3K27me3, or B-actin. **D and E**) Relative mRNA expression (ΔΔCT) by RT-qPCR normalized to GAPDH control. Quantitative PCR was performed once with three technical repeats per condition. Significance was calculated using Dunnet's Multiple Comparisons Test. ****p<0.0001, ***p<0.001, **p<0.01, *p<0.05. Error bars represent SD. Illustration. Illustrations created with BioRender.com.

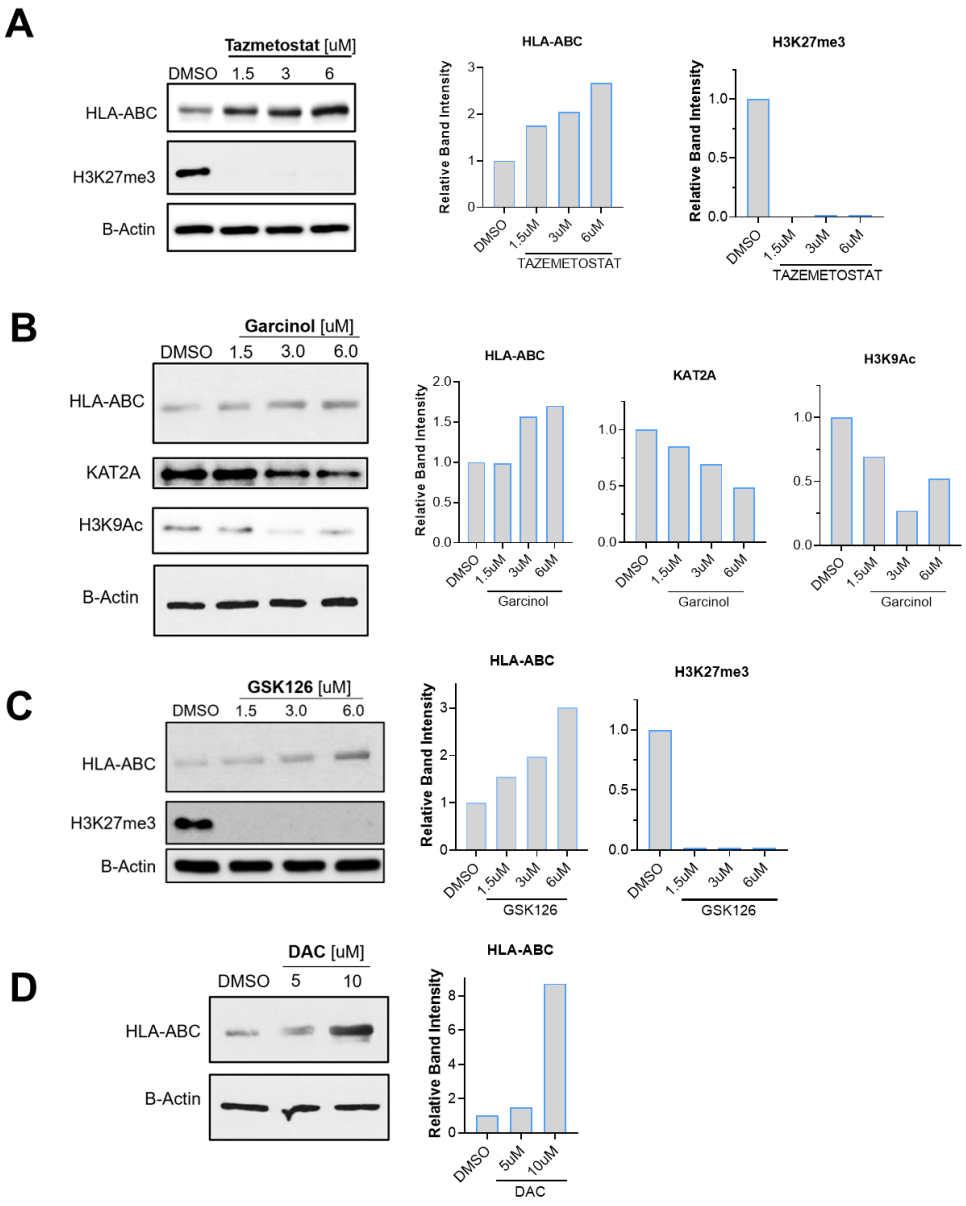

Figure 11. Pharmacologic Inhibitor Treatment of SCC90 Cell Line. A-D) Western blot analysis of WCL of SCC90 cell line following 7 day treatment with each respective inhibitor at the given concentration listed above. For each inhibitor, total HLA-ABC was detected. Additionally, in (**A**) and (**C**), global H3K27me3 was probed. In (**B**), KAT2A and global H3K9Ac were probed following garcinol treatment. B-Actin served as the loading control for each set of experiments. For all experiments, histograms quantify HLA-ABC expression relative to B-Actin for each given condition, respectively.

H3K27me3 levels (**Figure 10C**), suggesting a possible connection between the HAT activity of KAT2A and resultant H3K27me3 levels. Compared to the other inhibitors, decitabine showed the most robust increase in HLA-A, -B, and -C expression but the relatively smallest decrease in global H3K27me3 levels (**Figure 10B, 10C, & 10E** and **Figure 11D)**. This result may be explained by studies showing that DNMT inhibitors reactivate endogenous retroviruses and induce IFN responses, which can subsequently lead to increased MHC-I expression[382]. Thus, the effects of decitabine potentially circumvent the influence of HAT or PRC2-related activity. Given that PRC2-DNMT interactions are also known to affect DNMT activity directly[259], we tested MHC-I expression in HPV+ HNSCC cells treated with GSK126 in combination with decitabine[383] and observed a synergistic increase in *HLA-B* transcription (**Figure 10E**).

To determine if the increase in MHC-I expression by EZH2 inhibition is correlated to locus-specific H3K27me3 levels, we performed Cleavage Under Targets and Release Using Nuclease (CUT&RUN) analysis with GSK126 treated SCC90 cells and analyzed whole-genome levels of H3K27me3 and H3K4me3 (**Figure 12**). The gene loci for the HLA-A, -B, and -C are bivalent in nature[160], and the maintenance of H3K4me3 readies the gene for rapid activation with the abolishment of the H3K27me3 repressive mark in their promoters[236]. Following EZH2 inhibition, genome wide loss of H3K27me3 peaked in proximity to the transcriptional start sites of genes (**Figure 12A)**, and that (~26%) of H3K27me3 was lost within 1kb of known promoter regions (**Figure 12B**). H3K27me3 signal diminished at the *HLA-B* and *-C* gene loci and in proximity to H3K4me3 signal (**Figure 12C)**.

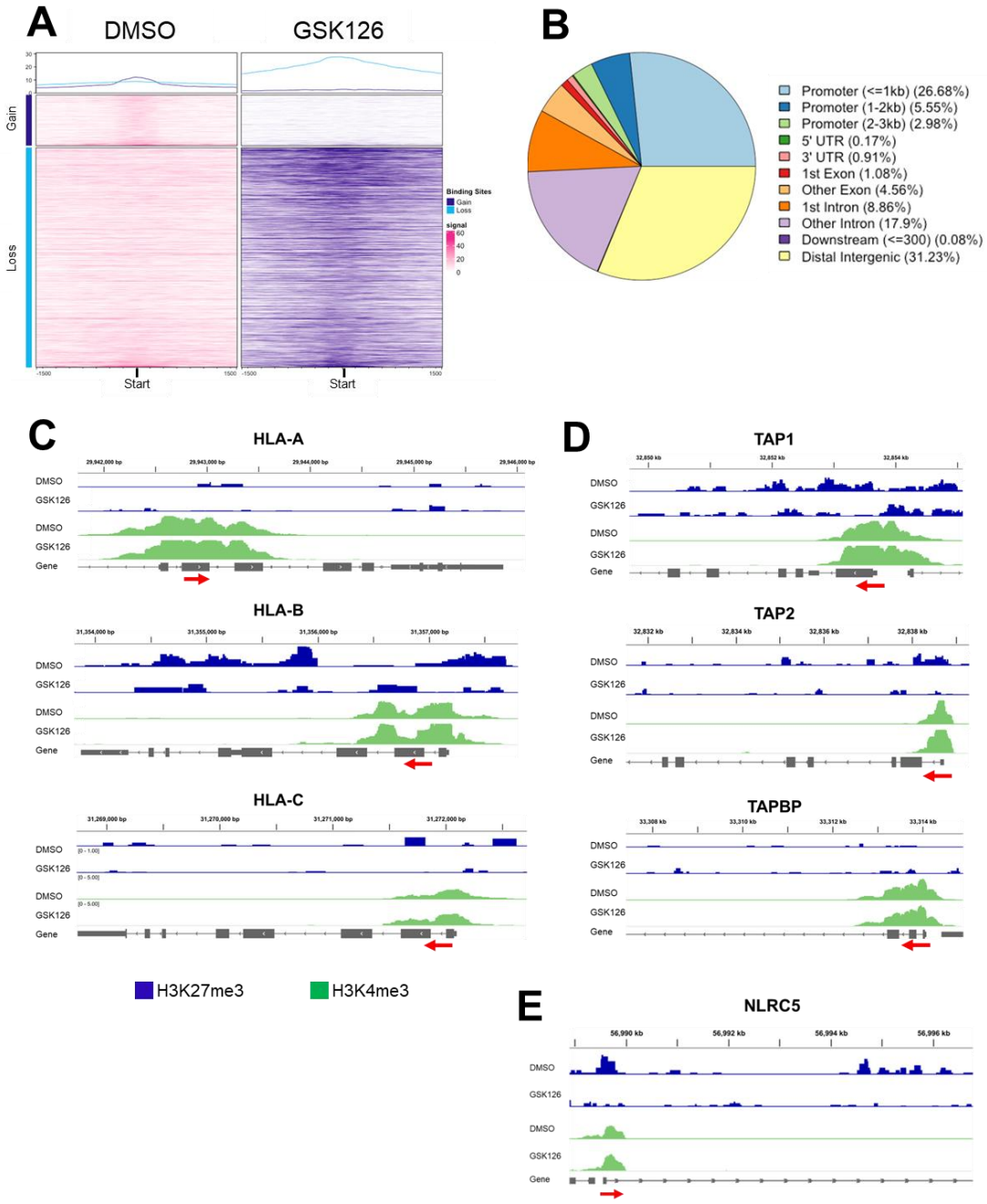

Figure 12. CUT&RUN Reveals H3K27me3 Changes Gene Loci with EZH2i. SCC90 treated with (0.1%)DMSO or GSK126 [6uM] for 7 days. **A)** H3K27me3 (loss/gain) signal plot relative to the transcription "start" sites genome wide. **B**) Annotation pie chart indicating (%) of genomic features affected by H3K27me3 changes. **C-E**) H3K27me3 signal from (**C**) *HLA-A,B,C* (**D**) *TAP* genes (**E**) *NLRC5*. Value axes (Kb) correspond to position on gene specific chromosomes. Blue and green peaks correspond to H3K27me3 or H3K4me3, respectively. Gene coding regions are shown in grey. Red arrows indicate the direction of the reading frame at promoter sites approximated by H3K4me3 signal.

decreases in H3K27me3 occurred at *TAP1*, *TAP2*, and *NLRC5* loci but not at *TAPBP* (**Figure 12D and E)**. Taken together, these results show that EZH2 inhibition decreases H3K27me3 at gene loci important for MHC-I expression in HPV+ HNSCC similar to what has been observed in other cancers[160]

PRC2 activity can limit the response of cancer cells to IFN-γ stimulation[160]. We postulated that with increased PRC2 activity in the HPV+ HNSCC cell lines that the effects of IFN-γ stimulation may be reduced. To test this, we treated SCC90 cells with IFN-γ for 24hrs following EZH2 inhibition and quantified changes in MHC-I upregulation. Flow cytometry experiments to detect surface expression of MHC-I (**Figure 13A)** show that without the application of EZH2 inhibitor, the upregulation of MHC-I by IFN-γ is reduced. We observed an initial increase in MHC-I surface expression with IFN-γ treatment in the DMSO treated cells, although there was no significant difference in MHC-I expression following an increased dose of IFN-γ in DMSO-treated cells. In contrast, EZH2 inhibitor treatment resulted in higher levels of MHC-I versus DMSO, with or without IFN-γ treatment, and after EZH2 inhibition, high dose IFN-γ significantly increased MHC-I over the low dose level. This suggests that with EZH2i, cells have a greater potential to respond to IFN-γ than without (**Figure 13A**). The same trends in expression of MHC-I are reflected in the western blot of WCL samples made from the experiments evaluated in the flow cytometry (**Figure 13B)**. **Figure 13B** shows that total HLA-ABC protein plateau in DMSO treated cells following IFN-γ treatment, but continues to increase in combination with EZH2 inhibition. Despite the limited response of IFN-γ to increase MHC-I, impediment does not appear to be related to a failure in the initiation step of the IFN-γ response, given the similar increase in total STAT1 and activated phosphorylated STAT1-Ser727 protein levels observed in both DMSO- and GSK126-treated groups (**Figure**

13B). This result could imply that despite IFN-γ receptor binding and STAT1 activation, there is a failure in either STAT1 mobilization or downstream transcription initiation, limiting MHC-I expression. The latter idea is supported by increased expression of antigen presentation machinery (APM) proteins TAP1, TAP2, TAPBP, and B2M following EZH2i treatment. (**Figure 13C**). The increased mRNA levels seen in (**Figure 13C)** also correlate with decreased H3K27me3 signal at gene specific loci (**Figure 12D)**. However, the NLRC5 mRNA level was paradoxically decreased following GSK126 treatment despite the concurrent H3K27me3 signal decrease at the *NLRC5* locus in the CUT&RUN experiment (**Figure 12E**). This may indicate the activity of other unknown elements regulating NRLC5. Overall, these results suggest that while IFN-γ initiates an interferon response in the HPV+ HNSCC cells, downstream upregulation of MHC-I is attenuated without the synchronized inhibition of EZH2.

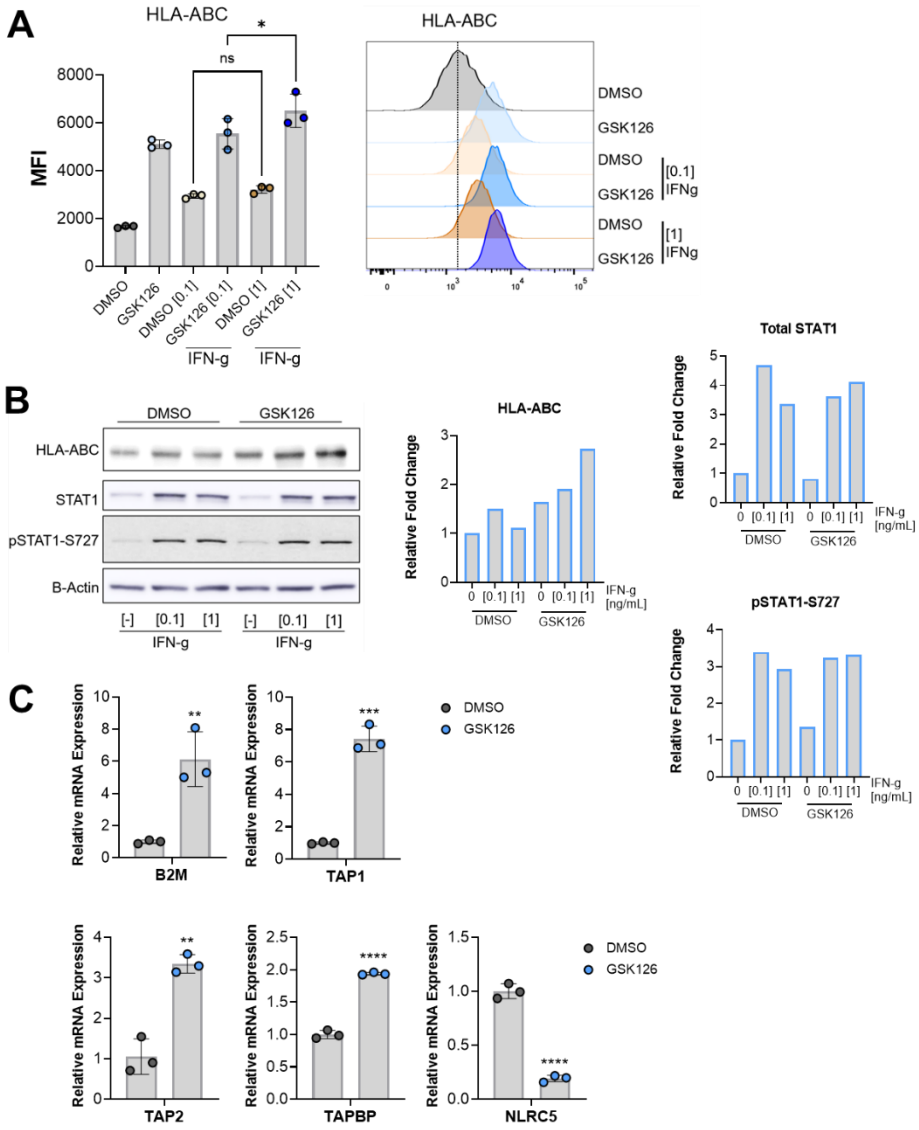

Figure 13. PRC2 limits the response to IFN-γ. A) Surface expression of total HLA-ABC detected by flow cytometry following drug treatment. SCC90 cells were treated for 3 days with DMSO (0.1%) or GSK126 [6uM] then received vehicle (PBS), [0.1], or [1] ng/mL IFN-γ. Significant p-values were calculated by Tukey's 2-way multiple comparisons test. **B**) Western blot of WCL from SCC90 cells following drug treatment probed for total HLA-ABC, total STAT1, phospho-STAT1 Ser727, or B-actin. Panels on the (right) quantify western blots relative to DMSO control. **C**) Relative mRNA expression (ΔΔCT) by RT-qPCR normalized to GAPDH for APM genes following treatment. Significant p-values were calculated using an unpaired student's T-test. ****p<0.0001, ***p<0.001, **p<0.01, *p<0.05. PCR experiments were performed once with three technical repeats. Error bars depict SD. We thank Dr. Jamie Bernard for the gift of pSTAT1-S727 antibody.

In silico analysis predicts E2Fs and MYC as the drivers of MHC-I downregulation

To delve deeper into understanding the mechanism underlying PRC2- and SAGA-mediated repression of MHC-I, we determined potential genetic drivers in our SCC90 CRISPR/Cas9 screen data using the upstream regulator analysis[376]. Analysis predicted the transcription factor, E2F1, was the most significant upstream regulator responsible for MHC-I downregulation (**Figure 14A)**. In HPV+ cells, E2Fs are highly activated by HPV E7-mediated inhibition of retinoblastoma protein (pRB) family members[21]. Furthermore, the PRC2 core members, EZH2 and EED were identified as downstream targets of E2F1 (**Figure 14B**). For clarity, the algorithm's scoring of E2F1 (in part) was based on the prominence of EZH2 and EED in the screen dataset, as well as their known associations with E2F1. Indeed, it has been previously demonstrated that E2F1 drives expression of *EZH2*, *EED*, and *SUZ12*[384-389]. In addition, HPV16 E7 mediated release of E2F drives EZH2 transcription[224], and the knockdown of HPV E6/E7 expression correlates with

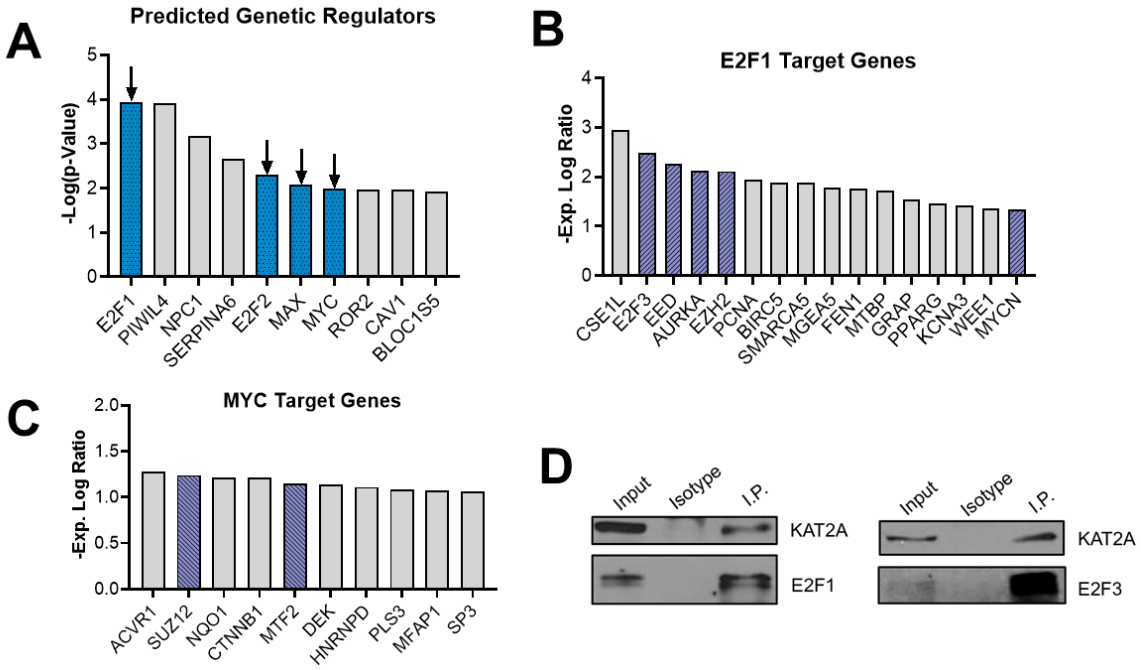

Figure 14. Computational Prediction of Genetic Upstream Regulators of MHC-I. A) Upstream regulator analysis prediction of genes based on the SCC90 ranked dataset. **B** and **C**) indicate known downstream targets of E2F1 or MYC harvested from the ranked dataset. **D**) Western blots of co-immunoprecipitations for KAT2A probed with E2F1 or E2F3 antibody compared to SCC90 WCL (input) and isotype control (IgG).

decreased E2F1 and EZH2 levels in HPV+ HNSCC cells[390]. Beyond E2F1, it is also possible that several other E2F family members could be driving these observations, given their known similarities in both sequence homology and promoter binding[36]. For instance, E2F3 was a robust and significant negative regulator of MHC-I in both SCC90 (Z= -4.18) and N/Tert-1_E6/E7 screens (Z= -1.92). Like E2F1, E2F3 can also positively regulate EZH2 transcription[391]. We confirmed that overexpression of the transcriptional activator E2F3a (E2F3 splice product) results in the upregulation of EZH2 transcription and total protein (**Figure 15**).

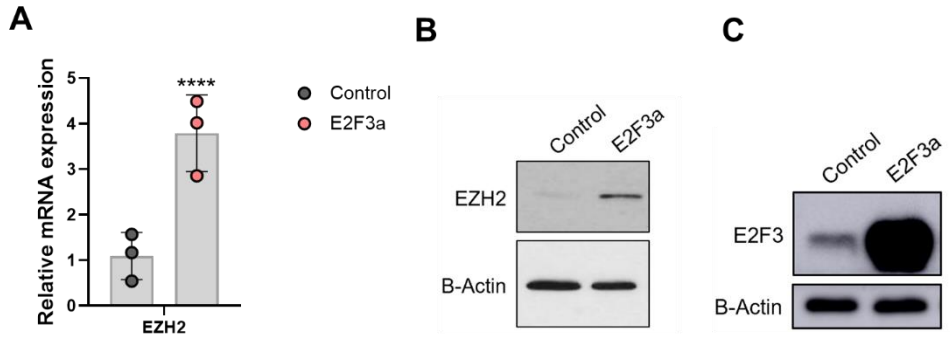

Figure 15. E2F3a overexpression upregulates EZH2. A) Relative EZH2 mRNA expression (ΔΔCT) by RT-qPCR normalized to GAPDH control from 293FT cells over-expressing pCMV-Neo/Bam-empty vector (control) or pCMV-E23Fa. Significant p-values were calculated using an unpaired student's T-test. ****p<0.0001, ***p<0.001, **p<0.01, *p<0.05. PCR experiments were performed once per condition with three technical repeats. Error bars depict SD. **B**) Western blot of WCL from 293FT cells following transient transfection of vector control (pCMV-Neo/Bam-empty) or pCMV-E23Fa and probed for EZH2 and B-actin, or **C**) probed for total E2F3 expression and B-actin.

In addition to E2Fs, the MYC proto-oncogene and its binding partner, MAX, were two of the most significant targets predicted in our upstream regulator analysis (**Figure 14A**). MYC activity is known to be upregulated by the HPV oncogene E6 and leads to significant cellular proliferation and transformation[42]. Intriguingly, our CRISPR/Cas9 screen data showed that *MYCN* (i.e., N-MYC) and its known stabilizer, Aurora Kinase A (*AURKA*)[392], were significant negative MHC-I regulators (**Figure 3B**). Both *MYCN* and *AURKA* were also significant downstream targets of E2F1, as determined in our upstream analysis (**Figure 14B**). The analysis also showed *SUZ12* and *MTF2* as among our dataset's most significant downstream targets of MYC (**Figure 14C**). Gene expression analysis of the TCGA data using Timer2.0 showed increased expression of N-MYC in HPV+ HNSCC patient samples relative to normal or HPV-negative HNSCC samples, and that there is a robust positive correlation between N-MYC and PRC2 expression (**Figure 16A and 16B**). However, c-MYC levels were not increased in the HNSCC TCGA data

compared to normal samples, although PRC2 genes did still significantly correlate with c-MYC in HNSCC overall (data not shown, but is accessible at http://timer.cistrome.org/). Next, we assessed N-MYC expression by western blot of WCL or by qRT-PCR in three HPV+ HNSCC cell lines relative to normal keratinocytes and determined that N-MYC was upregulated in all three of the lines tested (**Figure 16C and 16D**). Contrasting again, c-MYC transcript was significantly increased only in the SCC2 cell line, while levels in SCC90 and SCC152 were unremarkable relative to control (**Figure 16E)**.

SAGA is an important transcriptional coactivator for MYC (both c-MYC and N-MYC) and E2F[56,296,314,318,325,354-357], and KAT2A is reciprocally transcribed by both MYC and E2F[360]. MYC is stabilized by KAT2A via direct acetylation resulting in increased E2F1 transcription[329], demonstrating a reciprocal interplay between KAT2A, MYC, and E2F1. In light of this relationship and our analysis in (**Figure 14A-C**), we hypothesized that dysregulated KAT2A increases MYC- and E2F-mediated transcription of PRC2 genes in HPV+ HNSCC. To test the hypothesis, we first analyzed TCGA HNSCC patient data and revealed highly significant positive correlations between KAT2A expression and PRC2 genes (**Figure 17A)**. We also confirmed previous studies[343,356] that KAT2A binds to E2Fs through coimmunoprecipitations of E2F1 and E2F3, further implicating KAT2A's role as a transcriptional coactivator (**Figure 14D)**. Further, we show that KAT2A knockout in both SCC90 and SCC152 cell lines results in transcriptional downregulation of all PRC2 core members, EZH2, EED, or SUZ12*,* with the effect on *EED* transcription the most pronounced (**Figure 17B**). To follow the knockout experiments, treatment of SCC90 cells with GSK4027, a contemporary KAT2A/KAT2B inhibitor that targets the bromodomain of KAT2A/B, revealed increased total surface expression of MHC-I (**Figure 18A**).

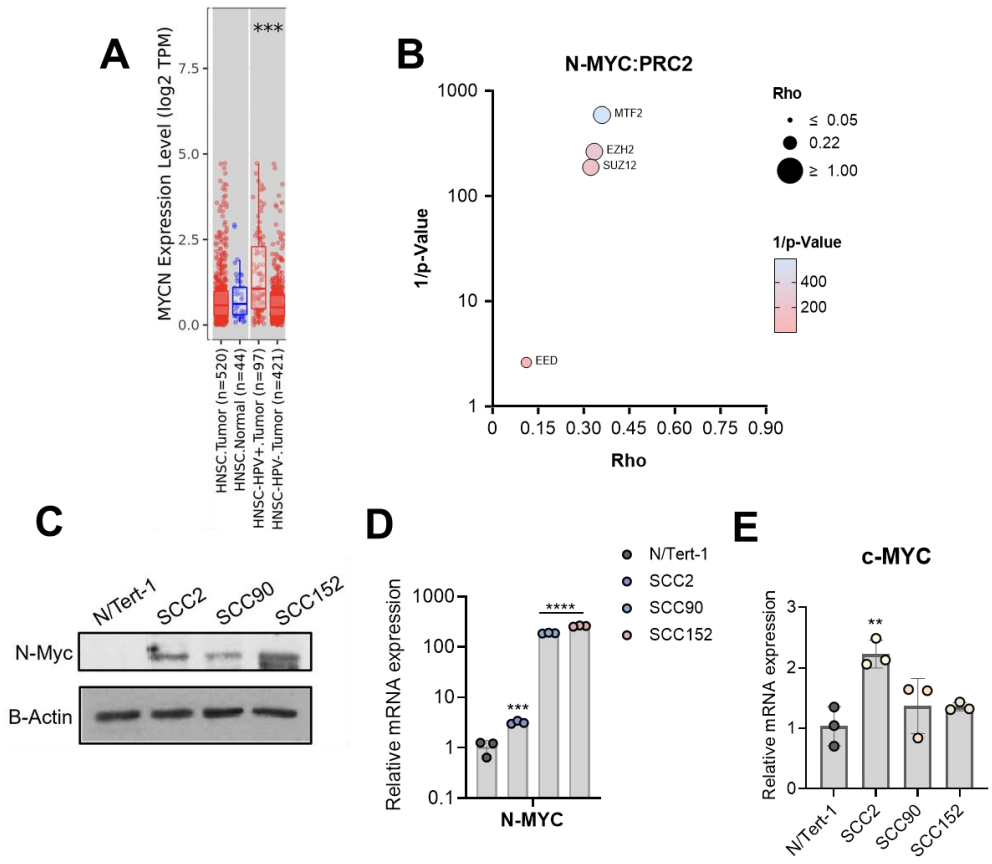

Figure 16. **N-MYC Expression is Increased in HPV+ HNSCC**.
A) Differential gene expression data obtained from Timer 2.0 for *MYCN*. **B**) Timer 2.0 derived correlation between N-MYC and PRC2.1 members from HPV+ HNSCC samples. **C**) Western blot analysis of WCL from N/Tert-1 keratinocyte cells (control) or HPV+ HNSCC cell lines probed for N-MYC or B-actin expression. **D**) Relative mRNA expression (ΔΔCT) by RT-qPCR normalized to GAPDH control for N-MYC expression or **E**) c-MYC expression in HPV+HNSCC cell lines versus keratinocyte control (N/Tert-1). Significant p-values were calculated using an unpaired student's T-test. ****p<0.0001, ***p<0.001, **p<0.01, *p<0.05. PCR experiments were performed once per condition with three technical repeats. Error bars depict SD.

Corroboration by additional experiments with GSK4027 treatment showed total HLA-ABC protein levels increased with concomitant decreases in KAT2A, EZH2, EED, and SUZ12 (**Figure 18B**). Thus, this evidence supports the hypothesis that dysregulation of KAT2A/SAGA contributes to the repression of MHC-I gene transcription by coactivating MYC and E2F to induce PRC2 expression.

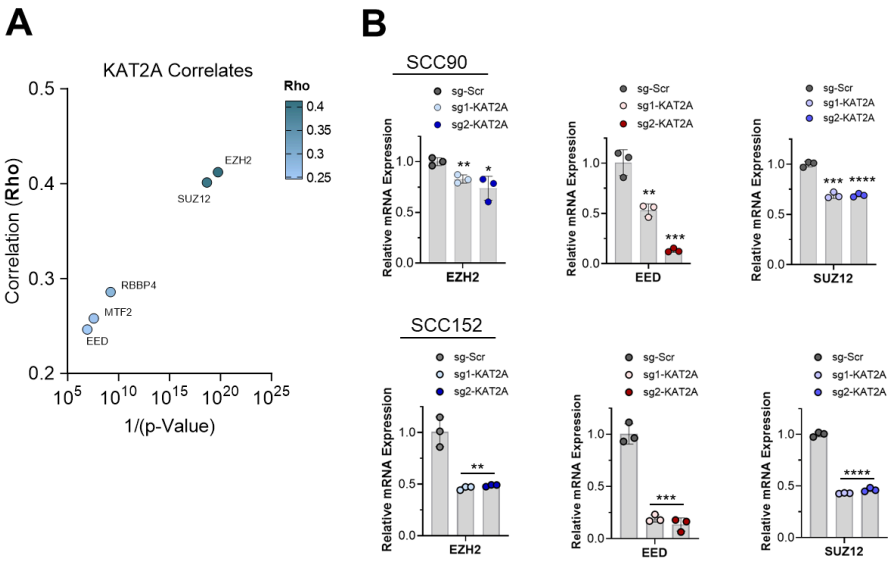

Figure 17. KAT2A is a correlates with PRC2 Gene Transcription. A) Correlation of KAT2A with PRC2 genes by TIMER2.0 using TCGA HNSCC datasets. **B**) qRT-PCR for EZH2, EED, or SUZ12 normalized to B-actin (ΔΔCT) in SCC90 and SCC152 sg-KAT2A or sg-Scr treated cells. Significance was calculated using an unpaired student's T-test. ****p<0.0001, ***p<0.001, **p<0.01, *p<0.05. PCR experiments were performed once per condition with three technical repeats. Error bars depict SD.

KAT2A levels correlate with diminished tumor immune cell infiltration

Efficient MHC-I expression is critical to the propagation of an antitumor immune response, and our data suggests that upregulated KAT2A/SAGA complex is negatively regulating MHC-I expression. Thus, dysregulated KAT2A may have negative ramifications for both antitumor immune cell responses and immune therapy efficacy. To better predict the

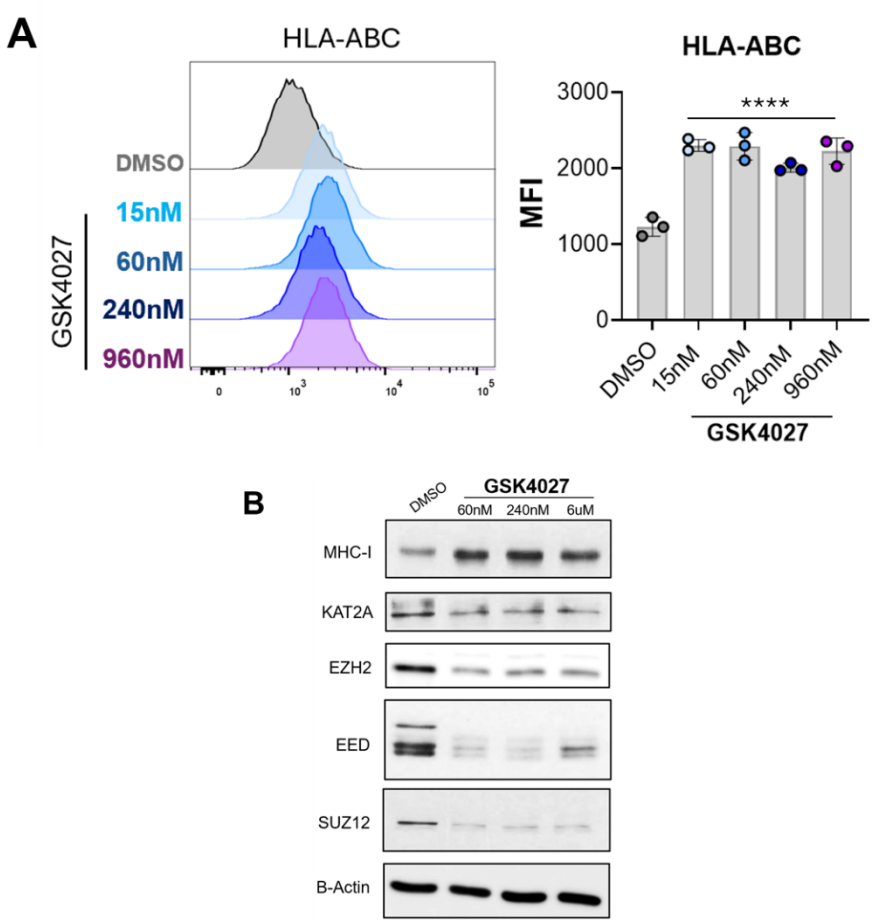

Figure 18. GSK4027 KAT2A Inhibitor Increases MHC-I expression and Depletes PRC2 Genes. A) Surface expression of total HLA-ABC was detected by flow cytometry following GSK4027 treatment for 7 days in SCC90 cells at the respective concentrations. **B**) Western blot analysis of WCL from SCC90 cells treated for 7 days with GSK4027 and probed for total HLA-ABC (MHC-I), KAT2A, EZH2, EED, SUZ12, or B-actin. Significance p-values: ****p<0.0001, ***p<0.001, **p<0.01, *p<0.05.

result of KAT2A upregulation in HPV+ HNSCC, we performed gene expression analysis using the TCGA patient datasets to estimate tumor immune cell infiltration (**Figure 19A**). Using Timer2.0 software to analyze HNSCC patient samples (n=522), we observed robust negative correlations between KAT2A expression and CD8+ T cells, dendritic cells (DC), natural killer cells (NK), and Macrophages (MC) infiltrating into the TME (**Figure 19A**). Conversely, the same analysis showed a strong positive correlation with myeloid-

derived suppressor cells (MDSCs), M2 macrophages (M2), and CD4+ T cells. For comparison, we conducted the same analysis with HLA-B expression and immune cell infiltration in the HNSCC dataset. We found that a near opposite result was true, and HLA-B expression correlates positively with CD8+, CD4+, DC, and NK cell tumor infiltration and negatively with M2 and MDSCs (**Figure 19B**).

We next compared KAT2A to HLA class I expression using the HPV+ HNSCC TCGA data on Timer2.0. We found a significant negative correlation between KAT2A expression and HLA-A, B, and C, and most prominently, HLA-E expression (**Figure 19C**). For comparison, we considered a similar HAT, KAT5, to HLA expression and found no significant correlations apart from HLA-E, which positively correlated (**Figure 19D**). Ultimately, these data indicate that KAT2A expression negatively correlates with the expression of most class I HLAs and will negatively impact the recruitment of immune effector cells (e.g., CD8+, DC, or NK cells) into tumors, limiting antitumor immune responses and possibly the efficacy of therapy.

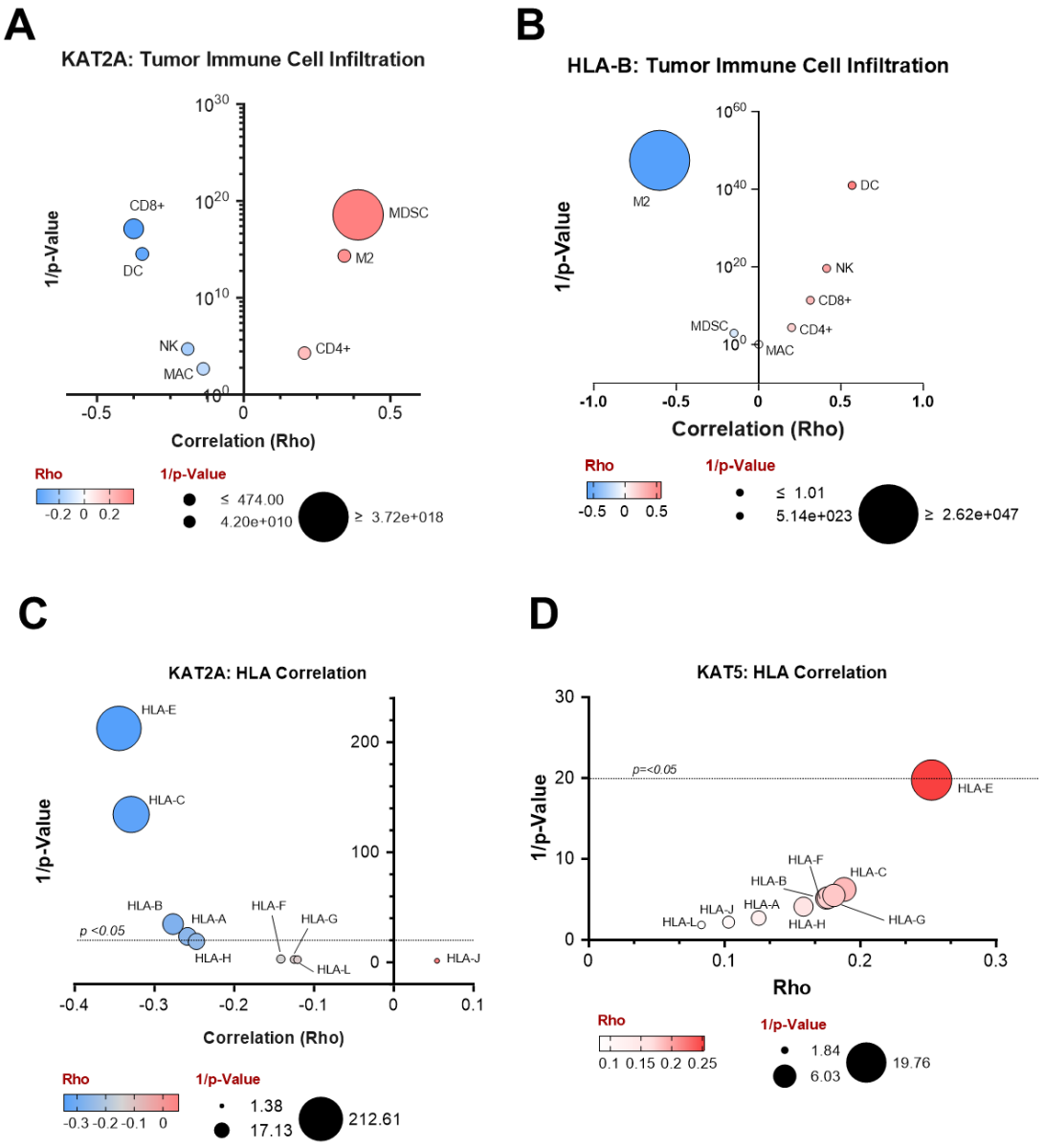

Figure 19. **KAT2A expression correlates with decreased CD8+ T Cell Infiltration and HLA Gene Expression in Head and Neck Cancer Samples**. **A**) Using TCGA Head and Neck tumor sample data (n=522), TIMER2.0 software correlates KAT2A or **B**) HLA-B expression with immune cell infiltration levels (includes tumor purity adjustment). **C**) Correlation of KAT2A or **D**) KAT5 with HLA genes from HPV+ HNSCC TCGA sample data (n=98) prepared with TIMER2.0 software. Dotted lines demarcate significant p-Value (<0.05).

2.3 Conclusions

Our CRISPR/Cas9 screens in HPV+ HNSCC revealed that several epigenetic regulators, including members of PRC1 and PRC2, were highly significant hits among the top negative MHC-I regulator genes. This result was consistent with previous findings that revealed PRC2 as part of an evolutionarily conserved mechanism to promote cancer immune evasion[160]. Furthermore, we revealed that cellular E2Fs and MYC family proto-oncogenes are the predicted drivers of inhibition of MHC-I expression. Our screens showed that an additional epigenetic regulator, KAT2A , was a top hit among negative MHC-I regulators. KAT2A operates through its greater complex, SAGA, which is a known transcriptional coactivator for E2F and MYC transcriptional programs. E2F and MYC are highly activated in HPV+ cells and are known to promote the expression of PRC2 genes[250,385]. We validated the results of our screening with additional genetic knockout experiments, small molecule pharmacologic inhibition, and related our findings to TCGA patient datasets. Overall, these results suggest that HPV upregulates PRC2 through the action of SAGA plus MYC and E2F transcription, and that the subsequent downregulation of MHC-I related gene transcription contributes to cancer immune evasion.

CHAPTER 3

Inhibition of Aurora Kinase A Increases MHC-I Expression in HPV+ HNSCC

Contributions to Science

The work in this chapter was conceptualized by Nicholas Giacobbi. The final figures for this chapter were generated by Nicholas Giacobbi. The experiments in this chapter were performed by Nicholas Giacobbi with contributions from Lexi Vu, Conchai Yang, Evelyn Gomez, and Dr. Mohamed Khalil.

3.1 Abstract

The MYC family of proto-oncogenes are important regulators of gene transcription in normal cells, but they often become dysregulated during the course of many cancers. In HPV+ HNSCC, activated c-MYC is known to drive the aberrant proliferation of cells. We recently showed that c-MYC can upregulate the expression of the ubiquitin ligase, MARCHF8, which targets important immune receptors for degradation and contributes to immune evasion. MYC can also increase the expression of PRC2 genes known to decrease MHC-I expression across cancers. Thus, the inhibition of MYC family members may be valuable in the treatment of cancer by increasing antitumor immunity and reducing the proliferation of cancer cells. Because MYC family members are notoriously difficult to target directly, we utilized the small molecule inhibitor of Aurora Kinase A (AURKA), MLN8237, to target MYC indirectly. AURKA is known to stabilize MYC proteins and therefore, its disruption decreases MYC. Here we show that application of MLN8237 can deplete MYC, MARCHF8, PRC2, and may increase antitumor immunity by increasing MHC-I expression.

3.2 Introduction

The activation of the MYC family of proto-oncogenes is associated with the progression of many cancers[393-395]. There are three MYC family paralogs: Cellular-MYC (c-MYC), Neuronal (N-MYC)[396,397], or Lung-MYC (L-MYC)[398,399], which are expressed in different tissue types and at various stages of development[400,401]. In HPV+ tumors, MYC family members can be activated or upregulated to contribute to cancer progression[49,402-404]. For example, the immortalization of primary keratinocytes by human telomerase (hTERT) is mediated by HPV oncoprotein E6 via c-MYC transcription factor binding on the hTERT promoter to upregulate transcription[42,43,405,406]. Our lab has also demonstrated that the transcription of the E3 ubiquitin ligase Membrane-associated RING-CH protein 8 (MARCHF8) is upregulated by activated c-MYC, and that increased MARCHF8 targets cell surface immune receptors for degradation contributing to immune evasion[45].

In addition to c-MYC activation, we show that in three HPV+HNSCC cell lines tested, that N-MYC expression is upregulated (**Figure 16**). The expression of N-MYC is usually restricted to developing embryos, maintaining pluripotency stem cells, or the proliferation of cells in the CNS[50,407,408], and N-MYC expression in oral keratinocytes is not usual. This suggests that its expression may be contributing to pathological changes, with higher N-MYC expression known to be associated with cancer aggressiveness[409-411]. In neuroblastomas, the effect of N-MYC was reported to promote immunosuppression[412,413]. Bernards et al. in 1986, were among early researchers who showed that N-MYC amplification decreases expression of MHC-I in neuroblastoma cells[57], but the exact mechanism by which N-MYC downregulates MHC-I is still not fully elucidated. Possible mechanisms may relate to recent reports which show N-MYC binding directly with EZH2 to mediate transcriptional repression of specific genes[248,249],

or to the observations that both N-MYC and C-MYC can drive the expression of PRC2 genes[250], which can result in repressed MHC-I transcription[160]. Regardless, it is still unclear what the specific roles for N-MYC expression in HPV+ cancers are, or if they relate to MHC-I regulation and immunosuppression. Thus, the goal of this study was to determine if abrogation of N-MYC can affect MHC-I expression in HPV+ HNSCC.

MYC family members have been exceedingly difficult to therapeutically target directly[393,395]. As an alternative strategy, some compounds can target MYC indirectly through the inhibition of its binding partners, thereby functionally downregulating MYC and its activity[414,415]. Aurora Kinase A stabilizes N-MYC by inhibiting the E3 ubiquitin ligase SCF(FbxW7), which targets N-MYC for proteasomal degradation; application of AURKA inhibitors (AURKAi) leads to N-MYC degradation[416-419]. In this work we evaluated the AURKAi, MLN8237 (Alisertib), its effect on N-MYC, and MHC-I expression in HPV+ HNSCC. Our data show that MLN8237 treatment reduces N-MYC protein levels and suggests that decreased N-MYC may alleviate both the transcriptional and post-translational downregulation of MHC-I, with N-MYC being the common node involved in both mechanisms. Overall, we hypothesize that aberrant N-MYC expression is negatively regulating MHC-I in HPV+HNSCC, and that its inhibition leads to restoration of MHC-I expression.

3.2 Results

Treatment of HPV+ HNSCC with MLN8237 Degrades N-MYC and Increases MHC-I

N-MYC and its stabilizer, AURKA, were both identified as significant negative regulators of MHC-I in our SCC90 CRISPR/ Cas9 screen (**Figure 3B**). Relative levels of N-MYC mRNA transcript and protein were upregulated in all three of the HPV+ HNSCC cell lines we tested (SCC-2, 90, & 152) (**Figure 16**). We postulated that disrupting N-MYC/AURKA could increase MHC-I expression, and to test this, we treated SCC90 cells with different doses of MLN8237 and evaluated the expression of MHC-I. **Figure 20A** shows that with MLN8237 treatment, N-MYC protein levels decrease and correlate with an increase in total HLA-ABC protein. Likewise, mRNA levels of HLA-A, B, or C significantly increase in the MLN8237 treated samples compared to DMSO (**Figure 20B**). We performed similar experiments using lower doses of MLN8237 (**Figure 21A**) and observed a significant increase in the relative mRNA transcript levels of HLA-B, but neither HLA-A nor HLA-C. Increased transcript coincided with increased surface expression of total HLA-A/B/C as detected by flow cytometry (**Figure 21B**). Because the effect on HLA-A, B, and C transcription resembled our previous experimental results with EZH2 inhibition (**Figure 8**), we estimated that EZH2 could be involved in a common pathway with AURKA/N-MYC, and we tested both EZH2 and AUKRA inhibitors together. Interestingly, we observed a synergistic effect toward increased MHC-I expression by co-treating with MLN8237 and GSK126 (EZH2i) (**Figure 21A and 21B**). Together, these results suggest MHC-I is being negatively regulated at the transcription level by N-MYC mediated activity.

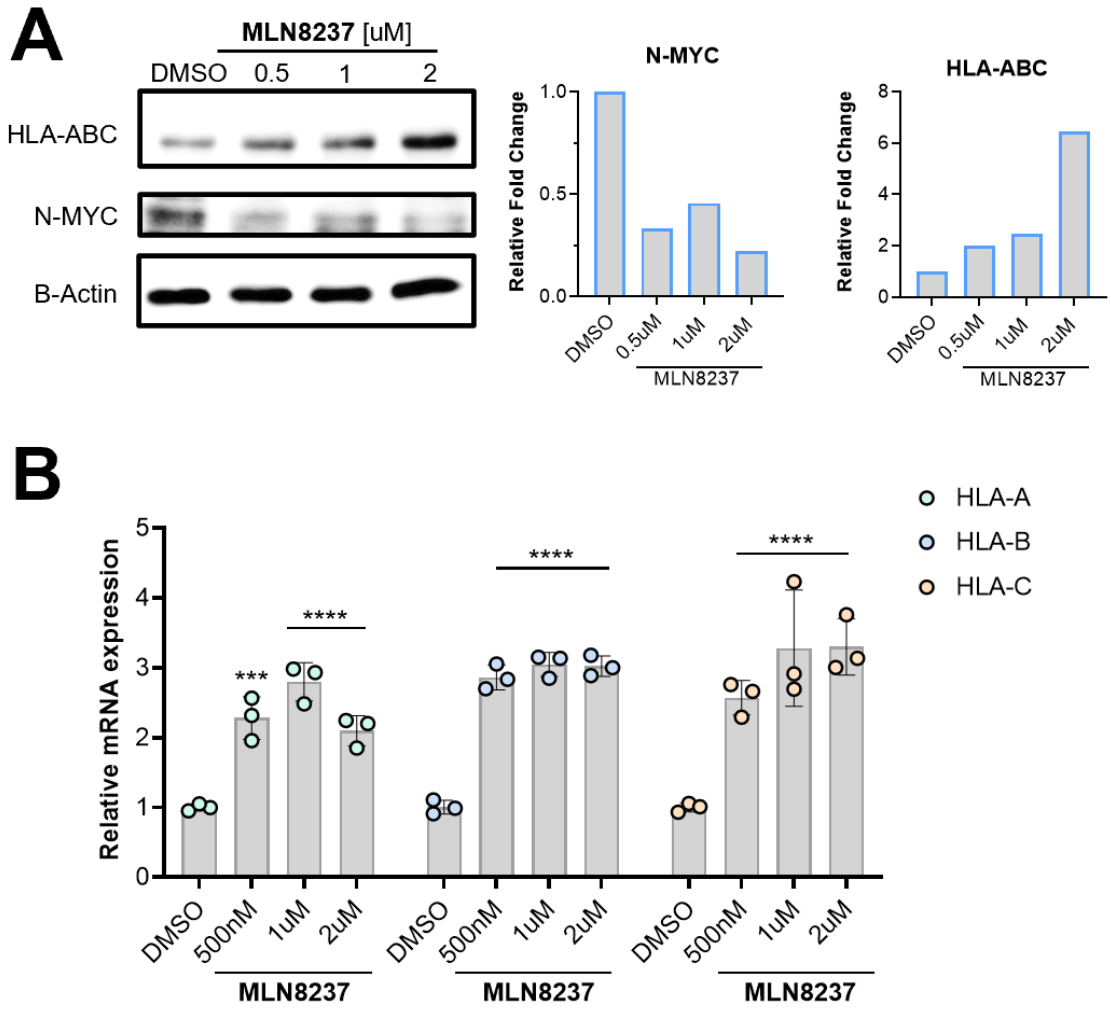

Figure 20. MLN8237 Treatment Decreases N-MYC Expression and Upregulates MHC-I in HPV+HNSCC. A) Western blot of WCL prepared from SCC90 cells treated with MLN8237 or (0.1%)DMSO (Control) and probed for total HLA-ABC or N-MYC. Relative quantification of N-MYC or HLA-ABC compared to B-Actin is depicted in the histograms on the right. **B)** RT-qPCR for relative expression of HLA-A, B, and C, normalized to GAPDH (ΔΔCT), in DMSO or MLN8237 treated cells. Statistical significance was determined by One-way ANOVA relative to DMSO control. ****p<0.0001, ***p<0.001, **p<0.01, *p<0.01. PCR experiments were performed once with three technical repeats per condition. Error bars represent SD.

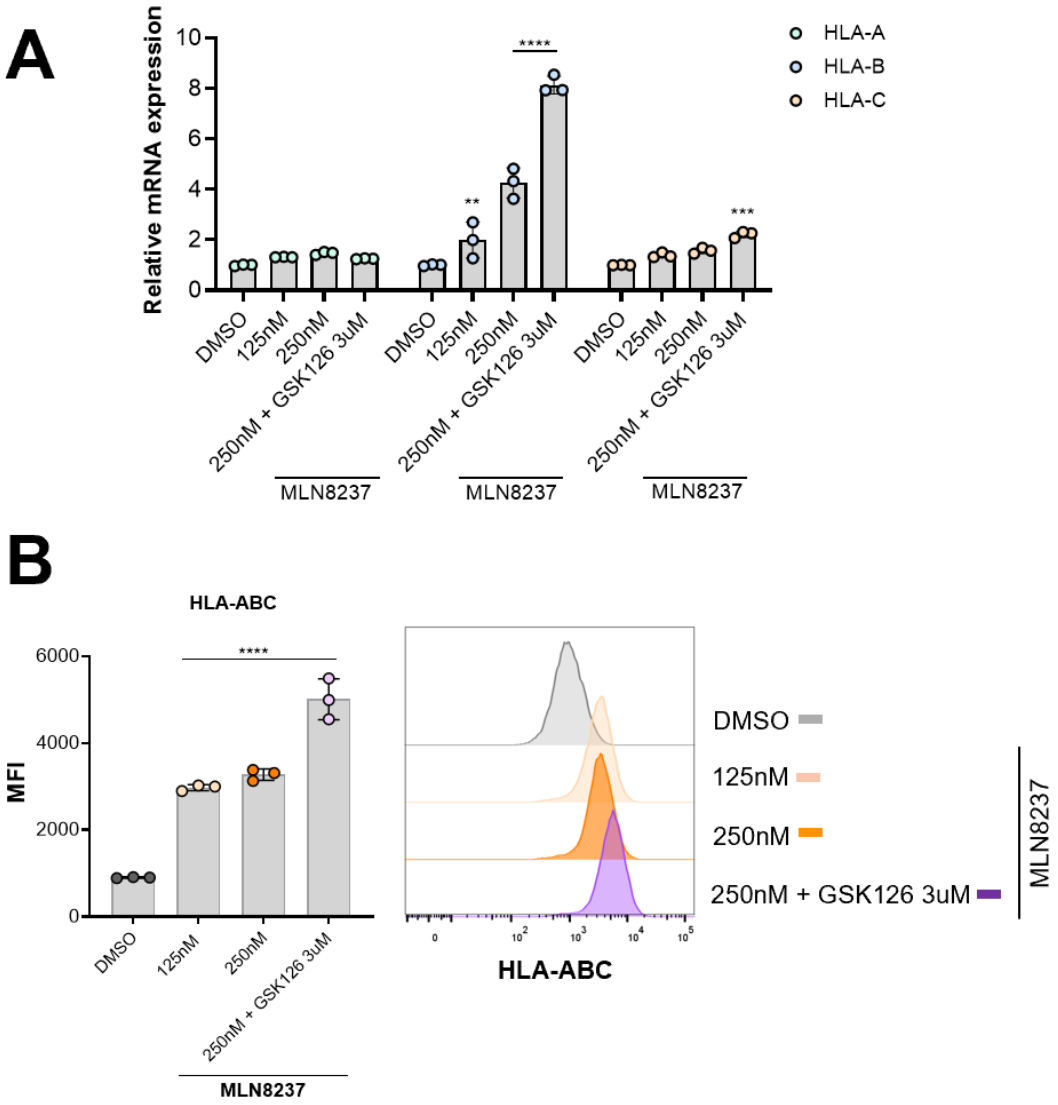

Figure 21. MLN8237 and EZH2i Synergize to Increases Expression of MHC-I. A) RT-qPCR for relative expression of HLA-A, B, and C, normalized to GAPDH (ΔΔCT) with samples prepared from SCC90 cells treated with (0.1%)DMSO or MLN8237. **B)** Surface expression of total HLA-ABC detected by flow cytometry with mean fluorescent intensity (MFI) representing three experiments are shown. Statistical significance was determined by One-way ANOVA relative to DMSO control. ****p<0.0001, ***p<0.001, **p<0.01, *p<0.01. PCR Experiments were performed once with three technical repeats per condition. Error bars represent SD.

MLN8237 Inhibits the Expression of MARCHF8 Ubiquitin Ligase

The E3 ubiquitin ligase MARCHF8 is upregulated in HPV+ HNSCC cell lines and contributes to immune evasion by targeting cell surface immune receptors for degradation, and the upregulation of MARCHF8 was due to increased promoter activation by the c-MYC/MAX complex[45]. Given the similarities in both their homology and activity[401], it is possible that N-MYC and c-MYC could both drive the upregulation of the same gene targets (i.e., MARCHF8). Other reports also do show that MLN8237 treatment reduces c-MYC levels along with N-MYC[420-423], and we hypothesized that MLN8237 treatment will downregulate MARCHF8 expression in our HPV+HNSCC cell lines. To test this, we evaluated the transcript levels of MARCHF8 in SCC90 following treatment with MLN8237. **Figure 22A** shows that MLN8237 reduces the level of MARCHF8 mRNA transcript, and correlates with decreased MARCHF8 protein expression as detected by western blot (**Figure 22B**). Because MYC proteins are known to interact with KAT2A/TRRAP to mediate transcriptional activation[296], and KAT2A can stabilize MYC directly[329], we postulated that depletion of KAT2A would also reduce MARCHF8 levels. **Figure 22C** shows that in both sg-KAT2A treated SCC90 and SCC152 cells, the level of MARCHF8 transcript decreases. Together, these results indicate that MYC proteins co-activated by KAT2A activity drive the transcription of MARCHF8, and that MLN8237 is a bona fide MARCHF8 inhibitor.

Inhibition of AURKA Differentially Regulates PRC2 Expression

It is well established that activated MYC family members upregulate the transcription of various genes[395,424], although in the long-term, this effect can eventually contribute to transcriptional downregulation by the (over)production of repressor proteins[425].

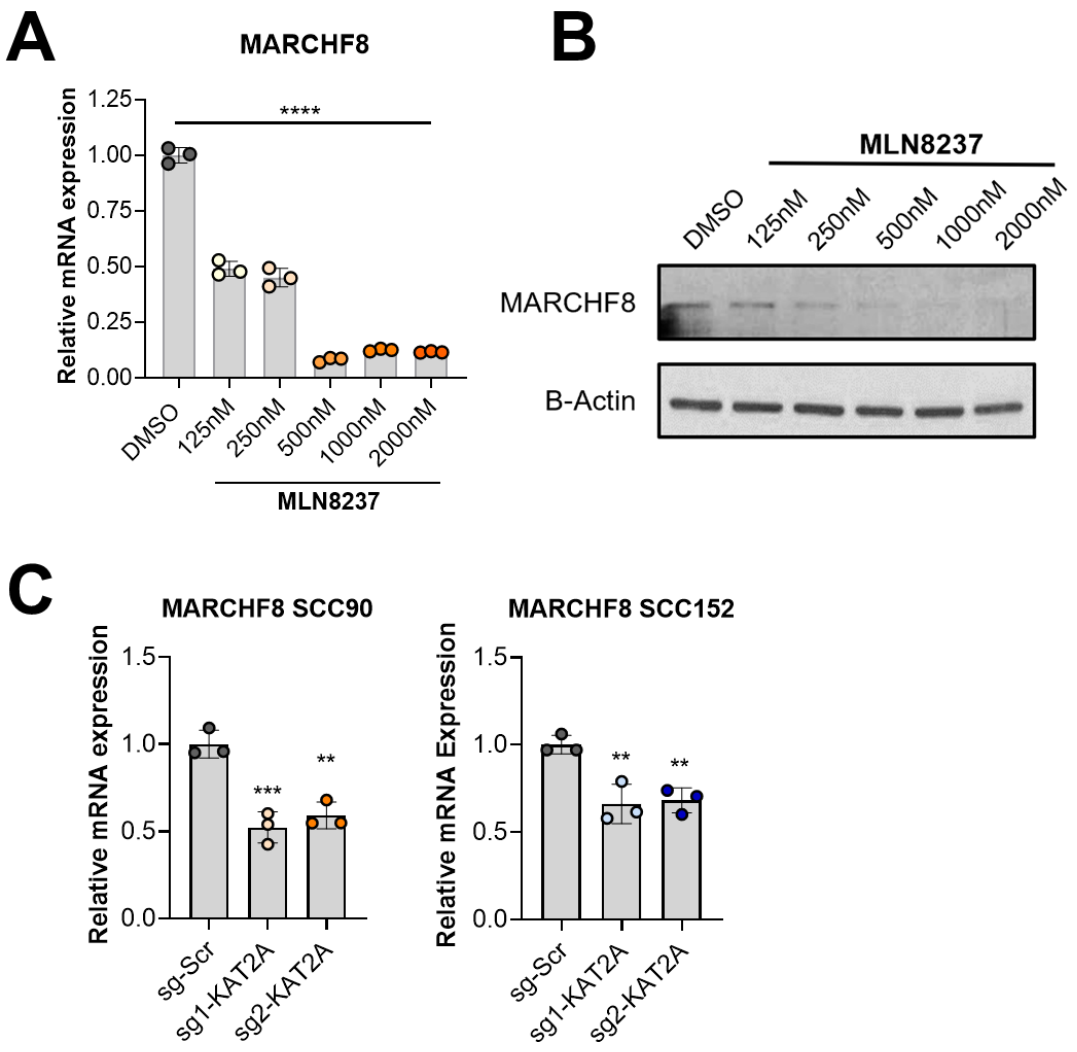

Figure 22. MLN8237 Treatment Decreases MARCHF8 Expression. A) RT-qPCR for relative expression of MARCHF8 normalized to GAPDH (ΔΔCT) in samples prepared from SCC90 cells treated with (0.1%) DMSO or MLN8237. **B)** Using WCL from the same cells compared in (A), total MARCHF8 protein levels are shown by western blot. **C**) RT-qPCR comparing cas9 expressing SCC90 or SCC152 cells transfected with small guide scrambled control (sg-Scr) or sg-KAT2A for the relative expression of MARCHF8 normalized to B-actin (ΔΔCT). Statistical significance was determined by Dunnet's Multiple Comparison Test relative to the DMSO control. ****p<0.0001, ***p<0.001,**p<0.01, *p<0.01. PCR Experiments were performed once with three technical repeats per condition. Error bars represent SD.

Both c-MYC and N-MYC can promote the expression of PRC2 core genes *EZH2*, *EED*, and *SUZ12* through a KAT2A-mediated mechanism[250]. Thus, we hypothesized that

MLN8237 treatment could decrease the expression of PRC2 genes depleting MYC. **Figure 23** shows that with MLN8237 treatment of SCC90 cells, *EED* is significantly downregulated, but the expression of both *EZH2* and *SUZ12* were upregulated. The differential effect of MLN8237 on PRC2 transcript levels suggests that MYC alone is not fully responsible for controlling the expression of PRC2 genes.

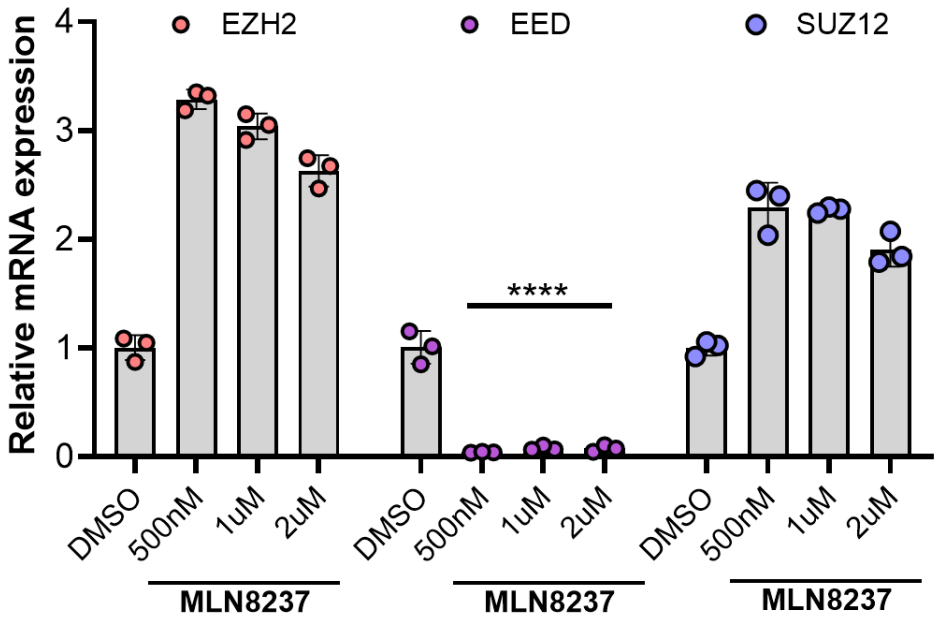

Figure 23. Differential Regulation of PRC2 Genes with MLN8237 Treatment. A) RT-qPCR for relative mRNA levels of EZH2, EED, or SUZ12 normalized to B-actin (ΔΔCT) in samples prepared from SCC90 cells treated with (0.1%) DMSO or MLN8237. Statistical significance was determined by One-way ANOVA relative to DMSO control. ****p<0.0001, ***p<0.001, **p<0.01, *p<0.01. PCR Experiments were performed once with three technical repeats per condition. Error bars represent SD.

MLN8237 Decreases Cell Viability but Increases MHC-I in mEERL Cells

Aurora Kinase A is a mitotic serine/threonine kinase that is tightly linked to cell cycle regulation through control of the mitotic spindle and centrosomes[426]. AURKA peaks in concentration at the G2 to M-Phase transition in the cell cycle[427]. MYC proteins are

also well known for their influence on the cell cycle, mostly affecting the G1 to S-Phase transition[428,429]. We evaluated the effect of MLN8237 on HPV+ mouse cancer cells (mEERL) by measuring their growth and viability. **Figure 24A** shows that with increasing concentration of MLN8237, both cell number (y-axis) and viability (%) decrease substantially after 48hrs of treatment. Compared to DMSO control, the lowest dose of MLN8237 tested, [31.25nM], reduced cell growth by >2-fold, and >10-fold at the highest dose [500nM]. Decreased growth correlated with decreased cell viability as measured by trypan blue staining. Brightfield microscopy images in **Figure 24B** show that MLN8237 treatment alters the morphology of treated cells relative to the DMSO control at 48hrs, with cell diameter appearing to also increase, although direct measurements were not taken. The effects of the drug treatment were observable as early as 24hrs in the lowest treatment dose [31.25nM] (data not shown). Despite the changes in mEERL cell growth, MLN8237 treatment still significantly increased MHC-I transcription (i.e., H2Db and H2K) in similar fashion to the human treated cells (**Figures 24C and 24D**). Taken together, MLN8237 treatment increased MHC-I expression, and reduces the growth of HPV+ tumor cells.

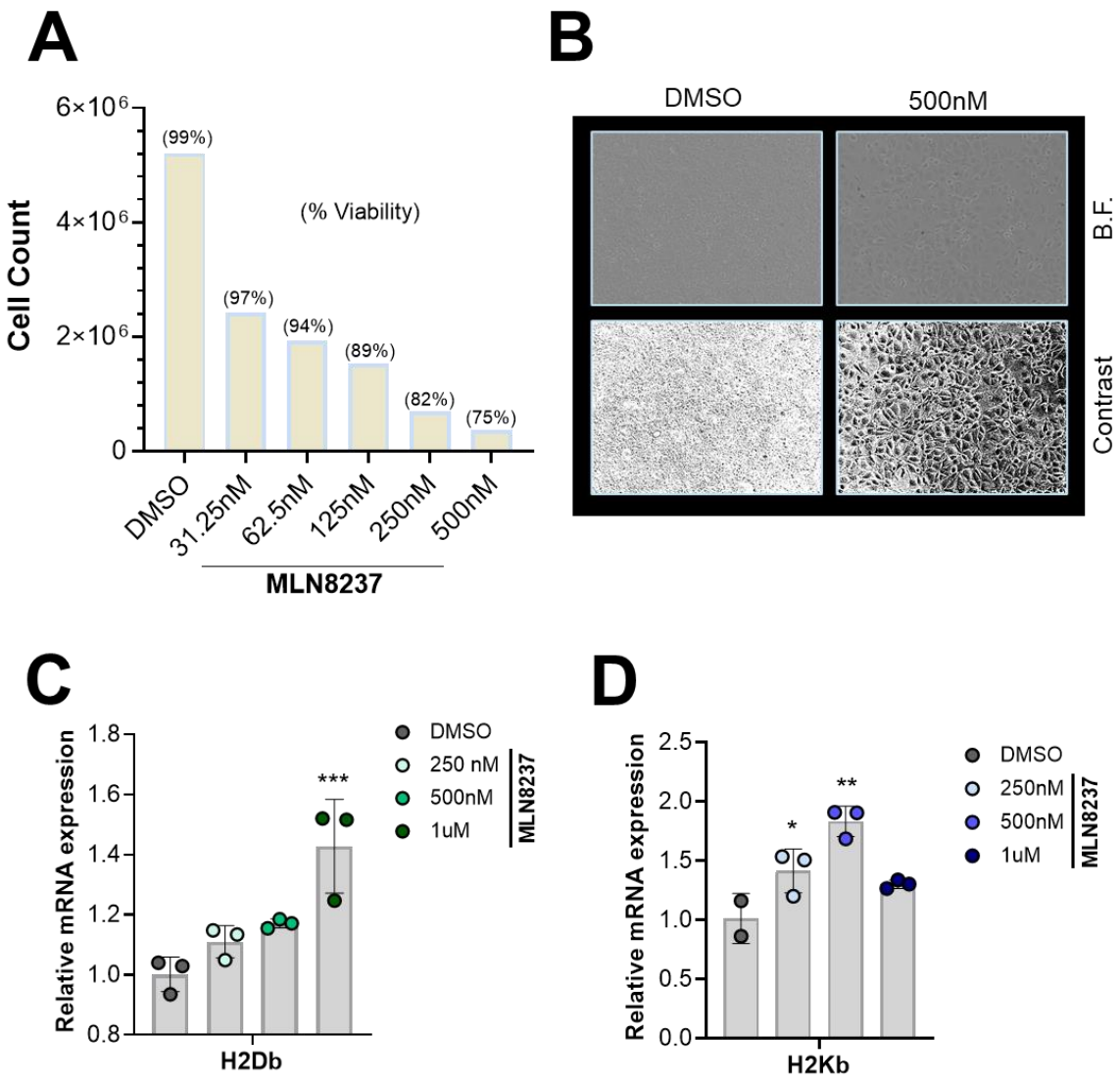

Figure 24. MLN8237 Decreases Cancer Cell Viability. A) Cell growth and viability assay in mEERL cells treated with DMSO or MLN8237. Briefly, cells were treated with DMSO or MLN8237 and incubated for 48hrs. Cells were then collected, stained with trypan blue, and counted. Viability (%) and cell counts were determined by cell cytometer. **C & D)** RT-qPCR for relative mRNA expression of H2Db or H2Kb transcript normalized to mouse B-actin (ΔΔCT) in samples prepared from mEERL cells treated with DMSO or MLN8237. Statistical significance was determined by One-way ANOVA relative to DMSO control. ****p<0.0001, ***p<0.001, **p<0.01, *p<0.01. Experiments were performed once with technical repeats provided as shown. Error bars represent SD.

3.3 Conclusions

We sought to determine the impact of the abnormal expression of N-MYC on MHC-I in HPV+ HNSCC cell lines. Because there is a paucity of direct methods to deplete MYC family members[415], we utilized the AURKAi, MLN8237, and treatment with MLN8237 successfully depleted the level of N-MYC protein in the cell lines tested. Based on our previous findings (**Chapter 2**), we hypothesized that aberrant N-MYC expression may contribute to increased levels of PRC2 and subsequent downregulation of MHC-I expression. MLN8237 treatment of HPV+ HNSCC increased MHC-I expression at the transcriptional level, total protein, and surface expression, and decreased transcript levels of the PRC2 core member, EED. This suggests that N-MYC may be increasing the expression of EED and PRC2 activity, consistent with our hypothesis.

Given that MYC is also responsible for expression of the ubiquitin ligase MARCHF8[45], we hypothesized that disruption of MYC family members with MLN8237 could result in reduced MARCHF8 levels. Indeed, we found that MLN8237 treatment decreased MARCHF8 transcript and total protein levels across multiple experiments, suggesting that MLN8237 may serve as a viable MARCHF8 inhibitor. Lastly, because MYC is coactivated by the SAGA complex through the activity of KAT2A, we hypothesized that KAT2A knockout would also dysregulate transcription of MARCHF8. In multiple HPV+ HNSCC cell lines, knockout of KAT2A decreased the transcript levels of MARCHF8 consistent with our hypothesis. Overall, our findings suggest that N-MYC, coactivated by KAT2A, is driving multiple oncogenic gene expression programs, and that inhibition of N-MYC can increase MHC-I in HPV+ HNSCC.

CHAPTER 4

The chemokine CXCL14 as a potential immunotherapeutic agent for cancer therapy

Part of this chapter was adapted from the original article entitled, "The Chemokine CXCL14 as a Potential Immunotherapeutic Agent for Cancer Therapy" published in Viruses. 2024 Feb 16;16(2):302. doi: 10.3390/v16020302.

Authors: **Nicholas S. Giacobbi**, Shreya Mullapudi, Harrison Nabors, and Dohun Pyeon

Contributions to Science

The work in this chapter was conceptualized by Nicholas Giacobbi, Dr. Dohun Pyeon, and Dr. Yasser Aldhamen. The final figures for this chapter were generated by Nicholas Giacobbi. Experiments were performed by Nicholas Giacobbi, with contributions from Shreya Mullapudi, Harrison Nabors, and Sarah Roosa.

4.1 Abstract

There is great enthusiasm toward the development of novel immunotherapies for the treatment of cancer, and given their roles in immune system regulation, chemokines stand out as promising candidates for use in new cancer therapies. Many previous studies have shown how chemokine signaling pathways could be targeted to halt cancer progression. We and others have revealed that the chemokine CXCL14 promotes antitumor immune responses, suggesting that CXCL14 may be effective for cancer immunotherapy. However, it is still unknown what mechanism governs CXCL14-mediated antitumor activity, how to deliver CXCL14, what dose to apply, and what combinations with existing therapy may boost antitumor immune responses in cancer patients. Here, we provide updates on the role of CXCL14 in cancer progression, examine new pathways that may relate to CXCL14 antitumor immune responses, describe the development and construction of a CXCL14 immunotherapeutic agent.

4.2 Introduction

The Goal of Cancer Immunotherapy

The goal of cancer immunotherapy is to activate antitumor immune responses. To date, the use of chemokines has shown limited efficacy in doing so as monotherapies[104,430]. However, given their critical functions in immune cell regulation, chemokines could still be honed for effective combination immunotherapies[431]. Indeed, some recent studies have shown that the response to immune checkpoint blockade targeting PD-1 and PD-L1 relies on T-cell recruitment by CXCL9 and CXCL10 expression and CXCR3 signaling[432-434]. Inversely, the Combination of BL8040 and Pembrolizumab in Patients with Metastatic Pancreatic Cancer (COMBAT) clinical trial, which examined a CXCR4 antagonist (BL-8040) in combination with a PD-1 inhibitor (pembrolizumab) and chemotherapy, exhibited promising results in treating pancreatic ductal adenocarcinoma[435,436], demonstrating that the negation of specific chemokine signaling may also serve as a viable strategy for effective immunotherapy. Using chemokines has shown an important impact on chimeric antigen receptor (CAR) T-cell therapy. While CAR T-cell therapies have been effective in treating some leukemias, lymphomas, and myelomas, they are less effective in treating solid tumors due to limited CAR T-cell infiltration into the TME[120,437,438]. Thus, attracting T cells by chemokines has been suggested to overcome this limitation of CAR T-cell therapy. For example, Wang et al. utilized an adenoviral vector to express CXCL11[438], which recruits T cells into peripheral tissues [439]. As T cells express high levels of CXCR3, a CXCL11 receptor, CXCL11 could be used as a strong chemoattractant to recruit CAR T cells into the TME. Ultimately, Wang et al. revealed that CAR T-cell therapy alone is ineffective in inhibiting tumor growth and requires the addition of CXCL11 to achieve a significant antitumor response[438]. It is

important to reiterate that although chemokines (or their blockade) can be combined with ICIs or CAR T-cell therapies, an unfettered application of chemokines across situations may be ineffective or even harmful. Thus, prior evidence consistent with an antitumor response and safety in each context should be necessary for selecting chemokines and preparing regimens for treatment.

Developing CXCL14 as an Immunotherapeutic Agent

Based on the antitumor activity of CXCL14 through immune activation in several cancers[38,116,126,127,129,440], we propose that CXCL14 could be used in cancer immunotherapy, particularly in treating HPV+ cancers. This possibility is further supported by the association of high CXCL14 expression with better patient survival in multiple cancers, including HNSCC and CxCa[125]. Furthermore, new evidence from Pan et al. has shown that CXCL14 expression is associated with an enhanced response to immunotherapy in renal cell carcinoma[441].

CXCL14 has many beneficial features as a therapeutic agent. CXCL14 is a small soluble protein with a size of ~10 kDa and can be delivered by several different vehicles, such as viral vectors, liposomes, and nanoparticles. Because CXCL14 is constitutively expressed by many cell types throughout the body for maintaining homeostasis[98], it is less likely to trigger any adversary effects commonly caused by proinflammatory chemokines[442]. This could be a key advantage of using CXCL14 compared to other cytokines (e.g., IL-2), many of which have been shown to cause high toxicity or trigger immune suppression via regulatory T cells[443]. Lastly, CXCL14 has dual functions in enhancing antitumor responses by recruiting natural killer (NK) and T cells into the TME and upregulating MHC-I expression on tumor cells to enhance antigen

presentation[98,125,126,441]. Thus, CXCL14 has great potential as an immunotherapeutic agent in novel combination immunotherapy with an ICI, particularly for ICI nonresponders.

Understanding the Mechanism of CXCL14-Mediated Tumor Suppression

CXCL14 upregulates MHC-I expression in HPV+ HNSCC cells and increases the infiltration of NK, CD4+, and CD8+ T cells into the TME[125]. However, the native CXCL14 receptor(s) and their signaling pathways required for MHC-I upregulation and immune cell chemotaxis remain to be elucidated. Tanegashima et al. found that CXCL14 binds to CpG oligodeoxynucleotides (ODNs) to induce toll-like receptor 9 (TLR9) signaling in dendritic cells[444]. Later, it was identified that the N-terminal loop structure of CXCL14, distinct from other CXC chemokines, is required for DNA recognition and internalization[445]. TLR9 activation also requires the N-terminal domain at amino acids 1–12 and the 40S loop at amino acids 41–47[445]. The evidence related to TLR9:CXCL14 signaling may also explain the orphan receptor status of CXCL14 with its activity outside the paradigm of typical CXC-CXCR receptor interactions. On the other hand, Witte et al. have shown that CXCL14 binds to CXCR4 to mediate platelet and monocyte chemotaxis[446], but the possibility of CXCR4 as the receptor for CXCL14 is controversial and lacks a definitive conclusion[447-450]. Despite these findings, it is still unclear whether TLR9 and/or CXCR4 are involved in MHC-I upregulation and/or NK and T cell recruitment by CXCL14. Although CXCR4 is highly expressed on T cells and is important for T cell chemotaxis[451], there is no evidence that the CXCL14-CXCR4 axis plays any role in T cell recruitment to the TME. Kouzeli et al. have shown that CXCL14 synergistically enhances interactions of CXCL13, CCL19, and CCL21 with their receptors to increase immune cell chemotaxis *in vitro*[452]. Thus, it is possible that CXCL14 plays a broad and non-linear role in MHC-I upregulation and lymphocyte chemotaxis beyond a direct ligand-receptor interaction.

Developing Effective Delivery Tools for CXCL14

A pharmacologic approach to restore CXCL14 may be possible using the DNA methyltransferase inhibitor (DNMTi) decitabine (5-aza-2'-deoxycytidine). We have previously shown that decitabine treatment reverses CXCL14 promoter hypermethylation and upregulates CXCL14 expression in HPV+ cancer cells[126]. Other groups have also shown the effectiveness of decitabine in upregulating CXCL14 to treat cancer[118,453,454]. However, the expression of many genes is affected by DNA methylation. Given the global impact on DNA methylation by decitabine, treatment may cause undesired effects and/or drug-related toxicity in patients beyond restoring CXCL14 expression. Thus, developing methods for the ectopic delivery of CXCL14 may be necessary to use CXCL14 as an immunotherapeutic agent. Potential methods for CXCL14 delivery include the administration of recombinant CXCL14 protein directly into the TME and CXCL14 gene using nanoparticles, liposomes, or viral vectors. Because each method has clear advantages and disadvantages, as previously documented[455-458], effective CXCL14 delivery may depend on these technical limitations and patients' circumstances (e.g., immunocompromised condition). For instance, the direct application of recombinant CXCL14 protein may be challenged by the lack of posttranslational modifications required for its proper functions[113,459]. Nanoparticles and liposomes have been shown to be effective in previous cancer therapies but are still limited by their route of administration and biodistribution[460]. On the other hand, viral vectors, such as adenovirus and vaccinia virus, have been shown to effectively deliver chemokine genes and boost antitumor immune responses as an additional benefit, given their documented role in innate immune activation[461,462]. Conversely, pre-existing immunity can quickly eliminate these viruses

and block successful CXCL14 delivery[463]. Thus, further tests are warranted to determine the most effective methods for CXCL14 delivery.

CXCL14 Therapeutic Dose and Combination Therapy

Determining the CXCL14 levels required for inducing effective antitumor immunity while being safe for a patient to receive is crucial for the success of using a CXCL14 immunotherapeutic agent. We have previously shown that restoring the physiological levels of CXCL14 in HPV+ HNSCC cells significantly suppresses tumor growth in immunocompetent syngeneic mice[126]. Our results support the notion of CXCL14-stimulated antitumor immunity for treating HPV+ HNSCC, however the optimal therapeutic dose of CXCL14 for a human patient is still unknown. Furthermore, given that tumorigenic mechanisms can be unique to each patient and coupled with the elaborate complexities of individual TMEs[464,465], the effective level of CXCL14 required for individual treatment may vary significantly among different patients. Even if therapeutic levels of CXCL14 could be clinically attained, the local application of CXCL14 to (or from) a single tumor site may not instigate an adequate immune response to promote cancer clearance in patients with advanced metastatic disease. This point is especially relevant in HPV+ HNSCC, where ~50% of cases have an unidentified primary tumor, and cells have already migrated from the initial tumor site[466]. Although some studies have indicated that high systemic levels of CXCL14 are safe in humans or mice[119,467], applying CXCL14 systemically may be impractical and still have unforeseen negative consequences. Thus, the local administration of CXCL14 directly into the TME could be an alternative approach to induce adaptive antitumor immune responses in combination with other immune-modulating therapies (e.g., a tumor vaccine). Previous studies have shown that delivering HPV epitope vaccines results in tumor suppression[209,212]. Thus, we hypothesize that

combinations of CXCL14 with an HPV tumor vaccine will further augment antitumor responses by enhancing T-cell infiltration and MHC-I antigen presentation, leading to robust tumor suppression[125,126]. From this basis, we sought to further explore the properties of CXCL14 related to its antitumor mechanisms and to prepare a CXCL14 transgene immunotherapy for the stimulation of antitumor immunity.

4.3 Results

Optimizing CXCL14 Protein Stability

To begin development of an effective CXCL14 immunotherapy, the protein stability of CXCL14 (and chemokines generally) needs to be improved due to its short half-life[468]. Based on a previous report of protein degrons, the amino acid motifs that facilitate protein degradation, we hypothesized that the deletion of two consecutive glutamates (CXCL14-dEE) at the carboxy-terminus stabilizes CXCL14 protein[98,469]. To test the hypothesis, we first analyzed the structure of CXCL14-dEE compared to wildtype CXCL14 (CXCL14-WT), using AlphaFold[470,471] and SWISS-MODEL[472-476]. The *in silico* analysis of the CXCL14-dEE structure did not show any significant alterations in protein folding or tertiary conformation compared to CXCL14-WT, except the minor changes from the truncation of the two glutamates (**Figure 25**).

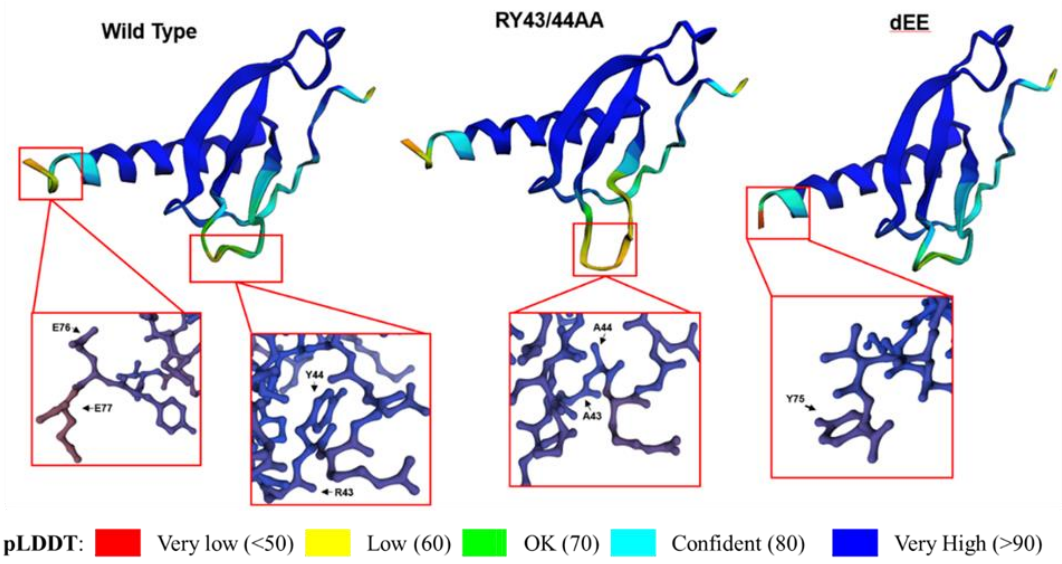

Figure 25. *In silico* structural analysis of wildtype and mutant CXCL14 proteins. Predicted folding representation of wildtype CXCL14, CXCL14-RY43/44AA, and CXCL14-dEE proteins were generated in ColabFold (v. 1.5.2), based on AlphaFold2[470,471]. Full protein structures are shown, along with detailed representations of mutated regions (red boxes) generated in SWISS-MODEL Workspace[472-476].

Figure 25. (Cont'd)
AlphaFold-predicted local distance difference test (pLDDT) represents a per-residue confidence score for each amino acid in the full peptide corresponding to the colored key.

To examine the functional changes of deleting the two glutamates, we performed cycloheximide (CHX) chase assays with MG-132-treated 293T cells expressing CXCL14-WT or CXCL14-dEE. Replacing MG-132 with CHX permits the evaluation of protein stability over time by inhibiting de novo protein synthesis (**Figure 26A**). MG-132 treatment does not increase levels of CXCL14-dEE to match that of CXCL14-WT, and subsequent CHX treatment showed a greatly reduced half-life of CXCL14-dEE. This result suggests that CXCL14-dEE is significantly less stable than CXCL14-WT. Additionally, Peterson et al. have shown that mutations in the "destruction-box" at arginine-43 and tyrosine-44 in CXCL14 stabilize CXCL14 protein by eliminating the E3 ligase recognition site (CXCL14-RY43/44AA)[477]. As expected, our *in silico* prediction of CXCL14-RY43/44AA protein structure showed no major changes compared to CXCL14-WT (**Figure 26A**). CHX treatment significantly enhanced the protein stability of CXCL14-RY43/44AA compared to CXCL14-WT, which is consistent with the previous result[477]. Interestingly, when cells were treated with CHX or MG-132 alone, CXCL14-RY43/44AA showed modest but consistently higher protein levels relative to CXCL14-WT. Additional chase experiments with brefeldin A treatment showed that CXCL14-RY43/44AA accumulated significantly faster than CXCL14-WT (**Figure 26B**). This suggests that the RY43/44AA mutation could contribute to increasing intracellular CXCL14 levels by limiting its secretion. However, this possibility should be confirmed by further investigation.

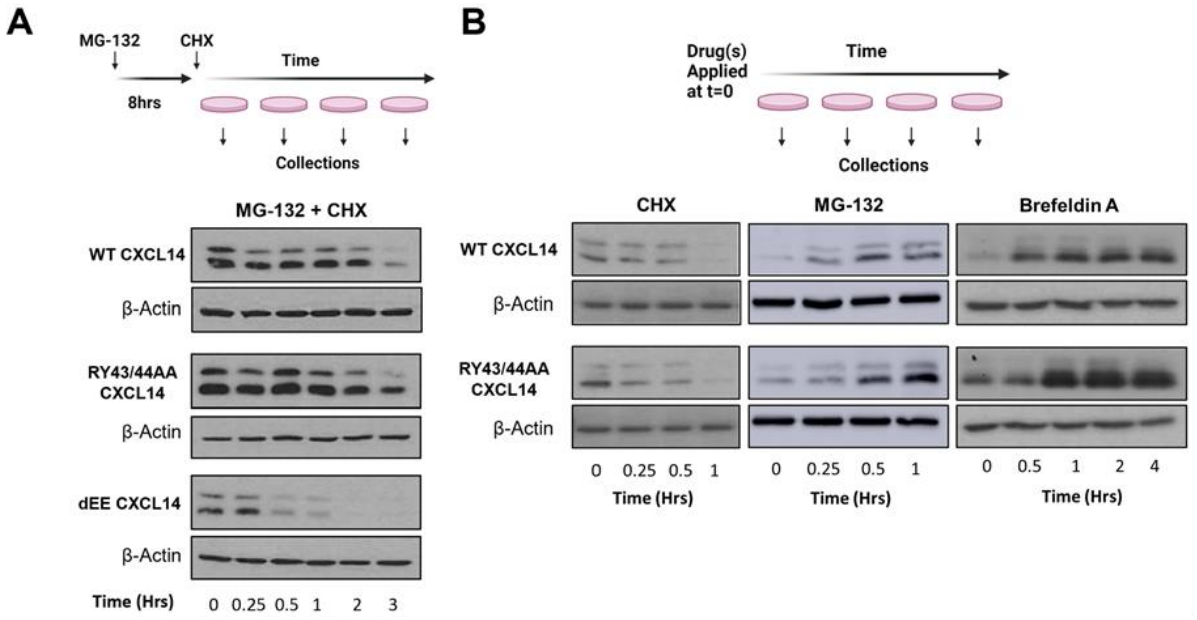

Figure 26. Protein stability of wildtype and mutant CXCL14 proteins. **A)** Western blots with whole cell lysate prepared from 293T cells transiently transfected with pCDH_ wild type CXCL14 (CXCL14-WT), CXCL14 with RY43/44AA substitution (CXCL14-RY43/44AA), or CXCL14 with the deletion of two glutamates at the C-terminus (CXCL14-dEE). After 24 h, cells were treated with MG-132 [10 μM] for 8 h and CHX [50 μg/mL] as previously described[45]. **B)** Western blots with whole cell extract prepared from 293T cells transiently transfected with CXCL14-WT or CXCL14-RY43/44AA. After 24 h, cells were treated with MG-132, CHX, or Brefeldin A [5 μg/mL]. Illustrations created with BioRender.com.

CXCL14 Expression Inhibits Virus Growth

Given the downregulation of CXCL14 during the course of HPV infection and cancer progression[126], it may be that HPV evolved to downregulate CXCL14 expression as part of an immune evasion strategy. To examine the potential of CXCL14 antiviral activity, we evaluated virus growth with the over-expression of CXCL14. CXCL14 was over-expressed for 24 hours in 293FT cells, then cells were challenged with increasing multiplicities of infection (MOI) of adenoviral vectors expressing green fluorescent protein (Ad5-GFP). At 72hrs post infection, we quantified the level of GFP by fluorescent microscopy to gauge the proportion of virally infected cells. Importantly, Ad5-

adenoviruses replicate in 293FT cells by receiving the virus oncoprotein E1A *in trans* (from the cells) and with the remainder of the viral genome in the Ad5 vector. The expression of GFP from the Ad5 following infection provides a proxy signal for the relative measurement of viral gene expression and growth. **Figure 27A** illustrates our experimental setup. Figure **27B** exemplifies the brightfield and GFP channel images analyzed in the experiment. The level of CXCL14 protein expression after 72hrs post infection is shown by western blotting of whole cell lysate (WCL) (**Figure27C**). In **Figure 28A**, the histogram depicts the quantification of GFP signal in CXCL14 cells versus mock control cells. We found that in the cells overexpressing CXCL14, there was a significantly reduced GFP signal compared to control cells, corresponding to reduced virus infection at nearly all MOIs tested. A similar repeat experiment was performed (**Figure 28B**), and again, over expression of CXCL14 inhibited virus propagation across MOIs in our experimental system compared to empty vector control (**Figure 28B**).

As an alternative approach to evaluate the effect of CXCL14 on virus growth, we performed a head-to-head growth comparison of Ad5-GFP and adenovirus expressing CXCL14 (Ad5-CXCL14) in 293T cells. We infected cells with equal amounts of virus,and quantified virus growth over time by collecting supernatant and calculating the absolute number of virus genomes by qPCR[478]. **Figure 29** provides an illustration of our experimental scheme. Strikingly, the growth of Ad5-CXCL14 was significantly reduced (>30-fold) during the exponential growth phase of the virus (48 to 72hrs) relative to Ad5-GFP (**Figure 30A**). **Figures 30B and 30C** show that both GFP and CXCL14 expression increases at similar rates from 18-96hrs, peaking at around 72hrs post infection. This indicates that the expression of CXCL14 negatively correlates with the significantly reduced levels of Ad5-CXCL14 virus (compared to Ad5-GFP) and suggests that CXCL14

is inhibiting virus growth. Overall, the results from **Figures 2 & 4** indicate that CXCL14 inhibits virus growth and may suggest that CXCL14 has an antiviral function.

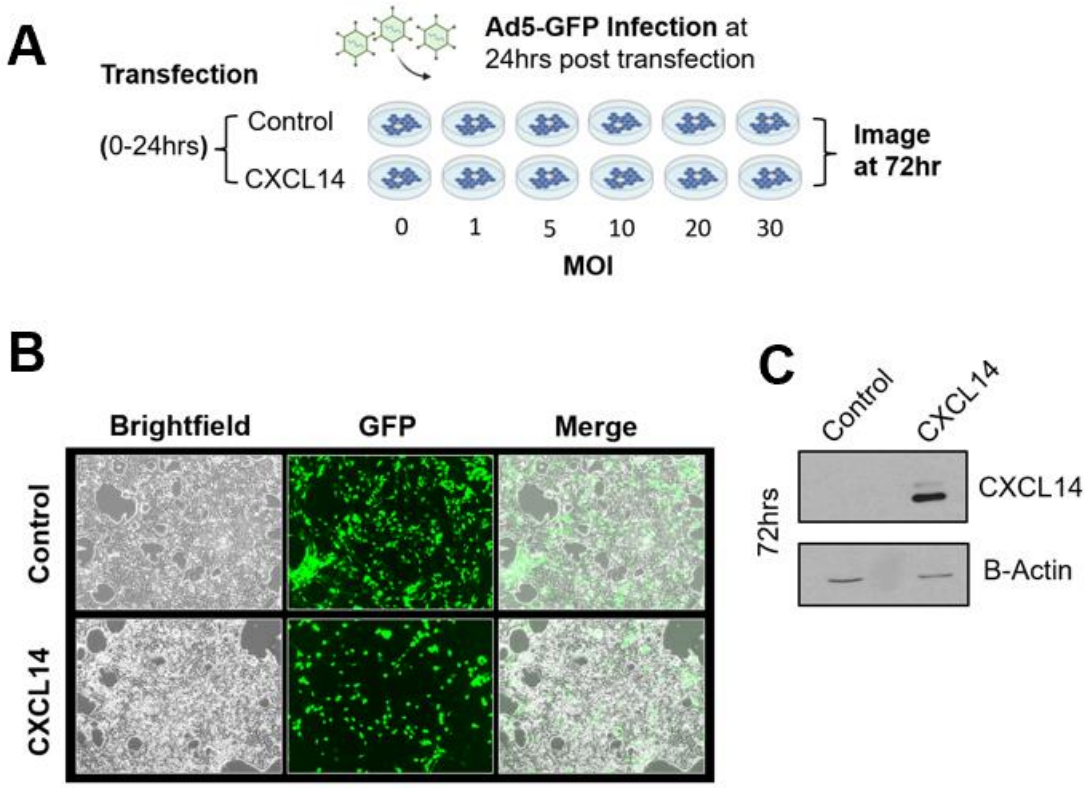

Figure 27. CXCL14 Expression and Ad5-GFP Infection. A) Illustrated experimental setup to compare effect of virus growth in the presence of CXCL14. Briefly, 5e5 293FT cells were plated on day one and transfected with pCDH_CXCL14-3xFLAG the next day. 24-hrs post transfection, cells were infected with Ad5-GFP at their respective MOI. 72-hrs post infection, GFP signal was captured by fluorescent microscopy and quantified by ImageJ software. **B)** Examples of brightfield and GFP images analyzed and compared in the experiment. **C)** Western Blot of WCL from cells transfected with pCDH_CXCL14-3xFLAG or mock transfected control. WCL was probed for CXCL14 (anti-FLAG) or beta-actin (loading control). Illustrations created with BioRender.com.

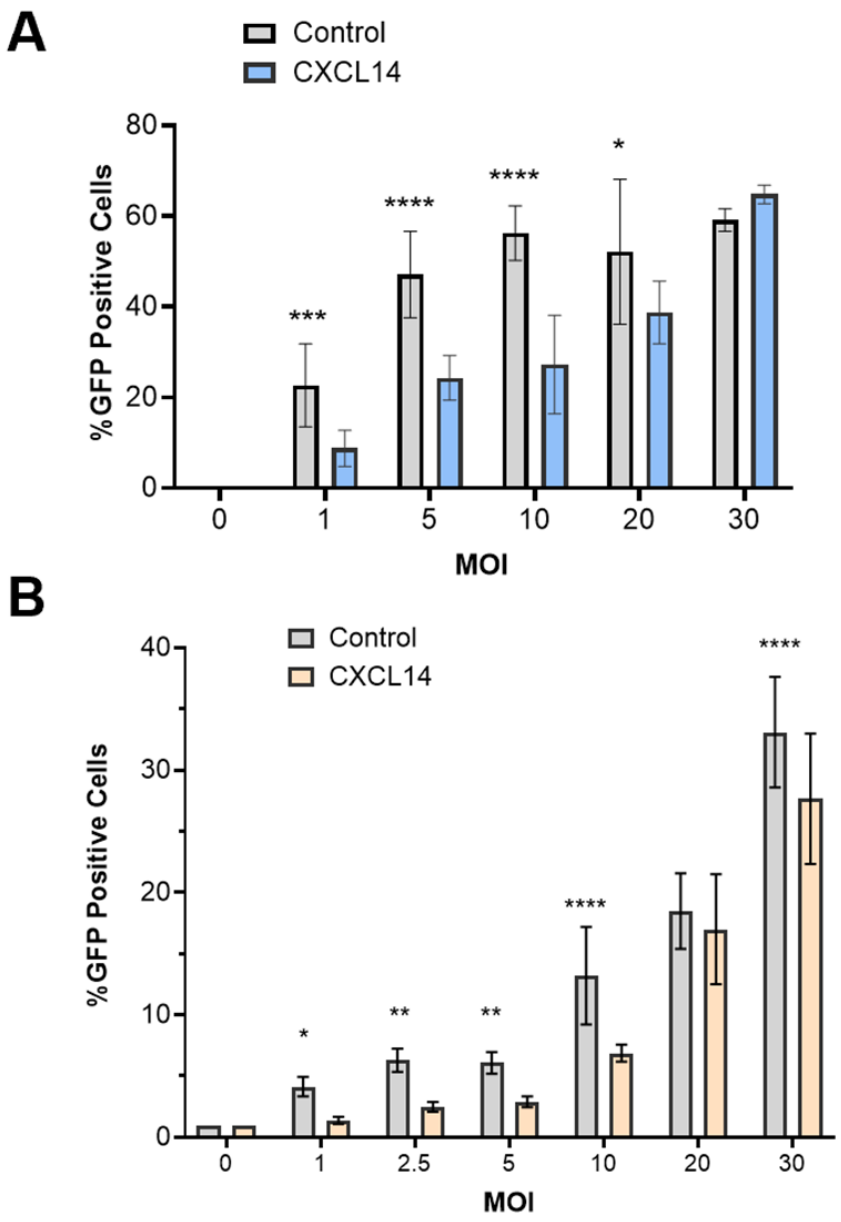

Figure 28. CXCL14 inhibits adenoviral growth. Following transfection of CXCL14 for 24hrs, cells were challenged with Ad5-GFP at increasing MOIs. Virus input (vp/mL) was determined as described[479]. GFP signal was captured by fluorescent microscopy at 72 hours post infection. GFP positive signal relative to the total brightfield area of cell coverage was estimated using ImageJ software (%GFP Positive Cells). Significance was calculated by Fisher's Least Significant Difference test. ****p<0.0001, ***p<0.001, **p<0.01, *p<0.05. Error bars represent SD. **A)** Compares 293FT cells transfected with pCDH-CXCL14 to mock transfected controls. **B)** Compares 293FT cells transfected with pLenti6-CXCL14 to pLenti6-empty vector control.

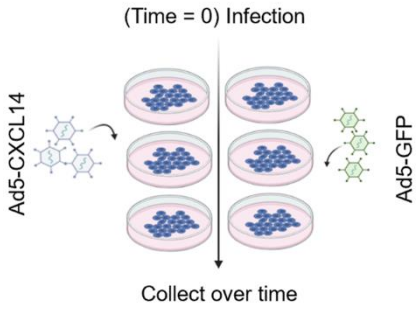

Figure 29. Experimental Setup of Ad5-GFP versus Ad5-CXCL14 Growth. Approximately 1e6 293FT cells were plated in parallel in individual 3.5cm dishes corresponding to each time point (0, 6, 18, 24, 48, 72, or 96hrs). Equal virus inputs (1e10 viral genome copies) of Ad5-CXCL14 or Ad5-GFP input were added to each respective plate in a final volume of 2mL. At each timepoint, total supernatant was collected and frozen at -80°C. From each supernatant, virus DNA was purified and used to measure absolute genome copy numbers. Resultant values are plotted in **Figure 30A**. Illustrations created with BioRender.com.

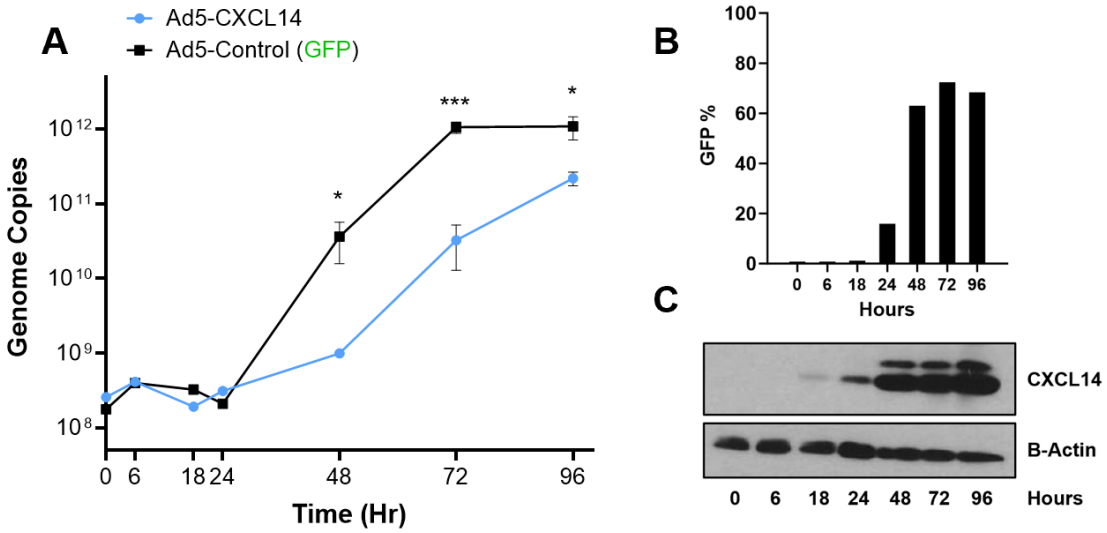

Figure 30. CXCL14 Expressing Adenovirus Demonstrates Attenuated Growth. A) Quantification of viral genome copies by RT-qPCR at each time point from Ad5-CXCL14 or Ad5-GFP viral infections. **B)** Expression of GFP signal overtime from cells infected by Ad5-GFP. The %GFP-positive cells were measured via fluorescent microscopy and quantified by Image J software. **C**) Western blot of whole cell lysates probing for CXCL14-3xFLAG prepared from 293FT cells infected with Ad5-CXCL14. Significance was

Figure 30. (Cont'd)
calculated using Student' T-test. ****p<0.0001, ***p<0.001, **p<0.01, *p<0.05. Error bars represent SD. Illustrations created with BioRender.com.

CXCL14 Downregulates Integrin Receptor Expression

To elucidate on the mechanisms underlying decreased virus growth with the overexpression of CXCL14, we considered viral entry as a possible point where CXCL14 may restrict the virus. Both papillomaviruses and adenoviruses utilize common receptors to enter host cells (e.g., integrins) and initiate infection[480-483]. For example, Integrin alpha V beta5 (αvβ5) is a protein heterodimer used to bind the cell to extracellular matrix[484], and is required for internalization of adenovirus, with some evidence even suggesting it as a primary receptor for virus attachment[485,486]. Several integrins subunits, with ITGA5 among them, were upregulated and were associated with high-risk HPV+ HNSCC and cervical cancer groups[481], suggesting possible involvement with HPV infections as well. However, we are unaware of evidence that shows CXCL14 can regulate the expression of integrins, but given the possible importance of integrin expression in HPV+ HNSCC[481] and viral entry, we chose to evaluate if CXCL14 can affect integrin expression. Following Ad5-GFP infection, the relative mRNA expression of the integrin subunits, ITGAV or ITGB5, were quantified. **Figure 31** indicates that both ITGAV and ITGB5 transcription was significantly downregulated at the time of infection in cells expressing CXCL14 relative to control cells, but the effect on ITGB5 was more dramatic. There was also a steady increase in the level of ITGB5 mRNA level over the course of infection, although levels did not meet control values (**Figure 31B**). These observations suggest that the expression of the integrin αvβ5 subunits could be regulated by a CXCL14-mediated pathway. Additionally, the increase in ITGB5 over time might suggest a virus-related mechanism to increase ITGB5

expression and cellular susceptibility. This data may help to explain the meaning of HPV downregulation of CXCL14, along with a need for ITGB5 to help viral entry[485]. However, more studies are required to confirm this possibility, to establish that CXCL14 is regulating integrin expression, and if it is truly related to an antiviral mechanism.

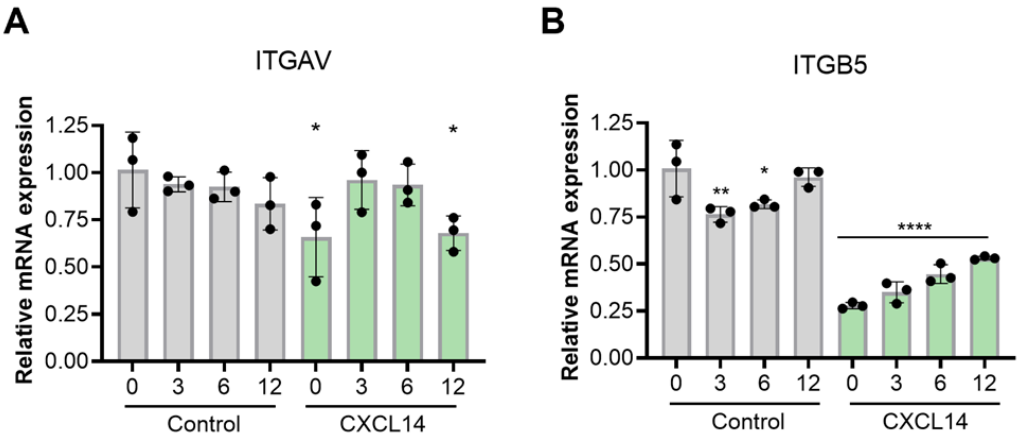

Figure 31. CXCL14 Downregulates Integrin Expression. Relative mRNA expression (ΔΔCT) by RT-qPCR, normalized to GAPDH control for ITGAV (**A**) or ITGB5 (**B**) expression. Following mock (control) or CXCL14 transfection, cells were infected by Ad5-GFP (MOI=5). Cells were collected at corresponding time points (0, 3, 6, and 12hrs post infection) for total RNA purification and downstream RT-qPCR. Significance p-values were calculated using Dunnett's Multiple Comparisons Test. ****p<0.0001, ***p<0.001, **p<0.01, *p<0.05. Experiments were performed once with three technical replicates per condition. Error bars depict SD.

CXCL14 Activates TLR9 Signaling

During HPV infection, host cells can detect viral double-stranded DNA (i.e., unmethylated CpG dsDNA) via Toll-like receptor 9 (TLR9) and subsequently induce an immune response which can lead to increased MHC-I expression[487]. However, HPV has evolved counter-mechanisms which can block TLR9 signaling[74,75]. CXCL14 can bind to CpG oligodeoxynucleotides (ODNs) to induce TLR9 signaling as part of an adaptive immune mechanism[444]. Therefore, we hypothesized that CXCL14 augments activation of

TLR9 signaling to mediate control of viral infections. We quantified TLR9 activation following the overexpression of CXCL14 and Ad5-GFP infection over time. **Figure 32** shows the relative mRNA expression levels of interleukin-12a (IL-12a) as a read-out of TLR9 activation[445]. We also quantified the level of tumor necrosis factor alpha (TNF-α) and interleukin-1β (IL-1b) for comparison. Relative to the control sample, CXCL14 expression increased the level of IL-12a transcript significantly at 0hr (prior to infection). IL-12a levels peaked at 3hrs post infection in the CXCL14 expressing cells, then appeared to retract later at 6 and 12hrs. Control cells also showed increased IL-12a signal, but they did not reach statistical significance until 12hrs post infection, and overall, were lower when compared to CXCL14 expressing cells at matching timepoints. This suggests that CXCL14 expression affects TLR9 activation. In contrast, TNF-α signaling did not demonstrate significant changes between control and CXCL14 expressing cells, but the relative levels of TNF-α expression did trend upward overall. For example, at 3hrs post infection, the CXCL14 group narrowly missed significance with $p=0.0527$, and may indicate some influence by CXCL14 and/or cellular response to the virus. Lastly, IL-1b signal was below our threshold of detection in both the experimental and control groups, and may be unaffected by CXCL14 (data not shown). Taken together, these results suggest that CXCL14 is influencing TLR9 activation and may help contribute to an antiviral mechanism.

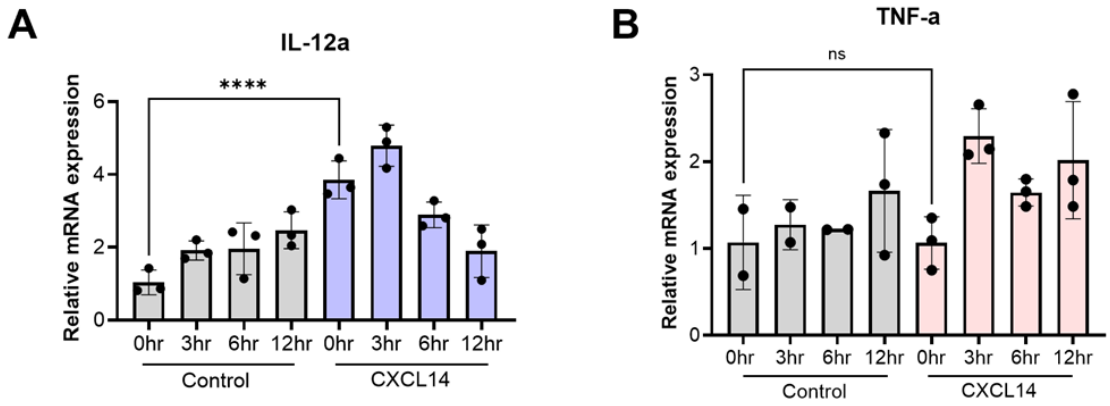

Figure 32. CXCL14 Activates TLR9 Signaling. Relative mRNA expression by RT-qPCR, normalized to GAPDH control (ΔΔCT) for IL-12a **(A)** or TNF-α **(B)** expression. Following mock (control) or CXCL14 transfection, cells were infected by Ad5-GFP (MOI=5). Cells were collected at corresponding time points (0, 3, 6, and 12hr) and analyzed as above by RT-qPCR. Significance p-values were calculated using Dunnett's Multiple Comparisons Test. ****p<0.0001,***p<0.001, **p<0.01, *p<0.05. Experiments were performed once with technical replicates as shown. Error bars depict SD.

Adenoviral Transgene Vector Construction for Delivery of CXCL14 and HPV Epitope Vaccine

We have prepared a novel transgene cassette comprised of the mature mouse CXCL14 (lacking signal peptide) chemokine with a 3xFLAG tag, a P2A self-cleavage site from porcine teschovirus-1[488], and a chimera of five fused truncated viral epitopes from HPV16 E6 and E7 (HPV-Epitopes) which are flanked by a human calreticulin signal peptide (spCRT) and KDEL sequences (**Figure 33A**). The HPV epitope chimera incorporates regions with predicted immunogenicity and presentation via MHC-I, as calculated by the Immune Epitope Database & Tools (IEDB) (**Table1**)[489,490]. **Table 1** shows the allele, peptide sequence, and score for peptides which are predicted to be presented via MHC-I from the chimera sequence. The cassette design provides space to incorporate two open reading frames separated by the P2A site for efficient expression

Allele	Length	Peptide	Score	Rank
HLA-A*01:01	10	HGDTPTLHEY	0.853261	0.05
HLA-B*57:01	9	RAHYNIVTF	0.829208	0.18
HLA-B*58:01	9	RAHYNIVTF	0.765275	0.14
HLA-A*01:01	9	VAEPDRAHY	0.743705	0.08
HLA-A*68:02	10	ETTDLTIHDI	0.723534	0.08
HLA-B*40:01	9	LEDLLMGTL	0.712717	0.15
HLA-B*15:01	9	RAHYNIVTF	0.699828	0.13
HLA-A*32:01	9	RAHYNIVTF	0.686351	0.04
HLA-A*02:01	9	YMLDLQPET	0.683365	0.14
HLA-A*68:02	10	EVYDFAFRDL	0.639435	0.11
HLA-B*35:01	9	VAEPDRAHY	0.617238	0.16
HLA-A*02:06	9	YMLDLQPET	0.608163	0.16
HLA-A*02:01	9	TLHEYMLDL	0.587294	0.21
HLA-B*15:01	9	TLRLCVEVY	0.553514	0.24

Table 1. Immune Epitope Database & Tools Analysis of HPV E6 and E7 sequence. Predicated peptides for loading into class I HLA- alleles and their corresponding immune score generated by IEDB (http://tools.iedb.org/main/).

of both CXCL14 and HPV-Epitopes[488]. The spCRT and KDEL sequences flanking the HPV-epitopes promote endoplasmic reticulum retention which contributes to enhanced presentation of viral epitopes via MHC-I for robust T cell responses, as previously shown in HPV+ HNSCC[491]. **Figure 33B** shows a western blot of WCL from 293T cell transiently transfected with the full gene cassette versus controls. Both the full-length version and the ribosomal skip fragments (“cleaved” product) of CXCL14 and HPV-Epitope products were detected (**Figure 33B**)[492]. At longer exposure times, the E7 antibody was also able to detect the full-length expression (data not shown). **Figure 34** summarizes the overall mechanism we predict the transgene therapy can achieve. Based

on this mechanism, we hypothesize that the expression of the CXCL14 and HPV-epitope cassette in tumor cells will drive antitumor immunity leading to their clearance.

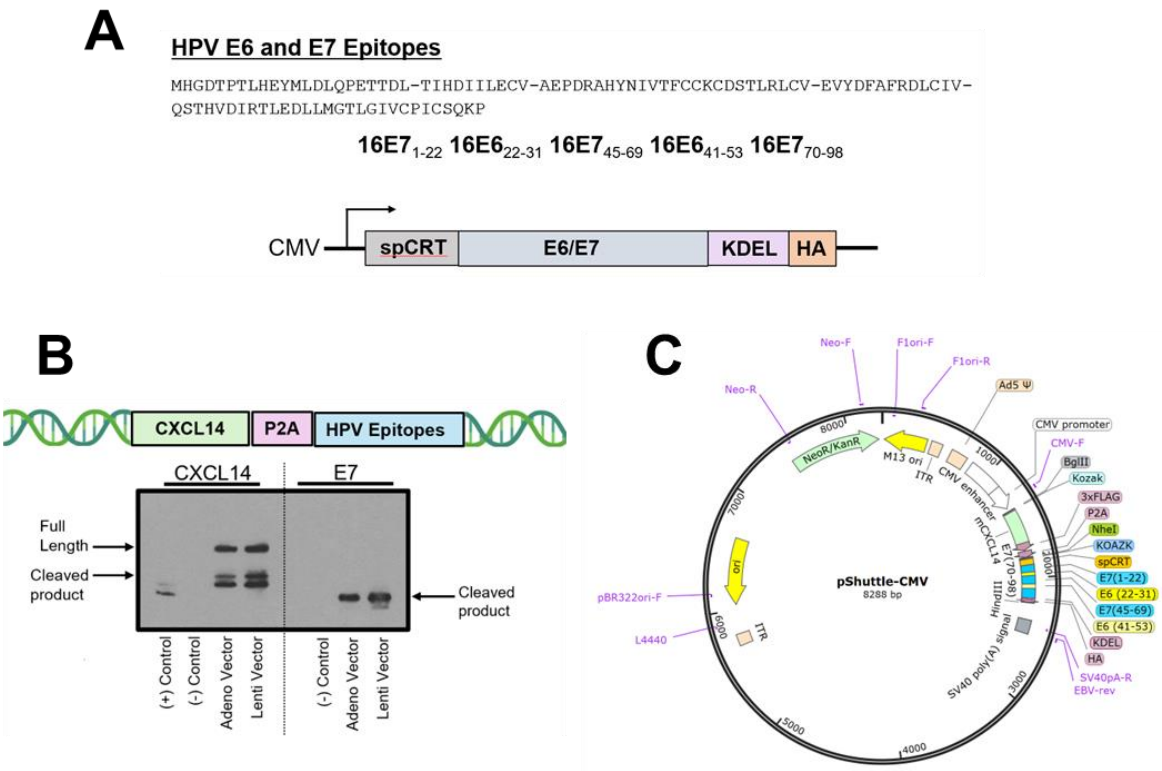

Figure 33. Construction and Expression of CXCL14 and HPV Epitope Transgene Cassette. **A)** The complete amino acid sequence for the chimera of HPV16 E6/E7 truncations. Each portion (separated by a hyphen) corresponds to the amino acid number (subscript) from the wildtype sequence. The transcription of the chimera is driven by the CMV promoter. spCRT = signal peptide of human calreticulin; KDEL = lysine, aspartic acid, glutamic acid, leucine peptide; HA = human influenza hemagglutinin. **B**) Western blot of WCL prepared from 293FT cells transiently transfected with plasmid expressing the cassette for 48hrs. Adeno Vector = (pShuttle-CMV); Lenti Vector = (pLenti6) . **C**) Plasmid Map of pShuttle-CMV with cloned CXCL14 and HPV Epitope Transgene Cassette. Illustrations created with BioRender.com.

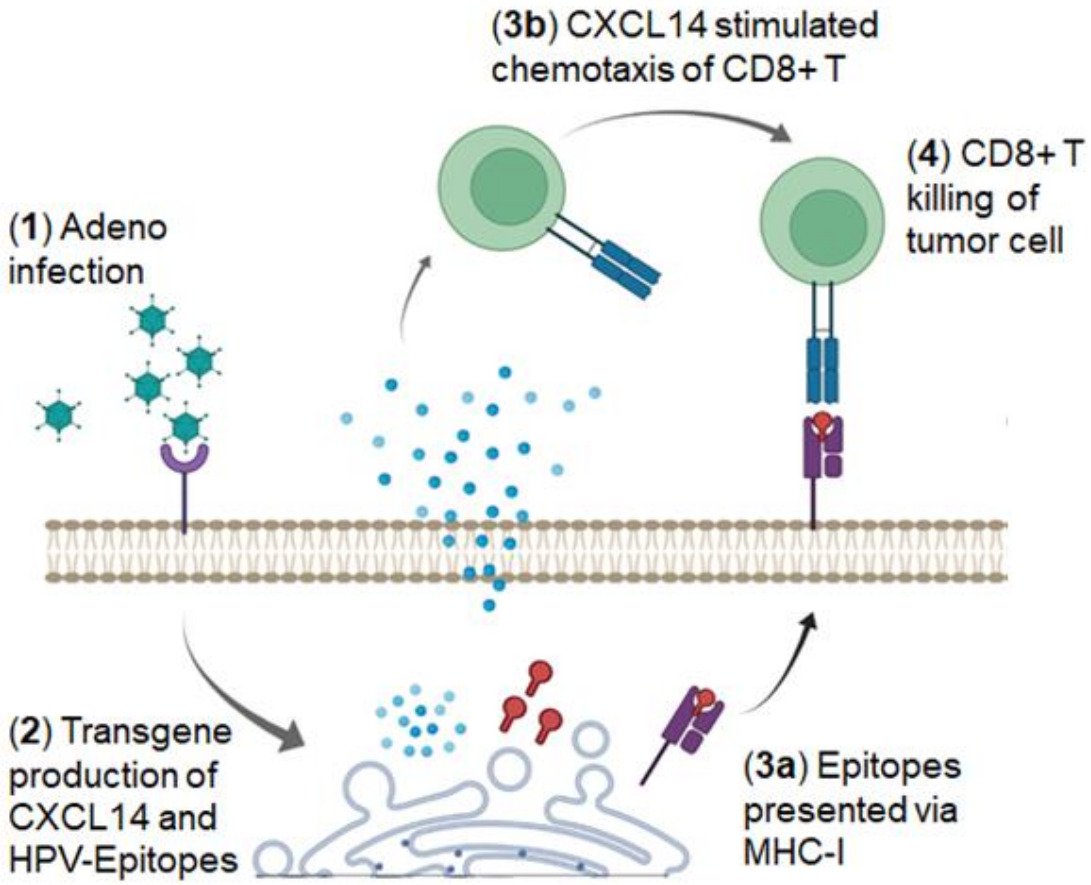

Figure 34. Overview of Hypothesized CXCL14 and HPV-Epitope Transgene Cassette Mediated Antitumor Mechanism in HPV+ HNSCC. (1) Ad5 transgene vector infection of tumor cells. (2) Expression of CXCL14 and HPV-Epitope sequences. (3a) CXCL14 increases MHC-I expression and presentation of packaged HPV-epitope sequences. (3b) Secreted CXCL14 signal attracts CD8+ T cells into the TME. (4) CD8+ Cytotoxic T cell antitumor response ensues. Illustrations created with BioRender.com.

4.4 Conclusions

Many studies have indicated that CXCL14 can have an important role in activating antitumor immunity, and given the appropriate context, the application (or restoration) of CXCL14 may be useful to augment current cancer therapies[98]. For example, in HPV+ HNSCC the expression of CXCL14 is dysregulated and restoration of CXCL14 promotes antitumor immunity[125]. While CXCL14 could be applied as a monotherapy, it is more likely to work in combination with other immunotherapy, such as a vaccine or alongside immune checkpoint blockade. Regardless, using CXCL14 as an immunotherapeutic agent is still challenged by limitations in understanding its antitumor mechanisms, its short half-life, and lack of a viable delivery methods. In this study, we attempted to address these issues in the hope of improving the rationale underlying the use of CXCL14, and to develop an effective method for its application. We show that CXCL14 expression limits adenoviral growth *in vitro*, and that antiviral signaling may be mediated through decreased expression of integrin subunits needed for viral entry and/or by increased TLR-9 activation. Preparation of CXCL14 mutant sequences, in an attempt to improve the stability of CXCL14, may be complicated by changes in the chemokines ability to be secreted. Lastly, we have developed a viral-based transgene platform for the multigene delivery of CXCL14 and an HPV-Epitope vaccine which was detected from multiple viral vectors. In conclusion, our results provide a vital next step in understanding CXCL14 antitumor immunity, and add new value to its potential as an immunotherapeutic agent.

CHAPTER 5

Discussion and future directions

Contributions to Science

The work in this chapter was conceptualized by Nicholas Giacobbi. The final figures for this chapter were generated by Nicholas Giacobbi. The experiments in this chapter were performed by Nicholas Giacobbi with contributions from Lexi Vu, Conchai Yang, and Dr. Mohamed Khalil. Table 2 was derived from the CRISPR/Cas9 screens described in Chapter 2.

5.1 Chapter 2: Epigenetic Immune Evasion

Immune surveillance is crucial for the elimination of cancer cells, and a key factor necessary for effective surveillance is the display of antigens by MHC-I molecules. MHC-I expression is required for the identification and destruction of cancer cells by the immune system, and with reduced expression, cancer cells can evade detection and persist at a higher rate. Attenuated MHC-I expression and antitumor immunity may also limit the effectiveness of current cancer therapies. In this study, we set out to understand the mechanisms that regulate MHC-I expression in HPV+ HNSCC.

A valuable clue about how MHC-I could be downregulated in HPV+ HNSCC came from a report on two Merkel cell carcinoma patients, which indicated that MHC-I expression was repressed by the transcriptional downregulation of *HLA-B* and *B2M* in relapsed patient tumors[493]. Subsequent work by Burr et al., showed that the transcriptional downregulation of MHC-I and APM was linked to epigenetic changes levied by dysregulated PRC2, and that the mechanism was observable in several other cancers[160]. Consistent with those observations, results from our genome-wide CRISPR/Cas9 screening identified core members of the PRC1/2 among the very top negative MHC-I regulators. This suggested that a similar mechanism to that observed by Burr et al. could be at play in HPV+ HNSCC. Ensuing validation through genetic and pharmacologic inhibition of PRC2 revealed an increase in MHC-I and APM mRNA expression, indicating that HPV also exploits PRC2 to promote immune evasion through transcriptional repression of MHC-I genes. However, we observed some opposing findings compared to Burr et al., particularly regarding their evidence that PRC2 inhibition derepresses *NLRC5* and enhances IRF1 binding at *HLA-B* and *-C* loci[160]. In contrast, our treatment of SCC90 cells with EZH2i (GSK126) instead drove the relative levels of

NLRC5 mRNA down. This result was unexpected given the known role of NRLC5 in enhancing MHC-I expression[494,495]. Additionally, our CUT&RUN analysis from GSK126 treated SCC90 cells shows apparent alleviation of H3K27me3 at the *NRLC5* locus (**Figure 12E**). This disparity has several possible explanations, the most buoyant being that increased MHC-I expression operates through an NLRC5 independent mechanism. Ironically, this possibility was confirmed by the researchers in Burr et al., when they showed that deletion of *NLRC5* only slightly limited an increase in MHC-I expression following EZH2i treatment[160]. Hence, NLRC5 may not be critical to PRC2 mediated inhibition of MHC-I expression in HPV+ HNSCC. However, this pathway and its relationship to other factors (e.g., IRF1) should be investigated further to better appreciate PRC2 mediated downregulation of MHC-I (and its restoration) in HPV+HNSCC.

Additional insights into the MHC-I/PRC2 pathway come from observations made by Sparbier et al., who connected the role MENIN (*MEN1**)*** to the downregulation of MHC-I[246]. Likewise, we also observed that MENIN was a significant negative MHC-I regulator in our CRISPR/Cas9 screens, which we validated by genetic knockout (**Figure 35**). Sparbier et. al., showed that MENIN negatively regulates MHC-I gene expression by sequestering the trithorax proteins (transcriptional promoters), KMT2A/B, away from bivalent promoters, permitting PRC2 mediated transcriptional repression[246]. With inhibition of MENIN, however, KMT2A/B activity tipped the balance in favor of transcriptional promotion of MHC-I gene expression[496]. Given our results with MENIN, additional work to examine the factors controlling bivalent gene expression in HPV+ HNSCC, is warranted, along with the possibility that MENIN(*MEN1*) could be novelly targeted (i.e., small molecule inhibitors) to limit immune evasion[497,498].

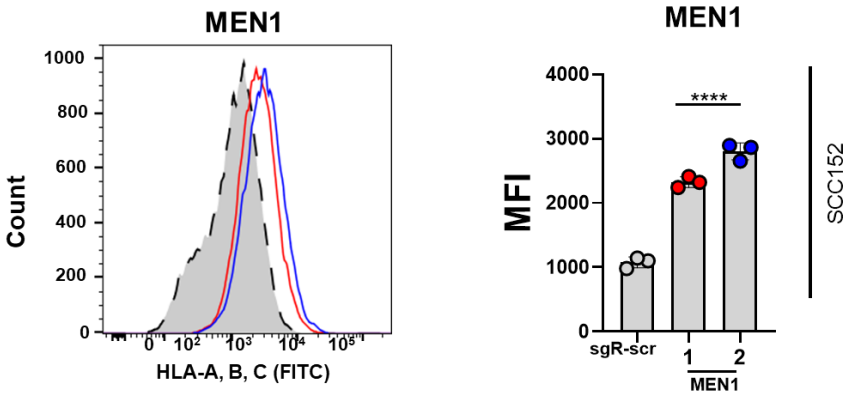

Figure 35. Genetic knockout of *MEN1* Increases MHC-I Expression. A) Surface expression of total HLA-ABC detection by flow cytometry following sg-RNA treatment for *MEN1* knockout or with scrambled control (sgR-scr) in SCC152 cells. Significance p-values were calculated using Dunnett's multiple comparisons test. ****p<0.0001, ***p<0.001, **p<0.01, *p<0.05.

Additional relevant negative MHC-I regulators found in our screens included *PCGF1* and *MTF2*. PCGF1 is a member of the PRC1 complex and is known to negatively control gene expression during differentiation of the embryo and can enhance PRC2.1-MTF2 activity[246,273,496]. MTF2 mediates the recruitment of PRC2 to target genes by recognizing both unmethylated CpG islands and an unwound DNA confirmation state which can selectively accommodate the winged-helix structure of MTF2[254]. MTF2 expression was increased in our HPV+ HNSCC cell lines (**Figure 5A-C**). Thus, it would be interesting to learn if the genes relevant to MHC-I regulation (e.g., HLAs or APMs) are targeted by PRC2 in and PRC2.1-MTF2 manner and should be examined. Specifically, CUT&RUN experiments could be used to locate MTF2 and the PRC2.1 complex in CGI promoter regions of HLA or APM genes, further suggesting their direct influence on specific genes and MHC-I expression.

The conspicuous reliance of PRC2 activity on the repression of MHC-I across all three of our CRISPR/Cas9 screens was reinforced by the "Top Canonical Pathways" analysis from IPA[376]. In each screen, PRC2 pathways were within the top 15 predicted negative MHC-I regulatory pathways of the hundreds identified (**Table 2**). IPA calculated significance (p-Value) and (Z-Score) based on the magnitude, direction, and known associations, and we then sorted the top hits by magnitude of negative Z-score (i.e., negative MHC-I regulators) and then significant p-Value. PRC2 pathways were named as either "PRC2 histone methylation" or by PRC2's association with "HOTAIR." **Table 2** juxtaposes the top 15 pathway hits and statistics calculated by IPA, but the full list of genes which make up a given pathway dataset can be found in the complete tables in the "**Canonical Pathways" supplemental figure 3**. Overall, pathway analysis provided another clear indication of the robust influence of PRC2 on MHC-I repression in HPV+ HNSCC.

Given the identification of HOTAIR in the SCC152 or SCC90 screens, follow-up experiments should include KO of the additional genes in the HOTAIR signatures and the evaluation of MHC-I expression. Increase in MHC-I may suggest the possible involvement of HOTAIR in aiding the targeting of PRC2 to gene loci important for MHC-I repression[289,290].

Another of the most valuable negative MHC-I regulator genes identified in the genome-wide screens was the lysine acetyltransferase, KAT2A. In general, KAT2A and the SAGA complex are notable for coactivating gene transcription rather than negating it[297]. Thus, at first it seemed counterintuitive that KAT2A would be one of the most significant negative MHC-I regulators in the HPV+ HNSCC cells. However, KAT2A/SAGA has been increasing reported to drive tumorigenic phenotypes and is shown to be

Table 2: List of Pathways from IPA Core Analysis

	SCC152		
	Pathway	**-log(p-value)**	**z-score**
1	Cell Cycle Control of Chromosomal Replication	1.81	-2.646
2	**HOTAIR Regulatory Pathway**	1.65	-2.887
3	Colorectal Cancer Metastasis Signaling	1.64	-2.673
4	Role of Osteoblasts in Rheumatoid Arthritis	1.42	-1.5
5	Neurovascular Coupling Signaling Pathway	1.41	-2.673
6	Pulmonary Fibrosis Idiopathic Signaling	1.39	-3.411
7	IL-10 Signaling	1.37	-1.155
8	Th17 Activation Pathway	1.34	-2.646
9	Role of JAK2 in Hormone-like Cytokine	1.3	-1.342
10	Multiple Sclerosis Signaling Pathway	1.22	-2.84
11	Macrophage Classical Activation Signaling	1.22	-2.714
12	Wound Healing Signaling Pathway	1.14	-1.5
13	Sirtuin Signaling Pathway	1.11	-0.577
14	PEDF Signaling	1.02	-0.447
15	BMP signaling pathway	0.923	-1
	SCC90		
	Pathway	**-log(p-value)**	**z-score**
1	BER (Base Excision Repair) Pathway	4.16	-3.162
2	CSDE1 Signaling Pathway	3.34	-2.53
3	Dolichyl-diphosphooligosaccharide Biosynthesis	2.84	-2
4	Antiproliferative Role of TOB in T Cell Signaling	2.83	-0.378
5	Mismatch Repair in Eukaryotes	2.63	-1.342
6	NER (Nucleotide Excision Repair, Enhanced)	2.57	-3.051
7	Assembly of RNA Polymerase II Complex	2.49	-2.828
8	FAT10 Cancer Signaling Pathway	2.31	-2.121
9	Autophagy	1.97	-2.828
10	Superpathway of Cholesterol Biosynthesis	1.91	-2.236
11	Cell Cycle: G2/M DNA Damage Checkpoint Regulation	1.77	-0.816
12	Chaperone Mediated Autophagy Signaling Pathway	1.73	-1.789
13	Adipogenesis pathway	1.51	-0.832
14	**HOTAIR Regulatory Pathway**	1.48	-3.207
15	Cell Cycle Control of Chromosomal Replication	1.48	-2.646
	N/Tert-1_E6E7		
	Pathway	**-log(p-value)**	**z-score**
1	Autism Signaling Pathway	3.2	-2.6
2	GNRH Signaling	2.97	-3.606
3	Androgen Signaling	2.81	-2.828
4	Rap1 signaling	2.78	-2
5	Synaptogenesis Signaling Pathway	2.71	-4.899
6	RHO GTPases activate PKNs	2.65	-2.236
7	Cardiac Hypertrophy Signaling	2.49	-3.742
8	Parkinson's Signaling Pathway	2.49	-2.294
9	S100 Family Signaling Pathway	2.35	-6.091
10	IGF-1 Signaling	2.34	-2.333
11	Melatonin Signaling	2.31	-1.134
12	Glutaminergic Receptor (Enhanced)	2.3	-4.082
13	G Beta Gamma Signaling	2.26	-3.606
14	Acetylcholine Receptor Signaling	2.24	-3.873
15	**PRC2 methylates histones and DNA**	2.23	-2.236

associated with cancer progression of the breast[499,500], lung[326,501], prostate[502,503], stomach[333], colon[325], and others[370,504,505]. KAT2A overexpression in HPV+ cervical

cancer is also implicated for its role in promoting dysregulated E2F and MYC activity and probably exacerbates their effects on cancer progression[329]. The relationship between KAT2A/SAGA and MYC transcriptional activation is well known, and its activation is important to both cellular transformation and to the establishment of oncogenesis[56,297,318,321,324,357].

We confirmed that the inhibition of KAT2A contributes to increased MHC-I expression and to decreased PRC2 expression. Our evidence was complemented by the TCGA HNSCC data that indicated strong positive correlations between KAT2A with PRC2 gene expression. Together, these results suggest that dysregulated KAT2A and the subsequent increase in PRC2 expression is at least partly responsible for the negative effects on MHC-I expression. However, it does not rule out the possibility that KAT2A affects PRC2 independent mechanisms, which can downregulate MHC-I expression, or that PRC2 could be co-opted by other transcriptional co-activators. The effect of KAT2B(PCAF) is also important to consider, as KAT2B is ~73% homologous to KAT2A, and can share overlapping functions[337,341]. KAT2B can also directly support EZH2 stability[330]. Examination of examination of KAT2B levels in the TCGA data shows a clear downregulation of KAT2B in the HNSCC relative to normal samples (via Timer2.0). Although KAT2B may not be dysregulated in the same way KAT2A is in HPV+ HNSCC, it does not preclude the possibility that KAT2B is supporting cancer progression or still compensating for KAT2A. We propose single KO experiments for KAT2B and evaluation of MHC-I and PRC2 expression in the future. Given the impact of GSK4027 (KAT2A/B inhibitor) treatment in the HPV+ cancer lines, a double KO experiments for KAT2A/B may also be necessary to test. However, a complete double KO may not be practical[337].

Genetic knockout experiments of the other SAGA complex members TADA1, USP22, and TAF6L, also showed similar increases in MHC-I expression to what was observed with KAT2A KO, suggesting that SAGA members are working together to repress MHC-I. An important next step in this study would be to isolate/over express the SAGA complex members and determine if their activity alone can drive MHC-I suppression or if the whole of the SAGA complex is required. USP22, for example, is known to act independently to promote immune evasion and drug resistance[319,335,506], and it would be valuable to have more understanding on the individual SAGA members.

Examination of HPV+ HNSCC TCGA samples showed a robust negative correlation between KAT2A expression and HLA-E, -B, and -C. This finding concurred with our previous report[38], and the apparent preferential targeting of *HLA-B*, and *-C* by PRC2 and/or KAT2A evident in the CRISPR/Cas9 screen validation experiments. We also observed that with *KAT2A* knockout, HLA-E expression was strongly upregulated in SCC152 cells, but relative HLA-E mRNA levels were somewhat decreased in SCC90 cells relative to control (**Figure 36**). This result was unexpected, given the strength of the association of HLA-E expression with KAT2A, and that the mRNA levels of HLA-E are downregulated in both SCC90 and SCC152 cell lines compared to N/Tert-1 control cells (**Figure 36**). Regardless, these observations suggest that KAT2A cannot be solely responsible for the control of HLA-E in SCC90 cells and that an additional unknown factor(s) is maintaining the suppression of HLA-E that is absent in SCC152 cells. This result was especially interesting because SCC90 and SCC152 were derived from separate secondary tumors from the same patient, but approximately one year apart[361]. We reported that in keratinocytes expressing high-risk HPV E7, distal CpG islands near the *HLA-E* gene locus were hypermethylated, leading to downregulated HLA-E

expression[38], but it is currently unclear what the DNA methylation status of CpG islands near *HLA-E* is in SCC90 or SCC152 cells. Experiments to gain that understanding may be a crucial first step in differentiating the differences in HLA-E expression between the HPV+ HNSCC cell lines, and how/if it may relate to KAT2A repression.

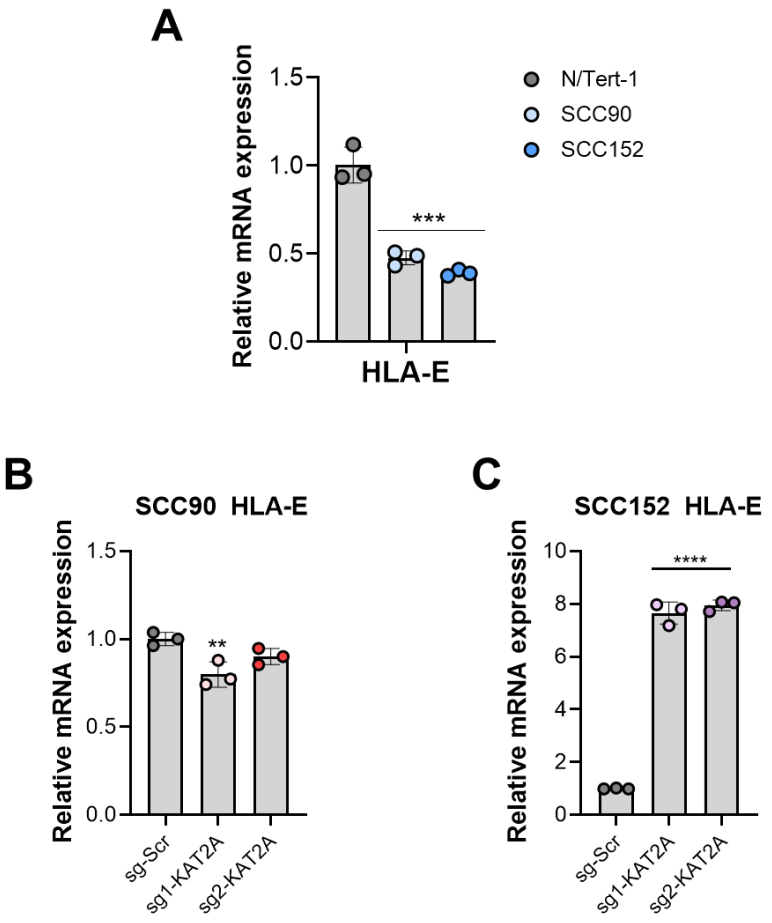

Figure 36. Expression of HLA-E is Differentially Regulated by KAT2A in HPV+HNSCC. A) Relative mRNA expression by RT-qPCR normalized to B-Actin control (ΔΔCT) for HLA-E expression in N/Tert-1 versus SCC90 or SCC152, or **B and C**) Control sgRNA treated cells versus sgRNA-KAT2A knockouts in SCC90 or SCC152. Significant p-values were calculated using an unpaired student's T-test. ****p<0.0001, ***p<0.001,**p<0.01, *p<0.05.(A) Represents one experiment of a duplicate. (B and C) represent single experiments. Each experiment has three technical repeats per condition. Error bars represent SD.

The pharmacologic validation experiments of our CRISPR/Cas9 screen results in this study are encouraging for the application of small molecule epigenetic inhibitors to help treat HPV+ HNSCC. The inhibition of EZH2 by GSK126 or Tazemetostat was able to increase MHC-I, and EZH2 inhibition correlated with reduced of H3K27me3 at HLA/APM genes. Additionally, we also tested a third EZH2 inhibitor, DZNEP. Both GSK126 and Tazemetostat directly target the action of EZH2 by competing with its cofactor, S-adenosylmethionine (SAM), to inhibit its activity[507]. Alternatively, DZNEP (3-Deazaneplanocin A), targets EZH2 indirectly by targeting S-adenosylhomocysteine (SAH) hydrolase, allowing SAH levels to increase, which then competes with SAM and inhibits EZH2[508]. Similar to our results in (**Figures 10-13**) DZNEP was able to increase MHC-I levels with a concomitant decrease in H3K27me3 across several at several doses (**Figure 37).** Thus, through multiple small molecules targeting different points in the mechanism, we confirm our results of PRC2 mediated downregulation of MHC-I.

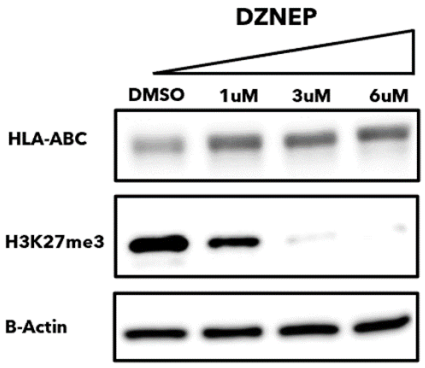

Figure 37. Pharmacologic Inhibitor Treatment of SCC90 Cell Line. A-D) Western blot analysis of WCL from SCC90 cells after 7 day treatment with DZNEP (3-Deazaneplanocin A) at the concentrations listed or (0.1%) DMSO. Total HLA-ABC, global H3K27me3, and B-Actin (loading control) were probed in each experiment.

Although these results are hopeful, an additional point may need to be addressed in regard to PRC2. EZH1 and EZH2 are both able to operate in the context of PRC2[509]. Compensation by EZH1, or worse, selection for an EZH1 driven cancer could occur with inhibition of EZH2[510]. Thus, it may be prudent to evaluate the potential effects of EZH1 inhibition (beyond MHC-I expression alone) in the HPV+ HNSCC cell lines as well. Valemetostat is dual EZH1/EZH2 inhibitor and could be more valuable than a single EZH2 targeting agent[511,512].

The development of GSK4027 was a welcome improvement from the other known KAT2A/B targeting drugs[513]. Other small molecules, including Butyrolactone 3 and CPTH2, have been reported to target KAT2A/B[354,355]. We attempted to use these drugs, but both drugs required high working concentrations (>1-500uM), and their cellular toxicity obstructed a fair assessment of KAT2A depletion (data not shown). Interestingly, Garcinol was effective at depleting KAT2A, H3K9Ac levels, and increased MHC-I levels. However, again at higher concentrations (>6uM), its effect was potently deleterious to cells in as

little as 16-24 hours. Fortunately, GSK4027 targets KAT2A/B with much greater affinity in the conserved c-terminal bromodomain (asparagine and tyrosine residues) required for detecting acetylated lysine[513]. What is interesting about the effect of GSK4027 in our experiments is that, presumably, it is not blocking HAT activity and only the bromodomain of KAT2A/B. The bromodomain is essential for "reading" the epigenetic/histone code (at acetylated lysine residues), and KAT2A/B's HAT activity should remain intact. Regardless, blocking the bromodomain could still explain how GSK4027 is depleting KAT2A and PRC2. If GSK4027 makes KAT2A unable to associate with MYC/E2Fs, or guide them to PRC2 genes, PRC2 might not be produced at the same level. Additionally, because MYC and E2F can drive KAT2A expression[329], the feed forward effect may also be lost, and KAT2A levels could fall. A simpler explanation may be that, if GSK4027 causes KAT2A activity to stagnant, it may linger such that it becomes more vulnerable to targeted degradation by cellular ubiquitin ligases. For now, it is unclear how exactly GSK4027 depletes PRC2 and KAT2A proteins, and it should be explored in future experiments.

CUT&RUN experiments to examine the frequency of MYC or E2Fs in binding sites of PRC2 genes would be a valuable confirmation of the KAT2A/SAGA coactivated upregulation of PRC2 and downstream MHC-I suppression. Next generation RNA-seq experiments in KAT2A KO cell lines and/or those treated with GSK4027 would also shed light on the transcriptional changes present with loss of KAT2A's influence. These results may also help to explain the previous observations of N-MYC and KAT2A sharing a significant overlap in their transcriptional targets[340].

N-MYC expression outside of the central nervous system in adults is unusual and aberrant expression can lead to significant effects on the epigenome[514] or contribute to

certain cancers[56,515]. N-MYC expression has even been directly linked to the development of immunosuppressive environments in cancer [413]. Thus, our detection of elevated N-MYC in all three HPV+ HNSCC cell lines may suggest that N-MYC is driving HPV+ cancer through an immunosuppressive mechanism. We have already alluded to the relationship of N-MYC toward EZH2 expression and activity[248,249,251], in addition to both c-MYC and N-MYC being known to directly regulate PRC2 gene expression[250]. Thus, it's plausible that N-MYC could be a main driver of the PRC2 mediated downregulation of MHC-I, and because KAT2A/SAGA coactivates N-MYC, they may augment the N-MYC oncogenic transcriptional program.

An additional explanation (or consequence) behind the atypical KAT2A and N-MYC expression in HNSCC could be part of the development of a dedifferentiated or "stem-cell like" state in tumor cells. KAT2A/SAGA has been implicated as a driver of "stemness" through multiple mechanisms, and its functions may be promoting expression of stem-like characteristics through epigenetic disruption of gene expression[341,344,516]. Namely of those genes typically implicated in the maintenance of cancer stem cells, e.g., OCT4, SOX2, NANOG CD44, STAT3, among others[517]. In (**Figure 38**) we compared HPV+ HNSCC cell lines to keratinocyte control cells and detected gargantuan increases in several of the Yamanaka factors[518] (e.g., SOX2 showed a >50,000-fold increase relative to control!) linked to stemness and neurogenic phenotypes[519-521].

Chang et al., identified the pRb/RBL2-E2F1/4-GCN5 axis as regulating the formation of cancer stem cells, they and were able to inhibit stem cell formation with GSK4027 or L-Moses (KAT2A/B bromodomain inhibitor)[343]! Importantly, negative control experiments (using GSK4028 or D-Moses) did not reproduce the effect. Chang et al. also determined that E2F1/4 and KAT2A (known associates[356]) was driving stem cell formation

through WNT/β-catenin pathway activation[343]. Amazingly, with the application of GSK4027 or L-Moses, CHIP-qPCR revealed robust reductions in H3K9Ac at WNT target genes, indicating that KAT2A mediated E2F coactivation was blocked[343]! These findings also speak to our earlier question regarding GSK4027 bromodomain targeting and the reduction in KAT2A/PRC2 levels (see above), and they could support the notion that targeting the bromodomain is still impactful enough to hinder the coactivator activity of KAT2A(SAGA) and its effect on gene transcription. Despite these exciting results by Chang et al., how exactly cancer stem cells link to HPV+ HNSCC progression, or if it impacts immune evasion directly, still remains obscure. However, these results are highly encouraging toward the pursuit of understanding the full range of KAT2A's effect on immune evasion and cancer progression in HPV+ HNSCC.

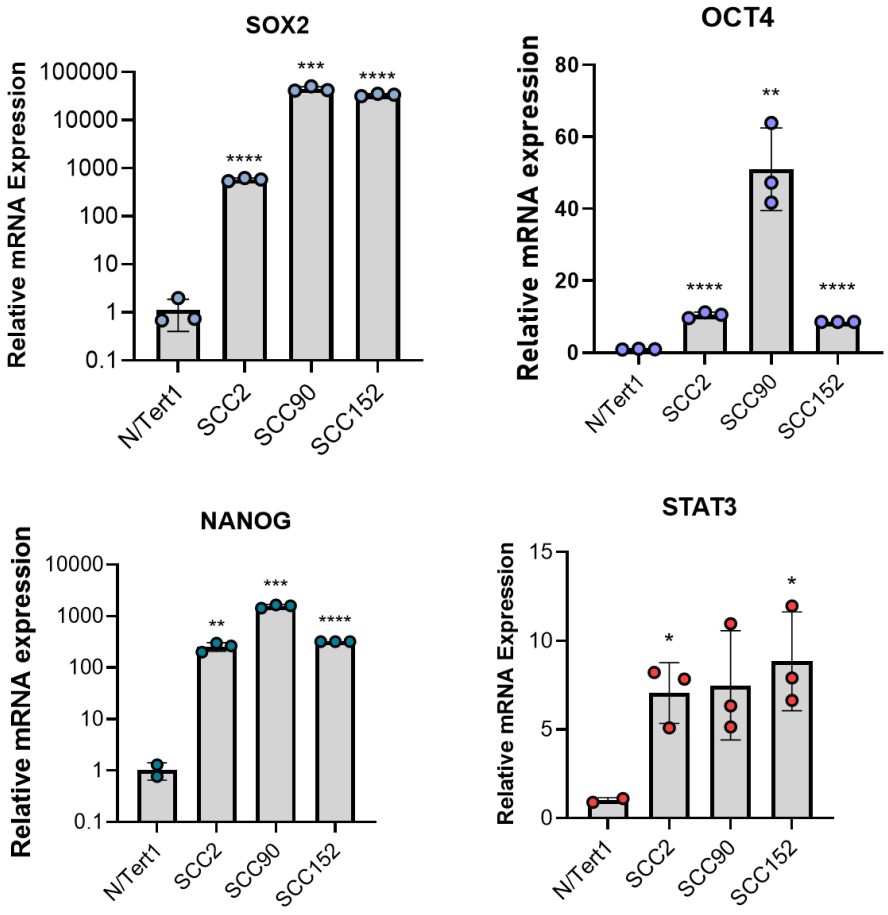

Figure 38. Cancer Stem Cell Genes are Highly Upregulated in HPV+HNSCC. Relative mRNA expression by RT-qPCR normalized to GAPDH (ΔΔCT) control for SOX2, OCT4, NANOG, and STAT3 expression in N/Tert-1 relative to HPV+HNSCC cell lines. Statistical significance was determined by an unpaired student's t-test. ****p<0.0001, ***p<0.001, **p<0.01, *p<0.01. Experiments were performed once with technical replicates shown for each condition. Error bars represent SD.

Lastly, it has not escaped our thoughts that the top gene common to all three of our CRISPR/Cas9 screens, *B3GNT5*, is playing an important role in MHC-I downregulation in HPV+HNSCC (**Figure 3D**). B3GNT5 is normally responsible for glycolipid synthesis[522]. The protease SPPL3 attenuates B3GNT5 activity, but when SPPL3 activity it lost, B3GNT5 can perversely layer glycosphingolipids on cell surface MHC-I and shield MHC-I from both antibodies and interactions with T-Cells[523,524]. The

shielding may explain the association of *B3GNT5* with low MHC-I expression in the CRISPR/Cas9 screens. That is, our antibody staining during flow cytometry may have reduced affinity yielding a low signal. In a similar study of MHC-I in lymphoma as ours, Dersh et al. identified an analogous axis involving SPPL3 and B3GNT2[158], further hinting that this mechanism could also limit interactions with CD8+ T cells in HPV+ HNSCC, but it is for now unclear.

To conclude, this work examined the mechanisms downregulating MHC-I in HPV+HNSCC. Through our investigation we learned that HPV is dysregulating epigenetic mechanisms linked to development as a means to evade antitumor immunity. **Figure 39** illustrates a summary of our main findings. Ultimately, we hope that this work provides novel experimental and therapeutic targets for future investigations in HPV+ HNSCC.

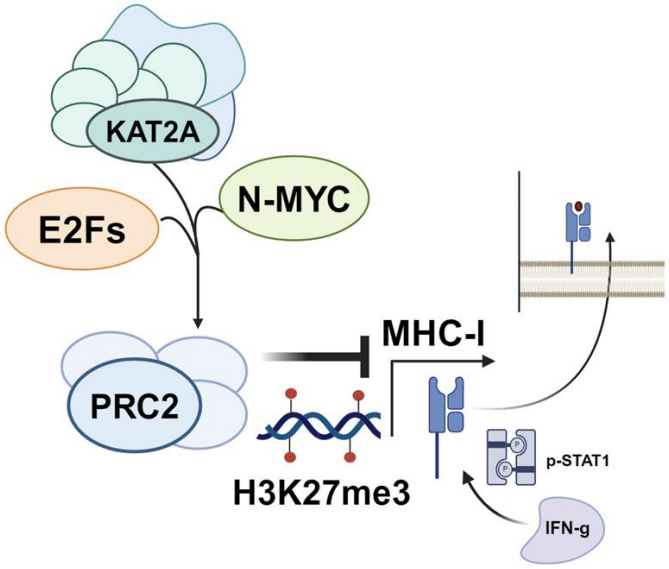

Figure 39. KAT2A/SAGA:PRC2 Axis: SAGA complex promotes PRC2 downregulation of MHC-I. Increased SAGA coactivation of E2Fs and MYC proteins, promotes the expression of PRC2 genes. Increased PRC2 expression results in increased H3K27me3 and downregulation of MHC-I expression. Illustrations created with BioRender.com.

5.2 Chapter 3: Inhibition of AURKA and N-MYC

We identified N-MYC and its stabilizer, AURKA, as negative MHC-I regulators from our CRISPR/Cas9 screen analysis, along with elevated levels of N-MYC expression in HPV+ HNSCC cells lines. Additionally, the ubiquitin ligase, MARCHF8, is upregulated by c-MYC in HPV+ HNSCC and is important for immune evasion[45]. Thus, we estimated that targeting MYC family members could be valuable in understanding the mechanisms of MHC-I downregulation and cancer progression, and so we chose to evaluate the effect of AURKAi, MLN8237, in HPV+ HNSCC.

MLN8237 (Alisertib) can bind AURKA preventing its kinase activity and allowing the induction of MYC degradation via the proteasome[417,418]. AURKAi treatment contributes to cancer regression in several preclinical models[427,525,526]. AURKA overexpression portends prognosis and chemotherapy resistance in patients with advanced oral squamous cell carcinoma[527], and AURKAi has even been proposed for use in HPV+ HNSCC due to E7 overexpression and sensitization to AURKA inhibition[528].

Our data confirms that MLN8237 depletes N-MYC and correlates with increases MHC-I transcript, protein, and cell surface expression in HPV+HNSCC (**Chapter 3**). Additional drug treatments targeting similar pathways (e.g., CD532) could also be tested to further verify our results[416]. Novel small molecules which abrogate AURKA, reduce both N-MYC and c-MYC levels more robustly than MLN8237, and have increased bioavailability have also been reported[529]. Some additional new hope for targeting MYC directly with a mutant c-terminal MYC peptide (Omomyc) which blocks MYC/MAX binding is also in clinical development[530]. Beyond the validation of MLN8237 results, these new

compounds could increase the therapeutic potential of MYC inhibition in cancer patients with MYC driven cancers and warrant additional evaluation in HPV+ HNSCC.

Some malignancies have been reported to have segregated activities for c-MYC and N-MYC, with the switch between them having important effects on cancer progression[531]. Future experiments should also more carefully evaluate the effects on N-MYC and c-MYC individually and determine what overlaps and differences each of the proto-oncogenes have on MHC-I expression in the context of HPV+ HNSCC.

Our lab has identified the E3 ubiquitin ligase MARCHF8 is an important regulator of cell surface immune receptors, capable of degrading death receptors and circumventing apoptosis in HPV+HNSCC[45]. Other reports show that MARCHF8 can target MHC-II for degradation, which leads to disruption T cell functions[532,533], and can negatively regulate cGAS-STING mediated innate immunity[534]. Therefore, the inhibition of MARCHF8 could be a valuable target to help drive antitumor immunity by blocking its ability to limit immune responses. Unfortunately, no MARCHF8 inhibitors currently exist, but here we show that MLN8237 treatment can significantly reduce the expression of MARCHF8 through the targeting of AURKA/MYC.

The depletion of MARCHF8 by inhibition of AURKA may have wide-reaching and significant ramifications in HPV+ HNSCC. AURKA was previously identified as a target of Cullin1(CUL1)-mediated degradation[535] and MARCHF8 stabilizes HPV E7 by targeting CUL1 for degradation[536]. This means that MARCHF8 permits the increase of E7 and AURKA activity with depletion of CUL1. Persistent AURKA also means that MYC proteins can be stabilized, and increased MYC will drive increased MARCHF8 and so on, possibly resulting in a feed-forward loop. Thus, the inhibition of AURKA/MYC may be able to block

this potential loop. In turn, decreased AURKA/MYC results in decreased growth promoting signals and will increase antitumor immunity (death receptor responses) with diminished levels of MARCHF8[45]. **Figure 40** illustrates the hypothetical feed forward loop connecting AURKA to MARCHF8 in HPV+ HNSCC.

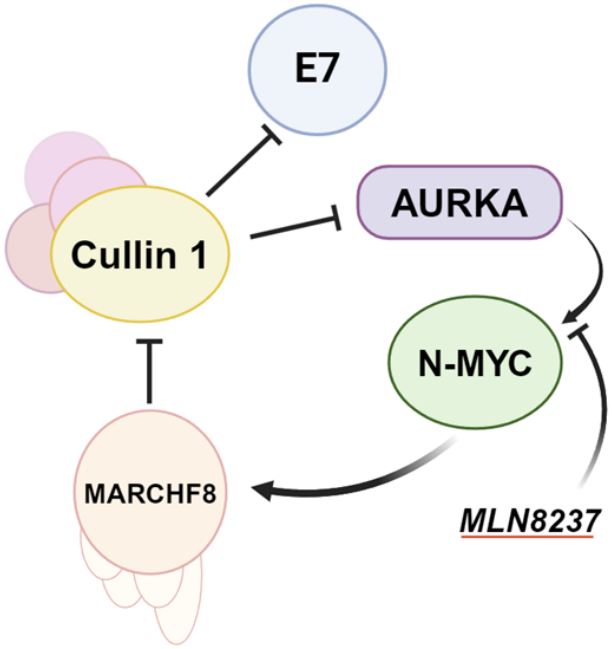

Figure 40. AURKA:MYC:MARCHF8 Axis Feed Forward Loop. MARCHF8 degrades CUL1 and allows E7 and AURKA to persist. Increased AURKA activity permits increased stability of MYC. Increased MYC drives MARCHF8 and establishes a feed forward loop. Illustrations created with BioRender.com.

The observed effect of MLN8237 treatment on MARCHF8 was complimented by the KAT2A knockout experiments that resulted in decreased MARCHF8 expression. This suggests that c-MYC and N-MYC are recruiting KAT2A to drive MARCHF8 transcription, further emphasizing the importance of dysregulated KAT2A in HPV+ HNSCC cancer progression. Furthermore, it may be also interesting to evaluate the effectiveness of KAT2A inhibitors on the levels of MARCHF8, as it could provide an additional option to

inhibit MARCHF8. Additionally, experiments to confirm both N-MYC and c-MYC can promote MARCHF8 expression are necessary. Specifically, experiments to show N-MYC/MAX on the MYC (E-Box) binding sites within the promoter region of MARCHF8 will be valuable in confirming the overall machanism[45].

PRC2 genes are also controlled by MYC driven transcription[250], and we estimated that, AURKA/MYC inhibition would decrease total PRC2. However, we found that only EED transcription was inhibited by MLN8237 treatment, and paradoxically, EZH2 and SUZ12 transcript increased. This may suggest that control of EZH2 and SUZ12 are driven by other transcriptional programs (e.g., E2Fs[385]) or that the EZH2 and SUZ12 transcripts are more durable with AURKA/MYC inhibition. Further evaluation of PRC2 protein levels and PRC2 activity will likely help to elucidate these possibilities and the ultimate consequences of MLN8237 treatment on PRC2 expression.

AURKA regulates cellular spindle formation and entry into mitosis, and inhibition of AURKA should limit cell cycle progression[427,537]. We observed obvious effects on cell growth in both our human and mouse HPV+ HNSCC, however we did not collect data on our human cell lines following treatment. In future experiments, we will thoroughly characterize the growth of our human HPV+ HNSCC cell lines by calculating growth rate and viability. Given previously investigations, we expect HPV+ human cancer cell growth/viability will be significantly reduced[528], and estimate that rates of apoptosis may increase due to increased mitotic disruption and death receptor expression[45]. In conclusion, this work characterizes MLN8237 inhibition of AURKA/MYC in HPV+ HNSCC. Our data suggests that AURKA/MYC is a critical node underlying tumor immune evasion, and that its disruption may be effective for HPV+ HNSCC treatment.

5.3 Chapter 4: CXCL14 as an Immunotherapeutic Agent

CXCL14 exhibits of an abundance of effects[98], but the full extent of CXCL14 signaling, cognate receptors, and mechanism(s) of tumor suppression are still not fully elucidated. Our investigation has provided new insights into CXCL14 antiviral functions, potential receptor activation, and the construction of a new transgene platform for future evaluation of CXCL14.

Across multiple assays, we detected that CXCL14 expression limits the growth of Ad5 virus. Although these results are promising, they may be confounded. That is, the observed effects are outside of the context of a typical infection and instead uses a producer cell-line system (293FT) to propagate the virus. 293T cells stably express a variety of viral oncoproteins which affect cell functions, and they also demonstrate limited immune expression and signaling[538,539]. These factors hinder an unbiased study of immune signaling pathways from these cells, and thus, a more relevant experimental system is necessitated. A better system to investigate the influence of CXCL14 on virus growth may include the HPV infection of primary human keratinocytes, mouse papillomavirus infections in mouse keratinocytes, or mouse papillomavirus infections *in vivo*.

Regardless of the potential antiviral effects by CXCL14, the lack of a known receptor or knowledge of what signaling pathways CXCL14 activates, prevents further progress into ultimately understanding the depth of CXCL14 antitumor responses. Future experiments should first focus on identifying the receptor binding partners of CXCL14. TLR9 activation by CXCL14 may be helpful in understanding the possible receptors[444]. Our data suggests an increase in TLR9 activation due to CXCL14 expression, but only

shows quantification of IL-12a as a readout. Further validation experiments are required to conclude a TLR9 specific mechanism. For example, treatment of cells with chloroquine to dysregulate endosomes and can abrogate TLR9 activation (in addition to other TLRs 3, 7, and 8), and help to initially narrow down the scope of investigation[540]. The use of TLR9-specific ODN agonists (positive controls) and scrambled ODN (negative controls) are necessary and could be used alongside additional TLR9 specific inhibitor treatments[541]. TLR-9 siRNA knockdown or sgRNA knockout experiments would also help to determine reliance on TLR9. Additionally, UNC93B1 is the trafficking chaperone for TLR9 release inside endosomes, and the induction of mutations in UNC93B1 can inhibit TLR9 release and its response[77,542]. Thus, repeat infection experiments with a mutated UNC93B1 (and non-functional TLR9) would show if TLR9 is being signaled. Furthermore, expression of fluorescently label TLR9 could be tracked from the ER in response to CXCL14 expression[76].

Identification of the pertinent receptors for CXCL14 is crucial to understanding the underlying mechanisms mediating antitumor activity. Given the evidence that CXCL14 may signal through G-protein coupled receptors, specifically the CXCR receptors (e.g., CXCR4)[446], a battery of possible GPCRs could be tested by the Presto-Tango[543] system from Addgene, or similar platform. In short, 293T cells overexpressing different GPCRs (~350) and treated with CXCL14 peptide, could be assayed for luciferase reporter activity. However, if CXCL14 requires critical post-translational modifications for receptor binding/activation, synthetic peptides may fail to solicit a response in the assay. The sequence of amino acids 40-47 is specifically notable as it forms the surface exposed, 40S-loop. This loop is rich in potential glycosylation sites that could be important for its function[113,477,544-546]. Thus, over-expression of CXCL14 from producer cell lines may need

to be integrated into the receptor experiments to ensure modifications are made. Additionally, the receptor for MHC-I upregulation may vary from what is required for chemotaxis by (i.e., on) immune cells, and will also need to be considered.

Given that the overexpression of CXCL14 upregulated MHC-I expression in tumor cells *in vitro* (i.e., without the influence of cell types), next generation RNA-seq experiments of CXCL14 overexpressing cells may be valuable to determine the underlying changes in transcription related to MHC-I upregulation. By extension, this strategy may also help to identify the receptor activated through signaling. Furthermore, because the increase in expression of MHC-I was observed in mouse (mEERL) tumor cells *in vitro*[125], it is necessary that this observation also be made in human HPV+ HNSCC cell lines expressing the human version of CXCL14 as well. Overlapping mechanism would strongly support the findings that CXCL14 overexpression alone can stimulate increased MHC-I expression.

With the evidence that CXCL14 drives antitumor immunity[125], CXCL14 (re)expression in HPV+ tumors through our transgene adenoviral vector may serve as a novel approach to study the antitumor effects and predict its therapeutic potential *in vitro*. First, to validate the efficacy of the chimeric HPV epitope peptide vaccine, mice could be immunized with synthesized versions of the full length peptide, individual peptide truncations, or truncations of permutations of the peptide sequence (in an attempt to recapitulate proteasomal processing). After allowing a memory response to ensue, total splenocytes could be harvested and re-exposed to peptides, and subsequent ELIPSOT assays to gauge IFN-γ production will permit the estimation of an established memory response. The presence or absence of CXCL14 may also be a factor to augment a

potential memory response and known positive and negative controls must be included to gauge the efficacy of the vaccine overall.

The *in vivo* infection of tumors with the CXCL14 and HPV-Epitope transgene adenoviral vectors would also serve as a direct measure of their effectiveness at stimulating antitumor immunity. Although, because the expression of transgenes is "transient" from the adenoviral system, the effect of CXCL14 and the vaccine would presumably need to be effective enough to inspire a long-term T cell memory response. One way this could be demonstrated is through multiple site injections of tumor cells (e.g., orally and on the flank) and application of treatment at only one site. If all tumor sites regress, it is more likely a system-wide memory response has been generated. Next generation RNA-seq and/or flow cytometry of tumor samples could detect the presence of CD8+ T memory cells along with the presence of other infiltrating immune cells. RNA-seq evaluation could also reveal changes in transcription relating to potential anti-tumor pathways in the infected (CXCL14) expressing tumor cells. Similar RNA-seq evaluation of tumor infiltrating CD8+ T cells or other immune cells may reveal novel signaling cascades upregulated in response to CXCL14 stimulated chemotaxis, and potential receptor candidates may be identified in this way.

It is still possible that strong T cell activation by CXCL14 and HPV-Epitope vaccination could induce T cell exhaustion. To overcome this potential problem, the addition of anti-PD-1 or PD-L1 inhibitors alongside the intratumoral injection of CXCL14 and HPV-Epitope could also be evaluated, along with monitoring the presence of T cell exhaustion markers (PD-1, CTLA-4, TIM-3). Thus, a combined therapy of CXCL14 and HPV-Epitope plus anti-PD-1/PD-L1 inhibitor may serve as a more effective treatment strategy. Additionally, there is evidence that the presence of PD1+ CD8+ T cell stem-like

cells may mean the difference between effective checkpoint blockade therapy as well as a response to an epitope vaccine or not[153]. Thus, the potential therapeutic value of the CXCL14-HPV epitope transgene therapy may be predicted by careful evaluation of target tumors for the presence of PD1+ CD8+ T cell stem cells[153].

5.4 Closing Remarks and Next Steps

Logically, understanding the processes of immune evasion by tumor cells and pathogens alike will directly inform on strategies to interdict those mechanisms. We chose to examine the factors inherent in the dysregulation of MHC-I expression, a key feature in CD8+ T cell activation and antitumor immunity, with the hope of identifying targets to improve the effectiveness of existing therapies and for the preparation of novel treatments for HPV+ HNSCC.

Each channel of our investigation, be it genetic genome-wide screening, pharmacologic inhibition, or *in silico* approaches, led us to the identification of epigenetic regulators (e.g., PRC2 and KAT2A) in the downregulation of MHC-I expression. Fundamentally, these epigenetic processes control gene expression at the transcriptional level, and alleviating their repression permitted increased MHC-I expression. Many small molecules which target those epigenetic regulators already exist, are in various stages of preclinical and clinical development, and may be valuable as part of combination strategies in the treatment of HPV+ HNSCC.

As an additional therapeutic option, and based our prior identification of CXCL14 as epigenetically downregulated during the course of HPV+ cancer progression, we prepared a combination transgene expression vector for CXCL14 and HPV epitope vaccine expression in tumor cells. We expect that transgene expression will increase MHC-I and stimulate antitumor immunity.

Our findings draw several important conclusions, and to the best of our knowledge, we are the first to report on them. We observed that PRC2 mediates downregulation of MHC-I expression in HPV+ HNSCC, and our observations are synonymous with previous reports of an evolutionarily conserved mechanism of PRC2 facilitated cancer immune evasion. Additionally, KAT2A and the SAGA complex coactivate dysregulated MYC and E2F family members to promote PRC2 gene expression. Lastly, the inhibition of KAT2A or MYC proto-oncogenes results in the decrease of PRC2 and MARCHF8 ubiquitin ligase gene expression in HPV+ HNSCC.

In summation, we hope that the implications of this work are a new perspective and foothold for future HPV+ HNSCC cancer research, the provision of new candidates for combination therapies to treat HPV+ HNSCC, and most importantly, to improve the lives of HPV+ HNSCC patients.

At this point, we propose the following experiments to continue the trajectory of this research. The data presented above strongly suggests that PRC2 mediated H3K27me3 is necessary for MHC-I transcriptional downregulation. Our CUT&RUN experiments, specifically, exhibit a correlation between the loss of promoter region H3K27me3 and an increase in HLA-B and C transcription following EZH2i (GSK126) treatment. However, not all genes that demonstrated decreased promoter H3K27me3 showed increased expression as a result (i.e., *NLRC5*). This may indicate the three-dimensional effects between chromatin regions, and at distant sites (e.g., upstream enhancer regions) away from the immediate gene promoter, may have a literally far-reaching effect on transcription. Long-range PRC2-H3K27me3 mediated interactions affecting gene expression have recently been mapped in human and mouse stem cells[547,548]. Using a similar strategy, we propose genome-wide High-throughput

Chromosome Conformation Capture (Hi-C) and High-throughput Chromatin Isolation by RNA Purification (Hi-CHIP) experiments could be used to map the H3K27me3 interactions in HPV+ HNSCC cells with and without EZH2/PRC2 inhibition.

From here, it is still difficult to predict the extent of the effects that dysregulated PRC2 has on the pattern of H3K27me3 and global chromatin structure in HPV+ HNSCC. Based on our current results, however, we can speculate about effects in regard to at least one gene. We hypothesize that with PRC2 inhibition, there will be an overall decrease in H3K27me3 levels, but the resultant pattern of H3K27me3 and chromatin structural confirmation will result in the *restriction* of *NLRC5* gene expression. It is also important to determine how the pattern of H3K27me3 would change with the abrogation of KAT2A. We hypothesize that KO of KAT2A will decrease PRC2 expression and resultant H3K27me3 levels.

Because we observed that PRC2 downregulates MHC-I heavy chain gene expression in human HPV+ HNSCC, we investigated for a similar event in mouse cells. In addition to the data in **Figure 7C** showing increased EZH2 and KAT2A protein levels in mEERL cells, **Figure 41** shows that the relative mRNA level of H2Db transcript is decreased in mEERL cells vs normal mouse keratinocytes. With these observations coupled with our data showing an increase in MHC-I expression following the inhibition of both PRC2 and KAT2A *in vitro*, we propose the use of small molecule inhibitors in syngeneic mouse models of HPV+ HNSCC. In mice injected with mEERL tumors, GSK4027, GSK126, Valmetostat, and combination GSK4027+GSK126, or GSK4027+Valmetostat, should be injected to determine their effects on tumor cell growth and tumor immune cell infiltration.

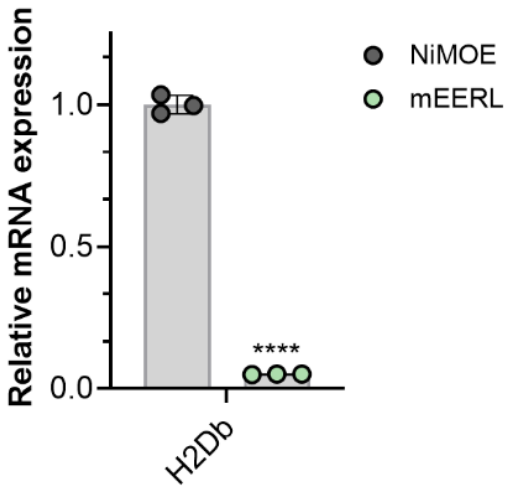

Figure 41. **H2Db mRNA expression is decreased in HPV+ mouse tumor cells**. RT-qPCR for relative mRNA expression of H2Db transcript normalized to mouse B-actin (ΔΔCT) in samples prepared from NiMOE or mEERL cells. Statistical significance was determined by an unpaired student's t-test. ****p<0.0001, ***p<0.001, **p<0.01, *p<0.01. Experiments were performed once with three technical repeats as shown. Error bars represent SD.

Lastly, with our observations of CXCL14 mediated antitumor immunity, and the antitumor efficacy of E6/E7 therapeutic vaccination[212], our combination adenoviral CXCL14 and HPV epitope transgene construct should be evaluated for its antitumor effects. Specifically, in vitro T cell activation assays (e.g., IFN-γ ELISPOT) to evaluate the establishment of immunological memory post vaccination, followed by *in vivo* intratumoral injection and evaluation of tumor growth. New evidence by Eberhardt et al. concluded that HPV E2 and E5 epitopes should also be considered for therapeutic vaccines to drive antitumor CD8+ T cell responses[153]. Downstream in our experiments, the incorporation of additional epitopes, like E2 and E5, (or swapping out of others) should also be evaluated to find the most effective and relevant therapeutic vaccine. Furthermore, other chemokines including CXCL9 and 10, should be compared with and alongside CXCL14 given their relationship toward the activation of T cells[106,107]. Hopefully, the right selection

of transgenes and combination immunotherapy will lead to robust and durable antitumor immunity *in vivo* and in HPV+ HNSCC patients.

CHAPTER 6

Methods and materials

Cell Culture and Cellular Transfection

In all cell culture experiments, cells were maintained in an automatically modulated incubator routinely measured at 37°C and (5%) CO2. Consistent ambient humidity of incubators was established with a pressure of ~760mm Hg and by the natural phase dynamics of liquid water from an open vessel containing ~1 liter of sterilized water. The approximate elevation of incubators was ~260 meters above sea level, and at latitude of ~42.70°N and longitude of -84.48° W.

HPV+ HNSCC Cell lines SCC2 (Cellosaurus #CVCL_7728), SCC90 (ATCC #CRL-3239), SCC152 (ATCC #CRL-3240), and 293FT (ATCC #CRL-3249) were maintained in accordance with their guidelines and handling information using 10% heat-inactivated FBS and 1% penicillin/streptomycin in 1x DMEM (DMEM-10). Keratinocyte serum-free medium with epidermal growth factor (EGF), bovine pituitary extract, and penicillin/streptomycin was used to maintain Normal (hTert) Immortalized human keratinocytes (N/Tert-1) cells or (N/Tert-1-E6E7)[549]. Normal immortalized mouse oral epithelial cells (NiMOE) and mouse oral epithelial cell expressing HPV16-E6 and E7, mutant H-Ras, and luciferase (mEERL) were acquired from John Lee[550]. All cell lines were maintained in their respective media for no more than four days before refeeding or were passaged at approximately 85% confluency. At the time of passage, cells were washed in 5mL of 1x PBS, aspirated, trypsinized in 1mL (0.25% Trypsin-EDTA ThermoFisher #25200056), and quenched in 9mL of DMEM-10. N/Tert-1 cells were resuspended in the same manner but were diluted in 9mL keratinocyte serum-free medium and spun down at 500xg and aspirated to remove any relic trypsin. Pellets were resuspended in appropriate volume of media and plated. Additional information for mEERL cell line propagation has been documented[45].

In general, all transfection procedures used throughout this study were consistent with the following specifications. For simplicity, the following description details plasmid transfection in a 10cm dish (Note: for smaller or larger containers, the volumes described were scaled according to volume of vessel and/or cell number used). First, 293FT cells were plated in a 10cm dish and grown for 16hrs to achieve a desired confluency of ~66%. At the time of transfection, Polyethylenimine (PEI) at a stock concentration of [1mg/mL] (Polysciences #9002-98-6) was diluted in 1.5mL Opti-MEM media. Gene-of-interest plasmids were diluted in a separate 1.5mL Opti-MEM (Fisher #31985070). The two dilutions were then combined and briefly vortexed (3mL) to achieve a (3:1) PEI to DNA ratio (e.g., 30ul PEI / 10ug Plasmid DNA). The transfection complex was then incubated at room temperature for ~20-30min. Concurrently, 293FT cells were given 7mL of Opti-MEM. Following incubation, transfection complexes were gently added to cell plates to produce a final volume of 10mL per plate. After 4-6hrs, transfection complex media was aspirated from transfected cell plates and fresh DMEM-10 was added (10mL). Cells were then grown ~48hrs prior to collection and downstream analysis.

Lentivirus Production and sgRNA Knockout/ Cell Line Preparation

The sgRNAs used for gene knockout were obtained from ChopChop (https://chopchop.cbu.uib.no/)[551-553] with sequences gleaned from Addgene in the Brunello sgRNA library (https://www.addgene.org/pooled-library/broadgpp-human-knockout-brunello/). **Table 3** lists the sgRNAs used in this study. The sgRNAs were cloned into sgOPTI (Addgene #85681) vector, a gift from Dr. Andrew Olive, as previously described[554]. Briefly, the sgOPTI vector was digested BsmBI v2 (NEB #R0739S). Next, linearized sgOPTI backbone was combined with sgRNA DNA duplex (IDT) and ligated

together with T4 ligase (NEB #0202). Ligated plasmids were then transformed into Stbl3 bacteria (ThermoFisher #C737303). Plasmid DNA was prepared by overnight bacterial culture and subsequent miniprep (IBI Scientific # IB47102). Plasmid constructs were validated by sanger sequencing (Genewiz/Azenta). Next, the sgRNAs containing plasmids (or alternative gene-of-interest containing plasmids) were co-transfected with the lentivirus packing plasmids, pCMV-VSVG (Addgene #8454) and pCMV-Delta 8.2 (Addgene #12263) (each gifted by Jerome Schaack) into 293FT cells with Polyethylenimine (PEI) at a stock concentration of [1mg/mL] and using a (3:1) PEI to DNA ratio and diluted in a final volume of 10mL Opti-MEM media. After 4-6 hours, the transfection complex was removed and fresh DMEM-10 was added. Plates were incubated until lentivirus containing supernatant was collected at 72hrs post transfection. Following collection, supernatant was centrifuged at 3000xg for 5 minutes to pellet cell carry-over. Cell-free virus suspension plus polybrene reagent [14ug/mL] was then used to infect the respective stably expressing Cas9 cell lines for 24-48hrs. Cas9 cells were produced prior by the same method (using lentiCas9-Blast, Addgene #52962) and were validated for Cas9 protein expression (data not shown). Cell lines were selected in blasticidin [8ug/mL] (selection for lentiCas9-Blast plasmid) and puromycin [4ug/mL] (selection for sgOPTI) for >7 days (and until control cells plates were 100% eradicated) prior to further analysis.

Cleavage Under Target and Release Using Nuclease (CUT&RUN)

Approximately 5e5 SCC90 cells were plated in 10cm dishes, grown 16hrs to reach a confluency of ~33-50%, and were incubated with DMEM-10 with (0.1%) DMSO (untreated control) or GSK126 [6uM] (Caymen #15415) in (0.1%) DMSO (Drug treated experimental) for 7 days. Media was refreshed twice after every three days with drug

added. Cells were trypsinized and resuspended in DMEM-10 media, pelleted at 500xg for 5 minutes, resuspended, counted. Next, CUT&RUN was performed using 5e5 SCC90 cells per target (n=2 replicates per target) using the CUTANA ChIC/CUT&RUN kit (Epicypher, version 3), in accordance with the user manual version 3.1 instructions. Antibody targets included H3K27me3 and H3K4me3. Genomic DNA was harvested from cells by column purification (Qiagen #56304) and DNA was quantified using the Qubit dsDNA HS kit. CUT&RUN sequencing libraries were prepared using the CUTANA CUT&RUN Library Prep kit (Epicypher, version 1), by user manual version 1.4. Sequencing libraries were analyzed by TapeStation (Agilent) and sequenced on the NovaSeq 6000 (Illumina) at 2x50 bp for 8-10e6 reads per library. Raw FASTQ files were processed using the nf-core CUT&RUN pipeline (nf-core/cutandrun v3.2.2). Trimmed FASTQ reads and spike-in reads were aligned to GRCh38 and K12-MG1655, respectively, using Bowtie2 v2.4.4. Peaks were called using SEACR v1.3 and consensus peaks were merged using bedtools v2.31.0. Genomic tracks were visualized using IGV desktop v2.16.1. Sequencing Reactions were performed by the VanAndel Institute Genomics Core (https://genomicscore.vai.org/) in Grand Rapids, Michigan. For the CUT&RUN procedure, preparation of sequencing libraries, and pipeline analysis of results (along with thoughtful discussion and reagents), we greatly thank the effort and expertise of John Vusich, and the oversight of his faculty advisor Dr. Eran Andrechek.

Preparation of Total RNA, Quantitative Reverse Transcription-Polymerase Chain Reaction (RT-qPCR)

The harvest of total RNA and elimination of genomic DNA was performed by RNeasy Plus Mini Kit (Qiagen #74104), quantified by NanoDrop, and stored at -80°C. Preparation of first-strand cDNA was prepared from (2ug) of total RNA using reverse

transcriptase consistent with manufacturer's instructions (Roche #04379012001). For RT-qPCR, reactions were assembled in a final volume of (20uL), SYBR green master mix (Applied Biosystems-ThermoFisher #A25741) (10uL), 1mM primers (5uL), and 100ng of cDNA (5uL) were combined, and RT-qPCR was performed in a Thermo-Fisher Quantstudio 3 or a Bio-Rad CFT Connect thermocycler. Primer sequence targets were also confirmed by Nucleotide Blast analysis (https://blast.ncbi.nlm.nih.gov/Blast.cgi). Physical primer oligos used are listed in (**Table 4**). Primers were diluted in double deionized water (ddH2O) at a stock concentration of [10uM] at stored at -20°C. Figures depicting RT-qPCR reactions describe the number of repeats and technical replicates performed, respectively. Additionally, they describe the utilized statistical testing and error bars.

Preparation of Whole Cell Lysate (WCL) and Western Blotting and Co-Immunoprecipitation

Whole cell lysates (WCL) were prepared from cultured cells, pelleted by centrifugation (500xg for 5 minutes), washed twice in 1xPBS solution, and incubated on ice for 30 minutes with periodic agitation in 1xRIPA buffer (Abcam #156034). Following incubation, lysates were centrifuged for 5 min at >10,000xg and WCL was decanted from pelleted cell debris. WCL was quantified by BCA assay (Pierce-ThermoFisher #23225) and NanoDrop by standard curves using bovine serum albumin standard. Western blot samples were prepared with (10ug-30ug) (depending on experimental conditions and were consistent among samples) of WCL diluted with (4x) Laemmli buffer (BioRad #1610747) with β-mercaptoethanol added (in accordance with BioRad instructions) and 1xPBS to a final volume of (20uL). Samples were boiled for 10min at 95-100°C. Samples were loaded into SDS-PAGE gels and electrophoresis was performed (Bio-Rad #

1658004) in accordance with manufacturer's recommendations. "Wet/Tank" Protein transfer was achieved using PVDF membranes (activated in 100% methanol) using (BioRad #1703930) and consistent with manufacturer's instructions. Following transfer, membranes were blocked in 10% milk, washed 3x in TBST, and treated with their respective primary and secondary antibodies with appropriate washing. **Table 5** lists all antibodies used in these studies. Finally, membranes were treated with Western HRP substrate (MilliporeSigma # WBLUC0100) and were subsequently developed using either X-Ray film and dip tank developer or digital reader (GE Amersham Western Blot System). Quantification of western blot band patterns was performed using ImageJ software Analysis to calculate the area under the curve for each respective band intensity and relative to its respective loading control (i.e., B-Actin signal).

For co-immunoprecipitations (Co-IP), pull-downs were performed using the Pierce Classic Magnetic IP/Co-IP Kit (ThermoFisher #88804) using (1-2mg) of WCL and the corresponding target antibody (5ug) in accordance with the manufacturer's instructions. Species corresponding IgG antibody for used for isotype control. Equal volumes of isotype control IP and target antibody IP samples were compared by subsequent western blot. Input control samples constitute the respective WCL. Subsequent western blotting was performed as described above. For both western blotting and Co-IP, all antibodies used for are listed in (**Table 5**).

Flow Cytometry

Cell samples for analysis were collected by trypsinization (described above) with an equal number of cells prepared for each sample (e.g., 1e6 cells/sample) and washed twice in 1x PBS. Cell suspensions were then pelleted at 500xg for 5 minutes and

resuspended in FACs (cell staining) buffer. Samples are then again pelleted and decanted. Cells were then agitated by flicking or very brief vortex. An appropriate volume of antibody (e.g., ~2uL) was added to each tube and tubes were gently (but thoroughly) mixed. Sample tubes were then incubated for ~30 minutes at 4°C in the dark. Following staining, cells were resuspended and washed twice in FACS buffer (BioLegend #420201). After decanting, cells were fixed via incubation in (4%) paraformaldehyde (BioLegend #420801) for ~30 minutes at 4°C in the dark. Samples were then FACs washed and resuspended in 500uL of FACs buffer and stored at 4°C until cytometric analysis. Experiments shown were performed in triplicate. Cytometric analysis was conducted by an LSRII flow cytometer (BD Biosciences) or by an Attune Flow cytometer (ThermoFisher) consistent with methods previously described[45,536]. Cytometric data was then analyzed and visualized by FlowJo v10.10 software. Antibodies used for detection are listed in (**Table 5**).

Cell Growth Curves and Viability Assay

In six well plates, ~1e6 mEERL cells were plated per well and grown overnight for 16hr. The following day, cell wells were treated with DMEM-10 containing (0.1%) DMSO or increasing concentrations of MLN8237 [31.25nM, 62.5nM, 125nM, 250nM, or 500nM] in (0.1%) DMSO, respectively, and incubated for 48hrs. Cells were then resuspended (as described above) and counted (Countess 3 Automated Cell Counter by Invitrogen), and the viability of cells was estimated by trypan blue staining. That is, equal volumes of cell sample suspensions were diluted with (0.4%) trypan blue and analyzed on Countess 3.

Mutagenesis Reactions

Mutagenesis reactions were performed using the QuikChange II Site-Directed Mutagenesis Kit (Agilent #200523) in accordance with the manufacturer's instructions.

Mutagenesis primers are listed in (**Table 4)**. Following mutagenesis and sanger sequencing conformation (Azenta/Genewiz), plasmids were transformed into XL-Gold cells and bacterial stocks were stored at -80°C.

Preparation of Adenovirus Transgene Vectors

The production of Ad5 transgene vectors followed the framework of the AdEasy Adenoviral Vector System (Agilent #240010), Luo et al. 2007[479], and from protocols generously donated by the Amalfitano Lab at Michigan State University. To begin, we cloned mouse CXCL14 (mCXCL14), HPV vaccine epitopes (HPV Epitopes), or the mCXCL14-P2A-HPV Epitopes sequences into the pShuttle-CMV plasmid. The vector is linearized by Pme I (NEB #R0560) digestion and precipitated with 100% Ethanol, 3M Sodium Acetate, and resuspended in purified ddH2O. Next, linear vectors were transformed via electroporation into BJ5183 cells (Agilent #200154) with pretransformed pAdEasy-1 (Agilent #240005). Homologous recombination between pShuttle and pAdEasy-1 results in complete pAd5-vector containing sequences of interest. pAd5 vectors were harvested by miniprep (IBI Scientific # IB47102) and retransformed into XL10-Gold cells (Agilent #200314). To verify homologous recombination events, purified pAd5-vectors were digested with Pac I (NEB #0547) with expected band sizes of ~30kb and 4.5kb or 3kb, depending on site of recombination (both outcomes are correct and vary based on the two potential sites of recombination). After isolation of digest confirmed pAd5 recombinant vectors, verification of whole plasmid sequencing was performed by Plasmidsaurus using Oxford Nanopore Technology with custom analysis and annotation (https://www.plasmidsaurus.com/). Next, pAd5 vectors were linearized by Pac I digestion and transfected into 293FT cells by PEI (as described above) or Calcium Phosphate

(Thermo cat# K2780-01). Following the appearance of significant cytopathic effect (CPE) after ~7-14 days, viral supernatant was transferred into a fresh plate of 293FT cells containing at least 50% fresh DMEM-10. Viruses were passaged 4-6x. Finally, to support higher viral titers, virus was passaged once more on ~35-90 15cm dishes of 293FT cells. After ~2-4days, cells were then collected and pellets were lysed in (5%) Deoxycholate, treated with [0.02M] MgCl2, DNase I, and RNase A both at [50ug/uL]. Virus particles were then purified from cell lysates by [1.33g/mL] CsCl gradient ultracentrifugation at, 3x subsequent dialysis in [10mM] Tris pH=8. Purified samples with diluted with 10% sucrose and the viral titer of the sample was determined. For titration, a fraction (5-50uL) was diluted in lysis buffer ((10%) SDS, [1M] Tris pH = 7.5, and [0.5M] EDTA pH = 8) and viral genome copies were measured by optical density via nanodrop. Note the expected (260/280) ratio = [1.33g/mL]. Viral particles (vp) per mL were estimated by the following equation ([A260 x 20 (dilution factor) x 10e12]/ [0.909] = vp/mL) and stocks were stored at -80°C. Additional experimental details can be found in (Agilent #240010 Instruction manual or in Luo et al. 2007[479]). We also graciously thank Sarah Roosa, Dr. Yasser Aldhamen, and Dr. Andrea Amalfitano, for reagents and supervision.

Adenovirus Growth Curves

Approximately 1e6 293FT cells were plated in parallel in individual 3.5cm dishes corresponding to each anticipated time point (0, 6, 18, 24, 48, 72, or 96hrs) making a total of (14) 3.5cm plates. Equal virus inputs were calculated by RT-qPCR (1E10 viral genome copies), and the appropriate amount of Ad5-CXCL14 or Ad5 expressing green fluorescent protein (Ad5-GFP) input was added to each respective plate in a final volume of 2mL of DMEM-10. At each respective timepoint (including time = 0hr), total supernatant was collected and frozen at -80°C. From each supernatant, virus DNA was purified (PureLink

Viral RNA/DNA Mini Kit #12280050) and used to measure absolute genome copy numbers by RT-qPCR as previously described[478]. To calculate absolute genome number, a standard curve of 10-fold dilutions ranging [10ng – 0.00001ng] was prepared using the pShuttle-CXCL14 plasmid. Primers for quantification of viral genomes are listed in (**Table 4**). Ad5-CXCL14 were prepared as described above. We humbly thank Sarah Roosa, Dr. Yasser Aldhamen, and Dr. Andrea Amalfitano for providing Ad5-GFP virus samples.

Fluorescence Microscopy and GFP Analysis of Ad5-GFP Viral Infections

In 6-well plates, ~5e5 293FT cells were plated per well and grown overnight for 16hrs. The next day, cells were transfected (as described above) with (2ug) of pCDH_CXCL14, pLenti6_CXCL14 or pLenti6-empty vector (control) plasmid and incubated for 24hrs*. The next day, cells were challenged with increasing multiplicities of infection (MOI) of Ad5-GFP virus. Virus was quantified by NanoDrop as previously described[479]. At 72 hours post infection (96hr post transfection of CXCL14), brightfield images and overlapping GFP signal were captured by fluorescence microscopy at equivalent locations in each well. Using ImageJ software, the brightfield (BF) area of cell coverage and the overlapping GFP signal were estimated for each given image field. Consistent threshold parameters were set and were subsequently applied to each image so as to measure uniformly. Next, %GFP was calculated by the ratio of GFP signal to brightfield area for each image, respectively. In experiment one, the average %GFP for MOI =1, 5, and 10 were based on (n) images (and their corresponding BF and GFP signal) were (n ≥10). For MOI = 20 and 30 (n ≥ 3). In Experiment 2, (n = ≥10) for all MOI shown. In both experiments, there was no detection of GFP at MOI = 0 but (n =3) images were still taken. *****(Note: that this description details two separate experiments: Experiment one compared pCDH-CXCL14 to mock transfected cells, and experiment two compared

pLenti6_empty-vector to pLenti6_CXCL14 transfected cells. All additional experimental details are the same.)

Stability Chase Experiments

In 6-well plates, 5e5 293FT cells were plated and grown overnight for 16hrs. The next day, cells were transfected (described above) with (2ug) of pCDH_CXCL14, pCDH_CXCL14-RY43/44AA, or pCDH_CXCL14-dEE. After 48hrs, cells were treated with cycloheximide (CHX) (Fisher #AC357420010) (50 µg/mL) or MG-132 (10 µM) (Fisher #474787) for 0hr, 0.25hrs, 0.5hrs, 1hr, and 2hr in a final volume of (2mL) DMEM-10 per well. For Brefeldin A (BioLegend #420601) treatment, cells were treated for 0hr, 0.5hrs, 1hr, 2hrs, or 4hrs in a final volume of (2mL) DMEM-10 per well with final concentration of (5 µg/mL). From each well, WCLs were prepared, and western blotting was performed (described above). Blots were probed with (1:5000) Anti-FLAG antibody (SigmaAldrich #F1804) (Note: all the CXCL14 constructs tested have a 3x-FLAG tag adjoined to the 3-prime end of the coding sequence. Following primary, blots received goat anti-mouse secondary antibody (Cell Signaling #7076S) at (1:10,000 dilution).

In double drug treatment chases using both MG-132 (10 µM) and CHX (50 µg/mL), following 24hrs post transfection, cells were treated with MG-132 in a volume of 2ml DMEM-10 for 8hrs. Cell wells were aspirated, and a fresh (2mL) DMEM-10 with CHX was added and cells treated for 0, 0.25hrs, 0.5hrs, 1hr, 2hrs, or 3hrs. From each well, WCLs were prepared, and western blotting was performed (described above). Blots were probed with (1:5000 dilution) Anti-FLAG primary antibody and (1:10,000 dilution) Goat anti-mouse secondary antibody. For all experiments, B-Actin-HRP conjugated primary antibody was probed (1:100K dilution) as the loading control.

Inhibitor Chase Experiments

In 6cm dishes, approximately 2e6 SCC90 cells were plated and permitted to grow for ~36hrs to achieve complete adherence to the plate and ~33-50% confluency. Next, growth media was aspirated and fresh DMEM-10 containing each respective inhibitor in (0.1%) DMSO or (0.1%) DMSO alone (control plates) was added. Inhibitors used were resuspended in DMSO, were acquired from Caymen Chemical (unless otherwise specified), and included GSK126 (#15415), EPZ6438-Tazemetostat (#16174), DZNEP (#13828), Garcinol (#10566), MLN8237 (#13602), and GSK4027 (#23421). Decitabine was purchased from Selleck Chemical (#506901). Cells were incubated at their respective concentrations (see given figures) for 7 days (unless otherwise specified). Fresh media and drug were added every third day of incubation. Cells were collected and processed as described above.

IFN-Gamma Treatment and GSK126 Treatment Assay

In 6cm dishes, ~2e6 SCC90 cells were plated and grown for ~36hrs to achieve complete adherence to the plate and ~33-50% confluency. Cells were treated for 3 days with DMSO (0.1%) or GSK126 [6uM] in (0.1%) DMSO in DMEM-10. After day 3, cells received fresh DMEM-10 plus drug and an additional [0.1] or [1] ng/mL IFN-γ (StemCell #78020), or vehicle (1xPBS) and incubated for 24hrs. Cells were then collected and analyzed by western blot and flow cytometry as described above.

Analysis by Tracking of Indels by Decomposition (TIDE)

From the transduced stably expressing sgRNA/Cas9 cell-lines, genomic DNA was harvested (Qiagen #56304). PCR was performed with Taq polymerase (New England BioLabs #M0495L) consistent with the manufacturer's instructions (https://www.neb.com/en-us/protocols/2012/10/04/pcr-using-hot-start-taq-dna-

polymerase-m0495) to amplify regions of interest with TIDE specific primer sequences corresponding to a given sgRNA target sequence (obtained from ChopChop, https://chopchop.cbu.uib.no/[551-553]). Primer Sequences are listed in **Table 4**. Amplicons were generated from the genomic DNA of both sgRNA edited and scrambled sgRNA (background sequence) non-targeting control samples. Amplicons were purified by PCR clean-up kit (Promega #A9281) and were analyzed by sanger sequencing (Azenta/Genewiz). Sequencing trace files for background and edited sequence reads were uploaded to the TIDE bioinformatic tool website (http://shinyapps.datacurators.nl/tide/) along with respective sgRNA sequences to determine (%) editing efficiency of target CRISPR/Cas9 treatment in accordance with guidelines from the developer.[365]

CRISPR Screen Preparation and Analysis

The Human Brunello CRISPR knockout pooled library was a gift from David Root and John Doench (Addgene #73178)[555], and was donated to us by Andrew Olive. Using the Brunello library, (4) sgRNAs targeting nearly every coding gene in humans plus an addition to 1000 non-targeting controls were packaged along with pCMV-VSVG (Addgene #8454) and pCMV-Delta 8.2 (Addgene #12263) (each gifted by Jerome Schaack) into 293FT cells with Polyethylenimine (PEI) at [1mg/mL] and using a (3:1) PEI to DNA ratio and diluted in a final volume of 3mL Opti-MEM media incubated for 20 minutes. Transfection complex was applied to ~8e6 293FT cells for 6 hours at 37°C. Media was then swapped with 5ml of complete DMEM-10. After 24 hours, viral supernatant was collected and fresh 5mL DMEM-10 added. This was repeated after an additional 24 hours. The total viral supernatant was filtered with a 0.22µM filter. [We thank Canchai Yang for

preparation of virus.] Viral supernatant was used to transduce SCC90, SCC152, or N/Tert-1_E6E7 cell lines for 6 hours in DMEM-10 plus polybrene [8ug/mL]. Media was swapped with DMEM-10 and incubated for 48 hours. Then media was replaced with DMEM-10 plus puromycin [4ug/mL] plus blasticidin [8ug/mL] and incubated to ensure selection of transduced cells. Cells were then collected and stained for MHC-I expression (as described above). [We thank Dr. Mohamed Khalil for cell selection, collection, and flow cytometry sample preparation]. The top and bottom 5% of MHC-I expressing cells were sorted in each end to achieve ~5e6 cell per group from duplicate experiments. Genomic DNA was harvested from the cells and PCR amplified as described[554,556]. PCR amplicons were sequenced on an Illumina NextSeq 500 in the Genomics Core at Michigan State University. Following the curation of the reads by removal of adapter sequences, we utilized the negative binomial regression model-based analysis of genome-wide CRISPR-Cas9 knockout (MAGeCK)[363]. MAGeCK analysis permitted mapping of the sequencing reads to the Brunello library index. The output from MAGeCK provided ranked lists of genes based on 4 independent sgRNAs that were used to curate the candidate gene list.

TCGA Patient Data Analysis

Analysis of “GDC TCGA Head and Neck Cancer (HNSC)” patient samples curated by TCGA (https://www.cancer.gov/ccg/research/genome-sequencing/tcga) were acquired from the University of California Santa Cruz (UCSC) at (https://xenabrowser.net/datapages/?dataset=TCGA-HNSC.htseq_fpkm.tsv&host=https%3A%2F%2Fgdc.xenahubs.net&removeHub=https%3A%2F%2Fxena.treehouse.gi.ucsc.edu%3A443). Version 07-19-2019. Patient samples were comprised of (n=546) patient samples, Illumina gene expression RNAseq data.

Authored by Genomic Data Commons. File download: (TCGA-HNSC.htseq_fpkm.tsv). Unique gene identifiers were cross referenced and respective given values (log2(fpkm+1)) were tabulated. Identifiers for “Normal” (11A), “Tumor” (01A/B), or “Metastatic” (06A) samples were then further analyzed in GraphPad Prism 10 to prepare violin plots.

RStudio Analysis of CRISPR/Cas9 Datasets

RStudio (https://posit.co/download/rstudio-desktop/) was used to analyze CRISPR/Cas9 datasets (described above). The generation of the “Volcano Plot” corresponding to the SCC90 dataset utilized the following RStudio libraries: (tidyverse), (ggrepel), and (RcolorBrewer). The ggPlot() function was used to plot all genes based on their respective log2FC and -log10(p-value). The generation of “Venn Diagrams” utilized the following RStudio libraries: (VennDiagram) and (readxl). The venn.plot() function was used to illustrate the overlap in genes from all three screens (N/Tert-1, SCC90, SCC152) after having met the Z-Score cutoff of ($Z = \pm 1.5$). That is, predicted top regulators candidate genes ranked by MAGeCK and normalized across screens where ($Z \leq -1.5$; $Z \geq 1.5$) and Z-score = [(log2FC-mean FC) / SD of mean]. The supplemental file for “**Supplemental Figure 1_Z-score Full**” is attached.

STRING Analysis

The MAGeCK derived ranked SCC90 CRISPR/Cas9 screen gene list (described above) was uploaded in STRING (https://string-db.org/)[368] using the “Proteins with Values/Ranks - Functional Enrichment Analysis” and set for “homo sapiens” to further analyze the ranked list of genes. The analysis is performed by uploading gene names and their associated LFC value from the ranked list. STRING scoring methods have been described[557]. The “Local Network Clusters” were arranged into a hierarchy based on their

computed enrichment score and associated false discovery rate (i.e., “Top of Input” (Negative MHC-I Regulators), “Bottom of Input” (Positive MHC-I Regulators), and” Both Ends” (where clusters overlapped in both top and bottom ends). Additional information, definitions, and technical details of the analysis can be found at (https://string-db.org/cgi/help?sessionId=bOBC0vSYiJLV). The derived “Local Network Clusters” were plotted in GraphPad Prism. Clusters corresponding to “Both Ends” along with redundant clusters from “Top of Input” (e.g., SAGA Complex (CL:6030)) were omitted from the tabulation for simplicity, and the most robust scoring cluster was maintained. The raw analysis is found in the “**Supplemental Figure 2_STRING Local Network Cluster**” supplemental download file.

TIMER2.0 Analysis

The *in silico* tool analysis of the head and neck cancer TCGA dataset was determined by TIMER2.0[373-375] (http://timer.cistrome.org/) generated in the lab of Dr. Xiaole Liu at the Dana Farber Cancer Institute. All TCGA data was collected from GDAC firehose website (http://firebrowse.org/).[375] All of the subsequent descriptions are based on descriptions put forth from (http://timer.cistrome.org/) and the cited works.[373-375]

For differential gene expression, each respective gene is selected under “Gene_DE.” Boxplots provide expression levels from the dataset; blue colored boxes represent normal (non-tumor) samples (n =44) and red represent tumor samples (n =520). Tumor samples are further divided into HPV-positive (HNSC-HPV+) (n= 97) or HPV-negative tumor samples (HNSC-HPV-) (n= 421). The criteria for HPV positive determination were not known. A request was made to the site operators for clarity, but no response has been issued. The Wilcoxon test was used to determine statistical significance and is denoted by asterisks (*: p-value < 0.05; **: p-value <0.01; ***: p-value <0.001). Box plots for

PRC2.1 genes EZH2, EED, SUZ12, and MTF2, along with SAGA genes KAT2A, TADA1, USP22, and TAF6L are shown, and plot images were captured from (http://timer.cistrome.org/) for display.

For Gene Correlation, TIMER2.0 (Gene_Corr) module permits the calculation of correlation between a given gene of interest and expression of another given gene as determined from the TCGA head and neck cancer dataset. For total head and neck cancer (HNSC) tumor samples (n =522), HPV-positive (HNSC-HPV+) (n= 98), or HPV-negative HNSC-HPV-) (n= 422) tumor samples. The statistical degree of correlation is determined by the "purity-adjusted" partial Spearman's rho (ρ) with positive correlation as $p<0.05$ and $\rho > 0$; negative correlation as $p<0.05$ and $\rho < 0$. For the figures generated in this work, values were downloaded from the TIMER2.0 website and plotted as Correlation versus significance (1/p-Value) for the displayed genes with GraphPad Prism.

The Gene Expression and Immune Infiltrate module on TIMER2.0 under "Immune" and "Gene" options, permits correlation of a respective gene with the tumor infiltration of different immune cell types. For total head and neck cancer (HNSC) tumor samples (n =522), HPV-positive (HNSC-HPV+) (n= 98), or HPV-negative HNSC-HPV-) (n= 422) tumor samples. The statistical degree of correlation is determined by the "purity-adjusted" partial Spearman's rho (ρ) with positive correlation as $p<0.05$ and $\rho > 0$; negative correlation as $p<0.05$ and $\rho < 0$. For all cell types listed (i.e., T cell CD4+, T cell CD8+, Macrophage (Mac), Macrophage M2, Myeloid Derived Suppressor Cells (MDSC), Myeloid Dendritic Cells (DC), values were gleaned from TIMER2.0 calculation. For NK cells (NK), TIMER2.0 supplies EPIC determined values, which were displayed in the figure.

IPA Analysis

Our CRISPR/Cas9 screen data were analyzed through the use of QIAGEN Ingenuity Pathway Analysis (https://digitalinsights.qiagen.com/products-overview/discovery-insights-portfolio/analysis-and-visualization/qiagen-ipa/)[376]. The analysis was used to identify pathways, genes, and pharmacologic agents that could hypothetically explain the observed gene expression changes in our screen datasets. To perform the analysis, experimental data values from our MAGeCK ranked lists generated from the CRISPR/Cas9 screens, were loaded into IPA with three criteria: gene name, Log2FC, and p-Value. Next, “Core Analysis” is performed. Core analysis can determine known canonical pathways enriched in the dataset and can predict potential upstream regulators (i.e., Upstream Regulator Analysis). Targets are assigned two statistical scores, an activation Z-score and an overlapping p-Value[376]. For p-Value, core analysis tests the null hypothesis that targets in our dataset (i.e., genes) do not overlap with known pathways, functions, etc., and p-Value is generated from the right-tailed Fischer Exact Test with significance $p<0.05$[376,558]. Z-score infers activation states (“activated” (+Z); “inhibited” (-Z)) based on IPA modeling and screens their pre-existing database (derived from existing literature) to make predictions based on the incidence of known targets, their directionality (i.e., positive or negative), and relationship to other associated targets[376,558]. More information on how the analysis statistics are calculated, and more about the IPA analysis in general, can be found in Kramer et al.[376] and can be found in the following online files published by Qiagen. (https://resources.qiagenbioinformatics.com/IPA_features/feature_highlight_upstream_downstream.pdf).

(http://pages.ingenuity.com/rs/ingenuity/images/0812%20upstream_regulator_analysis_whitepaper.pdf).

From the raw canonical pathway analysis, we sorted for negative Z-scores and then stratified based on the p-Value for each pathway. We listed the top 15 pathways in **Table 2.** Heading in red designate the list for each screen, and the headings in blue (i.e., "HOTAIR" or "PRC2 methylates histones and DNA") designate PRC2 associated pathways.

"Upstream regulator analysis" was also accessed from the core analysis. From the raw, unedited list of potential upstream targets, we segregated the pharmacological and genetic regulators based on molecule type. For genetic regulators, we chose the top 10 gene hits. Those hits had the molecule types of "transcription regulator," "transmembrane receptor," "kinase, growth factor," "transporter," or "other," but were all confirmed genes. For pharmacologic regulators, all compounds chosen were classified as "chemical drug," "chemical reagent," or "chemical - endogenous non-mammalian." For both genes and pharmacological agents, potential targets were only considered if they had both an attributed Z-Score and a p-Value. Additionally, the downstream targets from "E2F1" and "MYC" were also tabulated, and they were ranked on their original Log2FC (Expr Log Ratio) by IPA. The attached supplemental files "**Supplemental Figure 3_Canonical Pathways**" lists all identified pathways from our analysis, and "**Supplemental Figure 4_Upstream Regulator Analysis**", has the full and unedited predicted upstream regulator list, the isolated gene and pharmacologic lists, and all associated values and statistics.

AlphaFold 2.0 and SWISS-MODEL

Structure prediction of CXCL14 and CXCL14 mutant sequences were generated through the use of AlphaFold2.0 and SWISS-MODEL online structural analysis tools. The amino acid sequences of each protein were loaded in ColabFold (v. 1.5.2) (based on AlphaFold2)[470,471] (https://colab.research.google.com/drive/1J1G8OC6LZwT6Tqdz4uLRmnVzj7WWgUg1). Likewise, the same animo acid sequences were loaded into SWISS-MODEL Workspace[472-476]. The colored key denotes the AlphaFold-predicted local distance difference test (pLDDT) and is a per-residue confidence score for each amino acid. In the boxes highlighted in red, close-up regions where mutations were introduced are modeled and visualized by SWISS-MODEL.

Immune Epitope Database & Tools (IEDB) Analysis

Analysis of the HPV E6/E7 epitope chimera containing immunogenic epitopes which were derived from the full length E6 and E7 sequences. Starting with the full-length versions of HPV-16 E6 and E7 protein sequences (https://pave.niaid.nih.gov/locus_viewer?seq_id=HPV16REF), truncated animo acid segments were selected and then interspersed into a linked peptide chimera corresponding to the amino acid residues, E7(1-22), E6(22-31, E7(45-69), E6(41-53), E7 (70-98), respectively. Note that the residue numbers listed correspond to the full-length amino acid sequence from either 16-E7 or 16-E6. The chimera sequence [MHGDTPTLHEYMLDLQPETTDLTIHDIILECVAEPDRAHYNIVTFCCKCDSTLRLCVEV YDFAFRDLCIVQSTHVDIRTLEDLLMGTLGIVCPICSQKP] was then evaluated for the presence of immunogenic epitope sequences known to be presented via MHC-I

molecules via the IEDB epitope database **(**https://www.iedb.org/**)** and **(**http://tools.iedb.org/mhci/**).**

Statistical Analysis

Statistical analyses were performed using GraphPad Prism software. The mean +/- standard deviation (error bars) are represented on histograms (RT-qPCR and MFI). Significance (p = ≤0.05) was calculated using unpaired student's t-test or Dunnet's test for multiple comparisons and specific usage is specified in figure legends.

Generation of Diagrams and Illustrations

The depiction of diagrams and/or illustrations in figures 1,2,3,10,26,27,29,33,34,39, and 40 were created with BioRender.com (https://www.biorender.com/).

Data Availability

N/Tert-1_E6/E7, SCC90, and SCC152 CRISPR /Cas9 Screen Files to be Formally Deposited by the Pyeon Lab. All additional data files specified will be attached to submission electronically as supplemental files via Michigan State University ETD submission.

Table 3: List of sgRNA Targeting Sequences for CRISPR/Cas9 Knockout

Brunello #	Gene	Targeting Sequence	NCBI Ref Seq.
86266120	EED-1	AAGAGAATGATCCATACCAC	NM_003797.3
86255232	EED-2	TTGTGAATGACATTCATACA	NM_003797.3
148829740	EZH2-1	TTATGATGGGAAAGTACACG	NM_004456.4
148827244	EZH2-2	TTATCAGAAGGAAATTTCCG	NM_004456.4
64808013	MEN1-1	CCAGGCATGATCCTCAGACA	NM_130804.2
64809952	MEN1-2	GAACGTTGGTAGGGATGACG	NM_130804.2
31983100	SUZ12-1	GGAGACTATTCTTGATGGGA	NM_015355.2
31988435	SUZ12-2	GAGACTCTCTGAATTTCTAG	NM_015355.2
42120318	KAT2A-1	ATGAGATAAACCGACTGCTG	NM_021078.2

Table 3. (Cont'd)

42117757	KAT2A-2	TGGGGATGTCACCCATCACA	NM_021078.2
32851129	TAP1-1	CATCATGTCTCGGGTAACAG	NM_000593.5
32853380	TAP1-2	GGCTCCAAGAGCGAAAACGC	NM_000593.5
33313814	TAPBP-1	GATCGAGTGTTGGTTCGTGG	NM_172208.2
33313416	TAPBP-2	AAGCGGCTCATCTCGCAGTG	NM_172208.2
21015837	USP22-1	ACCTGGTGTGGACCCACGCG	NM_015276.1
21018000	USP22-2	TGGGGCTCTGCATCTCACAG	NM_015276.1
62782766	TAF6L-1	AGATCCTGGCAGATCCTGTG	NM_006473.3
62781928	TAF6L-2	GCAGACGAACTCCAAGATTG	NM_006473.3
166869775	TADA1-1	AGCTCATAGACTTCTCACAC	NM_053053.3
166876180	TADA1-2	AGAACTTAAGCGAGGCCCTG	NM_053053.3

Table 4: List of Primers

Name	Direction	Primer Sequence	Application
HLA-A	F	CTTGTAAAGTGTGAGACAGC	qPCR
HLA-A	R	CTTCAAGTCACAAAGGGAAG	qPCR
HLA-B	F	ATGTGTAGGAGGAAGAGTTC	qPCR
HLA-B	R	GAAGAAATCCTGCATCTCAG	qPCR
HLA-C	F	CATCACTTGTAAAGCCTGAG	qPCR
HLA-C	R	CTCTTGAAGTCACAAAGGAG	qPCR
HLA-E	F	TTCCGAGTGAATCTGCGGAC	qPCR
HLA-E	R	GTCGTAGGCGAACTGTTCATAC	qPCR
EZH2	F	AATCAGAGTACATGCGACTGAGA	qPCR
EZH2	R	GCTGTATCCTTCGCTGTTTCC	qPCR
EED	F	AAAGACCCCTGCTTCCAGATT	qPCR
EED	R	TTCCCCACTCGTAAACACCAA	qPCR
SUZ12	F	AGGCTGACCACGAGCTTTTC	qPCR
SUZ12	R	GGTGCTATGAGATTCCGAGTTC	qPCR
MTF2	F	TCAAACGTCTACCATTACAGTGG	qPCR
MTF2	R	TCCAGGGTGCAATCTATCCCA	qPCR
KAT2A	F	CTATGCCAGGCGAGAAGAGG	qPCR
KAT2A	R	TCGGCGTAGGTGAGGAAGTA	qPCR
NLRC5	F	GCTCGGCAACAAGAACCTGT	qPCR
NLRC5	R	GGTCCAAGGTCTCGTTCCT	qPCR
TAP1	F	GCAAGAAATAAAGACACTCA	qPCR
TAP1	R	AGCATACCTGAAATACTAGT	qPCR
TAP2	F	AACAACAAAGTCTTGATG	qPCR
TAP2	R	TTAATGTCTCACCCAAAA	qPCR
TAPBP	F	TCAAAGAAGAAAGCAGAGTG	qPCR
TAPBP	R	AGAGAGATTGGAGGGATTAG	qPCR
B2M	F	CCACTGAAAAAGATGAGTATGCCT	qPCR
B2M	R	CCAATCCAAATGCGGCATCTTCA	qPCR

Table 4. (Cont'd)

NANOG	F	TTTGTGGGCCTGAAGAAAACT	qPCR
NANOG	R	AGGGCTGTCCTGAATAAGCAG	qPCR
STAT3	F	CAGCAGCTTGACACACGGTA	qPCR
STAT3	R	AAACACCAAAGTGGCATGTGA	qPCR
OCT4(POUF1)	F	GGTCCGAGTGTGGTTCTGTA	qPCR
OCT4(POUF1)	R	CGAGGAGTACAGTGCAGTGA	qPCR
SOX2	F	GCCGAGTGGAAACTTTTGTCG	qPCR
SOX2	R	GGCAGCGTGTACTTATCCTTCT	qPCR
N-MYC	F	ACCCGGACGAAGATGACTTCT	qPCR
N-MYC	R	CAGCTCGTTCTCAAGCAGCAT	qPCR
c-MYC	F	CCTGGTGCTCCATGAGGAGAC	qPCR
c-MYC	R	CAGACTCTGACCTTTTGCCAGG	qPCR
HPV16-E6	F	CCACAGGAGCGACCCCGAAAGTTA	qPCR
HPV16-E6	R	CACGTCGCAGTAACTGTTGCTTGC	qPCR
HPV16-E7	F	GTGACAGCTCAGAGGAGGAGGATG	qPCR
HPV16-E7	R	ACGCACAACCGAAGCGTAGAGTCA	qPCR
MARCHF8	F	AGTGACATTCCACGTCATTGC	qPCR
MARCHF8	R	GATCTCCTCAGCAGTACGGTC	qPCR
GAPDH	F	GAAGGTGAAGGTCGGAGT	qPCR
GAPDH	R	CATGGGTGGAATCATATTGGAA	qPCR
B-Actin	F	TCACCCACACTGTGCCCATCTA	qPCR
B-Actin	R	TGAGGTAGTCAGTCAGGTCCCG	qPCR
H2Db	F	GGAGCCTCCTCCGTCCACTG	qPCR
H2Db	R	TACAATCTCGGAGAGACATT	qPCR
H2Kb	F	CGCGACGCTGCTGCGCACAG	qPCR
H2Kb	R	TACAATCTGGGAGAGACAGA	qPCR
B2M (mouse)	F	CCAGAGCAAGAGAGGTATCC	qPCR
B2M (mouse)	R	GAGTCCATCACAATGCCTGT	qPCR
ITGAV	F	CCTGTGCCTGTGTGGGTGAT	qPCR
ITGAV	R	GGTGGCGGACCCGTTTA	qPCR
ITGB5	F	TTGGCAGAGAACAACATCAACC	qPCR
ITGB5	R	TCCTCAGGCTGATCCCAGAC	qPCR
IL-12a	F	CCTTGCACTTCTGAAGAGATTGA	qPCR
IL-12a	R	ACAGGGCCATCATAAAAGAGGT	qPCR
TNF-alpha	F	GAGGCCAAGCCCTGGTATG	qPCR
TNF-alpha	R	CGGGCCGATTGATCTCAGC	qPCR
IL-1beta	F	CAGGCTGCTCTGGGATTCTC	qPCR
IL-1beta	R	GTCCTGGAAGGAGCACTTCAT	qPCR
USP22-sg1 Fwd	F	TCTGGCAGTTTTACTCTGGACA	TIDE
USP22-sg1 Rev	R	CAAAACAATGGAATGTGTCACC	TIDE
USP22-sg2 Fwd	F	CAGGTAACTCCTGCTCTCTGGT	TIDE
USP22-sg2 Rev	R	AGTAACAGAAATGTTCCCCTGC	TIDE
TAF6L-sg1 Fwd	F	TTGTAAGTGGCCTCTATCAGCA	TIDE
TAF6L-sg1 Rev	R	CAGGCACACACTATTTTGGAGA	TIDE
TAF6L-sg2 Fwd	F	CTGTCTTCCAGAAGAATACCGC	TIDE

Table 4. (Cont'd)

TAF6L-sg2 Rev	R	GGTAGCTTACAGGGACATGAGG	TIDE
TADA1-sg1 Fwd	F	AACCTAAAGCTGTGGTTCAAGC	TIDE
TADA1-sg1 Rev	R	TTTTGGATATCCCCTATTCTGC	TIDE
TADA1-sg2 Fwd	F	AGTTGGTTTTTGGGTTGTTGAT	TIDE
TADA1-sg2 Rev	R	CTGGACGCTGTGCTAGGG	TIDE
EED-1F	F	CTTTTTGGTTTTGCATACAGGA	TIDE
EED-1R	R	TTCTAAACTCATTGTTGGGGCT	TIDE
EED-2F	F	TCACAGGAGGTATTTTAAGGCAG	TIDE
EED-2R	R	GGATACATCAGCATCCACGTAA	TIDE
EZH2-1F	F	TCTGGAGAACTGGGTAAAGACA	TIDE
EZH2-1R	R	TAGCCCCTTTTTCCAAGAGAA	TIDE
EZH2-2F	F	TTTGTTTTTGACTGACTGGCAT	TIDE
EZH2-2R	R	GTTCTTCTGCTGTGCCCTTATC	TIDE
MEN1-1F	F	AGGACCCTCTTTCATTACCTCC	TIDE
MEN1-1R	R	GGGCTACTACAGTATGAAGGGG	TIDE
MEN1-2F	F	GAACGTTGGTAGGGATGACG	TIDE
MEN1-2R	R	GAGACCTTCTTCACCAGCTCAC	TIDE
SUZ12-1F	F	ATGAAGTAGCCATGCAGGAAAT	TIDE
SUZ12-1R	R	ATGAATTAGCATTTGGGGAAGA	TIDE
SUZ12-2F	F	CTACGTTGCAGTTCACTCTTCG	TIDE
SUZ12-2R	R	CAGAGCAAGACTCCATCTCAAA	TIDE
TAP1-1F	F	CTCATCACTTGGAACCTGTCTG	TIDE
TAP1-1R	R	GGTACCATTTTCCCACCTTCTT	TIDE
TAP1-2F	F	AGTACTGCTACTTCTCGCCGAC	TIDE
TAP1-2R	R	ATGAGATCAGCTCTCGGAACA	TIDE
TAP2-1F	F	CATCTCCCTCCCCTCTTATTCT	TIDE
TAP2-1R	R	TTAGTCTCCTGGAAGAAACCGA	TIDE
TAP2-2F	F	CAAATTGGAACACTGGGGTATT	TIDE
TAP2-2R	R	GTCGGTCCATGTAGGAGAAAAC	TIDE
TAPBP-1F	F	GCAGGTCACCAGACATACAAAC	TIDE
TAPBP-1R	R	ACTGAGATAGAGCTCAGGGTCG	TIDE
TAPBP-2F	F	TCCTTCTCTACACTCAGACCCC	TIDE
TAPBP-2R	R	ATATGCTGACCATCAGCCAAG	TIDE
pLenti-CXCL14-F	F	AGGCCTGGATCCGCCGCCACCATGAGGCTC	Cloning
pLenti-CXCL14-R	R	AGGCCTACCGGTCTACTTGTCATCGTCATCCTT	Cloning
pCDH_CXCL14	F	ACTAAAGAATTCGCCGCCACCATGAGGCTC	Cloning
pCDH_CXCL14	R	TTTAGTGGATCCCTACTTGTCATCGTCATC	Cloning
CXCL14_RY43/44AA	F	CACCAAGAGCATGTCCGCGGCCCGGGGCCAGGAGCAC	Mutagenesis
CXCL14_RY43/44AA	R	GTGCTCCTGGCCCCGGGCCGCGGACATGCTCTTGGTG	Mutagenesis
CXCL14_dEE	F	GAGAAGCGCAGGGTCTACGACTACAAAGACCATG	Mutagenesis
CXCL14_dEE	R	CATGGTCTTTGTAGTCGTAGACCCTGCGCTTCTC	Mutagenesis
pShuttle_CXCL14-F	F	GGTGGTAGATCTGCCGCCACCATGAGGCTC	Cloning
pShuttle_CXCL14-R	R	GATGACGATGACAAGTAGAAGCTTTGATCA	Cloning
pShuttle_NG01	F	TGATCAAGATCTGCCGCCACCATGAGGCTC	Cloning
pShuttle_NG01	R	AGGCCTGATATCCTAAGCGTAATCTGGAACATCGTA	Cloning

Table 4. (Cont'd)

pShuttle_HPV_Epitopes	F	AGGCCTAGATCTGCCGCCACCATGCTGCTATCCGTGCCG	Cloning
pShuttle_HPV_Epitopes	R	AGGCCTGATATCCTAAGCGTAATCTGGAACATCGTA	Cloning
ITR-Psi_F	F	CGACGGATGTGGCAAAAGT	Ad5 Titration
ITR-Psi_R:	R	CCGCCTAAAACCGCGCGAAAA	Ad5 Titration

Table 5: List of Antibodies

Antibody Name	**Application**	**Company**	**Product #**
HPV16 E7	Western Blot	ThermoFisher	28-0006
HLA-A/B/C	Western Blot	Protein Tech	15240-1-AP
MTF2 Rabbit PolyAb	Western Blot	Protein Tech	16208-1-AP
MARCH8 Rabbit PolyAb	Western Blot	Protein Tech	14119-1-AP
N-Myc Antibody (B8.4.B)	Western Blot	Santa Cruz	sc-53993
E2F3	Western Blot / CoIP	Santa Cruz	sc-56665
E2F-1 Antibody (KH95)	Western Blot / CoIP	Santa Cruz	sc-251x
GCN5 (KAT2A)	Western Blot	Santa Cruz	sc-365321
SUZ12	Western Blot	Santa Cruz	sc-271325
Ezh2 (D2C9) XP® Rabbit mAb #5246	Western Blot	Cell Signaling	5246S
EED (E4L6E) Antibody	Western Blot	Cell Signaling	85322S
MONOCLONAL ANTI-FLAG(R) M2	Western Blot	Sigma-Aldrich	F1804-200UG
Direct-Blot™ HRP anti-β-actin Antibody	Western Blot	BioLegend	664804
Anti-mouse IgG, HRP-linked Antibody Seconday	Western Blot	Cell Signaling	7076
Anti-rabbit IgG, HRP-linked Antibody Seconday	Western Blot	Cell Signaling	7074
Tri-Methyl-Histone H3 (Lys27) (C36B11) Rabbit mAb	Western Blot	Cell Signaling	9733
Acetyl-Histone H3 (Lys9) (C5B11) Rabbit mAb	Western Blot	Cell Signaling	9649
STAT1 (D1K9Y) Rabbit mAb	Western Blot	Cell Signaling	14994
Phospho-Stat1 (Ser727) Antibody	Western Blot	Cell Signaling	9177
FITC anti-human HLA-A,B,C Antibody	Flow Cytometry	BioLegend	311404
Rabbit IgG	CUT&RUN	Epicypher	13-0042
H3K4me3	CUT&RUN	Epicypher	13-0041
H3K27me3	CUT&RUN	Thermo Fisher	MA5-11198

REFERENCES

1. Powell, S.F., Vu, L., Spanos, W.C., and Pyeon, D. (2021). The Key Differences between Human Papillomavirus-Positive and -Negative Head and Neck Cancers: Biological and Clinical Implications. Cancers (Basel) *13*. 10.3390/cancers13205206.

2. Barsouk, A., Aluru, J.S., Rawla, P., Saginala, K., and Barsouk, A. (2023). Epidemiology, Risk Factors, and Prevention of Head and Neck Squamous Cell Carcinoma. Med Sci (Basel) *11*. 10.3390/medsci11020042.

3. Szymonowicz, K.A., and Chen, J. (2020). Biological and clinical aspects of HPV-related cancers. Cancer Biol Med *17*, 864-878. 10.20892/j.issn.2095-3941.2020.0370.

4. Gondal, T.A., Chaudhary, N., Bajwa, H., Rauf, A., Le, D., and Ahmed, S. (2023). Anal Cancer: The Past, Present and Future. Curr Oncol *30*, 3232-3250. 10.3390/curroncol30030246.

5. Gao, G., and Smith, D.I. (2016). Human Papillomavirus and the Development of Different Cancers. Cytogenet Genome Res *150*, 185-193. 10.1159/000458166.

6. Chaturvedi, A.K., Katki, H.A., Hildesheim, A., Rodriguez, A.C., Quint, W., Schiffman, M., Van Doorn, L.J., Porras, C., Wacholder, S., Gonzalez, P., et al. (2011). Human papillomavirus infection with multiple types: pattern of coinfection and risk of cervical disease. J Infect Dis *203*, 910-920. 10.1093/infdis/jiq139.

7. McDermott, J.D., and Bowles, D.W. (2019). Epidemiology of Head and Neck Squamous Cell Carcinomas: Impact on Staging and Prevention Strategies. Curr Treat Options Oncol *20*, 43. 10.1007/s11864-019-0650-5.

8. Conarty, J.P., and Wieland, A. (2023). The Tumor-Specific Immune Landscape in HPV+ Head and Neck Cancer. Viruses *15*. 10.3390/v15061296.

9. de Martel, C., Plummer, M., Vignat, J., and Franceschi, S. (2017). Worldwide burden of cancer attributable to HPV by site, country and HPV type. Int J Cancer *141*, 664-670. 10.1002/ijc.30716.

10. Hirth, J. (2019). Disparities in HPV vaccination rates and HPV prevalence in the United States: a review of the literature. Hum Vaccin Immunother *15*, 146-155. 10.1080/21645515.2018.1512453.

11. Beavis, A.L., and Levinson, K.L. (2016). Preventing Cervical Cancer in the United States: Barriers and Resolutions for HPV Vaccination. Front Oncol *6*, 19. 10.3389/fonc.2016.00019.

12. Mirabello, L., Clarke, M.A., Nelson, C.W., Dean, M., Wentzensen, N., Yeager, M., Cullen, M., Boland, J.F., Workshop, N.H., Schiffman, M., and Burk, R.D. (2018).

The Intersection of HPV Epidemiology, Genomics and Mechanistic Studies of HPV-Mediated Carcinogenesis. Viruses *10*. 10.3390/v10020080.

13. Hakim, A.A., and Dinh, T.A. (2009). Worldwide impact of the human papillomavirus vaccine. Curr Treat Options Oncol *10*, 44-53. 10.1007/s11864-009-0094-4.

14. Bruni, L., Serrano, B., Roura, E., Alemany, L., Cowan, M., Herrero, R., Poljak, M., Murillo, R., Broutet, N., Riley, L.M., and de Sanjose, S. (2022). Cervical cancer screening programmes and age-specific coverage estimates for 202 countries and territories worldwide: a review and synthetic analysis. Lancet Glob Health *10*, e1115-e1127. 10.1016/S2214-109X(22)00241-8.

15. Serrano, B., Ibanez, R., Robles, C., Peremiquel-Trillas, P., de Sanjose, S., and Bruni, L. (2022). Worldwide use of HPV self-sampling for cervical cancer screening. Prev Med *154*, 106900. 10.1016/j.ypmed.2021.106900.

16. Tota, J.E., Best, A.F., Zumsteg, Z.S., Gillison, M.L., Rosenberg, P.S., and Chaturvedi, A.K. (2019). Evolution of the Oropharynx Cancer Epidemic in the United States: Moderation of Increasing Incidence in Younger Individuals and Shift in the Burden to Older Individuals. J Clin Oncol *37*, 1538-1546. 10.1200/JCO.19.00370.

17. Nokovitch, L., Maquet, C., Crampon, F., Taihi, I., Roussel, L.M., Obongo, R., Virard, F., Fervers, B., and Deneuve, S. (2023). Oral Cavity Squamous Cell Carcinoma Risk Factors: State of the Art. J Clin Med *12*. 10.3390/jcm12093264.

18. Khariwala, S.S., Ma, B., Ruszczak, C., Carmella, S.G., Lindgren, B., Hatsukami, D.K., Hecht, S.S., and Stepanov, I. (2017). High Level of Tobacco Carcinogen-Derived DNA Damage in Oral Cells Is an Independent Predictor of Oral/Head and Neck Cancer Risk in Smokers. Cancer Prev Res (Phila) *10*, 507-513. 10.1158/1940-6207.CAPR-17-0140.

19. Ferraguti, G., Terracina, S., Petrella, C., Greco, A., Minni, A., Lucarelli, M., Agostinelli, E., Ralli, M., de Vincentiis, M., Raponi, G., et al. (2022). Alcohol and Head and Neck Cancer: Updates on the Role of Oxidative Stress, Genetic, Epigenetics, Oral Microbiota, Antioxidants, and Alkylating Agents. Antioxidants (Basel) *11*. 10.3390/antiox11010145.

20. Dayyani, F., Etzel, C.J., Liu, M., Ho, C.H., Lippman, S.M., and Tsao, A.S. (2010). Meta-analysis of the impact of human papillomavirus (HPV) on cancer risk and overall survival in head and neck squamous cell carcinomas (HNSCC). Head Neck Oncol *2*, 15. 10.1186/1758-3284-2-15.

21. Hoppe-Seyler, K., Bossler, F., Braun, J.A., Herrmann, A.L., and Hoppe-Seyler, F. (2018). The HPV E6/E7 Oncogenes: Key Factors for Viral Carcinogenesis and Therapeutic Targets. Trends Microbiol *26*, 158-168. 10.1016/j.tim.2017.07.007.

22. Ren, S., Gaykalova, D.A., Guo, T., Favorov, A.V., Fertig, E.J., Tamayo, P., Callejas-Valera, J.L., Allevato, M., Gilardi, M., Santos, J., et al. (2020). HPV E2, E4, E5 drive alternative carcinogenic pathways in HPV positive cancers. Oncogene *39*, 6327-6339. 10.1038/s41388-020-01431-8.

23. Bhatla, N., and Singhal, S. (2020). Primary HPV screening for cervical cancer. Best Pract Res Clin Obstet Gynaecol *65*, 98-108. 10.1016/j.bpobgyn.2020.02.008.

24. Pipas, J.M. (2019). DNA Tumor Viruses and Their Contributions to Molecular Biology. J Virol *93*. 10.1128/JVI.01524-18.

25. DiMaio, D. (2019). Small size, big impact: how studies of small DNA tumour viruses revolutionized biology. Philos Trans R Soc Lond B Biol Sci *374*, 20180300. 10.1098/rstb.2018.0300.

26. Munoz, N., Castellsague, X., Berrington de Gonzalez, A., and Gissmann, L. (2006). Chapter 1: HPV in the etiology of human cancer. Vaccine *24 Suppl 3*, S3/1-10. 10.1016/j.vaccine.2006.05.115.

27. Rice, G., and Rompolas, P. (2020). Advances in resolving the heterogeneity and dynamics of keratinocyte differentiation. Curr Opin Cell Biol *67*, 92-98. 10.1016/j.ceb.2020.09.004.

28. Doorbar, J. (2005). The papillomavirus life cycle. J Clin Virol *32 Suppl 1*, S7-15. 10.1016/j.jcv.2004.12.006.

29. Roman, A., and Munger, K. (2013). The papillomavirus E7 proteins. Virology *445*, 138-168. 10.1016/j.virol.2013.04.013.

30. Kirk, A., and Graham, S.V. (2024). The human papillomavirus late life cycle and links to keratinocyte differentiation. J Med Virol *96*, e29461. 10.1002/jmv.29461.

31. Vande Pol, S.B., and Klingelhutz, A.J. (2013). Papillomavirus E6 oncoproteins. Virology *445*, 115-137. 10.1016/j.virol.2013.04.026.

32. Sherman, L., Itzhaki, H., Jackman, A., Chen, J.J., Koval, D., and Schlegel, R. (2002). Inhibition of serum- and calcium-induced terminal differentiation of human keratinocytes by HPV 16 E6: study of the association with p53 degradation, inhibition of p53 transactivation, and binding to E6BP. Virology *292*, 309-320. 10.1006/viro.2001.1263.

33. Dyson, N. (1998). The regulation of E2F by pRB-family proteins. Genes Dev *12*, 2245-2262. 10.1101/gad.12.15.2245.

34. Munger, K., Baldwin, A., Edwards, K.M., Hayakawa, H., Nguyen, C.L., Owens, M., Grace, M., and Huh, K. (2004). Mechanisms of human papillomavirus-

induced oncogenesis. J Virol *78*, 11451-11460. 10.1128/JVI.78.21.11451-11460.2004.

35. Kent, L.N., and Leone, G. (2019). The broken cycle: E2F dysfunction in cancer. Nat Rev Cancer *19*, 326-338. 10.1038/s41568-019-0143-7.

36. Rabinovich, A., Jin, V.X., Rabinovich, R., Xu, X., and Farnham, P.J. (2008). E2F in vivo binding specificity: comparison of consensus versus nonconsensus binding sites. Genome Res *18*, 1763-1777. 10.1101/gr.080622.108.

37. Xu, X., Bieda, M., Jin, V.X., Rabinovich, A., Oberley, M.J., Green, R., and Farnham, P.J. (2007). A comprehensive ChIP-chip analysis of E2F1, E2F4, and E2F6 in normal and tumor cells reveals interchangeable roles of E2F family members. Genome Res *17*, 1550-1561. 10.1101/gr.6783507.

38. Cicchini, L., Blumhagen, R.Z., Westrich, J.A., Myers, M.E., Warren, C.J., Siska, C., Raben, D., Kechris, K.J., and Pyeon, D. (2017). High-Risk Human Papillomavirus E7 Alters Host DNA Methylome and Represses HLA-E Expression in Human Keratinocytes. Sci Rep *7*, 3633. 10.1038/s41598-017-03295-7.

39. Burgers, W.A., Blanchon, L., Pradhan, S., de Launoit, Y., Kouzarides, T., and Fuks, F. (2007). Viral oncoproteins target the DNA methyltransferases. Oncogene *26*, 1650-1655. 10.1038/sj.onc.1209950.

40. Scheffner, M., Huibregtse, J.M., Vierstra, R.D., and Howley, P.M. (1993). The HPV-16 E6 and E6-AP complex functions as a ubiquitin-protein ligase in the ubiquitination of p53. Cell *75*, 495-505. 10.1016/0092-8674(93)90384-3.

41. Stine, Z.E., Walton, Z.E., Altman, B.J., Hsieh, A.L., and Dang, C.V. (2015). MYC, Metabolism, and Cancer. Cancer Discov *5*, 1024-1039. 10.1158/2159-8290.CD-15-0507.

42. Veldman, T., Liu, X., Yuan, H., and Schlegel, R. (2003). Human papillomavirus E6 and Myc proteins associate in vivo and bind to and cooperatively activate the telomerase reverse transcriptase promoter. Proc Natl Acad Sci U S A *100*, 8211-8216. 10.1073/pnas.1435900100.

43. Liu, X., Yuan, H., Fu, B., Disbrow, G.L., Apolinario, T., Tomaic, V., Kelley, M.L., Baker, C.C., Huibregtse, J., and Schlegel, R. (2005). The E6AP ubiquitin ligase is required for transactivation of the hTERT promoter by the human papillomavirus E6 oncoprotein. J Biol Chem *280*, 10807-10816. 10.1074/jbc.M410343200.

44. Van Doorslaer, K., and Burk, R.D. (2012). Association between hTERT activation by HPV E6 proteins and oncogenic risk. Virology *433*, 216-219. 10.1016/j.virol.2012.08.006.

45. Khalil, M.I., Yang, C., Vu, L., Chadha, S., Nabors, H., Welbon, C., James, C.D., Morgan, I.M., Spanos, W.C., and Pyeon, D. (2023). HPV upregulates MARCHF8 ubiquitin ligase and inhibits apoptosis by degrading the death receptors in head and neck cancer. PLoS Pathog *19*, e1011171. 10.1371/journal.ppat.1011171.

46. Yuan, H., Krawczyk, E., Blancato, J., Albanese, C., Zhou, D., Wang, N., Paul, S., Alkhilaiwi, F., Palechor-Ceron, N., Dakic, A., et al. (2017). HPV positive neuroendocrine cervical cancer cells are dependent on Myc but not E6/E7 viral oncogenes. Sci Rep *7*, 45617. 10.1038/srep45617.

47. Wang, X., Jia, W., Wang, M., Liu, J., Zhou, X., Liang, Z., Zhang, Q., Long, S., Quzhen, S., Li, X., et al. (2022). Human papillomavirus integration perspective in small cell cervical carcinoma. Nat Commun *13*, 5968. 10.1038/s41467-022-33359-w.

48. Strieder, V., and Lutz, W. (2002). Regulation of N-myc expression in development and disease. Cancer Lett *180*, 107-119. 10.1016/s0304-3835(02)00020-4.

49. Herrick, J., Conti, C., Teissier, S., Thierry, F., Couturier, J., Sastre-Garau, X., Favre, M., Orth, G., and Bensimon, A. (2005). Genomic organization of amplified MYC genes suggests distinct mechanisms of amplification in tumorigenesis. Cancer Res *65*, 1174-1179. 10.1158/0008-5472.CAN-04-2802.

50. Rickman, D.S., Schulte, J.H., and Eilers, M. (2018). The Expanding World of N-MYC-Driven Tumors. Cancer Discov *8*, 150-163. 10.1158/2159-8290.CD-17-0273.

51. Swartling, F.J., Savov, V., Persson, A.I., Chen, J., Hackett, C.S., Northcott, P.A., Grimmer, M.R., Lau, J., Chesler, L., Perry, A., et al. (2012). Distinct neural stem cell populations give rise to disparate brain tumors in response to N-MYC. Cancer Cell *21*, 601-613. 10.1016/j.ccr.2012.04.012.

52. Yancopoulos, G.D., Nisen, P.D., Tesfaye, A., Kohl, N.E., Goldfarb, M.P., and Alt, F.W. (1985). N-myc can cooperate with ras to transform normal cells in culture. Proc Natl Acad Sci U S A *82*, 5455-5459. 10.1073/pnas.82.16.5455.

53. Seeger, R.C., Brodeur, G.M., Sather, H., Dalton, A., Siegel, S.E., Wong, K.Y., and Hammond, D. (1985). Association of multiple copies of the N-myc oncogene with rapid progression of neuroblastomas. N Engl J Med *313*, 1111-1116. 10.1056/NEJM198510313131802.

54. Brodeur, G.M., Seeger, R.C., Sather, H., Dalton, A., Siegel, S.E., Wong, K.Y., and Hammond, D. (1986). Clinical implications of oncogene activation in human neuroblastomas. Cancer *58*, 541-545. 10.1002/1097-0142(19860715)58:2+<541::aid-cncr2820581322>3.0.co;2-2.

55. Funa, K., Steinholtz, L., Nou, E., and Bergh, J. (1987). Increased expression of N-myc in human small cell lung cancer biopsies predicts lack of response to chemotherapy and poor prognosis. Am J Clin Pathol *88*, 216-220. 10.1093/ajcp/88.2.216.

56. Malone, C.F., Mabe, N.W., Forman, A.B., Alexe, G., Engel, K.L., Chen, Y.C., Soeung, M., Salhotra, S., Basanthakumar, A., Liu, B., et al. (2024). The KAT module of the SAGA complex maintains the oncogenic gene expression program in MYCN-amplified neuroblastoma. Sci Adv *10*, eadm9449. 10.1126/sciadv.adm9449.

57. Bernards, R., Dessain, S.K., and Weinberg, R.A. (1986). N-myc amplification causes down-modulation of MHC class I antigen expression in neuroblastoma. Cell *47*, 667-674. 10.1016/0092-8674(86)90509-x.

58. Sarma, J.V., and Ward, P.A. (2011). The complement system. Cell Tissue Res *343*, 227-235. 10.1007/s00441-010-1034-0.

59. Turvey, S.E., and Broide, D.H. (2010). Innate immunity. J Allergy Clin Immunol *125*, S24-32. 10.1016/j.jaci.2009.07.016.

60. Gallo, R.L., and Hooper, L.V. (2012). Epithelial antimicrobial defence of the skin and intestine. Nat Rev Immunol *12*, 503-516. 10.1038/nri3228.

61. Kurn, H., and Daly, D.T. (2024). Histology, Epithelial Cell. In StatPearls.

62. Sanchez-Danes, A., and Blanpain, C. (2018). Deciphering the cells of origin of squamous cell carcinomas. Nat Rev Cancer *18*, 549-561. 10.1038/s41568-018-0024-5.

63. Jamal, Z., and Anjum, F. (2024). Oropharyngeal Squamous Cell Carcinoma. In StatPearls.

64. Harden, M.E., and Munger, K. (2017). Human papillomavirus molecular biology. Mutat Res Rev Mutat Res *772*, 3-12. 10.1016/j.mrrev.2016.07.002.

65. Egawa, N., Egawa, K., Griffin, H., and Doorbar, J. (2015). Human Papillomaviruses; Epithelial Tropisms, and the Development of Neoplasia. Viruses *7*, 3863-3890. 10.3390/v7072802.

66. Doorbar, J. (2013). Latent papillomavirus infections and their regulation. Curr Opin Virol *3*, 416-421. 10.1016/j.coviro.2013.06.003.

67. Maglennon, G.A., McIntosh, P.B., and Doorbar, J. (2014). Immunosuppression facilitates the reactivation of latent papillomavirus infections. J Virol *88*, 710-716. 10.1128/JVI.02589-13.

68. Doorbar, J. (2023). The human Papillomavirus twilight zone - Latency, immune control and subclinical infection. Tumour Virus Res *16*, 200268. 10.1016/j.tvr.2023.200268.

69. Agudo, J. (2021). Immune privilege of skin stem cells: What do we know and what can we learn? Exp Dermatol *30*, 522-528. 10.1111/exd.14221.

70. Beutler, B. (2004). Innate immunity: an overview. Mol Immunol *40*, 845-859. 10.1016/j.molimm.2003.10.005.

71. Takeda, K., Kaisho, T., and Akira, S. (2003). Toll-like receptors. Annu Rev Immunol *21*, 335-376. 10.1146/annurev.immunol.21.120601.141126.

72. Martinez-Campos, C., Burguete-Garcia, A.I., and Madrid-Marina, V. (2017). Role of TLR9 in Oncogenic Virus-Produced Cancer. Viral Immunol *30*, 98-105. 10.1089/vim.2016.0103.

73. Michalak, E.M., Burr, M.L., Bannister, A.J., and Dawson, M.A. (2019). The roles of DNA, RNA and histone methylation in ageing and cancer. Nat Rev Mol Cell Biol *20*, 573-589. 10.1038/s41580-019-0143-1.

74. Hasan, U.A., Bates, E., Takeshita, F., Biliato, A., Accardi, R., Bouvard, V., Mansour, M., Vincent, I., Gissmann, L., Iftner, T., et al. (2007). TLR9 expression and function is abolished by the cervical cancer-associated human papillomavirus type 16. J Immunol *178*, 3186-3197. 10.4049/jimmunol.178.5.3186.

75. Pacini, L., Savini, C., Ghittoni, R., Saidj, D., Lamartine, J., Hasan, U.A., Accardi, R., and Tommasino, M. (2015). Downregulation of Toll-Like Receptor 9 Expression by Beta Human Papillomavirus 38 and Implications for Cell Cycle Control. J Virol *89*, 11396-11405. 10.1128/JVI.02151-15.

76. Latz, E., Schoenemeyer, A., Visintin, A., Fitzgerald, K.A., Monks, B.G., Knetter, C.F., Lien, E., Nilsen, N.J., Espevik, T., and Golenbock, D.T. (2004). TLR9 signals after translocating from the ER to CpG DNA in the lysosome. Nat Immunol *5*, 190-198. 10.1038/ni1028.

77. Kim, Y.M., Brinkmann, M.M., Paquet, M.E., and Ploegh, H.L. (2008). UNC93B1 delivers nucleotide-sensing toll-like receptors to endolysosomes. Nature *452*, 234-238. 10.1038/nature06726.

78. Hacker, H., Vabulas, R.M., Takeuchi, O., Hoshino, K., Akira, S., and Wagner, H. (2000). Immune cell activation by bacterial CpG-DNA through myeloid differentiation marker 88 and tumor necrosis factor receptor-associated factor (TRAF)6. J Exp Med *192*, 595-600. 10.1084/jem.192.4.595.

79. Kumagai, Y., Takeuchi, O., and Akira, S. (2008). TLR9 as a key receptor for the recognition of DNA. Adv Drug Deliv Rev *60*, 795-804. 10.1016/j.addr.2007.12.004.

80. Liu, T., Zhang, L., Joo, D., and Sun, S.C. (2017). NF-kappaB signaling in inflammation. Signal Transduct Target Ther *2*, 17023-. 10.1038/sigtrans.2017.23.

81. Kawai, T., and Akira, S. (2006). Innate immune recognition of viral infection. Nat Immunol *7*, 131-137. 10.1038/ni1303.

82. Giacobbi, N.S., Gupta, T., Coxon, A.T., and Pipas, J.M. (2015). Polyomavirus T antigens activate an antiviral state. Virology *476*, 377-385. 10.1016/j.virol.2014.12.032.

83. Lim, L., Hu, M.H., Fan, D., Tu, H.F., Tsai, Y.C., Cheng, M., Wang, S., Chang, C.L., Wu, T.C., and Hung, C.F. (2024). STAT1-Deficient HPV E6/E7-Associated Cancers Maintain Host Immunocompetency against Therapeutic Intervention. Vaccines (Basel) *12*. 10.3390/vaccines12040430.

84. Schoggins, J.W. (2019). Interferon-Stimulated Genes: What Do They All Do? Annu Rev Virol *6*, 567-584. 10.1146/annurev-virology-092818-015756.

85. Zhou, F. (2009). Molecular mechanisms of IFN-gamma to up-regulate MHC class I antigen processing and presentation. Int Rev Immunol *28*, 239-260. 10.1080/08830180902978120.

86. Ma, W., Lehner, P.J., Cresswell, P., Pober, J.S., and Johnson, D.R. (1997). Interferon-gamma rapidly increases peptide transporter (TAP) subunit expression and peptide transport capacity in endothelial cells. J Biol Chem *272*, 16585-16590. 10.1074/jbc.272.26.16585.

87. Han, J., Wu, M., and Liu, Z. (2023). Dysregulation in IFN-gamma signaling and response: the barricade to tumor immunotherapy. Front Immunol *14*, 1190333. 10.3389/fimmu.2023.1190333.

88. Newton, K., and Dixit, V.M. (2012). Signaling in innate immunity and inflammation. Cold Spring Harb Perspect Biol *4*. 10.1101/cshperspect.a006049.

89. Nauseef, W.M., and Borregaard, N. (2014). Neutrophils at work. Nat Immunol *15*, 602-611. 10.1038/ni.2921.

90. Coffman, R.L. (2010). Immunology. The origin of TH2 responses. Science *328*, 1116-1117. 10.1126/science.1192009.

91. Poto, R., Gambardella, A.R., Marone, G., Schroeder, J.T., Mattei, F., Schiavoni, G., and Varricchi, G. (2022). Basophils from allergy to cancer. Front Immunol *13*, 1056838. 10.3389/fimmu.2022.1056838.

92. Stone, K.D., Prussin, C., and Metcalfe, D.D. (2010). IgE, mast cells, basophils, and eosinophils. J Allergy Clin Immunol *125*, S73-80. 10.1016/j.jaci.2009.11.017.

93. Vivier, E., Tomasello, E., Baratin, M., Walzer, T., and Ugolini, S. (2008). Functions of natural killer cells. Nat Immunol *9*, 503-510. 10.1038/ni1582.

94. Dhar, P., and Wu, J.D. (2018). NKG2D and its ligands in cancer. Curr Opin Immunol *51*, 55-61. 10.1016/j.coi.2018.02.004.

95. Ginhoux, F., and Jung, S. (2014). Monocytes and macrophages: developmental pathways and tissue homeostasis. Nat Rev Immunol *14*, 392-404. 10.1038/nri3671.

96. Price, J.V., and Vance, R.E. (2014). The macrophage paradox. Immunity *41*, 685-693. 10.1016/j.immuni.2014.10.015.

97. Laing, K.J., and Secombes, C.J. (2004). Chemokines. Dev Comp Immunol *28*, 443-460. 10.1016/j.dci.2003.09.006.

98. Westrich, J.A., Vermeer, D.W., Colbert, P.L., Spanos, W.C., and Pyeon, D. (2020). The multifarious roles of the chemokine CXCL14 in cancer progression and immune responses. Mol Carcinog *59*, 794-806. 10.1002/mc.23188.

99. Wculek, S.K., Cueto, F.J., Mujal, A.M., Melero, I., Krummel, M.F., and Sancho, D. (2020). Dendritic cells in cancer immunology and immunotherapy. Nat Rev Immunol *20*, 7-24. 10.1038/s41577-019-0210-z.

100. Zhang, X., and Mosser, D.M. (2008). Macrophage activation by endogenous danger signals. J Pathol *214*, 161-178. 10.1002/path.2284.

101. Nagarsheth, N., Wicha, M.S., and Zou, W. (2017). Chemokines in the cancer microenvironment and their relevance in cancer immunotherapy. Nat Rev Immunol *17*, 559-572. 10.1038/nri.2017.49.

102. Ozga, A.J., Chow, M.T., and Luster, A.D. (2021). Chemokines and the immune response to cancer. Immunity *54*, 859-874. 10.1016/j.immuni.2021.01.012.

103. Drouillard, D., Craig, B.T., and Dwinell, M.B. (2023). Physiology of chemokines in the cancer microenvironment. Am J Physiol Cell Physiol *324*, C167-C182. 10.1152/ajpcell.00151.2022.

104. Markl, F., Huynh, D., Endres, S., and Kobold, S. (2022). Utilizing chemokines in cancer immunotherapy. Trends Cancer *8*, 670-682. 10.1016/j.trecan.2022.04.001.

105. Hoch, T., Schulz, D., Eling, N., Gomez, J.M., Levesque, M.P., and Bodenmiller, B. (2022). Multiplexed imaging mass cytometry of the chemokine milieus in

melanoma characterizes features of the response to immunotherapy. Sci Immunol *7*, eabk1692. 10.1126/sciimmunol.abk1692.

106. Farhood, B., Najafi, M., and Mortezaee, K. (2019). CD8(+) cytotoxic T lymphocytes in cancer immunotherapy: A review. J Cell Physiol *234*, 8509-8521. 10.1002/jcp.27782.

107. Karin, N. (2020). CXCR3 Ligands in Cancer and Autoimmunity, Chemoattraction of Effector T Cells, and Beyond. Front Immunol *11*, 976. 10.3389/fimmu.2020.00976.

108. Galeano Nino, J.L., Pageon, S.V., Tay, S.S., Colakoglu, F., Kempe, D., Hywood, J., Mazalo, J.K., Cremasco, J., Govendir, M.A., Dagley, L.F., et al. (2020). Cytotoxic T cells swarm by homotypic chemokine signalling. Elife *9*. 10.7554/eLife.56554.

109. Rubio, A.J., Porter, T., and Zhong, X. (2020). Duality of B Cell-CXCL13 Axis in Tumor Immunology. Front Immunol *11*, 521110. 10.3389/fimmu.2020.521110.

110. Ukita, M., Hamanishi, J., Yoshitomi, H., Yamanoi, K., Takamatsu, S., Ueda, A., Suzuki, H., Hosoe, Y., Furutake, Y., Taki, M., et al. (2022). CXCL13-producing CD4+ T cells accumulate in the early phase of tertiary lymphoid structures in ovarian cancer. JCI Insight *7*. 10.1172/jci.insight.157215.

111. Li, F., Kitajima, S., Kohno, S., Yoshida, A., Tange, S., Sasaki, S., Okada, N., Nishimoto, Y., Muranaka, H., Nagatani, N., et al. (2019). Retinoblastoma Inactivation Induces a Protumoral Microenvironment via Enhanced CCL2 Secretion. Cancer Res *79*, 3903-3915. 10.1158/0008-5472.CAN-18-3604.

112. Xu, W., Wu, Y., Liu, W., Anwaier, A., Tian, X., Su, J., Huang, H., Wei, G., Qu, Y., Zhang, H., and Ye, D. (2022). Tumor-associated macrophage-derived chemokine CCL5 facilitates the progression and immunosuppressive tumor microenvironment of clear cell renal cell carcinoma. Int J Biol Sci *18*, 4884-4900. 10.7150/ijbs.74647.

113. Hromas, R., Broxmeyer, H.E., Kim, C., Nakshatri, H., Christopherson, K., 2nd, Azam, M., and Hou, Y.H. (1999). Cloning of BRAK, a novel divergent CXC chemokine preferentially expressed in normal versus malignant cells. Biochem Biophys Res Commun *255*, 703-706. 10.1006/bbrc.1999.0257.

114. Frederick, M.J., Henderson, Y., Xu, X., Deavers, M.T., Sahin, A.A., Wu, H., Lewis, D.E., El-Naggar, A.K., and Clayman, G.L. (2000). In vivo expression of the novel CXC chemokine BRAK in normal and cancerous human tissue. Am J Pathol *156*, 1937-1950. 10.1016/S0002-9440(10)65067-5.

115. Bi, J., Liu, Q., Sun, Y., Hu, X., He, X., and Xu, C. (2021). CXCL14 inhibits the growth and promotes apoptosis of hepatocellular carcinoma cells via suppressing

Akt/mTOR pathway. J Recept Signal Transduct Res *41*, 593-603. 10.1080/10799893.2020.1837870.

116. Kumar, A., Mohamed, E., Tong, S., Chen, K., Mukherjee, J., Lim, Y., Wong, C.M., Boosalis, Z., Shai, A., Pieper, R.O., et al. (2022). CXCL14 Promotes a Robust Brain Tumor-Associated Immune Response in Glioma. Clin Cancer Res *28*, 2898-2910. 10.1158/1078-0432.CCR-21-2830.

117. Kim, H., Won, B.H., Choi, J.I., Lee, I., Lee, J.H., Park, J.H., Choi, Y.S., Kim, J.H., Cho, S., Lim, J.B., and Lee, B.S. (2022). BRAK and APRIL as novel biomarkers for ovarian tumors. Biomark Med *16*, 717-729. 10.2217/bmm-2021-1014.

118. Tessema, M., Klinge, D.M., Yingling, C.M., Do, K., Van Neste, L., and Belinsky, S.A. (2010). Re-expression of CXCL14, a common target for epigenetic silencing in lung cancer, induces tumor necrosis. Oncogene *29*, 5159-5170. 10.1038/onc.2010.255.

119. Yang, X.Y., Ozawa, S., Kato, Y., Maehata, Y., Izukuri, K., Ikoma, T., Kanamori, K., Akasaka, T., Suzuki, K., Iwabuchi, H., et al. (2019). C-X-C Motif Chemokine Ligand 14 is a Unique Multifunctional Regulator of Tumor Progression. Int J Mol Sci *20*. 10.3390/ijms20081872.

120. Wang, Y., Sun, Q., Ye, Y., Sun, X., Xie, S., Zhan, Y., Song, J., Fan, X., Zhang, B., Yang, M., et al. (2022). FGF-2 signaling in nasopharyngeal carcinoma modulates pericyte-macrophage crosstalk and metastasis. JCI Insight *7*. 10.1172/jci.insight.157874.

121. Augsten, M., Sjoberg, E., Frings, O., Vorrink, S.U., Frijhoff, J., Olsson, E., Borg, A., and Ostman, A. (2014). Cancer-associated fibroblasts expressing CXCL14 rely upon NOS1-derived nitric oxide signaling for their tumor-supporting properties. Cancer Res *74*, 2999-3010. 10.1158/0008-5472.CAN-13-2740.

122. Wei, S.T., Chiang, J.Y., Wang, H.L., Lei, F.J., Huang, Y.C., Wang, C.C., Cho, D.Y., and Hsieh, C.H. (2023). Hypoxia-induced CXC chemokine ligand 14 expression drives protumorigenic effects through activation of insulin-like growth factor-1 receptor signaling in glioblastoma. Cancer Sci *114*, 174-186. 10.1111/cas.15587.

123. Chang, T.M., Chiang, Y.C., Lee, C.W., Lin, C.M., Fang, M.L., Chi, M.C., Liu, J.F., and Kou, Y.R. (2023). CXCL14 promotes metastasis of non-small cell lung cancer through ACKR2-depended signaling pathway. Int J Biol Sci *19*, 1455-1470. 10.7150/ijbs.79438.

124. Mlecnik, B., Bindea, G., Angell, H.K., Maby, P., Angelova, M., Tougeron, D., Church, S.E., Lafontaine, L., Fischer, M., Fredriksen, T., et al. (2016). Integrative Analyses of Colorectal Cancer Show Immunoscore Is a Stronger Predictor of Patient Survival Than Microsatellite Instability. Immunity *44*, 698-711. 10.1016/j.immuni.2016.02.025.

125. Westrich, J.A., Vermeer, D.W., Silva, A., Bonney, S., Berger, J.N., Cicchini, L., Greer, R.O., Song, J.I., Raben, D., Slansky, J.E., et al. (2019). CXCL14 suppresses human papillomavirus-associated head and neck cancer through antigen-specific CD8(+) T-cell responses by upregulating MHC-I expression. Oncogene *38*, 7166-7180. 10.1038/s41388-019-0911-6.

126. Cicchini, L., Westrich, J.A., Xu, T., Vermeer, D.W., Berger, J.N., Clambey, E.T., Lee, D., Song, J.I., Lambert, P.F., Greer, R.O., et al. (2016). Suppression of Antitumor Immune Responses by Human Papillomavirus through Epigenetic Downregulation of CXCL14. mBio *7*. 10.1128/mBio.00270-16.

127. Dolinska, M., Cai, H., Mansson, A., Shen, J., Xiao, P., Bouderlique, T., Li, X., Leonard, E., Chang, M., Gao, Y., et al. (2023). Characterization of the bone marrow niche in patients with chronic myeloid leukemia identifies CXCL14 as a new therapeutic option. Blood *142*, 73-89. 10.1182/blood.2022016896.

128. Parikh, A., Shin, J., Faquin, W., Lin, D.T., Tirosh, I., Sunwoo, J.B., and Puram, S.V. (2020). Malignant cell-specific CXCL14 promotes tumor lymphocyte infiltration in oral cavity squamous cell carcinoma. J Immunother Cancer *8*. 10.1136/jitc-2020-001048.

129. Cao, B., Yang, Y., Pan, Y., Jia, Y., Brock, M.V., Herman, J.G., and Guo, M. (2013). Epigenetic silencing of CXCL14 induced colorectal cancer migration and invasion. Discov Med *16*, 137-147.

130. Gu, X.L., Ou, Z.L., Lin, F.J., Yang, X.L., Luo, J.M., Shen, Z.Z., and Shao, Z.M. (2012). Expression of CXCL14 and its anticancer role in breast cancer. Breast Cancer Res Treat *135*, 725-735. 10.1007/s10549-012-2206-2.

131. Sjoberg, E., Meyrath, M., Milde, L., Herrera, M., Lovrot, J., Hagerstrand, D., Frings, O., Bartish, M., Rolny, C., Sonnhammer, E., et al. (2019). A Novel ACKR2-Dependent Role of Fibroblast-Derived CXCL14 in Epithelial-to-Mesenchymal Transition and Metastasis of Breast Cancer. Clin Cancer Res *25*, 3702-3717. 10.1158/1078-0432.CCR-18-1294.

132. Wente, M.N., Mayer, C., Gaida, M.M., Michalski, C.W., Giese, T., Bergmann, F., Giese, N.A., Buchler, M.W., and Friess, H. (2008). CXCL14 expression and potential function in pancreatic cancer. Cancer Lett *259*, 209-217. 10.1016/j.canlet.2007.10.021.

133. Horny, K., Sproll, C., Peiffer, L., Furtmann, F., Gerhardt, P., Gravemeyer, J., Stoecklein, N.H., Spassova, I., and Becker, J.C. (2023). Mesenchymal-epithelial transition in lymph node metastases of oral squamous cell carcinoma is accompanied by ZEB1 expression. J Transl Med *21*, 267. 10.1186/s12967-023-04102-w.

134. Gowhari Shabgah, A., Haleem Al-Qaim, Z., Markov, A., Valerievich Yumashev, A., Ezzatifar, F., Ahmadi, M., Mohammad Gheibihayat, S., and Gholizadeh Navashenaq, J. (2021). Chemokine CXCL14; a double-edged sword in cancer development. Int Immunopharmacol *97*, 107681. 10.1016/j.intimp.2021.107681.

135. Budhwani, M., Turrell, G., Yu, M., Frazer, I.H., Mehdi, A.M., and Chandra, J. (2021). Immune-Inhibitory Gene Expression is Positively Correlated with Overall Immune Activity and Predicts Increased Survival Probability of Cervical and Head and Neck Cancer Patients. Front Mol Biosci *8*, 622643. 10.3389/fmolb.2021.622643.

136. Badoual, C., Combe, P., Gey, A., Granier, C., Roussel, H., De Guillebon, E., Oudard, S., and Tartour, E. (2013). [PD-1 and PDL-1 expression in cancer: significance and prognostic value]. Med Sci (Paris) *29*, 570-572. 10.1051/medsci/2013296005.

137. Paijens, S.T., Vledder, A., de Bruyn, M., and Nijman, H.W. (2021). Tumor-infiltrating lymphocytes in the immunotherapy era. Cell Mol Immunol *18*, 842-859. 10.1038/s41423-020-00565-9.

138. Nguyen, N., Bellile, E., Thomas, D., McHugh, J., Rozek, L., Virani, S., Peterson, L., Carey, T.E., Walline, H., Moyer, J., et al. (2016). Tumor infiltrating lymphocytes and survival in patients with head and neck squamous cell carcinoma. Head Neck *38*, 1074-1084. 10.1002/hed.24406.

139. Solomon, B., Young, R.J., Bressel, M., Urban, D., Hendry, S., Thai, A., Angel, C., Haddad, A., Kowanetz, M., Fua, T., et al. (2018). Prognostic Significance of PD-L1(+) and CD8(+) Immune Cells in HPV(+) Oropharyngeal Squamous Cell Carcinoma. Cancer Immunol Res *6*, 295-304. 10.1158/2326-6066.CIR-17-0299.

140. Raskov, H., Orhan, A., Christensen, J.P., and Gogenur, I. (2021). Cytotoxic CD8(+) T cells in cancer and cancer immunotherapy. Br J Cancer *124*, 359-367. 10.1038/s41416-020-01048-4.

141. Dhatchinamoorthy, K., Colbert, J.D., and Rock, K.L. (2021). Cancer Immune Evasion Through Loss of MHC Class I Antigen Presentation. Front Immunol *12*, 636568. 10.3389/fimmu.2021.636568.

142. Prokhnevska, N., Cardenas, M.A., Valanparambil, R.M., Sobierajska, E., Barwick, B.G., Jansen, C., Reyes Moon, A., Gregorova, P., delBalzo, L., Greenwald, R., et al. (2023). CD8(+) T cell activation in cancer comprises an initial activation phase in lymph nodes followed by effector differentiation within the tumor. Immunity *56*, 107-124 e105. 10.1016/j.immuni.2022.12.002.

143. Lever, M., Maini, P.K., van der Merwe, P.A., and Dushek, O. (2014). Phenotypic models of T cell activation. Nat Rev Immunol *14*, 619-629. 10.1038/nri3728.

144. Cemerski, S., and Shaw, A. (2006). Immune synapses in T-cell activation. Curr Opin Immunol *18*, 298-304. 10.1016/j.coi.2006.03.011.

145. Curtsinger, J.M., and Mescher, M.F. (2010). Inflammatory cytokines as a third signal for T cell activation. Curr Opin Immunol *22*, 333-340. 10.1016/j.coi.2010.02.013.

146. Curtsinger, J.M., Johnson, C.M., and Mescher, M.F. (2003). CD8 T cell clonal expansion and development of effector function require prolonged exposure to antigen, costimulation, and signal 3 cytokine. J Immunol *171*, 5165-5171. 10.4049/jimmunol.171.10.5165.

147. Dustin, M.L. (2014). The immunological synapse. Cancer Immunol Res *2*, 1023-1033. 10.1158/2326-6066.CIR-14-0161.

148. Spetz, J., Presser, A.G., and Sarosiek, K.A. (2019). T Cells and Regulated Cell Death: Kill or Be Killed. Int Rev Cell Mol Biol *342*, 27-71. 10.1016/bs.ircmb.2018.07.004.

149. Martin, M.D., and Badovinac, V.P. (2018). Defining Memory CD8 T Cell. Front Immunol *9*, 2692. 10.3389/fimmu.2018.02692.

150. Kaech, S.M., Wherry, E.J., and Ahmed, R. (2002). Effector and memory T-cell differentiation: implications for vaccine development. Nat Rev Immunol *2*, 251-262. 10.1038/nri778.

151. Zehn, D., Thimme, R., Lugli, E., de Almeida, G.P., and Oxenius, A. (2022). 'Stem-like' precursors are the fount to sustain persistent CD8(+) T cell responses. Nat Immunol *23*, 836-847. 10.1038/s41590-022-01219-w.

152. Jansen, C.S., Prokhnevska, N., Master, V.A., Sanda, M.G., Carlisle, J.W., Bilen, M.A., Cardenas, M., Wilkinson, S., Lake, R., Sowalsky, A.G., et al. (2019). An intra-tumoral niche maintains and differentiates stem-like CD8 T cells. Nature *576*, 465-470. 10.1038/s41586-019-1836-5.

153. Eberhardt, C.S., Kissick, H.T., Patel, M.R., Cardenas, M.A., Prokhnevska, N., Obeng, R.C., Nasti, T.H., Griffith, C.C., Im, S.J., Wang, X., et al. (2021). Functional HPV-specific PD-1(+) stem-like CD8 T cells in head and neck cancer. Nature *597*, 279-284. 10.1038/s41586-021-03862-z.

154. Groettrup, M., Kirk, C.J., and Basler, M. (2010). Proteasomes in immune cells: more than peptide producers? Nat Rev Immunol *10*, 73-78. 10.1038/nri2687.

155. Colbert, J.D., Cruz, F.M., and Rock, K.L. (2020). Cross-presentation of exogenous antigens on MHC I molecules. Curr Opin Immunol *64*, 1-8. 10.1016/j.coi.2019.12.005.

156. Blum, J.S., Wearsch, P.A., and Cresswell, P. (2013). Pathways of antigen processing. Annu Rev Immunol *31*, 443-473. 10.1146/annurev-immunol-032712-095910.

157. Raghavan, M., Del Cid, N., Rizvi, S.M., and Peters, L.R. (2008). MHC class I assembly: out and about. Trends Immunol *29*, 436-443. 10.1016/j.it.2008.06.004.

158. Dersh, D., Phelan, J.D., Gumina, M.E., Wang, B., Arbuckle, J.H., Holly, J., Kishton, R.J., Markowitz, T.E., Seedhom, M.O., Fridlyand, N., et al. (2021). Genome-wide Screens Identify Lineage- and Tumor-Specific Genes Modulating MHC-I- and MHC-II-Restricted Immunosurveillance of Human Lymphomas. Immunity *54*, 116-131 e110. 10.1016/j.immuni.2020.11.002.

159. Woods, G.M., Howson, L.J., Brown, G.K., Tovar, C., Kreiss, A., Corcoran, L.M., and Lyons, A.B. (2015). Immunology of a Transmissible Cancer Spreading among Tasmanian Devils. J Immunol *195*, 23-29. 10.4049/jimmunol.1500131.

160. Burr, M.L., Sparbier, C.E., Chan, K.L., Chan, Y.C., Kersbergen, A., Lam, E.Y.N., Azidis-Yates, E., Vassiliadis, D., Bell, C.C., Gilan, O., et al. (2019). An Evolutionarily Conserved Function of Polycomb Silences the MHC Class I Antigen Presentation Pathway and Enables Immune Evasion in Cancer. Cancer Cell *36*, 385-401 e388. 10.1016/j.ccell.2019.08.008.

161. Siddle, H.V., Kreiss, A., Tovar, C., Yuen, C.K., Cheng, Y., Belov, K., Swift, K., Pearse, A.M., Hamede, R., Jones, M.E., et al. (2013). Reversible epigenetic down-regulation of MHC molecules by devil facial tumour disease illustrates immune escape by a contagious cancer. Proc Natl Acad Sci U S A *110*, 5103-5108. 10.1073/pnas.1219920110.

162. Haist, M., Stege, H., Grabbe, S., and Bros, M. (2021). The Functional Crosstalk between Myeloid-Derived Suppressor Cells and Regulatory T Cells within the Immunosuppressive Tumor Microenvironment. Cancers (Basel) *13*. 10.3390/cancers13020210.

163. Saleh, R., and Elkord, E. (2019). Treg-mediated acquired resistance to immune checkpoint inhibitors. Cancer Lett *457*, 168-179. 10.1016/j.canlet.2019.05.003.

164. Huang, B., Pan, P.Y., Li, Q., Sato, A.I., Levy, D.E., Bromberg, J., Divino, C.M., and Chen, S.H. (2006). Gr-1+CD115+ immature myeloid suppressor cells mediate the development of tumor-induced T regulatory cells and T-cell anergy in tumor-bearing host. Cancer Res *66*, 1123-1131. 10.1158/0008-5472.CAN-05-1299.

165. Groth, C., Hu, X., Weber, R., Fleming, V., Altevogt, P., Utikal, J., and Umansky, V. (2019). Immunosuppression mediated by myeloid-derived suppressor cells (MDSCs) during tumour progression. Br J Cancer *120*, 16-25. 10.1038/s41416-018-0333-1.

166. Ku, A.W., Muhitch, J.B., Powers, C.A., Diehl, M., Kim, M., Fisher, D.T., Sharda, A.P., Clements, V.K., O'Loughlin, K., Minderman, H., et al. (2016). Tumor-induced MDSC act via remote control to inhibit L-selectin-dependent adaptive immunity in lymph nodes. Elife *5*. 10.7554/eLife.17375.

167. Umansky, V., Blattner, C., Gebhardt, C., and Utikal, J. (2016). The Role of Myeloid-Derived Suppressor Cells (MDSC) in Cancer Progression. Vaccines (Basel) *4*. 10.3390/vaccines4040036.

168. Davis, R.J., Van Waes, C., and Allen, C.T. (2016). Overcoming barriers to effective immunotherapy: MDSCs, TAMs, and Tregs as mediators of the immunosuppressive microenvironment in head and neck cancer. Oral Oncol *58*, 59-70. 10.1016/j.oraloncology.2016.05.002.

169. Wang, J., Huang, H., Lu, J., Bi, P., Wang, F., Liu, X., Zhang, B., Luo, Y., and Li, X. (2017). Tumor cells induced-M2 macrophage favors accumulation of Treg in nasopharyngeal carcinoma. Int J Clin Exp Pathol *10*, 8389-8401.

170. Kansy, B.A., Wehrs, T.P., Bruderek, K., Si, Y., Ludwig, S., Droege, F., Hasskamp, P., Henkel, U., Dominas, N., Hoffmann, T.K., et al. (2023). HPV-associated head and neck cancer is characterized by distinct profiles of CD8(+) T cells and myeloid-derived suppressor cells. Cancer Immunol Immunother *72*, 4367-4383. 10.1007/s00262-023-03571-8.

171. Snietura, M., Brewczynski, A., Kopec, A., and Rutkowski, T. (2020). Infiltrates of M2-Like Tumour-Associated Macrophages Are Adverse Prognostic Factor in Patients with Human Papillomavirus-Negative but Not in Human Papillomavirus-Positive Oropharyngeal Squamous Cell Carcinoma. Pathobiology *87*, 75-86. 10.1159/000505522.

172. Blank, C.U., Haining, W.N., Held, W., Hogan, P.G., Kallies, A., Lugli, E., Lynn, R.C., Philip, M., Rao, A., Restifo, N.P., et al. (2019). Defining 'T cell exhaustion'. Nat Rev Immunol *19*, 665-674. 10.1038/s41577-019-0221-9.

173. Baessler, A., and Vignali, D.A.A. (2024). T Cell Exhaustion. Annu Rev Immunol *42*, 179-206. 10.1146/annurev-immunol-090222-110914.

174. Momtaz, P., and Postow, M.A. (2014). Immunologic checkpoints in cancer therapy: focus on the programmed death-1 (PD-1) receptor pathway. Pharmgenomics Pers Med *7*, 357-365. 10.2147/PGPM.S53163.

175. Harrington, K.J., Burtness, B., Greil, R., Soulieres, D., Tahara, M., de Castro, G., Jr., Psyrri, A., Brana, I., Baste, N., Neupane, P., et al. (2023). Pembrolizumab With or Without Chemotherapy in Recurrent or Metastatic Head and Neck Squamous Cell Carcinoma: Updated Results of the Phase III KEYNOTE-048 Study. J Clin Oncol *41*, 790-802. 10.1200/JCO.21.02508.

176. Pestana, R.C., Becnel, M., Rubin, M.L., Torman, D.K., Crespo, J., Phan, J., Hanna, E., Bell, D., Glisson, B.S., Johnson, J.M., et al. (2020). Response rates and survival to systemic therapy after immune checkpoint inhibitor failure in recurrent/metastatic head and neck squamous cell carcinoma. Oral Oncol *101*, 104523. 10.1016/j.oraloncology.2019.104523.

177. Chow, L.Q.M. (2020). Head and Neck Cancer. N Engl J Med *382*, 60-72. 10.1056/NEJMra1715715.

178. Ruffin, A.T., Li, H., Vujanovic, L., Zandberg, D.P., Ferris, R.L., and Bruno, T.C. (2023). Improving head and neck cancer therapies by immunomodulation of the tumour microenvironment. Nat Rev Cancer *23*, 173-188. 10.1038/s41568-022-00531-9.

179. Joo, Y.H., Cho, K.J., Park, J.O., Kim, S.Y., and Kim, M.S. (2018). Surgical morbidity and mortality in patients after microvascular reconstruction for head and neck cancer. Clin Otolaryngol *43*, 502-508. 10.1111/coa.13006.

180. Bergamini, C., Ferris, R.L., Xie, J., Mariani, G., Ali, M., Holmes, W.C., Harrington, K., Psyrri, A., Cavalieri, S., and Licitra, L. (2021). Bleeding complications in patients with squamous cell carcinoma of the head and neck. Head Neck *43*, 2844-2858. 10.1002/hed.26772.

181. Brook, I. (2020). Late side effects of radiation treatment for head and neck cancer. Radiat Oncol J *38*, 84-92. 10.3857/roj.2020.00213.

182. Qin, T., Li, S., Henry, L.E., Liu, S., and Sartor, M.A. (2021). Molecular Tumor Subtypes of HPV-Positive Head and Neck Cancers: Biological Characteristics and Implications for Clinical Outcomes. Cancers (Basel) *13*. 10.3390/cancers13112721.

183. Qin, T., Li, S., Henry, L.E., Chou, E., Cavalcante, R.G., Garb, B.F., D'Silva, N.J., Rozek, L.S., and Sartor, M.A. (2023). Whole-genome CpG-resolution DNA Methylation Profiling of HNSCC Reveals Distinct Mechanisms of Carcinogenesis for Fine-scale HPV+ Cancer Subtypes. Cancer Res Commun *3*, 1701-1715. 10.1158/2767-9764.CRC-23-0009.

184. Parmar, K., Mohamed, A., Vaish, E., Thawani, R., Cetnar, J., and Thein, K.Z. (2022). Immunotherapy in head and neck squamous cell carcinoma: An updated review. Cancer Treat Res Commun *33*, 100649. 10.1016/j.ctarc.2022.100649.

185. Zanoni, D.K., Patel, S.G., and Shah, J.P. (2019). Changes in the 8th Edition of the American Joint Committee on Cancer (AJCC) Staging of Head and Neck Cancer: Rationale and Implications. Curr Oncol Rep *21*, 52. 10.1007/s11912-019-0799-x.

186. Machczynski, P., Majchrzak, E., Niewinski, P., Marchlewska, J., and Golusinski, W. (2020). A review of the 8th edition of the AJCC staging system for oropharyngeal cancer according to HPV status. Eur Arch Otorhinolaryngol *277*, 2407-2412. 10.1007/s00405-020-05979-9.

187. Billfalk-Kelly, A., Yu, E., Su, J., O'Sullivan, B., Waldron, J., Ringash, J., Bartlett, E., Perez-Ordonez, B., Weinreb, I., Bayley, A., et al. (2019). Radiologic Extranodal Extension Portends Worse Outcome in cN+ TNM-8 Stage I Human Papillomavirus-Mediated Oropharyngeal Cancer. Int J Radiat Oncol Biol Phys *104*, 1017-1027. 10.1016/j.ijrobp.2019.03.047.

188. Chaturvedi, A.K., Engels, E.A., Pfeiffer, R.M., Hernandez, B.Y., Xiao, W., Kim, E., Jiang, B., Goodman, M.T., Sibug-Saber, M., Cozen, W., et al. (2011). Human papillomavirus and rising oropharyngeal cancer incidence in the United States. J Clin Oncol *29*, 4294-4301. 10.1200/JCO.2011.36.4596.

189. Ang, K.K., Harris, J., Wheeler, R., Weber, R., Rosenthal, D.I., Nguyen-Tan, P.F., Westra, W.H., Chung, C.H., Jordan, R.C., Lu, C., et al. (2010). Human papillomavirus and survival of patients with oropharyngeal cancer. N Engl J Med *363*, 24-35. 10.1056/NEJMoa0912217.

190. DiBlasi, M., McNamara, R., Jayne, C., Berzansky, I., Pottle, C., and Colden, D. (2024). Two brothers with human papillomavirus-positive oropharyngeal squamous cell carcinoma of the tonsil: A case report. SAGE Open Med Case Rep *12*, 2050313X241271762. 10.1177/2050313X241271762.

191. Slebos, R.J., Yi, Y., Ely, K., Carter, J., Evjen, A., Zhang, X., Shyr, Y., Murphy, B.M., Cmelak, A.J., Burkey, B.B., et al. (2006). Gene expression differences associated with human papillomavirus status in head and neck squamous cell carcinoma. Clin Cancer Res *12*, 701-709. 10.1158/1078-0432.CCR-05-2017.

192. Matlung, S.E., Wilhelmina van Kempen, P.M., Bovenschen, N., van Baarle, D., and Willems, S.M. (2016). Differences in T-cell infiltrates and survival between HPV+ and HPV- oropharyngeal squamous cell carcinoma. Future Sci OA *2*, FSO88. 10.4155/fso.15.88.

193. Huang, S.H., Perez-Ordonez, B., Liu, F.F., Waldron, J., Ringash, J., Irish, J., Cummings, B., Siu, L.L., Kim, J., Weinreb, I., et al. (2012). Atypical clinical behavior of p16-confirmed HPV-related oropharyngeal squamous cell carcinoma treated with radical radiotherapy. Int J Radiat Oncol Biol Phys *82*, 276-283. 10.1016/j.ijrobp.2010.08.031.

194. Bulut, O.C., Lindel, K., Hauswald, H., Brandt, R., Klauschen, F., Wolf, J., Wolf, T., Plinkert, P.K., Simon, C., Weichert, W., and Stenzinger, A. (2014). Clinical and molecular characteristics of HNSCC patients with brain metastases: a retrospective study. Eur Arch Otorhinolaryngol *271*, 1715-1722. 10.1007/s00405-013-2665-z.

195. Rischin, D., Young, R.J., Fisher, R., Fox, S.B., Le, Q.T., Peters, L.J., Solomon, B., Choi, J., O'Sullivan, B., Kenny, L.M., and McArthur, G.A. (2010). Prognostic significance of p16INK4A and human papillomavirus in patients with oropharyngeal cancer treated on TROG 02.02 phase III trial. J Clin Oncol *28*, 4142-4148. 10.1200/JCO.2010.29.2904.

196. Ferris, R.L., Blumenschein, G., Jr., Fayette, J., Guigay, J., Colevas, A.D., Licitra, L., Harrington, K., Kasper, S., Vokes, E.E., Even, C., et al. (2016). Nivolumab for Recurrent Squamous-Cell Carcinoma of the Head and Neck. N Engl J Med *375*, 1856-1867. 10.1056/NEJMoa1602252.

197. Cohen, E.E.W., Soulieres, D., Le Tourneau, C., Dinis, J., Licitra, L., Ahn, M.J., Soria, A., Machiels, J.P., Mach, N., Mehra, R., et al. (2019). Pembrolizumab versus methotrexate, docetaxel, or cetuximab for recurrent or metastatic head-and-neck squamous cell carcinoma (KEYNOTE-040): a randomised, open-label, phase 3 study. Lancet *393*, 156-167. 10.1016/S0140-6736(18)31999-8.

198. Burtness, B., Harrington, K.J., Greil, R., Soulieres, D., Tahara, M., de Castro, G., Jr., Psyrri, A., Baste, N., Neupane, P., Bratland, A., et al. (2019). Pembrolizumab alone or with chemotherapy versus cetuximab with chemotherapy for recurrent or metastatic squamous cell carcinoma of the head and neck (KEYNOTE-048): a randomised, open-label, phase 3 study. Lancet *394*, 1915-1928. 10.1016/S0140-6736(19)32591-7.

199. Ferris, R.L., Spanos, W.C., Leidner, R., Goncalves, A., Martens, U.M., Kyi, C., Sharfman, W., Chung, C.H., Devriese, L.A., Gauthier, H., et al. (2021). Neoadjuvant nivolumab for patients with resectable HPV-positive and HPV-negative squamous cell carcinomas of the head and neck in the CheckMate 358 trial. J Immunother Cancer *9*. 10.1136/jitc-2021-002568.

200. Luo, X., Qiu, Y., Fitzsimonds, Z.R., Wang, Q., Chen, Q., and Lei, Y.L. (2024). Immune escape of head and neck cancer mediated by the impaired MHC-I antigen presentation pathway. Oncogene *43*, 388-394. 10.1038/s41388-023-02912-2.

201. Zhou, L., Mudianto, T., Ma, X., Riley, R., and Uppaluri, R. (2020). Targeting EZH2 Enhances Antigen Presentation, Antitumor Immunity, and Circumvents Anti-PD-1 Resistance in Head and Neck Cancer. Clin Cancer Res *26*, 290-300. 10.1158/1078-0432.CCR-19-1351.

202. Kopytko, P., Piotrowska, K., Janisiak, J., and Tarnowski, M. (2021). Garcinol-A Natural Histone Acetyltransferase Inhibitor and New Anti-Cancer Epigenetic Drug. Int J Mol Sci *22*. 10.3390/ijms22062828.

203. Mladenov, E., Magin, S., Soni, A., and Iliakis, G. (2013). DNA double-strand break repair as determinant of cellular radiosensitivity to killing and target in radiation therapy. Front Oncol *3*, 113. 10.3389/fonc.2013.00113.

204. Huang, R.X., and Zhou, P.K. (2020). DNA damage response signaling pathways and targets for radiotherapy sensitization in cancer. Signal Transduct Target Ther *5*, 60. 10.1038/s41392-020-0150-x.

205. Oike, T., Ogiwara, H., Torikai, K., Nakano, T., Yokota, J., and Kohno, T. (2012). Garcinol, a histone acetyltransferase inhibitor, radiosensitizes cancer cells by inhibiting non-homologous end joining. Int J Radiat Oncol Biol Phys *84*, 815-821. 10.1016/j.ijrobp.2012.01.017.

206. Oike, T., Ogiwara, H., Amornwichet, N., Nakano, T., and Kohno, T. (2014). Chromatin-regulating proteins as targets for cancer therapy. J Radiat Res *55*, 613-628. 10.1093/jrr/rrt227.

207. Li, F., Shanmugam, M.K., Chen, L., Chatterjee, S., Basha, J., Kumar, A.P., Kundu, T.K., and Sethi, G. (2013). Garcinol, a polyisoprenylated benzophenone modulates multiple proinflammatory signaling cascades leading to the suppression of growth and survival of head and neck carcinoma. Cancer Prev Res (Phila) *6*, 843-854. 10.1158/1940-6207.CAPR-13-0070.

208. Peng, S., Ji, H., Trimble, C., He, L., Tsai, Y.C., Yeatermeyer, J., Boyd, D.A., Hung, C.F., and Wu, T.C. (2004). Development of a DNA vaccine targeting human papillomavirus type 16 oncoprotein E6. J Virol *78*, 8468-8476. 10.1128/JVI.78.16.8468-8476.2004.

209. Zhao, X., Yang, F., Mariz, F., Osen, W., Bolchi, A., Ottonello, S., and Muller, M. (2020). Combined prophylactic and therapeutic immune responses against human papillomaviruses induced by a thioredoxin-based L2-E7 nanoparticle vaccine. PLoS Pathog *16*, e1008827. 10.1371/journal.ppat.1008827.

210. Lamikanra, A., Pan, Z.K., Isaacs, S.N., Wu, T.C., and Paterson, Y. (2001). Regression of established human papillomavirus type 16 (HPV-16) immortalized tumors in vivo by vaccinia viruses expressing different forms of HPV-16 E7 correlates with enhanced CD8(+) T-cell responses that home to the tumor site. J Virol *75*, 9654-9664. 10.1128/JVI.75.20.9654-9664.2001.

211. Harrington, K.J., Kong, A., Mach, N., Chesney, J.A., Fernandez, B.C., Rischin, D., Cohen, E.E.W., Radcliffe, H.S., Gumuscu, B., Cheng, J., et al. (2020). Talimogene Laherparepvec and Pembrolizumab in Recurrent or Metastatic Squamous Cell Carcinoma of the Head and Neck (MASTERKEY-232): A Multicenter, Phase 1b Study. Clin Cancer Res *26*, 5153-5161. 10.1158/1078-0432.CCR-20-1170.

212. Peng, S., Ferrall, L., Gaillard, S., Wang, C., Chi, W.Y., Huang, C.H., Roden, R.B.S., Wu, T.C., Chang, Y.N., and Hung, C.F. (2021). Development of DNA Vaccine Targeting E6 and E7 Proteins of Human Papillomavirus 16 (HPV16) and HPV18 for Immunotherapy in Combination with Recombinant Vaccinia Boost and PD-1 Antibody. mBio *12*. 10.1128/mBio.03224-20.

213. Nakao, S., Arai, Y., Tasaki, M., Yamashita, M., Murakami, R., Kawase, T., Amino, N., Nakatake, M., Kurosaki, H., Mori, M., et al. (2020). Intratumoral expression of IL-7 and IL-12 using an oncolytic virus increases systemic sensitivity to immune checkpoint blockade. Sci Transl Med *12*. 10.1126/scitranslmed.aax7992.

214. Goldberg, A.D., Allis, C.D., and Bernstein, E. (2007). Epigenetics: a landscape takes shape. Cell *128*, 635-638. 10.1016/j.cell.2007.02.006.

215. Sharma, S., Kelly, T.K., and Jones, P.A. (2010). Epigenetics in cancer. Carcinogenesis *31*, 27-36. 10.1093/carcin/bgp220.

216. Hanahan, D. (2022). Hallmarks of Cancer: New Dimensions. Cancer Discov *12*, 31-46. 10.1158/2159-8290.CD-21-1059.

217. Margueron, R., and Reinberg, D. (2010). Chromatin structure and the inheritance of epigenetic information. Nat Rev Genet *11*, 285-296. 10.1038/nrg2752.

218. Gibney, E.R., and Nolan, C.M. (2010). Epigenetics and gene expression. Heredity (Edinb) *105*, 4-13. 10.1038/hdy.2010.54.

219. Bird, A.P., and Wolffe, A.P. (1999). Methylation-induced repression--belts, braces, and chromatin. Cell *99*, 451-454. 10.1016/s0092-8674(00)81532-9.

220. Lyko, F. (2018). The DNA methyltransferase family: a versatile toolkit for epigenetic regulation. Nat Rev Genet *19*, 81-92. 10.1038/nrg.2017.80.

221. Steenbergen, R.D., Snijders, P.J., Heideman, D.A., and Meijer, C.J. (2014). Clinical implications of (epi)genetic changes in HPV-induced cervical precancerous lesions. Nat Rev Cancer *14*, 395-405. 10.1038/nrc3728.

222. Au Yeung, C.L., Tsang, W.P., Tsang, T.Y., Co, N.N., Yau, P.L., and Kwok, T.T. (2010). HPV-16 E6 upregulation of DNMT1 through repression of tumor suppressor p53. Oncol Rep *24*, 1599-1604. 10.3892/or_00001023.

223. Sartor, M.A., Dolinoy, D.C., Jones, T.R., Colacino, J.A., Prince, M.E., Carey, T.E., and Rozek, L.S. (2011). Genome-wide methylation and expression differences in HPV(+) and HPV(-) squamous cell carcinoma cell lines are consistent with divergent mechanisms of carcinogenesis. Epigenetics *6*, 777-787. 10.4161/epi.6.6.16216.

224. Holland, D., Hoppe-Seyler, K., Schuller, B., Lohrey, C., Maroldt, J., Durst, M., and Hoppe-Seyler, F. (2008). Activation of the enhancer of zeste homologue 2 gene by the human papillomavirus E7 oncoprotein. Cancer Res *68*, 9964-9972. 10.1158/0008-5472.CAN-08-1134.

225. Bohl, S.R., Bullinger, L., and Rucker, F.G. (2018). Epigenetic therapy: azacytidine and decitabine in acute myeloid leukemia. Expert Rev Hematol *11*, 361-371. 10.1080/17474086.2018.1453802.

226. Fili, C., Candoni, A., Zannier, M.E., Olivieri, J., Imbergamo, S., Caizzi, M., Nadali, G., Di Bona, E., Ermacora, A., Gottardi, M., et al. (2019). Efficacy and toxicity of Decitabine in patients with acute myeloid leukemia (AML): A multicenter real-world experience. Leuk Res *76*, 33-38. 10.1016/j.leukres.2018.11.015.

227. Nie, J., Liu, L., Li, X., and Han, W. (2014). Decitabine, a new star in epigenetic therapy: the clinical application and biological mechanism in solid tumors. Cancer Lett *354*, 12-20. 10.1016/j.canlet.2014.08.010.

228. Ye, C., Jiang, N., Zheng, J., Zhang, S., Zhang, J., and Zhou, J. (2024). Epigenetic therapy: Research progress of decitabine in the treatment of solid tumors. Biochim Biophys Acta Rev Cancer *1879*, 189066. 10.1016/j.bbcan.2023.189066.

229. Degli Esposti, D., Sklias, A., Lima, S.C., Beghelli-de la Forest Divonne, S., Cahais, V., Fernandez-Jimenez, N., Cros, M.P., Ecsedi, S., Cuenin, C., Bouaoun, L., et al. (2017). Unique DNA methylation signature in HPV-positive head and neck squamous cell carcinomas. Genome Med *9*, 33. 10.1186/s13073-017-0419-z.

230. Nakagawa, T., Kurokawa, T., Mima, M., Imamoto, S., Mizokami, H., Kondo, S., Okamoto, Y., Misawa, K., Hanazawa, T., and Kaneda, A. (2021). DNA Methylation and HPV-Associated Head and Neck Cancer. Microorganisms *9*. 10.3390/microorganisms9040801.

231. Bannister, A.J., and Kouzarides, T. (2011). Regulation of chromatin by histone modifications. Cell Res *21*, 381-395. 10.1038/cr.2011.22.

232. Strahl, B.D., and Allis, C.D. (2000). The language of covalent histone modifications. Nature *403*, 41-45. 10.1038/47412.

233. Allshire, R.C., and Madhani, H.D. (2018). Ten principles of heterochromatin formation and function. Nat Rev Mol Cell Biol *19*, 229-244. 10.1038/nrm.2017.119.

234. Maeshima, K., Iida, S., Shimazoe, M.A., Tamura, S., and Ide, S. (2024). Is euchromatin really open in the cell? Trends Cell Biol *34*, 7-17. 10.1016/j.tcb.2023.05.007.

235. Papp, B., and Muller, J. (2006). Histone trimethylation and the maintenance of transcriptional ON and OFF states by trxG and PcG proteins. Genes Dev *20*, 2041-2054. 10.1101/gad.388706.

236. Blanco, E., Gonzalez-Ramirez, M., Alcaine-Colet, A., Aranda, S., and Di Croce, L. (2020). The Bivalent Genome: Characterization, Structure, and Regulation. Trends Genet *36*, 118-131. 10.1016/j.tig.2019.11.004.

237. Schmitges, F.W., Prusty, A.B., Faty, M., Stutzer, A., Lingaraju, G.M., Aiwazian, J., Sack, R., Hess, D., Li, L., Zhou, S., et al. (2011). Histone methylation by PRC2 is inhibited by active chromatin marks. Mol Cell *42*, 330-341. 10.1016/j.molcel.2011.03.025.

238. Glancy, E., Choy, N., and Eckersley-Maslin, M.A. (2024). Bivalent chromatin: a developmental balancing act tipped in cancer. Biochem Soc Trans *52*, 217-229. 10.1042/BST20230426.

239. Schuettengruber, B., and Cavalli, G. (2009). Recruitment of polycomb group complexes and their role in the dynamic regulation of cell fate choice. Development *136*, 3531-3542. 10.1242/dev.033902.

240. Conway, E., Healy, E., and Bracken, A.P. (2015). PRC2 mediated H3K27 methylations in cellular identity and cancer. Curr Opin Cell Biol *37*, 42-48. 10.1016/j.ceb.2015.10.003.

241. Lee, T.I., Jenner, R.G., Boyer, L.A., Guenther, M.G., Levine, S.S., Kumar, R.M., Chevalier, B., Johnstone, S.E., Cole, M.F., Isono, K., et al. (2006). Control of developmental regulators by Polycomb in human embryonic stem cells. Cell *125*, 301-313. 10.1016/j.cell.2006.02.043.

242. Yamanaka, S. (2007). Strategies and new developments in the generation of patient-specific pluripotent stem cells. Cell Stem Cell *1*, 39-49. 10.1016/j.stem.2007.05.012.

243. Yamanaka, S. (2008). Induction of pluripotent stem cells from mouse fibroblasts by four transcription factors. Cell Prolif *41 Suppl 1*, 51-56. 10.1111/j.1365-2184.2008.00493.x.

244. Caretti, G., Di Padova, M., Micales, B., Lyons, G.E., and Sartorelli, V. (2004). The Polycomb Ezh2 methyltransferase regulates muscle gene expression and skeletal muscle differentiation. Genes Dev *18*, 2627-2638. 10.1101/gad.1241904.

245. Comet, I., Riising, E.M., Leblanc, B., and Helin, K. (2016). Maintaining cell identity: PRC2-mediated regulation of transcription and cancer. Nat Rev Cancer *16*, 803-810. 10.1038/nrc.2016.83.

246. Sparbier, C.E., Gillespie, A., Gomez, J., Kumari, N., Motazedian, A., Chan, K.L., Bell, C.C., Gilan, O., Chan, Y.C., Popp, S., et al. (2023). Targeting Menin disrupts the KMT2A/B and polycomb balance to paradoxically activate bivalent genes. Nat Cell Biol *25*, 258-272. 10.1038/s41556-022-01056-x.

247. Cao, W., Younis, R.H., Li, J., Chen, H., Xia, R., Mao, L., Chen, W., and Ren, H. (2011). EZH2 promotes malignant phenotypes and is a predictor of oral cancer development in patients with oral leukoplakia. Cancer Prev Res (Phila) *4*, 1816-1824. 10.1158/1940-6207.CAPR-11-0130.

248. Dardenne, E., Beltran, H., Benelli, M., Gayvert, K., Berger, A., Puca, L., Cyrta, J., Sboner, A., Noorzad, Z., MacDonald, T., et al. (2016). N-Myc Induces an EZH2-Mediated Transcriptional Program Driving Neuroendocrine Prostate Cancer. Cancer Cell *30*, 563-577. 10.1016/j.ccell.2016.09.005.

249. Wang, L., Chen, C., Song, Z., Wang, H., Ye, M., Wang, D., Kang, W., Liu, H., and Qing, G. (2022). EZH2 depletion potentiates MYC degradation inhibiting neuroblastoma and small cell carcinoma tumor formation. Nat Commun *13*, 12. 10.1038/s41467-021-27609-6.

250. Neri, F., Zippo, A., Krepelova, A., Cherubini, A., Rocchigiani, M., and Oliviero, S. (2012). Myc regulates the transcription of the PRC2 gene to control the expression of developmental genes in embryonic stem cells. Mol Cell Biol *32*, 840-851. 10.1128/MCB.06148-11.

251. Zhang, X.Y., DeSalle, L.M., Patel, J.H., Capobianco, A.J., Yu, D., Thomas-Tikhonenko, A., and McMahon, S.B. (2005). Metastasis-associated protein 1 (MTA1) is an essential downstream effector of the c-MYC oncoprotein. Proc Natl Acad Sci U S A *102*, 13968-13973. 10.1073/pnas.0502330102.

252. Hojfeldt, J.W., Laugesen, A., Willumsen, B.M., Damhofer, H., Hedehus, L., Tvardovskiy, A., Mohammad, F., Jensen, O.N., and Helin, K. (2018). Accurate H3K27 methylation can be established de novo by SUZ12-directed PRC2. Nat Struct Mol Biol *25*, 225-232. 10.1038/s41594-018-0036-6.

253. Wu, H., Zeng, H., Dong, A., Li, F., He, H., Senisterra, G., Seitova, A., Duan, S., Brown, P.J., Vedadi, M., et al. (2013). Structure of the catalytic domain of EZH2 reveals conformational plasticity in cofactor and substrate binding sites and explains oncogenic mutations. PLoS One *8*, e83737. 10.1371/journal.pone.0083737.

254. van Mierlo, G., Veenstra, G.J.C., Vermeulen, M., and Marks, H. (2019). The Complexity of PRC2 Subcomplexes. Trends Cell Biol *29*, 660-671. 10.1016/j.tcb.2019.05.004.

255. Jiao, L., and Liu, X. (2015). Structural basis of histone H3K27 trimethylation by an active polycomb repressive complex 2. Science *350*, aac4383. 10.1126/science.aac4383.

256. Margueron, R., Justin, N., Ohno, K., Sharpe, M.L., Son, J., Drury, W.J., 3rd, Voigt, P., Martin, S.R., Taylor, W.R., De Marco, V., et al. (2009). Role of the

polycomb protein EED in the propagation of repressive histone marks. Nature *461*, 762-767. 10.1038/nature08398.

257. Cao, R., and Zhang, Y. (2004). SUZ12 is required for both the histone methyltransferase activity and the silencing function of the EED-EZH2 complex. Mol Cell *15*, 57-67. 10.1016/j.molcel.2004.06.020.

258. Yang, Y., and Li, G. (2020). Post-translational modifications of PRC2: signals directing its activity. Epigenetics Chromatin *13*, 47. 10.1186/s13072-020-00369-1.

259. Vire, E., Brenner, C., Deplus, R., Blanchon, L., Fraga, M., Didelot, C., Morey, L., Van Eynde, A., Bernard, D., Vanderwinden, J.M., et al. (2006). The Polycomb group protein EZH2 directly controls DNA methylation. Nature *439*, 871-874. 10.1038/nature04431.

260. Liu, X., and Liu, X. (2022). PRC2, Chromatin Regulation, and Human Disease: Insights From Molecular Structure and Function. Front Oncol *12*, 894585. 10.3389/fonc.2022.894585.

261. Riising, E.M., Comet, I., Leblanc, B., Wu, X., Johansen, J.V., and Helin, K. (2014). Gene silencing triggers polycomb repressive complex 2 recruitment to CpG islands genome wide. Mol Cell *55*, 347-360. 10.1016/j.molcel.2014.06.005.

262. Gretarsson, K.H., Abini-Agbomson, S., Gloor, S.L., Weinberg, D.N., McCuiston, J.L., Kumary, V.U.S., Hickman, A.R., Sahu, V., Lee, R., Xu, X., et al. (2024). Cancer-associated DNA hypermethylation of Polycomb targets requires DNMT3A dual recognition of histone H2AK119 ubiquitination and the nucleosome acidic patch. Sci Adv *10*, eadp0975. 10.1126/sciadv.adp0975.

263. Schlesinger, Y., Straussman, R., Keshet, I., Farkash, S., Hecht, M., Zimmerman, J., Eden, E., Yakhini, Z., Ben-Shushan, E., Reubinoff, B.E., et al. (2007). Polycomb-mediated methylation on Lys27 of histone H3 pre-marks genes for de novo methylation in cancer. Nat Genet *39*, 232-236. 10.1038/ng1950.

264. Ohm, J.E., McGarvey, K.M., Yu, X., Cheng, L., Schuebel, K.E., Cope, L., Mohammad, H.P., Chen, W., Daniel, V.C., Yu, W., et al. (2007). A stem cell-like chromatin pattern may predispose tumor suppressor genes to DNA hypermethylation and heritable silencing. Nat Genet *39*, 237-242. 10.1038/ng1972.

265. Rush, M., Appanah, R., Lee, S., Lam, L.L., Goyal, P., and Lorincz, M.C. (2009). Targeting of EZH2 to a defined genomic site is sufficient for recruitment of Dnmt3a but not de novo DNA methylation. Epigenetics *4*, 404-414. 10.4161/epi.4.6.9392.

266. Wang, X., Paucek, R.D., Gooding, A.R., Brown, Z.Z., Ge, E.J., Muir, T.W., and Cech, T.R. (2017). Molecular analysis of PRC2 recruitment to DNA in chromatin

and its inhibition by RNA. Nat Struct Mol Biol *24*, 1028-1038. 10.1038/nsmb.3487.

267. Macrae, T.A., Fothergill-Robinson, J., and Ramalho-Santos, M. (2023). Regulation, functions and transmission of bivalent chromatin during mammalian development. Nat Rev Mol Cell Biol *24*, 6-26. 10.1038/s41580-022-00518-2.

268. Laugesen, A., Hojfeldt, J.W., and Helin, K. (2019). Molecular Mechanisms Directing PRC2 Recruitment and H3K27 Methylation. Mol Cell *74*, 8-18. 10.1016/j.molcel.2019.03.011.

269. Hojfeldt, J.W., Hedehus, L., Laugesen, A., Tatar, T., Wiehle, L., and Helin, K. (2019). Non-core Subunits of the PRC2 Complex Are Collectively Required for Its Target-Site Specificity. Mol Cell *76*, 423-436 e423. 10.1016/j.molcel.2019.07.031.

270. de Potter, B., Raas, M.W.D., Seidl, M.F., Verrijzer, C.P., and Snel, B. (2023). Uncoupled evolution of the Polycomb system and deep origin of non-canonical PRC1. Commun Biol *6*, 1144. 10.1038/s42003-023-05501-x.

271. Kim, J.J., and Kingston, R.E. (2022). Context-specific Polycomb mechanisms in development. Nat Rev Genet *23*, 680-695. 10.1038/s41576-022-00499-0.

272. Fursova, N.A., Blackledge, N.P., Nakayama, M., Ito, S., Koseki, Y., Farcas, A.M., King, H.W., Koseki, H., and Klose, R.J. (2019). Synergy between Variant PRC1 Complexes Defines Polycomb-Mediated Gene Repression. Mol Cell *74*, 1020-1036 e1028. 10.1016/j.molcel.2019.03.024.

273. Sugishita, H., Kondo, T., Ito, S., Nakayama, M., Yakushiji-Kaminatsui, N., Kawakami, E., Koseki, Y., Ohinata, Y., Sharif, J., Harachi, M., et al. (2021). Variant PCGF1-PRC1 links PRC2 recruitment with differentiation-associated transcriptional inactivation at target genes. Nat Commun *12*, 5341. 10.1038/s41467-021-24894-z.

274. Casanova, M., Preissner, T., Cerase, A., Poot, R., Yamada, D., Li, X., Appanah, R., Bezstarosti, K., Demmers, J., Koseki, H., and Brockdorff, N. (2011). Polycomblike 2 facilitates the recruitment of PRC2 Polycomb group complexes to the inactive X chromosome and to target loci in embryonic stem cells. Development *138*, 1471-1482. 10.1242/dev.053652.

275. Perino, M., van Mierlo, G., Karemaker, I.D., van Genesen, S., Vermeulen, M., Marks, H., van Heeringen, S.J., and Veenstra, G.J.C. (2018). MTF2 recruits Polycomb Repressive Complex 2 by helical-shape-selective DNA binding. Nat Genet *50*, 1002-1010. 10.1038/s41588-018-0134-8.

276. Perino, M., van Mierlo, G., Loh, C., Wardle, S.M.T., Zijlmans, D.W., Marks, H., and Veenstra, G.J.C. (2020). Two Functional Axes of Feedback-Enforced PRC2 Recruitment in Mouse Embryonic Stem Cells. Stem Cell Reports *15*, 1287-1300. 10.1016/j.stemcr.2020.07.007.

277. Petracovici, A., and Bonasio, R. (2021). Distinct PRC2 subunits regulate maintenance and establishment of Polycomb repression during differentiation. Mol Cell *81*, 2625-2639 e2625. 10.1016/j.molcel.2021.03.038.

278. Fabbri, M., Garzon, R., Cimmino, A., Liu, Z., Zanesi, N., Callegari, E., Liu, S., Alder, H., Costinean, S., Fernandez-Cymering, C., et al. (2007). MicroRNA-29 family reverts aberrant methylation in lung cancer by targeting DNA methyltransferases 3A and 3B. Proc Natl Acad Sci U S A *104*, 15805-15810. 10.1073/pnas.0707628104.

279. Lopez-Bertoni, H., Lal, B., Li, A., Caplan, M., Guerrero-Cazares, H., Eberhart, C.G., Quinones-Hinojosa, A., Glas, M., Scheffler, B., Laterra, J., and Li, Y. (2015). DNMT-dependent suppression of microRNA regulates the induction of GBM tumor-propagating phenotype by Oct4 and Sox2. Oncogene *34*, 3994-4004. 10.1038/onc.2014.334.

280. Pang, Y., Liu, J., Li, X., Xiao, G., Wang, H., Yang, G., Li, Y., Tang, S.C., Qin, S., Du, N., et al. (2018). MYC and DNMT3A-mediated DNA methylation represses microRNA-200b in triple negative breast cancer. J Cell Mol Med *22*, 6262-6274. 10.1111/jcmm.13916.

281. Zhao, X., Lwin, T., Zhang, X., Huang, A., Wang, J., Marquez, V.E., Chen-Kiang, S., Dalton, W.S., Sotomayor, E., and Tao, J. (2013). Disruption of the MYC-miRNA-EZH2 loop to suppress aggressive B-cell lymphoma survival and clonogenicity. Leukemia *27*, 2341-2350. 10.1038/leu.2013.94.

282. Suzuki, R., Honda, S., and Kirino, Y. (2012). PIWI Expression and Function in Cancer. Front Genet *3*, 204. 10.3389/fgene.2012.00204.

283. Iwasaki, Y.W., Siomi, M.C., and Siomi, H. (2015). PIWI-Interacting RNA: Its Biogenesis and Functions. Annu Rev Biochem *84*, 405-433. 10.1146/annurev-biochem-060614-034258.

284. Firmino, N., Martinez, V.D., Rowbotham, D.A., Enfield, K.S.S., Bennewith, K.L., and Lam, W.L. (2016). HPV status is associated with altered PIWI-interacting RNA expression pattern in head and neck cancer. Oral Oncol *55*, 43-48. 10.1016/j.oraloncology.2016.01.012.

285. Yan, J., Dutta, B., Hee, Y.T., and Chng, W.J. (2019). Towards understanding of PRC2 binding to RNA. RNA Biol *16*, 176-184. 10.1080/15476286.2019.1565283.

286. Balas, M.M., Hartwick, E.W., Barrington, C., Roberts, J.T., Wu, S.K., Bettcher, R., Griffin, A.M., Kieft, J.S., and Johnson, A.M. (2021). Establishing RNA-RNA interactions remodels lncRNA structure and promotes PRC2 activity. Sci Adv *7*. 10.1126/sciadv.abc9191.

287. Kaneko, S., Son, J., Bonasio, R., Shen, S.S., and Reinberg, D. (2014). Nascent RNA interaction keeps PRC2 activity poised and in check. Genes Dev *28*, 1983-1988. 10.1101/gad.247940.114.

288. Friedman, J.M., Liang, G., Liu, C.C., Wolff, E.M., Tsai, Y.C., Ye, W., Zhou, X., and Jones, P.A. (2009). The putative tumor suppressor microRNA-101 modulates the cancer epigenome by repressing the polycomb group protein EZH2. Cancer Res *69*, 2623-2629. 10.1158/0008-5472.CAN-08-3114.

289. Zhu, C., Wang, X., Wang, Y., and Wang, K. (2022). Functions and underlying mechanisms of lncRNA HOTAIR in cancer chemotherapy resistance. Cell Death Discov *8*, 383. 10.1038/s41420-022-01174-3.

290. Rinn, J.L., Kertesz, M., Wang, J.K., Squazzo, S.L., Xu, X., Brugmann, S.A., Goodnough, L.H., Helms, J.A., Farnham, P.J., Segal, E., and Chang, H.Y. (2007). Functional demarcation of active and silent chromatin domains in human HOX loci by noncoding RNAs. Cell *129*, 1311-1323. 10.1016/j.cell.2007.05.022.

291. Yang, Y., Jiang, C., Yang, Y., Guo, L., Huang, J., Liu, X., Wu, C., and Zou, J. (2018). Silencing of LncRNA-HOTAIR decreases drug resistance of Non-Small Cell Lung Cancer cells by inactivating autophagy via suppressing the phosphorylation of ULK1. Biochem Biophys Res Commun *497*, 1003-1010. 10.1016/j.bbrc.2018.02.141.

292. Zhou, Y., Wang, Y., Lin, M., Wu, D., and Zhao, M. (2021). LncRNA HOTAIR promotes proliferation and inhibits apoptosis by sponging miR-214-3p in HPV16 positive cervical cancer cells. Cancer Cell Int *21*, 400. 10.1186/s12935-021-02103-7.

293. Cheng, Y., Song, Z., Fang, X., and Tang, Z. (2024). Polycomb repressive complex 2 and its core component EZH2: potential targeted therapeutic strategies for head and neck squamous cell carcinoma. Clin Epigenetics *16*, 54. 10.1186/s13148-024-01666-2.

294. Krebs, A.R., Karmodiya, K., Lindahl-Allen, M., Struhl, K., and Tora, L. (2011). SAGA and ATAC histone acetyl transferase complexes regulate distinct sets of genes and ATAC defines a class of p300-independent enhancers. Mol Cell *44*, 410-423. 10.1016/j.molcel.2011.08.037.

295. Spiegelman, B.M., and Heinrich, R. (2004). Biological control through regulated transcriptional coactivators. Cell *119*, 157-167. 10.1016/j.cell.2004.09.037.

296. McMahon, S.B., Wood, M.A., and Cole, M.D. (2000). The essential cofactor TRRAP recruits the histone acetyltransferase hGCN5 to c-Myc. Mol Cell Biol *20*, 556-562. 10.1128/MCB.20.2.556-562.2000.

297. Cheon, Y., Kim, H., Park, K., Kim, M., and Lee, D. (2020). Dynamic modules of the coactivator SAGA in eukaryotic transcription. Exp Mol Med *52*, 991-1003. 10.1038/s12276-020-0463-4.

298. Baptista, T., Grunberg, S., Minoungou, N., Koster, M.J.E., Timmers, H.T.M., Hahn, S., Devys, D., and Tora, L. (2017). SAGA Is a General Cofactor for RNA Polymerase II Transcription. Mol Cell *68*, 130-143 e135. 10.1016/j.molcel.2017.08.016.

299. Herbst, D.A., Esbin, M.N., Louder, R.K., Dugast-Darzacq, C., Dailey, G.M., Fang, Q., Darzacq, X., Tjian, R., and Nogales, E. (2021). Structure of the human SAGA coactivator complex. Nat Struct Mol Biol *28*, 989-996. 10.1038/s41594-021-00682-7.

300. Yayli, G., Bernardini, A., Mendoza Sanchez, P.K., Scheer, E., Damilot, M., Essabri, K., Morlet, B., Negroni, L., Vincent, S.D., Timmers, H.T.M., and Tora, L. (2023). ATAC and SAGA co-activator complexes utilize co-translational assembly, but their cellular localization properties and functions are distinct. Cell Rep *42*, 113099. 10.1016/j.celrep.2023.113099.

301. Spedale, G., Timmers, H.T., and Pijnappel, W.W. (2012). ATAC-king the complexity of SAGA during evolution. Genes Dev *26*, 527-541. 10.1101/gad.184705.111.

302. Jin, Q., Yu, L.R., Wang, L., Zhang, Z., Kasper, L.H., Lee, J.E., Wang, C., Brindle, P.K., Dent, S.Y., and Ge, K. (2011). Distinct roles of GCN5/PCAF-mediated H3K9ac and CBP/p300-mediated H3K18/27ac in nuclear receptor transactivation. EMBO J *30*, 249-262. 10.1038/emboj.2010.318.

303. Nagy, Z., and Tora, L. (2007). Distinct GCN5/PCAF-containing complexes function as co-activators and are involved in transcription factor and global histone acetylation. Oncogene *26*, 5341-5357. 10.1038/sj.onc.1210604.

304. Riss, A., Scheer, E., Joint, M., Trowitzsch, S., Berger, I., and Tora, L. (2015). Subunits of ADA-two-A-containing (ATAC) or Spt-Ada-Gcn5-acetyltrasferase (SAGA) Coactivator Complexes Enhance the Acetyltransferase Activity of GCN5. J Biol Chem *290*, 28997-29009. 10.1074/jbc.M115.668533.

305. Cieniewicz, A.M., Moreland, L., Ringel, A.E., Mackintosh, S.G., Raman, A., Gilbert, T.M., Wolberger, C., Tackett, A.J., and Taverna, S.D. (2014). The bromodomain of Gcn5 regulates site specificity of lysine acetylation on histone H3. Mol Cell Proteomics *13*, 2896-2910. 10.1074/mcp.M114.038174.

306. Guelman, S., Kozuka, K., Mao, Y., Pham, V., Solloway, M.J., Wang, J., Wu, J., Lill, J.R., and Zha, J. (2009). The double-histone-acetyltransferase complex ATAC is essential for mammalian development. Mol Cell Biol *29*, 1176-1188. 10.1128/MCB.01599-08.

307. Vermeulen, M., Eberl, H.C., Matarese, F., Marks, H., Denissov, S., Butter, F., Lee, K.K., Olsen, J.V., Hyman, A.A., Stunnenberg, H.G., and Mann, M. (2010). Quantitative interaction proteomics and genome-wide profiling of epigenetic histone marks and their readers. Cell *142*, 967-980. 10.1016/j.cell.2010.08.020.

308. Bian, C., Xu, C., Ruan, J., Lee, K.K., Burke, T.L., Tempel, W., Barsyte, D., Li, J., Wu, M., Zhou, B.O., et al. (2011). Sgf29 binds histone H3K4me2/3 and is required for SAGA complex recruitment and histone H3 acetylation. EMBO J *30*, 2829-2842. 10.1038/emboj.2011.193.

309. Hassan, A.H., Prochasson, P., Neely, K.E., Galasinski, S.C., Chandy, M., Carrozza, M.J., and Workman, J.L. (2002). Function and selectivity of bromodomains in anchoring chromatin-modifying complexes to promoter nucleosomes. Cell *111*, 369-379. 10.1016/s0092-8674(02)01005-x.

310. Ornaghi, P., Ballario, P., Lena, A.M., Gonzalez, A., and Filetici, P. (1999). The bromodomain of Gcn5p interacts in vitro with specific residues in the N terminus of histone H4. J Mol Biol *287*, 1-7. 10.1006/jmbi.1999.2577.

311. Yayli, G., Bernardini, A., Sanchez, P.K.M., Scheer, E., Damilot, M., Essabri, K., Morlet, B., Negroni, L., Vincent, S.D., Timmers, H.M., and Tora, L. (2023). ATAC and SAGA coactivator complexes utilize co-translational assembly, but their cellular localization properties and functions are distinct. bioRxiv. 10.1101/2023.08.03.551787.

312. Zhao, Y., Lang, G., Ito, S., Bonnet, J., Metzger, E., Sawatsubashi, S., Suzuki, E., Le Guezennec, X., Stunnenberg, H.G., Krasnov, A., et al. (2008). A TFTC/STAGA module mediates histone H2A and H2B deubiquitination, coactivates nuclear receptors, and counteracts heterochromatin silencing. Mol Cell *29*, 92-101. 10.1016/j.molcel.2007.12.011.

313. Zhang, X.Y., Pfeiffer, H.K., Thorne, A.W., and McMahon, S.B. (2008). USP22, an hSAGA subunit and potential cancer stem cell marker, reverses the polycomb-catalyzed ubiquitylation of histone H2A. Cell Cycle *7*, 1522-1524. 10.4161/cc.7.11.5962.

314. McMahon, S.B., Van Buskirk, H.A., Dugan, K.A., Copeland, T.D., and Cole, M.D. (1998). The novel ATM-related protein TRRAP is an essential cofactor for the c-Myc and E2F oncoproteins. Cell *94*, 363-374. 10.1016/s0092-8674(00)81479-8.

315. Yin, B.K., and Wang, Z.Q. (2021). Beyond HAT Adaptor: TRRAP Liaisons with Sp1-Mediated Transcription. Int J Mol Sci *22*. 10.3390/ijms222212445.

316. Ard, P.G., Chatterjee, C., Kunjibettu, S., Adside, L.R., Gralinski, L.E., and McMahon, S.B. (2002). Transcriptional regulation of the mdm2 oncogene by p53 requires TRRAP acetyltransferase complexes. Mol Cell Biol *22*, 5650-5661. 10.1128/MCB.22.16.5650-5661.2002.

317. Chen, Y.C., and Dent, S.Y.R. (2021). Conservation and diversity of the eukaryotic SAGA coactivator complex across kingdoms. Epigenetics Chromatin *14*, 26. 10.1186/s13072-021-00402-x.

318. Mustachio, L.M., Roszik, J., Farria, A., and Dent, S.Y.R. (2020). Targeting the SAGA and ATAC Transcriptional Coactivator Complexes in MYC-Driven Cancers. Cancer Res *80*, 1905-1911. 10.1158/0008-5472.CAN-19-3652.

319. Schrecengost, R.S., Dean, J.L., Goodwin, J.F., Schiewer, M.J., Urban, M.W., Stanek, T.J., Sussman, R.T., Hicks, J.L., Birbe, R.C., Draganova-Tacheva, R.A., et al. (2014). USP22 regulates oncogenic signaling pathways to drive lethal cancer progression. Cancer Res *74*, 272-286. 10.1158/0008-5472.CAN-13-1954.

320. Flinn, E.M., Wallberg, A.E., Hermann, S., Grant, P.A., Workman, J.L., and Wright, A.P. (2002). Recruitment of Gcn5-containing complexes during c-Myc-dependent gene activation. Structure and function aspects. J Biol Chem *277*, 23399-23406. 10.1074/jbc.M201704200.

321. Hirsch, C.L., Coban Akdemir, Z., Wang, L., Jayakumaran, G., Trcka, D., Weiss, A., Hernandez, J.J., Pan, Q., Han, H., Xu, X., et al. (2015). Myc and SAGA rewire an alternative splicing network during early somatic cell reprogramming. Genes Dev *29*, 803-816. 10.1101/gad.255109.114.

322. Patel, J.H., Du, Y., Ard, P.G., Phillips, C., Carella, B., Chen, C.J., Rakowski, C., Chatterjee, C., Lieberman, P.M., Lane, W.S., et al. (2004). The c-MYC oncoprotein is a substrate of the acetyltransferases hGCN5/PCAF and TIP60. Mol Cell Biol *24*, 10826-10834. 10.1128/MCB.24.24.10826-10834.2004.

323. Liu, X., Vorontchikhina, M., Wang, Y.L., Faiola, F., and Martinez, E. (2008). STAGA recruits Mediator to the MYC oncoprotein to stimulate transcription and cell proliferation. Mol Cell Biol *28*, 108-121. 10.1128/MCB.01402-07.

324. Zhang, N., Ichikawa, W., Faiola, F., Lo, S.Y., Liu, X., and Martinez, E. (2014). MYC interacts with the human STAGA coactivator complex via multivalent contacts with the GCN5 and TRRAP subunits. Biochim Biophys Acta *1839*, 395-405. 10.1016/j.bbagrm.2014.03.017.

325. Han, X., and Chen, J. (2022). KAT2A affects tumor metabolic reprogramming in colon cancer progression through epigenetic activation of E2F1. Hum Cell *35*, 1140-1158. 10.1007/s13577-022-00707-3.

326. Mustachio, L.M., Roszik, J., Farria, A.T., Guerra, K., and Dent, S.Y. (2019). Repression of GCN5 expression or activity attenuates c-MYC expression in non-small cell lung cancer. Am J Cancer Res *9*, 1830-1845.

327. Chen, Y.C., Bhaskara, G.B., Lu, Y., Lin, K., and Dent, S.Y.R. (2024). The SAGA acetyltransferase module is required for the maintenance of MAF and MYC

oncogenic gene expression programs in multiple myeloma. Genes Dev. 10.1101/gad.351789.124.

328. Downey, M. (2021). Non-histone protein acetylation by the evolutionarily conserved GCN5 and PCAF acetyltransferases. Biochim Biophys Acta Gene Regul Mech *1864*, 194608. 10.1016/j.bbagrm.2020.194608.

329. Qiao, L., Zhang, Q., Zhang, W., and Chen, J.J. (2018). The lysine acetyltransferase GCN5 contributes to human papillomavirus oncoprotein E7-induced cell proliferation via up-regulating E2F1. J Cell Mol Med *22*, 5333-5345. 10.1111/jcmm.13806.

330. Wan, J., Zhan, J., Li, S., Ma, J., Xu, W., Liu, C., Xue, X., Xie, Y., Fang, W., Chin, Y.E., and Zhang, H. (2015). PCAF-primed EZH2 acetylation regulates its stability and promotes lung adenocarcinoma progression. Nucleic Acids Res *43*, 3591-3604. 10.1093/nar/gkv238.

331. Martinez-Balbas, M.A., Bauer, U.M., Nielsen, S.J., Brehm, A., and Kouzarides, T. (2000). Regulation of E2F1 activity by acetylation. EMBO J *19*, 662-671. 10.1093/emboj/19.4.662.

332. Mao, X., Gluck, N., Li, D., Maine, G.N., Li, H., Zaidi, I.W., Repaka, A., Mayo, M.W., and Burstein, E. (2009). GCN5 is a required cofactor for a ubiquitin ligase that targets NF-kappaB/RelA. Genes Dev *23*, 849-861. 10.1101/gad.1748409.

333. Zhang, C., and Huang, Z. (2024). KAT2A Promotes the Succinylation of PKM2 to Inhibit its Activity and Accelerate Glycolysis of Gastric Cancer. Mol Biotechnol *66*, 1446-1457. 10.1007/s12033-023-00778-z.

334. Zhang, X.Y., Varthi, M., Sykes, S.M., Phillips, C., Warzecha, C., Zhu, W., Wyce, A., Thorne, A.W., Berger, S.L., and McMahon, S.B. (2008). The putative cancer stem cell marker USP22 is a subunit of the human SAGA complex required for activated transcription and cell-cycle progression. Mol Cell *29*, 102-111. 10.1016/j.molcel.2007.12.015.

335. Guo, J., Zhao, J., Fu, W., Xu, Q., and Huang, D. (2022). Immune Evasion and Drug Resistance Mediated by USP22 in Cancer: Novel Targets and Mechanisms. Front Immunol *13*, 918314. 10.3389/fimmu.2022.918314.

336. Fischer, V., Plassard, D., Ye, T., Reina-San-Martin, B., Stierle, M., Tora, L., and Devys, D. (2021). The related coactivator complexes SAGA and ATAC control embryonic stem cell self-renewal through acetyltransferase-independent mechanisms. Cell Rep *36*, 109598. 10.1016/j.celrep.2021.109598.

337. Yamauchi, T., Yamauchi, J., Kuwata, T., Tamura, T., Yamashita, T., Bae, N., Westphal, H., Ozato, K., and Nakatani, Y. (2000). Distinct but overlapping roles of histone acetylase PCAF and of the closely related PCAF-B/GCN5 in mouse

embryogenesis. Proc Natl Acad Sci U S A *97*, 11303-11306. 10.1073/pnas.97.21.11303.

338. Lin, W., Srajer, G., Evrard, Y.A., Phan, H.M., Furuta, Y., and Dent, S.Y. (2007). Developmental potential of Gcn5(-/-) embryonic stem cells in vivo and in vitro. Dev Dyn *236*, 1547-1557. 10.1002/dvdy.21160.

339. Hirsch, C.L., Wrana, J.L., and Dent, S.Y.R. (2017). KATapulting toward Pluripotency and Cancer. J Mol Biol *429*, 1958-1977. 10.1016/j.jmb.2016.09.023.

340. Martinez-Cerdeno, V., Lemen, J.M., Chan, V., Wey, A., Lin, W., Dent, S.R., and Knoepfler, P.S. (2012). N-Myc and GCN5 regulate significantly overlapping transcriptional programs in neural stem cells. PLoS One *7*, e39456. 10.1371/journal.pone.0039456.

341. Walters, B.W., Tan, T.J., Tan, C.T., Dube, C.T., Lee, K.T., Koh, J., Ong, Y.H.B., Tan, V.X.H., Jahan, F.R.S., Lim, X.N., et al. (2023). Divergent functions of histone acetyltransferases KAT2A and KAT2B in keratinocyte self-renewal and differentiation. J Cell Sci *136*. 10.1242/jcs.260723.

342. Seruggia, D., Oti, M., Tripathi, P., Canver, M.C., LeBlanc, L., Di Giammartino, D.C., Bullen, M.J., Nefzger, C.M., Sun, Y.B.Y., Farouni, R., et al. (2019). TAF5L and TAF6L Maintain Self-Renewal of Embryonic Stem Cells via the MYC Regulatory Network. Mol Cell *74*, 1148-1163 e1147. 10.1016/j.molcel.2019.03.025.

343. Chang, C.H., Liu, F., Militi, S., Hester, S., Nibhani, R., Deng, S., Dunford, J., Rendek, A., Soonawalla, Z., Fischer, R., et al. (2024). The pRb/RBL2-E2F1/4-GCN5 axis regulates cancer stem cell formation and G0 phase entry/exit by paracrine mechanisms. Nat Commun *15*, 3580. 10.1038/s41467-024-47680-z.

344. Collier, A.J., Bendall, A., Fabian, C., Malcolm, A.A., Tilgner, K., Semprich, C.I., Wojdyla, K., Nisi, P.S., Kishore, K., Roamio Franklin, V.N., et al. (2022). Genome-wide screening identifies Polycomb repressive complex 1.3 as an essential regulator of human naive pluripotent cell reprogramming. Sci Adv *8*, eabk0013. 10.1126/sciadv.abk0013.

345. Domingues, A.F., Kulkarni, R., Giotopoulos, G., Gupta, S., Vinnenberg, L., Arede, L., Foerner, E., Khalili, M., Adao, R.R., Johns, A., et al. (2020). Loss of Kat2a enhances transcriptional noise and depletes acute myeloid leukemia stem-like cells. Elife *9*. 10.7554/eLife.51754.

346. Moris, N., Edri, S., Seyres, D., Kulkarni, R., Domingues, A.F., Balayo, T., Frontini, M., and Pina, C. (2018). Histone Acetyltransferase KAT2A Stabilizes Pluripotency with Control of Transcriptional Heterogeneity. Stem Cells *36*, 1828-1838. 10.1002/stem.2919.

347. Schuren, A.B., Costa, A.I., and Wiertz, E.J. (2016). Recent advances in viral evasion of the MHC Class I processing pathway. Curr Opin Immunol *40*, 43-50. 10.1016/j.coi.2016.02.007.

348. Westrich, J.A., Warren, C.J., and Pyeon, D. (2017). Evasion of host immune defenses by human papillomavirus. Virus Res *231*, 21-33. 10.1016/j.virusres.2016.11.023.

349. Kim, K.H., and Roberts, C.W. (2016). Targeting EZH2 in cancer. Nat Med *22*, 128-134. 10.1038/nm.4036.

350. Wassef, M., and Margueron, R. (2017). The Multiple Facets of PRC2 Alterations in Cancers. J Mol Biol *429*, 1978-1993. 10.1016/j.jmb.2016.10.012.

351. Sparmann, A., and van Lohuizen, M. (2006). Polycomb silencers control cell fate, development and cancer. Nat Rev Cancer *6*, 846-856. 10.1038/nrc1991.

352. Lechner, M., Fenton, T., West, J., Wilson, G., Feber, A., Henderson, S., Thirlwell, C., Dibra, H.K., Jay, A., Butcher, L., et al. (2013). Identification and functional validation of HPV-mediated hypermethylation in head and neck squamous cell carcinoma. Genome Med *5*, 15. 10.1186/gm419.

353. Zhao, L., Yu, Y., Wu, J., Bai, J., Zhao, Y., Li, C., Sun, W., and Wang, X. (2014). Role of EZH2 in oral squamous cell carcinoma carcinogenesis. Gene *537*, 197-202. 10.1016/j.gene.2014.01.006.

354. Farria, A., Li, W., and Dent, S.Y. (2015). KATs in cancer: functions and therapies. Oncogene *34*, 4901-4913. 10.1038/onc.2014.453.

355. White, J., Derheimer, F.A., Jensen-Pergakes, K., O'Connell, S., Sharma, S., Spiegel, N., and Paul, T.A. (2024). Histone lysine acetyltransferase inhibitors: an emerging class of drugs for cancer therapy. Trends Pharmacol Sci *45*, 243-254. 10.1016/j.tips.2024.01.010.

356. Lang, S.E., McMahon, S.B., Cole, M.D., and Hearing, P. (2001). E2F transcriptional activation requires TRRAP and GCN5 cofactors. J Biol Chem *276*, 32627-32634. 10.1074/jbc.M102067200.

357. Liu, X., Tesfai, J., Evrard, Y.A., Dent, S.Y., and Martinez, E. (2003). c-Myc transformation domain recruits the human STAGA complex and requires TRRAP and GCN5 acetylase activity for transcription activation. J Biol Chem *278*, 20405-20412. 10.1074/jbc.M211795200.

358. Goos, H., Kinnunen, M., Salokas, K., Tan, Z., Liu, X., Yadav, L., Zhang, Q., Wei, G.H., and Varjosalo, M. (2022). Human transcription factor protein interaction networks. Nat Commun *13*, 766. 10.1038/s41467-022-28341-5.

359. Wang, Y.W., Chang, H.S., Lin, C.H., and Yu, W.C. (2007). HPV-18 E7 conjugates to c-Myc and mediates its transcriptional activity. Int J Biochem Cell Biol *39*, 402-412. 10.1016/j.biocel.2006.09.006.
360. Yin, Y.W., Jin, H.J., Zhao, W., Gao, B., Fang, J., Wei, J., Zhang, D.D., Zhang, J., and Fang, D. (2015). The Histone Acetyltransferase GCN5 Expression Is Elevated and Regulated by c-Myc and E2F1 Transcription Factors in Human Colon Cancer. Gene Expr *16*, 187-196. 10.3727/105221615X14399878166230.

361. White, J.S., Weissfeld, J.L., Ragin, C.C., Rossie, K.M., Martin, C.L., Shuster, M., Ishwad, C.S., Law, J.C., Myers, E.N., Johnson, J.T., and Gollin, S.M. (2007). The influence of clinical and demographic risk factors on the establishment of head and neck squamous cell carcinoma cell lines. Oral Oncol *43*, 701-712. 10.1016/j.oraloncology.2006.09.001.

362. Sanson, K.R., Hanna, R.E., Hegde, M., Donovan, K.F., Strand, C., Sullender, M.E., Vaimberg, E.W., Goodale, A., Root, D.E., Piccioni, F., and Doench, J.G. (2018). Optimized libraries for CRISPR-Cas9 genetic screens with multiple modalities. Nat Commun *9*, 5416. 10.1038/s41467-018-07901-8.

363. Li, W., Xu, H., Xiao, T., Cong, L., Love, M.I., Zhang, F., Irizarry, R.A., Liu, J.S., Brown, M., and Liu, X.S. (2014). MAGeCK enables robust identification of essential genes from genome-scale CRISPR/Cas9 knockout screens. Genome Biol *15*, 554. 10.1186/s13059-014-0554-4.

364. Boyle, L.H., Hermann, C., Boname, J.M., Porter, K.M., Patel, P.A., Burr, M.L., Duncan, L.M., Harbour, M.E., Rhodes, D.A., Skjodt, K., et al. (2013). Tapasin-related protein TAPBPR is an additional component of the MHC class I presentation pathway. Proc Natl Acad Sci U S A *110*, 3465-3470. 10.1073/pnas.1222342110.

365. Brinkman, E.K., Chen, T., Amendola, M., and van Steensel, B. (2014). Easy quantitative assessment of genome editing by sequence trace decomposition. Nucleic Acids Res *42*, e168. 10.1093/nar/gku936.

366. Blees, A., Januliene, D., Hofmann, T., Koller, N., Schmidt, C., Trowitzsch, S., Moeller, A., and Tampe, R. (2017). Structure of the human MHC-I peptide-loading complex. Nature *551*, 525-528. 10.1038/nature24627.

367. Benko, S., Kovacs, E.G., Hezel, F., and Kufer, T.A. (2017). NLRC5 Functions beyond MHC I Regulation-What Do We Know So Far? Front Immunol *8*, 150. 10.3389/fimmu.2017.00150.

368. Szklarczyk, D., Kirsch, R., Koutrouli, M., Nastou, K., Mehryary, F., Hachilif, R., Gable, A.L., Fang, T., Doncheva, N.T., Pyysalo, S., et al. (2023). The STRING database in 2023: protein-protein association networks and functional enrichment analyses for any sequenced genome of interest. Nucleic Acids Res *51*, D638-D646. 10.1093/nar/gkac1000.

369. Fischer, S., and Liefke, R. (2023). Polycomb-like Proteins in Gene Regulation and Cancer. Genes (Basel) *14*. 10.3390/genes14040938.

370. Haque, M.E., Jakaria, M., Akther, M., Cho, D.Y., Kim, I.S., and Choi, D.K. (2021). The GCN5: its biological functions and therapeutic potentials. Clin Sci (Lond) *135*, 231-257. 10.1042/CS20200986.

371. Commons, G.D. https://xenabrowser.net/datapages/?host=https%3A%2F%2Fgdc.xenahubs.net&dataset=TCGA-HNSC.htseq_fpkm-uq.tsv.

372. Goldman, M.J., Craft, B., Hastie, M., Repecka, K., McDade, F., Kamath, A., Banerjee, A., Luo, Y., Rogers, D., Brooks, A.N., et al. (2020). Visualizing and interpreting cancer genomics data via the Xena platform. Nat Biotechnol *38*, 675-678. 10.1038/s41587-020-0546-8.

373. Li, B., Severson, E., Pignon, J.C., Zhao, H., Li, T., Novak, J., Jiang, P., Shen, H., Aster, J.C., Rodig, S., et al. (2016). Comprehensive analyses of tumor immunity: implications for cancer immunotherapy. Genome Biol *17*, 174. 10.1186/s13059-016-1028-7.

374. Li, T., Fan, J., Wang, B., Traugh, N., Chen, Q., Liu, J.S., Li, B., and Liu, X.S. (2017). TIMER: A Web Server for Comprehensive Analysis of Tumor-Infiltrating Immune Cells. Cancer Res *77*, e108-e110. 10.1158/0008-5472.CAN-17-0307.

375. Li, T., Fu, J., Zeng, Z., Cohen, D., Li, J., Chen, Q., Li, B., and Liu, X.S. (2020). TIMER2.0 for analysis of tumor-infiltrating immune cells. Nucleic Acids Res *48*, W509-W514. 10.1093/nar/gkaa407.

376. Kramer, A., Green, J., Pollard, J., Jr., and Tugendreich, S. (2014). Causal analysis approaches in Ingenuity Pathway Analysis. Bioinformatics *30*, 523-530. 10.1093/bioinformatics/btt703.

377. Lopez-Banuelos, L., and Vega, L. (2022). Inhibition of acetylation, is it enough to fight cancer? Crit Rev Oncol Hematol *176*, 103752. 10.1016/j.critrevonc.2022.103752.

378. Schobert, R., and Biersack, B. (2019). Chemical and Biological Aspects of Garcinol and Isogarcinol: Recent Developments. Chem Biodivers *16*, e1900366. 10.1002/cbdv.201900366.

379. Hoy, S.M. (2020). Tazemetostat: First Approval. Drugs *80*, 513-521. 10.1007/s40265-020-01288-x.

380. Dhillon, S. (2020). Decitabine/Cedazuridine: First Approval. Drugs *80*, 1373-1378. 10.1007/s40265-020-01389-7.

381. Patnaik, E., Madu, C., and Lu, Y. (2023). Epigenetic Modulators as Therapeutic Agents in Cancer. Int J Mol Sci *24*. 10.3390/ijms241914964.

382. Chiappinelli, K.B., Strissel, P.L., Desrichard, A., Li, H., Henke, C., Akman, B., Hein, A., Rote, N.S., Cope, L.M., Snyder, A., et al. (2015). Inhibiting DNA Methylation Causes an Interferon Response in Cancer via dsRNA Including Endogenous Retroviruses. Cell *162*, 974-986. 10.1016/j.cell.2015.07.011.

383. Zhang, L., Li, H.T., Shereda, R., Lu, Q., Weisenberger, D.J., O'Connell, C., Machida, K., An, W., Lenz, H.J., El-Khoueiry, A., et al. (2022). DNMT and EZH2 inhibitors synergize to activate therapeutic targets in hepatocellular carcinoma. Cancer Lett *548*, 215899. 10.1016/j.canlet.2022.215899.

384. Kirmizis, A., Bartley, S.M., and Farnham, P.J. (2003). Identification of the polycomb group protein SU(Z)12 as a potential molecular target for human cancer therapy. Mol Cancer Ther *2*, 113-121.

385. Bracken, A.P., Pasini, D., Capra, M., Prosperini, E., Colli, E., and Helin, K. (2003). EZH2 is downstream of the pRB-E2F pathway, essential for proliferation and amplified in cancer. EMBO J *22*, 5323-5335. 10.1093/emboj/cdg542.

386. Santos, M., Martinez-Fernandez, M., Duenas, M., Garcia-Escudero, R., Alfaya, B., Villacampa, F., Saiz-Ladera, C., Costa, C., Oteo, M., Duarte, J., et al. (2014). In vivo disruption of an Rb-E2F-Ezh2 signaling loop causes bladder cancer. Cancer Res *74*, 6565-6577. 10.1158/0008-5472.CAN-14-1218.

387. Lee, S.R., Roh, Y.G., Kim, S.K., Lee, J.S., Seol, S.Y., Lee, H.H., Kim, W.T., Kim, W.J., Heo, J., Cha, H.J., et al. (2015). Activation of EZH2 and SUZ12 Regulated by E2F1 Predicts the Disease Progression and Aggressive Characteristics of Bladder Cancer. Clin Cancer Res *21*, 5391-5403. 10.1158/1078-0432.CCR-14-2680.

388. Du, L., Fakih, M.G., Rosen, S.T., and Chen, Y. (2020). SUMOylation of E2F1 Regulates Expression of EZH2. Cancer Res *80*, 4212-4223. 10.1158/0008-5472.CAN-20-1259.

389. Wu, Z.L., Zheng, S.S., Li, Z.M., Qiao, Y.Y., Aau, M.Y., and Yu, Q. (2010). Polycomb protein EZH2 regulates E2F1-dependent apoptosis through epigenetically modulating Bim expression. Cell Death Differ *17*, 801-810. 10.1038/cdd.2009.162.

390. Khattri, M., Amako, Y., Gibbs, J.R., Collura, J.L., Arora, R., Harold, A., Li, M.Y., Harms, P.W., Ezhkova, E., and Shuda, M. (2023). Methyltransferase-independent function of enhancer of zeste homologue 2 maintains tumorigenicity induced by human oncogenic papillomavirus and polyomavirus. Tumour Virus Res *16*, 200264. 10.1016/j.tvr.2023.200264.

391. Tao, T., Liu, D., Liu, C., Xu, B., Chen, S., Yin, Y., Ang, L., Huang, Y., Zhang, X., and Chen, M. (2014). Autoregulatory feedback loop of EZH2/miR-200c/E2F3 as a driving force for prostate cancer development. Biochim Biophys Acta *1839*, 858-865. 10.1016/j.bbagrm.2014.07.001.

392. Otto, T., Horn, S., Brockmann, M., Eilers, U., Schuttrumpf, L., Popov, N., Kenney, A.M., Schulte, J.H., Beijersbergen, R., Christiansen, H., et al. (2009). Stabilization of N-Myc is a critical function of Aurora A in human neuroblastoma. Cancer Cell *15*, 67-78. 10.1016/j.ccr.2008.12.005.

393. Krenz, B., Lee, J., Kannan, T., and Eilers, M. (2024). Immune evasion: An imperative and consequence of MYC deregulation. Mol Oncol. 10.1002/1878-0261.13695.

394. Meyer, N., and Penn, L.Z. (2008). Reflecting on 25 years with MYC. Nat Rev Cancer *8*, 976-990. 10.1038/nrc2231.

395. Dhanasekaran, R., Deutzmann, A., Mahauad-Fernandez, W.D., Hansen, A.S., Gouw, A.M., and Felsher, D.W. (2022). The MYC oncogene - the grand orchestrator of cancer growth and immune evasion. Nat Rev Clin Oncol *19*, 23-36. 10.1038/s41571-021-00549-2.

396. Schwab, M., Alitalo, K., Klempnauer, K.H., Varmus, H.E., Bishop, J.M., Gilbert, F., Brodeur, G., Goldstein, M., and Trent, J. (1983). Amplified DNA with limited homology to myc cellular oncogene is shared by human neuroblastoma cell lines and a neuroblastoma tumour. Nature *305*, 245-248. 10.1038/305245a0.

397. Kohl, N.E., Kanda, N., Schreck, R.R., Bruns, G., Latt, S.A., Gilbert, F., and Alt, F.W. (1983). Transposition and amplification of oncogene-related sequences in human neuroblastomas. Cell *35*, 359-367. 10.1016/0092-8674(83)90169-1.

398. Saksela, K. (1987). Expression of the L-myc gene is under positive control by short-lived proteins. Oncogene *1*, 291-296.

399. Zimmerman, K.A., Yancopoulos, G.D., Collum, R.G., Smith, R.K., Kohl, N.E., Denis, K.A., Nau, M.M., Witte, O.N., Toran-Allerand, D., Gee, C.E., and et al. (1986). Differential expression of myc family genes during murine development. Nature *319*, 780-783. 10.1038/319780a0.

400. DePinho, R., Mitsock, L., Hatton, K., Ferrier, P., Zimmerman, K., Legouy, E., Tesfaye, A., Collum, R., Yancopoulos, G., Nisen, P., and et al. (1987). Myc family of cellular oncogenes. J Cell Biochem *33*, 257-266. 10.1002/jcb.240330404.

401. Liu, R., Shi, P., Wang, Z., Yuan, C., and Cui, H. (2020). Molecular Mechanisms of MYCN Dysregulation in Cancers. Front Oncol *10*, 625332. 10.3389/fonc.2020.625332.

402. Abba, M.C., Laguens, R.M., Dulout, F.N., and Golijow, C.D. (2004). The c-myc activation in cervical carcinomas and HPV 16 infections. Mutat Res *557*, 151-158. 10.1016/j.mrgentox.2003.10.005.

403. Peter, M., Rosty, C., Couturier, J., Radvanyi, F., Teshima, H., and Sastre-Garau, X. (2006). MYC activation associated with the integration of HPV DNA at the MYC locus in genital tumors. Oncogene *25*, 5985-5993. 10.1038/sj.onc.1209625.

404. Sastre-Garau, X., Favre, M., Couturier, J., and Orth, G. (2000). Distinct patterns of alteration of myc genes associated with integration of human papillomavirus type 16 or type 45 DNA in two genital tumours. J Gen Virol *81*, 1983-1993. 10.1099/0022-1317-81-8-1983.

405. Liu, X., Dakic, A., Zhang, Y., Dai, Y., Chen, R., and Schlegel, R. (2009). HPV E6 protein interacts physically and functionally with the cellular telomerase complex. Proc Natl Acad Sci U S A *106*, 18780-18785. 10.1073/pnas.0906357106.

406. Damania, B., and Pipas, J.M. (2009). DNA tumor viruses (Springer Science + Business Media).

407. Stanton, B.R., and Parada, L.F. (1992). The N-myc proto-oncogene: developmental expression and in vivo site-directed mutagenesis. Brain Pathol *2*, 71-83.

408. Stanton, B.R., Perkins, A.S., Tessarollo, L., Sassoon, D.A., and Parada, L.F. (1992). Loss of N-myc function results in embryonic lethality and failure of the epithelial component of the embryo to develop. Genes Dev *6*, 2235-2247. 10.1101/gad.6.12a.2235.

409. Tomlinson, F.H., Jenkins, R.B., Scheithauer, B.W., Keelan, P.A., Ritland, S., Parisi, J.E., Cunningham, J., and Olsen, K.D. (1994). Aggressive medulloblastoma with high-level N-myc amplification. Mayo Clin Proc *69*, 359-365. 10.1016/s0025-6196(12)62221-6.

410. Lee, J.K., Phillips, J.W., Smith, B.A., Park, J.W., Stoyanova, T., McCaffrey, E.F., Baertsch, R., Sokolov, A., Meyerowitz, J.G., Mathis, C., et al. (2016). N-Myc Drives Neuroendocrine Prostate Cancer Initiated from Human Prostate Epithelial Cells. Cancer Cell *29*, 536-547. 10.1016/j.ccell.2016.03.001.

411. Brodeur, G.M. (2018). Spontaneous regression of neuroblastoma. Cell Tissue Res *372*, 277-286. 10.1007/s00441-017-2761-2.

412. Zimmerli, D., Brambillasca, C.S., Talens, F., Bhin, J., Linstra, R., Romanens, L., Bhattacharya, A., Joosten, S.E.P., Da Silva, A.M., Padrao, N., et al. (2022). MYC promotes immune-suppression in triple-negative breast cancer via inhibition of interferon signaling. Nat Commun *13*, 6579. 10.1038/s41467-022-34000-6.

413. Raieli, S., Di Renzo, D., Lampis, S., Amadesi, C., Montemurro, L., Pession, A., Hrelia, P., Fischer, M., and Tonelli, R. (2021). MYCN Drives a Tumor Immunosuppressive Environment Which Impacts Survival in Neuroblastoma. Front Oncol *11*, 625207. 10.3389/fonc.2021.625207.

414. Muller, I., Larsson, K., Frenzel, A., Oliynyk, G., Zirath, H., Prochownik, E.V., Westwood, N.J., and Henriksson, M.A. (2014). Targeting of the MYCN protein with small molecule c-MYC inhibitors. PLoS One *9*, e97285. 10.1371/journal.pone.0097285.

415. Wang, C., Zhang, J., Yin, J., Gan, Y., Xu, S., Gu, Y., and Huang, W. (2021). Alternative approaches to target Myc for cancer treatment. Signal Transduct Target Ther *6*, 117. 10.1038/s41392-021-00500-y.

416. Richards, M.W., Burgess, S.G., Poon, E., Carstensen, A., Eilers, M., Chesler, L., and Bayliss, R. (2016). Structural basis of N-Myc binding by Aurora-A and its destabilization by kinase inhibitors. Proc Natl Acad Sci U S A *113*, 13726-13731. 10.1073/pnas.1610626113.

417. Manfredi, M.G., Ecsedy, J.A., Chakravarty, A., Silverman, L., Zhang, M., Hoar, K.M., Stroud, S.G., Chen, W., Shinde, V., Huck, J.J., et al. (2011). Characterization of Alisertib (MLN8237), an investigational small-molecule inhibitor of aurora A kinase using novel in vivo pharmacodynamic assays. Clin Cancer Res *17*, 7614-7624. 10.1158/1078-0432.CCR-11-1536.

418. Gorgun, G., Calabrese, E., Hideshima, T., Ecsedy, J., Perrone, G., Mani, M., Ikeda, H., Bianchi, G., Hu, Y., Cirstea, D., et al. (2010). A novel Aurora-A kinase inhibitor MLN8237 induces cytotoxicity and cell-cycle arrest in multiple myeloma. Blood *115*, 5202-5213. 10.1182/blood-2009-12-259523.

419. Sehdev, V., Peng, D., Soutto, M., Washington, M.K., Revetta, F., Ecsedy, J., Zaika, A., Rau, T.T., Schneider-Stock, R., Belkhiri, A., and El-Rifai, W. (2012). The aurora kinase A inhibitor MLN8237 enhances cisplatin-induced cell death in esophageal adenocarcinoma cells. Mol Cancer Ther *11*, 763-774. 10.1158/1535-7163.MCT-11-0623.

420. Wang, L., Arras, J., Katsha, A., Hamdan, S., Belkhiri, A., Ecsedy, J., and El-Rifai, W. (2017). Cisplatin-resistant cancer cells are sensitive to Aurora kinase A inhibition by alisertib. Mol Oncol *11*, 981-995. 10.1002/1878-0261.12066.

421. Li, Y., Li, X., Pu, J., Yang, Q., Guan, H., Ji, M., Shi, B., Chen, M., and Hou, P. (2018). c-Myc Is a Major Determinant for Antitumor Activity of Aurora A Kinase Inhibitor MLN8237 in Thyroid Cancer. Thyroid *28*, 1642-1654. 10.1089/thy.2018.0183.

422. Katsha, A., Wang, L., Arras, J., Omar, O.M., Ecsedy, J., Belkhiri, A., and El-Rifai, W. (2017). Activation of EIF4E by Aurora Kinase A Depicts a Novel Druggable

Axis in Everolimus-Resistant Cancer Cells. Clin Cancer Res *23*, 3756-3768. 10.1158/1078-0432.CCR-16-2141.

423. Dauch, D., Rudalska, R., Cossa, G., Nault, J.C., Kang, T.W., Wuestefeld, T., Hohmeyer, A., Imbeaud, S., Yevsa, T., Hoenicke, L., et al. (2016). A MYC-aurora kinase A protein complex represents an actionable drug target in p53-altered liver cancer. Nat Med *22*, 744-753. 10.1038/nm.4107.

424. Patange, S., Ball, D.A., Wan, Y., Karpova, T.S., Girvan, M., Levens, D., and Larson, D.R. (2022). MYC amplifies gene expression through global changes in transcription factor dynamics. Cell Rep *38*, 110292. 10.1016/j.celrep.2021.110292.

425. Rahl, P.B., and Young, R.A. (2014). MYC and transcription elongation. Cold Spring Harb Perspect Med *4*, a020990. 10.1101/cshperspect.a020990.

426. Marumoto, T., Honda, S., Hara, T., Nitta, M., Hirota, T., Kohmura, E., and Saya, H. (2003). Aurora-A kinase maintains the fidelity of early and late mitotic events in HeLa cells. J Biol Chem *278*, 51786-51795. 10.1074/jbc.M306275200.

427. Otto, T., and Sicinski, P. (2017). Cell cycle proteins as promising targets in cancer therapy. Nat Rev Cancer *17*, 93-115. 10.1038/nrc.2016.138.

428. Garcia-Gutierrez, L., Bretones, G., Molina, E., Arechaga, I., Symonds, C., Acosta, J.C., Blanco, R., Fernandez, A., Alonso, L., Sicinski, P., et al. (2019). Myc stimulates cell cycle progression through the activation of Cdk1 and phosphorylation of p27. Sci Rep *9*, 18693. 10.1038/s41598-019-54917-1.

429. Dong, P., Maddali, M.V., Srimani, J.K., Thelot, F., Nevins, J.R., Mathey-Prevot, B., and You, L. (2014). Division of labour between Myc and G1 cyclins in cell cycle commitment and pace control. Nat Commun *5*, 4750. 10.1038/ncomms5750.

430. Propper, D.J., and Balkwill, F.R. (2022). Harnessing cytokines and chemokines for cancer therapy. Nat Rev Clin Oncol *19*, 237-253. 10.1038/s41571-021-00588-9.

431. Homey, B., Muller, A., and Zlotnik, A. (2002). Chemokines: agents for the immunotherapy of cancer? Nat Rev Immunol *2*, 175-184. 10.1038/nri748.

432. Chow, M.T., Ozga, A.J., Servis, R.L., Frederick, D.T., Lo, J.A., Fisher, D.E., Freeman, G.J., Boland, G.M., and Luster, A.D. (2019). Intratumoral Activity of the CXCR3 Chemokine System Is Required for the Efficacy of Anti-PD-1 Therapy. Immunity *50*, 1498-1512 e1495. 10.1016/j.immuni.2019.04.010.

433. House, I.G., Savas, P., Lai, J., Chen, A.X.Y., Oliver, A.J., Teo, Z.L., Todd, K.L., Henderson, M.A., Giuffrida, L., Petley, E.V., et al. (2020). Macrophage-Derived

CXCL9 and CXCL10 Are Required for Antitumor Immune Responses Following Immune Checkpoint Blockade. Clin Cancer Res *26*, 487-504. 10.1158/1078-0432.CCR-19-1868.

434. Dangaj, D., Bruand, M., Grimm, A.J., Ronet, C., Barras, D., Duttagupta, P.A., Lanitis, E., Duraiswamy, J., Tanyi, J.L., Benencia, F., et al. (2019). Cooperation between Constitutive and Inducible Chemokines Enables T Cell Engraftment and Immune Attack in Solid Tumors. Cancer Cell *35*, 885-900 e810. 10.1016/j.ccell.2019.05.004.

435. Bockorny, B., Semenisty, V., Macarulla, T., Borazanci, E., Wolpin, B.M., Stemmer, S.M., Golan, T., Geva, R., Borad, M.J., Pedersen, K.S., et al. (2020). BL-8040, a CXCR4 antagonist, in combination with pembrolizumab and chemotherapy for pancreatic cancer: the COMBAT trial. Nat Med *26*, 878-885. 10.1038/s41591-020-0880-x.

436. Gong, R., and Ren, H. (2020). Targeting chemokines/chemokine receptors: a promising strategy for enhancing the immunotherapy of pancreatic ductal adenocarcinoma. Signal Transduct Target Ther *5*, 149. 10.1038/s41392-020-00267-8.

437. Sterner, R.C., and Sterner, R.M. (2021). CAR-T cell therapy: current limitations and potential strategies. Blood Cancer J *11*, 69. 10.1038/s41408-021-00459-7.

438. Wang, G., Zhang, Z., Zhong, K., Wang, Z., Yang, N., Tang, X., Li, H., Lu, Q., Wu, Z., Yuan, B., et al. (2023). CXCL11-armed oncolytic adenoviruses enhance CAR-T cell therapeutic efficacy and reprogram tumor microenvironment in glioblastoma. Mol Ther *31*, 134-153. 10.1016/j.ymthe.2022.08.021.

439. Gao, Q., and Zhang, Y. (2021). CXCL11 Signaling in the Tumor Microenvironment. Adv Exp Med Biol *1302*, 41-50. 10.1007/978-3-030-62658-7_4.

440. Lu, J., Chatterjee, M., Schmid, H., Beck, S., and Gawaz, M. (2016). CXCL14 as an emerging immune and inflammatory modulator. J Inflamm (Lond) *13*, 1. 10.1186/s12950-015-0109-9.

441. Pan, Q., Liu, R., Zhang, X., Cai, L., Li, Y., Dong, P., Gao, J., Liu, Y., and He, L. (2023). CXCL14 as a potential marker for immunotherapy response prediction in renal cell carcinoma. Ther Adv Med Oncol *15*, 17588359231217966. 10.1177/17588359231217966.

442. Fajgenbaum, D.C., and June, C.H. (2020). Cytokine Storm. N Engl J Med *383*, 2255-2273. 10.1056/NEJMra2026131.

443. Wrangle, J.M., Patterson, A., Johnson, C.B., Neitzke, D.J., Mehrotra, S., Denlinger, C.E., Paulos, C.M., Li, Z., Cole, D.J., and Rubinstein, M.P. (2018). IL-

2 and Beyond in Cancer Immunotherapy. J Interferon Cytokine Res *38*, 45-68. 10.1089/jir.2017.0101.

444. Tanegashima, K., Takahashi, R., Nuriya, H., Iwase, R., Naruse, N., Tsuji, K., Shigenaga, A., Otaka, A., and Hara, T. (2017). CXCL14 Acts as a Specific Carrier of CpG DNA into Dendritic Cells and Activates Toll-like Receptor 9-mediated Adaptive Immunity. EBioMedicine *24*, 247-256. 10.1016/j.ebiom.2017.09.012.

445. Iwase, R., Naruse, N., Nakagawa, M., Saito, R., Shigenaga, A., Otaka, A., Hara, T., and Tanegashima, K. (2021). Identification of Functional Domains of CXCL14 Involved in High-Affinity Binding and Intracellular Transport of CpG DNA. J Immunol *207*, 459-469. 10.4049/jimmunol.2100030.

446. Witte, A., Rohlfing, A.K., Dannenmann, B., Dicenta, V., Nasri, M., Kolb, K., Sudmann, J., Castor, T., Rath, D., Borst, O., et al. (2021). The chemokine CXCL14 mediates platelet function and migration via direct interaction with CXCR4. Cardiovasc Res *117*, 903-917. 10.1093/cvr/cvaa080.

447. Otte, M., Kliewer, A., Schutz, D., Reimann, C., Schulz, S., and Stumm, R. (2014). CXCL14 is no direct modulator of CXCR4. FEBS Lett *588*, 4769-4775. 10.1016/j.febslet.2014.11.009.

448. Tanegashima, K., Suzuki, K., Nakayama, Y., Tsuji, K., Shigenaga, A., Otaka, A., and Hara, T. (2013). CXCL14 is a natural inhibitor of the CXCL12-CXCR4 signaling axis. FEBS Lett *587*, 1731-1735. 10.1016/j.febslet.2013.04.046.

449. Hara, T., and Tanegashima, K. (2014). CXCL14 antagonizes the CXCL12-CXCR4 signaling axis. Biomol Concepts *5*, 167-173. 10.1515/bmc-2014-0007.

450. Collins, P.J., McCully, M.L., Martinez-Munoz, L., Santiago, C., Wheeldon, J., Caucheteux, S., Thelen, S., Cecchinato, V., Laufer, J.M., Purvanov, V., et al. (2017). Epithelial chemokine CXCL14 synergizes with CXCL12 via allosteric modulation of CXCR4. FASEB J *31*, 3084-3097. 10.1096/fj.201700013R.

451. Kumar, A., Humphreys, T.D., Kremer, K.N., Bramati, P.S., Bradfield, L., Edgar, C.E., and Hedin, K.E. (2006). CXCR4 physically associates with the T cell receptor to signal in T cells. Immunity *25*, 213-224. 10.1016/j.immuni.2006.06.015.

452. Kouzeli, A., Collins, P.J., Metzemaekers, M., Meyrath, M., Szpakowska, M., Artinger, M., Struyf, S., Proost, P., Chevigne, A., Legler, D.F., et al. (2020). CXCL14 Preferentially Synergizes With Homeostatic Chemokine Receptor Systems. Front Immunol *11*, 561404. 10.3389/fimmu.2020.561404.

453. Guo, J., Chang, C., Yang, L.Y., Cai, H.Q., Chen, D.X., Zhang, Y., Cai, Y., Wang, J.J., Wei, W.Q., Hao, J.J., and Wang, M.R. (2022). Dysregulation of CXCL14 promotes malignant phenotypes of esophageal squamous carcinoma cells via

regulating SRC and EGFR signaling. Biochem Biophys Res Commun *609*, 75-83. 10.1016/j.bbrc.2022.03.144.

454. Song, E.Y., Shurin, M.R., Tourkova, I.L., Gutkin, D.W., and Shurin, G.V. (2010). Epigenetic mechanisms of promigratory chemokine CXCL14 regulation in human prostate cancer cells. Cancer Res *70*, 4394-4401. 10.1158/0008-5472.CAN-10-0427.

455. Bulcha, J.T., Wang, Y., Ma, H., Tai, P.W.L., and Gao, G. (2021). Viral vector platforms within the gene therapy landscape. Signal Transduct Target Ther *6*, 53. 10.1038/s41392-021-00487-6.

456. Yun, C.O., Hong, J., and Yoon, A.R. (2022). Current clinical landscape of oncolytic viruses as novel cancer immunotherapeutic and recent preclinical advancements. Front Immunol *13*, 953410. 10.3389/fimmu.2022.953410.

457. Shalhout, S.Z., Miller, D.M., Emerick, K.S., and Kaufman, H.L. (2023). Therapy with oncolytic viruses: progress and challenges. Nat Rev Clin Oncol *20*, 160-177. 10.1038/s41571-022-00719-w.

458. Dogbey, D.M., Torres, V.E.S., Fajemisin, E., Mpondo, L., Ngwenya, T., Akinrinmade, O.A., Perriman, A.W., and Barth, S. (2023). Technological advances in the use of viral and non-viral vectors for delivering genetic and non-genetic cargos for cancer therapy. Drug Deliv Transl Res *13*, 2719-2738. 10.1007/s13346-023-01362-3.

459. Mortier, A., Van Damme, J., and Proost, P. (2008). Regulation of chemokine activity by posttranslational modification. Pharmacol Ther *120*, 197-217. 10.1016/j.pharmthera.2008.08.006.

460. Gavas, S., Quazi, S., and Karpinski, T.M. (2021). Nanoparticles for Cancer Therapy: Current Progress and Challenges. Nanoscale Res Lett *16*, 173. 10.1186/s11671-021-03628-6.

461. Zhu, J., Martinez, J., Huang, X., and Yang, Y. (2007). Innate immunity against vaccinia virus is mediated by TLR2 and requires TLR-independent production of IFN-beta. Blood *109*, 619-625. 10.1182/blood-2006-06-027136.

462. Shirley, J.L., de Jong, Y.P., Terhorst, C., and Herzog, R.W. (2020). Immune Responses to Viral Gene Therapy Vectors. Mol Ther *28*, 709-722. 10.1016/j.ymthe.2020.01.001.

463. Zaiss, A.K., Machado, H.B., and Herschman, H.R. (2009). The influence of innate and pre-existing immunity on adenovirus therapy. J Cell Biochem *108*, 778-790. 10.1002/jcb.22328.

464. Binnewies, M., Roberts, E.W., Kersten, K., Chan, V., Fearon, D.F., Merad, M., Coussens, L.M., Gabrilovich, D.I., Ostrand-Rosenberg, S., Hedrick, C.C., et al. (2018). Understanding the tumor immune microenvironment (TIME) for effective therapy. Nat Med *24*, 541-550. 10.1038/s41591-018-0014-x.
465. Melero, I., Castanon, E., Alvarez, M., Champiat, S., and Marabelle, A. (2021). Intratumoural administration and tumour tissue targeting of cancer immunotherapies. Nat Rev Clin Oncol *18*, 558-576. 10.1038/s41571-021-00507-y.

466. Ren, J., Yang, W., Su, J., Ren, X., Fazelzad, R., Albert, T., Habbous, S., Goldstein, D.P., de Almeida, J.R., Hansen, A., et al. (2019). Human papillomavirus and p16 immunostaining, prevalence and prognosis of squamous carcinoma of unknown primary in the head and neck region. Int J Cancer *145*, 1465-1474. 10.1002/ijc.32164.

467. Izukuri, K., Suzuki, K., Yajima, N., Ozawa, S., Ito, S., Kubota, E., and Hata, R. (2010). Chemokine CXCL14/BRAK transgenic mice suppress growth of carcinoma cell transplants. [corrected]. Transgenic Res *19*, 1109-1117. 10.1007/s11248-010-9384-7.

468. Hillyer, P., and Male, D. (2005). Expression of chemokines on the surface of different human endothelia. Immunol Cell Biol *83*, 375-382. 10.1111/j.1440-1711.2005.01345.x.

469. Koren, I., Timms, R.T., Kula, T., Xu, Q., Li, M.Z., and Elledge, S.J. (2018). The Eukaryotic Proteome Is Shaped by E3 Ubiquitin Ligases Targeting C-Terminal Degrons. Cell *173*, 1622-1635 e1614. 10.1016/j.cell.2018.04.028.

470. Mirdita, M., Schutze, K., Moriwaki, Y., Heo, L., Ovchinnikov, S., and Steinegger, M. (2022). ColabFold: making protein folding accessible to all. Nat Methods *19*, 679-682. 10.1038/s41592-022-01488-1.

471. Jumper, J., Evans, R., Pritzel, A., Green, T., Figurnov, M., Ronneberger, O., Tunyasuvunakool, K., Bates, R., Zidek, A., Potapenko, A., et al. (2021). Highly accurate protein structure prediction with AlphaFold. Nature *596*, 583-589. 10.1038/s41586-021-03819-2.

472. Waterhouse, A., Bertoni, M., Bienert, S., Studer, G., Tauriello, G., Gumienny, R., Heer, F.T., de Beer, T.A.P., Rempfer, C., Bordoli, L., et al. (2018). SWISS-MODEL: homology modelling of protein structures and complexes. Nucleic Acids Res *46*, W296-W303. 10.1093/nar/gky427.

473. Studer, G., Rempfer, C., Waterhouse, A.M., Gumienny, R., Haas, J., and Schwede, T. (2020). QMEANDisCo-distance constraints applied on model quality estimation. Bioinformatics *36*, 2647. 10.1093/bioinformatics/btaa058.

474. Bienert, S., Waterhouse, A., de Beer, T.A., Tauriello, G., Studer, G., Bordoli, L., and Schwede, T. (2017). The SWISS-MODEL Repository-new features and functionality. Nucleic Acids Res *45*, D313-D319. 10.1093/nar/gkw1132.

475. Guex, N., Peitsch, M.C., and Schwede, T. (2009). Automated comparative protein structure modeling with SWISS-MODEL and Swiss-PdbViewer: a historical perspective. Electrophoresis *30 Suppl 1*, S162-173. 10.1002/elps.200900140.

476. Bertoni, M., Kiefer, F., Biasini, M., Bordoli, L., and Schwede, T. (2017). Modeling protein quaternary structure of homo- and hetero-oligomers beyond binary interactions by homology. Sci Rep *7*, 10480. 10.1038/s41598-017-09654-8.

477. Peterson, F.C., Thorpe, J.A., Harder, A.G., Volkman, B.F., and Schwarze, S.R. (2006). Structural determinants involved in the regulation of CXCL14/BRAK expression by the 26 S proteasome. J Mol Biol *363*, 813-822. 10.1016/j.jmb.2006.08.057.

478. Ma, L., Bluyssen, H.A., De Raeymaeker, M., Laurysens, V., van der Beek, N., Pavliska, H., van Zonneveld, A.J., Tomme, P., and van Es, H.H. (2001). Rapid determination of adenoviral vector titers by quantitative real-time PCR. J Virol Methods *93*, 181-188. 10.1016/s0166-0934(01)00257-9.

479. Luo, J., Deng, Z.L., Luo, X., Tang, N., Song, W.X., Chen, J., Sharff, K.A., Luu, H.H., Haydon, R.C., Kinzler, K.W., et al. (2007). A protocol for rapid generation of recombinant adenoviruses using the AdEasy system. Nat Protoc *2*, 1236-1247. 10.1038/nprot.2007.135.

480. Kasuga, I., Hogg, J.C., Pare, P.D., Hayashi, S., Sedgwick, E.G., Ruan, J., Wallace, A.M., He, J.Q., Zhang, X., and Sandford, A.J. (2009). Role of genetic susceptibility to latent adenoviral infection and decreased lung function. Respir Med *103*, 1672-1680. 10.1016/j.rmed.2009.05.008.

481. Kwon, E.J., Lee, H.R., Lee, J.H., Seo, C., Ha, M., Roh, J., Kim, Y.H., and Jang, J.Y. (2022). Identification of differentially expressed genes and pathways for risk stratification in HPV-associated cancers governing different anatomical sites. Front Biosci (Landmark Ed) *27*, 2. 10.31083/j.fbl2701002.

482. Stasiak, A.C., and Stehle, T. (2020). Human adenovirus binding to host cell receptors: a structural view. Med Microbiol Immunol *209*, 325-333. 10.1007/s00430-019-00645-2.

483. Aksoy, P., Gottschalk, E.Y., and Meneses, P.I. (2017). HPV entry into cells. Mutat Res Rev Mutat Res *772*, 13-22. 10.1016/j.mrrev.2016.09.004.

484. Zuidema, A., Wang, W., Kreft, M., Te Molder, L., Hoekman, L., Bleijerveld, O.B., Nahidiazar, L., Janssen, H., and Sonnenberg, A. (2018). Mechanisms of integrin alphaVbeta5 clustering in flat clathrin lattices. J Cell Sci *131*. 10.1242/jcs.221317.

485. Summerford, C., Bartlett, J.S., and Samulski, R.J. (1999). AlphaVbeta5 integrin: a co-receptor for adeno-associated virus type 2 infection. Nat Med *5*, 78-82. 10.1038/4768.

486. Lyle, C., and McCormick, F. (2010). Integrin alphavbeta5 is a primary receptor for adenovirus in CAR-negative cells. Virol J *7*, 148. 10.1186/1743-422X-7-148.

487. Wagner, H. (2004). The immunobiology of the TLR9 subfamily. Trends Immunol *25*, 381-386. 10.1016/j.it.2004.04.011.

488. Liu, Z., Chen, O., Wall, J.B.J., Zheng, M., Zhou, Y., Wang, L., Vaseghi, H.R., Qian, L., and Liu, J. (2017). Systematic comparison of 2A peptides for cloning multi-genes in a polycistronic vector. Sci Rep *7*, 2193. 10.1038/s41598-017-02460-2.

489. Vita, R., Mahajan, S., Overton, J.A., Dhanda, S.K., Martini, S., Cantrell, J.R., Wheeler, D.K., Sette, A., and Peters, B. (2019). The Immune Epitope Database (IEDB): 2018 update. Nucleic Acids Res *47*, D339-D343. 10.1093/nar/gky1006.

490. Tools, I.E.D. (2024). IEDB. www.iedb.org.

491. Perez-Trujillo, J.J., Garza-Morales, R., Barron-Cantu, J.A., Figueroa-Parra, G., Garcia-Garcia, A., Rodriguez-Rocha, H., Garcia-Juarez, J., Munoz-Maldonado, G.E., Saucedo-Cardenas, O., Montes-De-Oca-Luna, R., and Loera-Arias, M.J. (2017). DNA vaccine encoding human papillomavirus antigens flanked by a signal peptide and a KDEL sequence induces a potent therapeutic antitumor effect. Oncol Lett *13*, 1569-1574. 10.3892/ol.2017.5635.

492. Donnelly, M.L.L., Luke, G., Mehrotra, A., Li, X., Hughes, L.E., Gani, D., and Ryan, M.D. (2001). Analysis of the aphthovirus 2A/2B polyprotein 'cleavage' mechanism indicates not a proteolytic reaction, but a novel translational effect: a putative ribosomal 'skip'. J Gen Virol *82*, 1013-1025. 10.1099/0022-1317-82-5-1013.

493. Paulson, K.G., Voillet, V., McAfee, M.S., Hunter, D.S., Wagener, F.D., Perdicchio, M., Valente, W.J., Koelle, S.J., Church, C.D., Vandeven, N., et al. (2018). Acquired cancer resistance to combination immunotherapy from transcriptional loss of class I HLA. Nat Commun *9*, 3868. 10.1038/s41467-018-06300-3.

494. Kobayashi, K.S., and van den Elsen, P.J. (2012). NLRC5: a key regulator of MHC class I-dependent immune responses. Nat Rev Immunol *12*, 813-820. 10.1038/nri3339.

495. Meissner, T.B., Li, A., Biswas, A., Lee, K.H., Liu, Y.J., Bayir, E., Iliopoulos, D., van den Elsen, P.J., and Kobayashi, K.S. (2010). NLR family member NLRC5 is a transcriptional regulator of MHC class I genes. Proc Natl Acad Sci U S A *107*, 13794-13799. 10.1073/pnas.1008684107.

496. Wang, X.Q.D., and Dou, Y. (2023). Dissecting MENIN in bivalent gene regulation. Nat Cell Biol *25*, 209-210. 10.1038/s41556-022-01063-y.

497. Liu, P., Shi, C., Qiu, L., Shang, D., Lu, Z., Tu, Z., and Liu, H. (2024). Menin signaling and therapeutic targeting in breast cancer. Curr Probl Cancer *51*, 101118. 10.1016/j.currproblcancer.2024.101118.

498. Thomas, X. (2024). Small Molecule Menin Inhibitors: Novel Therapeutic Agents Targeting Acute Myeloid Leukemia with KMT2A Rearrangement or NPM1 Mutation. Oncol Ther *12*, 57-72. 10.1007/s40487-024-00262-x.

499. Oh, J.H., Lee, J.Y., Kim, K.H., Kim, C.Y., Jeong, D.S., Cho, Y., Nam, K.T., and Kim, M.H. (2020). Elevated GCN5 expression confers tamoxifen resistance by upregulating AIB1 expression in ER-positive breast cancer. Cancer Lett *495*, 145-155. 10.1016/j.canlet.2020.09.017.

500. Zhao, L., Pang, A., and Li, Y. (2018). Function of GCN5 in the TGF-beta1-induced epithelial-to-mesenchymal transition in breast cancer. Oncol Lett *16*, 3955-3963. 10.3892/ol.2018.9134.

501. Zhao, C., Li, Y., Qiu, W., He, F., Zhang, W., Zhao, D., Zhang, Z., Zhang, E., Ma, P., Liu, Y., et al. (2018). C5a induces A549 cell proliferation of non-small cell lung cancer via GDF15 gene activation mediated by GCN5-dependent KLF5 acetylation. Oncogene *37*, 4821-4837. 10.1038/s41388-018-0298-9.

502. Lu, D., Song, Y., Yu, Y., Wang, D., Liu, B., Chen, L., Li, X., Li, Y., Cheng, L., Lv, F., et al. (2021). KAT2A-mediated AR translocation into nucleus promotes abiraterone-resistance in castration-resistant prostate cancer. Cell Death Dis *12*, 787. 10.1038/s41419-021-04077-w.

503. Shao, G., Liu, Y., Ma, T., Zhang, L., Yuan, M., and Zhao, S. (2018). GCN5 inhibition prevents IL-6-induced prostate cancer metastases through PI3K/PTEN/Akt signaling by inactivating Egr-1. Biosci Rep *38*. 10.1042/BSR20180816.

504. Lin, S., Qiu, L., Liang, K., Zhang, H., Xian, M., Chen, Z., Wei, J., Fu, S., Gong, X., Ding, K., et al. (2022). KAT2A/E2F1 Promotes Cell Proliferation and Migration via Upregulating the Expression of UBE2C in Pan-Cancer. Genes (Basel) *13*. 10.3390/genes13101817.

505. Farria, A.T., Mustachio, L.M., Akdemir, Z.H.C., and Dent, S.Y.R. (2019). GCN5 HAT inhibition reduces human Burkitt lymphoma cell survival through reduction of MYC target gene expression and impeding BCR signaling pathways. Oncotarget *10*, 5847-5858. 10.18632/oncotarget.27226.
506. Li, Q., Zhang, L., You, W., Xu, J., Dai, J., Hua, D., Zhang, R., Yao, F., Zhou, S., Huang, W., et al. (2022). PRDM1/BLIMP1 induces cancer immune evasion by modulating the USP22-SPI1-PD-L1 axis in hepatocellular carcinoma cells. Nat Commun *13*, 7677. 10.1038/s41467-022-35469-x.

507. Li, C., Wang, Y., Gong, Y., Zhang, T., Huang, J., Tan, Z., and Xue, L. (2021). Finding an easy way to harmonize: a review of advances in clinical research and combination strategies of EZH2 inhibitors. Clin Epigenetics *13*, 62. 10.1186/s13148-021-01045-1.

508. Hanaki, S., and Shimada, M. (2021). Targeting EZH2 as cancer therapy. J Biochem *170*, 1-4. 10.1093/jb/mvab007.

509. Lee, S.H., Li, Y., Kim, H., Eum, S., Park, K., and Lee, C.H. (2022). The role of EZH1 and EZH2 in development and cancer. BMB Rep *55*, 595-601. 10.5483/BMBRep.2022.55.12.174.

510. Mochizuki-Kashio, M., Aoyama, K., Sashida, G., Oshima, M., Tomioka, T., Muto, T., Wang, C., and Iwama, A. (2015). Ezh2 loss in hematopoietic stem cells predisposes mice to develop heterogeneous malignancies in an Ezh1-dependent manner. Blood *126*, 1172-1183. 10.1182/blood-2015-03-634428.

511. Keam, S.J. (2022). Valemetostat Tosilate: First Approval. Drugs *82*, 1621-1627. 10.1007/s40265-022-01800-5.

512. Izutsu, K., Makita, S., Nosaka, K., Yoshimitsu, M., Utsunomiya, A., Kusumoto, S., Morishima, S., Tsukasaki, K., Kawamata, T., Ono, T., et al. (2023). An open-label, single-arm phase 2 trial of valemetostat for relapsed or refractory adult T-cell leukemia/lymphoma. Blood *141*, 1159-1168. 10.1182/blood.2022016862.

513. Humphreys, P.G., Bamborough, P., Chung, C.W., Craggs, P.D., Gordon, L., Grandi, P., Hayhow, T.G., Hussain, J., Jones, K.L., Lindon, M., et al. (2017). Discovery of a Potent, Cell Penetrant, and Selective p300/CBP-Associated Factor (PCAF)/General Control Nonderepressible 5 (GCN5) Bromodomain Chemical Probe. J Med Chem *60*, 695-709. 10.1021/acs.jmedchem.6b01566.

514. He, S., Liu, Z., Oh, D.Y., and Thiele, C.J. (2013). MYCN and the epigenome. Front Oncol *3*, 1. 10.3389/fonc.2013.00001.

515. Matthay, K.K., Maris, J.M., Schleiermacher, G., Nakagawara, A., Mackall, C.L., Diller, L., and Weiss, W.A. (2016). Neuroblastoma. Nat Rev Dis Primers *2*, 16078. 10.1038/nrdp.2016.78.

516. Arede, L., and Pina, C. (2021). Buffering noise: KAT2A modular contributions to stabilization of transcription and cell identity in cancer and development. Exp Hematol *93*, 25-37. 10.1016/j.exphem.2020.10.003.

517. Yu, S.S., and Cirillo, N. (2020). The molecular markers of cancer stem cells in head and neck tumors. J Cell Physiol *235*, 65-73. 10.1002/jcp.28963.

518. Liu, X., Huang, J., Chen, T., Wang, Y., Xin, S., Li, J., Pei, G., and Kang, J. (2008). Yamanaka factors critically regulate the developmental signaling network in mouse embryonic stem cells. Cell Res *18*, 1177-1189. 10.1038/cr.2008.309.

519. Boumahdi, S., Driessens, G., Lapouge, G., Rorive, S., Nassar, D., Le Mercier, M., Delatte, B., Caauwe, A., Lenglez, S., Nkusi, E., et al. (2014). SOX2 controls tumour initiation and cancer stem-cell functions in squamous-cell carcinoma. Nature *511*, 246-250. 10.1038/nature13305.

520. Kaneko, Y., Suenaga, Y., Islam, S.M., Matsumoto, D., Nakamura, Y., Ohira, M., Yokoi, S., and Nakagawara, A. (2015). Functional interplay between MYCN, NCYM, and OCT4 promotes aggressiveness of human neuroblastomas. Cancer Sci *106*, 840-847. 10.1111/cas.12677.

521. Izumi, H., Kaneko, Y., and Nakagawara, A. (2020). The Role of MYCN in Symmetric vs. Asymmetric Cell Division of Human Neuroblastoma Cells. Front Oncol *10*, 570815. 10.3389/fonc.2020.570815.

522. Pucci, M., Duca, M., Malagolini, N., and Dall'Olio, F. (2022). Glycosyltransferases in Cancer: Prognostic Biomarkers of Survival in Patient Cohorts and Impact on Malignancy in Experimental Models. Cancers (Basel) *14*. 10.3390/cancers14092128.

523. Jongsma, M.L.M., de Waard, A.A., Raaben, M., Zhang, T., Cabukusta, B., Platzer, R., Blomen, V.A., Xagara, A., Verkerk, T., Bliss, S., et al. (2021). The SPPL3-Defined Glycosphingolipid Repertoire Orchestrates HLA Class I-Mediated Immune Responses. Immunity *54*, 132-150 e139. 10.1016/j.immuni.2020.11.003.

524. Jongsma, M.L.M., de Waard, A.A., Raaben, M., Zhang, T., Cabukusta, B., Platzer, R., Blomen, V.A., Xagara, A., Verkerk, T., Bliss, S., et al. (2021). The SPPL3-defined glycosphingolipid repertoire orchestrates HLA class I-mediated immune responses. Immunity *54*, 387. 10.1016/j.immuni.2021.01.016.

525. Brockmann, M., Poon, E., Berry, T., Carstensen, A., Deubzer, H.E., Rycak, L., Jamin, Y., Thway, K., Robinson, S.P., Roels, F., et al. (2013). Small molecule inhibitors of aurora-a induce proteasomal degradation of N-myc in childhood neuroblastoma. Cancer Cell *24*, 75-89. 10.1016/j.ccr.2013.05.005.

526. Gustafson, W.C., Meyerowitz, J.G., Nekritz, E.A., Chen, J., Benes, C., Charron, E., Simonds, E.F., Seeger, R., Matthay, K.K., Hertz, N.T., et al. (2014). Drugging

MYCN through an allosteric transition in Aurora kinase A. Cancer Cell *26*, 414-427. 10.1016/j.ccr.2014.07.015.

527. Li, Y., and Zhang, J. (2015). AURKA is a predictor of chemotherapy response and prognosis for patients with advanced oral squamous cell carcinoma. Tumour Biol *36*, 3557-3564. 10.1007/s13277-014-2992-8.

528. Shaikh, M.H., Idris, A., Johnson, N.W., Fallaha, S., Clarke, D.T.W., Martin, D., Morgan, I.M., Gabrielli, B., and McMillan, N.A.J. (2018). Aurora kinases are a novel therapeutic target for HPV-positive head and neck cancers. Oral Oncol *86*, 105-112. 10.1016/j.oraloncology.2018.09.006.

529. Chang, C.P., Yeh, T.K., Chen, C.T., Wang, W.P., Chen, Y.T., Tsai, C.H., Chen, Y.F., Ke, Y.Y., Wang, J.Y., Chen, C.P., et al. (2024). Discovery of a Long Half-Life AURKA Inhibitor to Treat MYC-Amplified Solid Tumors as a Monotherapy and in Combination with Everolimus. Mol Cancer Ther *23*, 766-779. 10.1158/1535-7163.MCT-23-0602.

530. Garralda, E., Beaulieu, M.E., Moreno, V., Casacuberta-Serra, S., Martinez-Martin, S., Foradada, L., Alonso, G., Masso-Valles, D., Lopez-Estevez, S., Jauset, T., et al. (2024). MYC targeting by OMO-103 in solid tumors: a phase 1 trial. Nat Med *30*, 762-771. 10.1038/s41591-024-02805-1.

531. Mundo, L., Ambrosio, M.R., Raimondi, F., Del Porro, L., Guazzo, R., Mancini, V., Granai, M., Jim Rocca, B., Lopez, C., Bens, S., et al. (2019). Molecular switch from MYC to MYCN expression in MYC protein negative Burkitt lymphoma cases. Blood Cancer J *9*, 91. 10.1038/s41408-019-0252-2.

532. Ishido, S., and Kajikawa, M. (2019). MHC class II fine tuning by ubiquitination: lesson from MARCHs. Immunogenetics *71*, 197-201. 10.1007/s00251-018-1094-y.

533. Bayer-Santos, E., Durkin, C.H., Rigano, L.A., Kupz, A., Alix, E., Cerny, O., Jennings, E., Liu, M., Ryan, A.S., Lapaque, N., et al. (2016). The Salmonella Effector SteD Mediates MARCH8-Dependent Ubiquitination of MHC II Molecules and Inhibits T Cell Activation. Cell Host Microbe *20*, 584-595. 10.1016/j.chom.2016.10.007.

534. Yang, X., Shi, C., Li, H., Shen, S., Su, C., and Yin, H. (2022). MARCH8 attenuates cGAS-mediated innate immune responses through ubiquitylation. Sci Signal *15*, eabk3067. 10.1126/scisignal.abk3067.

535. Coon, T.A., Glasser, J.R., Mallampalli, R.K., and Chen, B.B. (2012). Novel E3 ligase component FBXL7 ubiquitinates and degrades Aurora A, causing mitotic arrest. Cell Cycle *11*, 721-729. 10.4161/cc.11.4.19171.

536. Khalil, M.I., Yang, C., Vu, L., Chadha, S., Nabors, H., James, C.D., Morgan, I.M., and Pyeon, D. (2024). The membrane-associated ubiquitin ligase MARCHF8 stabilizes the human papillomavirus oncoprotein E7 by degrading CUL1 and UBE2L3 in head and neck cancer. J Virol *98*, e0172623. 10.1128/jvi.01726-23.

537. Nikonova, A.S., Astsaturov, I., Serebriiskii, I.G., Dunbrack, R.L., Jr., and Golemis, E.A. (2013). Aurora A kinase (AURKA) in normal and pathological cell division. Cell Mol Life Sci *70*, 661-687. 10.1007/s00018-012-1073-7.

538. Ferreira, C.B., Sumner, R.P., Rodriguez-Plata, M.T., Rasaiyaah, J., Milne, R.S., Thrasher, A.J., Qasim, W., and Towers, G.J. (2020). Lentiviral Vector Production Titer Is Not Limited in HEK293T by Induced Intracellular Innate Immunity. Mol Ther Methods Clin Dev *17*, 209-219. 10.1016/j.omtm.2019.11.021.

539. Reus, J.B., Trivino-Soto, G.S., Wu, L.I., Kokott, K., and Lim, E.S. (2020). SV40 Large T Antigen Is Not Responsible for the Loss of STING in 293T Cells but Can Inhibit cGAS-STING Interferon Induction. Viruses *12*. 10.3390/v12020137.

540. Yasuda, H., Leelahavanichkul, A., Tsunoda, S., Dear, J.W., Takahashi, Y., Ito, S., Hu, X., Zhou, H., Doi, K., Childs, R., et al. (2008). Chloroquine and inhibition of Toll-like receptor 9 protect from sepsis-induced acute kidney injury. Am J Physiol Renal Physiol *294*, F1050-1058. 10.1152/ajprenal.00461.2007.

541. Javmen, A., Szmacinski, H., Lakowicz, J.R., and Toshchakov, V.Y. (2018). Blocking TIR Domain Interactions in TLR9 Signaling. J Immunol *201*, 995-1006. 10.4049/jimmunol.1800194.

542. Majer, O., Liu, B., Woo, B.J., Kreuk, L.S.M., Van Dis, E., and Barton, G.M. (2019). Release from UNC93B1 reinforces the compartmentalized activation of select TLRs. Nature *575*, 371-374. 10.1038/s41586-019-1611-7.

543. Kroeze, W.K., Sassano, M.F., Huang, X.P., Lansu, K., McCorvy, J.D., Giguere, P.M., Sciaky, N., and Roth, B.L. (2015). PRESTO-Tango as an open-source resource for interrogation of the druggable human GPCRome. Nat Struct Mol Biol *22*, 362-369. 10.1038/nsmb.3014.

544. Xiong, X., Liao, X., Qiu, S., Xu, H., Zhang, S., Wang, S., Ai, J., and Yang, L. (2022). CXCL8 in Tumor Biology and Its Implications for Clinical Translation. Front Mol Biosci *9*, 723846. 10.3389/fmolb.2022.723846.

545. Bednarska, N.G., Wren, B.W., and Willcocks, S.J. (2017). The importance of the glycosylation of antimicrobial peptides: natural and synthetic approaches. Drug Discov Today *22*, 919-926. 10.1016/j.drudis.2017.02.001.

546. Cai, Z., Wei, Q., Li, X., Luan, Y., and Dong, S. (2020). Chemical Syntheses and Biological Evaluation of CXCL14 and Its Site-Selectively Modified Methionine Sulfoxide-Containing Derivatives. J Org Chem *85*, 1740-1747. 10.1021/acs.joc.9b02730.

547. Kraft, K., Yost, K.E., Murphy, S.E., Magg, A., Long, Y., Corces, M.R., Granja, J.M., Wittler, L., Mundlos, S., Cech, T.R., et al. (2022). Polycomb-mediated genome architecture enables long-range spreading of H3K27 methylation. Proc Natl Acad Sci U S A *119*, e2201883119. 10.1073/pnas.2201883119.

548. Lin, X., Leicher, R., Liu, S., and Zhang, B. (2021). Cooperative DNA looping by PRC2 complexes. Nucleic Acids Res *49*, 6238-6248. 10.1093/nar/gkab441.

549. Dickson, M.A., Hahn, W.C., Ino, Y., Ronfard, V., Wu, J.Y., Weinberg, R.A., Louis, D.N., Li, F.P., and Rheinwald, J.G. (2000). Human keratinocytes that express hTERT and also bypass a p16(INK4a)-enforced mechanism that limits life span become immortal yet retain normal growth and differentiation characteristics. Mol Cell Biol *20*, 1436-1447. 10.1128/MCB.20.4.1436-1447.2000.

550. Spanos, W.C., Nowicki, P., Lee, D.W., Hoover, A., Hostager, B., Gupta, A., Anderson, M.E., and Lee, J.H. (2009). Immune response during therapy with cisplatin or radiation for human papillomavirus-related head and neck cancer. Arch Otolaryngol Head Neck Surg *135*, 1137-1146. 10.1001/archoto.2009.159.

551. Labun, K., Montague, T.G., Gagnon, J.A., Thyme, S.B., and Valen, E. (2016). CHOPCHOP v2: a web tool for the next generation of CRISPR genome engineering. Nucleic Acids Res *44*, W272-276. 10.1093/nar/gkw398.

552. Labun, K., Montague, T.G., Krause, M., Torres Cleuren, Y.N., Tjeldnes, H., and Valen, E. (2019). CHOPCHOP v3: expanding the CRISPR web toolbox beyond genome editing. Nucleic Acids Res *47*, W171-W174. 10.1093/nar/gkz365.

553. Montague, T.G., Cruz, J.M., Gagnon, J.A., Church, G.M., and Valen, E. (2014). CHOPCHOP: a CRISPR/Cas9 and TALEN web tool for genome editing. Nucleic Acids Res *42*, W401-407. 10.1093/nar/gku410.

554. Gilliland, H.N., Beckman, O.K., and Olive, A.J. (2023). A Genome-Wide Screen in Macrophages Defines Host Genes Regulating the Uptake of Mycobacterium abscessus. mSphere *8*, e0066322. 10.1128/msphere.00663-22.

555. Doench, J.G., Fusi, N., Sullender, M., Hegde, M., Vaimberg, E.W., Donovan, K.F., Smith, I., Tothova, Z., Wilen, C., Orchard, R., et al. (2016). Optimized sgRNA design to maximize activity and minimize off-target effects of CRISPR-Cas9. Nat Biotechnol *34*, 184-191. 10.1038/nbt.3437.

556. Kiritsy, M.C., Ankley, L.M., Trombley, J., Huizinga, G.P., Lord, A.E., Orning, P., Elling, R., Fitzgerald, K.A., and Olive, A.J. (2021). A genetic screen in macrophages identifies new regulators of IFNgamma-inducible MHCII that contribute to T cell activation. Elife *10*. 10.7554/eLife.65110.

557. von Mering, C., Jensen, L.J., Snel, B., Hooper, S.D., Krupp, M., Foglierini, M., Jouffre, N., Huynen, M.A., and Bork, P. (2005). STRING: known and predicted protein-protein associations, integrated and transferred across organisms. Nucleic Acids Res *33*, D433-437. 10.1093/nar/gki005.
558. Mullen, L. (2022). Introduction to the IPA Core Analysis. https://tv.qiagenbioinformatics.com/photo/44601141/introduction-to-the-ipa-core.